PROTEIN-INTERCALATED BENTONITE FOR BIO-COMPOSITES

A thesis

submitted in fulfillment

of the requirements for the degree

of

Doctor of Philosophy

in Materials and Process Engineering

at

The University of Waikato

by

MUHAMMAD RASHID SHAMSUDDIN

THE UNIVERSITY OF
WAIKATO
Te Whare Wānanga o Waikato

2013

ABSTRACT

The application of clays in various fields such as agriculture [1, 2], mining [1], construction [3], petroleum derivatives recovery [4], waste water treatment [5-8] and material reinforcements [9-11] is closely related to their unique properties including small particle size with high surface negativity and hydrophilic nature. This work investigated the potential use of bentonite clay for treatment of meat rendering waste water by adsorption and utilizing the spent bentonite for bioplastic fillers. Models were applied to predict the organic adsorption and the sedimentation of clay particles in solution.

Various clays including bentonite are typically used in polymers to enhance composite properties at a very low level of loading [10, 12-17]. As bio-composite fillers, bentonite is modified with organics such as alkylammonium [18], amines [19] and gelatin [20] to improve compatibility with the matrix polymer. The use of these materials can be expensive and therefore, more attention has been directed to using waste sources such as meat processing waste [21, 22]. One type of waste, stickwater which contains approximately 4-5 % protein, 1-2 % fat and < 1 % minerals, could become a low-cost organic modifier for bentonite [23, 24]. Stickwater has a biological oxygen demand (BOD) of 150 000 mg/L, coloured, odorous and its treatment can be expensive [24-27].

Currently, stickwater is mostly dried and added to blood and bone meal in meat rendering plants. Where no further unit operations are carried out on stickwater, the stickwater must be treated to reduce the BOD. Depending on the the scale of operation, a plant can produce up to 30 000 L of stickwater at 2-5 % solids per day [28]. Waste water treatment costs NZ$ 0.90 per kg solids [29] or approximately NZ$ 1350 per day. The main protein in stickwater is gelatin, a denatured form of collagen. Extracting protein from stickwater by adsorption can reduce the treatment charges by decreasing the BOD as well as producing organically-modified bentonite for use as a bio-composite filler.

Gelatin has a large numbers of side groups and can be easily crosslinked and adsorbed [30]. Locally mined bentonite in the form of calcium and sodium bentonite, CaBt and NaBt respectively, costs NZ$ 20 per tonne [31] and has a high gelatin adsorption capacity of up to 405 mg protein per gram bentonite (mg/g). For 30 000 kg stickwater, treatment using sodium bentonite costs around NZ$ 74 per day (this excludes operating and other material costs). Gelatin adsorption from stickwater gave a lower adsorption capacity of 246 mg/g due to competition between mineral and fat solutes with gelatin for binding sites on the adsorbent. Adsorption of solutes by bentonite occurred on the surface and within the interlayer spacings as revealed by x-ray diffraction (XRD) and thermogravimetric analysis (TGA).

Settling or sedimentation of particles from solution was studied to find an alternative to centrifugation for solid recovery after treatment. At 2 % protein concentration, settling was obtained for CaBt in gelatin at pH 3 whereas in stickwater, both CaBt and NaBt settled at pH 3. The highest clay recovery was obtained after overnight settling at 91 and 95 % for CaBt in gelatin and stickwater at pH 3. Conditions that favoured settling corresponded to low gelatin adsorption.

Bentonite consists of aluminosilicate layers and upon organic adsorption, intercalation and exfoliation can be achieved [20, 32]. As reinforcement materials, this leads to fillers with a very high aspect ratio in matrix polymers such as in bloodmeal-based plastic, also known as Novatein Thermoplastic Protein or NTP. In NTP, the highest improvement in tensile strength and Young's modulus was at 23 % (11.45 MPa) and 17 % (727.45 MPa) at 0.5 parts stickwater-modified NaBt per hundred of bloodmeal (pph_{BM}). For elongation at break, the highest increase of 23.5 % was achieved for unmodified NaBt at 0.5 $pph_{BM.}$ These improvements also correspond with enhancements in glass transitition temperature (T_g) of composites and increased basal spacing (*d*-value) of bentonite. Transmission electron microscope (TEM) analysis confirmed the exfoliation of fillers for organically-modified bentonite. These observations, particularly at low filler dosage strongly suggest the formation of nanocomposites.

ACKNOWLEDGEMENTS

A big thank you to my supervisors, Dr. Johan Verbeek and Dr. Mark Lay for being there when I needed them. They are like my beacon of light in the forest of darkness. When the going was tough, they set my arse on fire to make sure I did not go astray. When there was no hope in my experiments, they paved the way by making truck-load of suggestions. When I was struggling financially, they were not around to catch me working full-time. Special thanks to Mark for taking me on countless hikings.

Thanks to all my research colleagues who had inspired me directly or indirectly and shaped my research to what it is now; especially the three stooges - Aaron, Jim, Talia and the rest – Sisira, Tan, Asma, Jasneet, Jeanie, Faisal and the Malaysians. The lab and office are less colourful without you guys.

Thanks to all the lab technicians; Lisa Li, Indar Singh, Yuanji Zhang, Helen Turner, Annette Rodgers, Chris McKinnon, Chris Wang and Brett Nichols for the helpful guidance and valuable thoughts. Thanks to Ivan Bell, the science store keeper for stocking up chemicals and disposables. A big thank you to the science librarian, Cheryl Ward for some midas touch on Words and Endnote. A pleasant thank to the floor cleaner, Liz for being positive and friendly and for keeping the office clean.

Thanks to department academics; Assoc. Prof. Dr. Brian Gabbitas for the generous assistance on TEM, Assoc. Prof. Dr. Alan Langdon for sharing the knowledge on XRD and BET, Prof. Janis Swan for her expertise on NZ meat industry and Kim Pickering for bringing cakes during CAKE meetings.

Special thanks to my kiwi family here in NZ; the Kirks, the Greers and the Marrets in Hastings for providing me jobs and B&B when my pocket grew thin, the Gilligans and the Malaysian community in Hamilton for their encouragements and hospitality.

Utterly important, to my parents back in Malaysia; mum, dad and all my family members for the limitless supports throughout the journey. Though they are 11 flight hours away but they are always close in my heart. I just cannot thank you enough. May The Almighty God shower them with love and endless blessings.

TABLE OF CONTENTS

LIST OF FIGURES

LIST OF TABLES

NOMENCLATURE

Latin letters

$[P]$	concentration of solutes	$[S]$	concentration of binding sites
$[SP]$	concentration of filled binding sites with solutes	a_{ts} (m^2)	cross sectional area of a column
b (J/mol)	Temkin isotherm constant	Bt	bentonite
C (mg/ml)	instantaneous concentration	C_D	drag coefficient
C_e (mg/ml)	equilibrium concentration	C_f (mg/ml)	final concentration
C_o (mg/ml)	initial concentration	C_r (mg/g)	amount of adsorbed solute on solid-phase
C_{rmax} (mg/g)	maximum amount of adsorbed solute on solid-phase	C_u (0.05108 mm^2/s^2)	Ubbelohde tube constant
d_{001}	first diffraction peak	D_{cp} (μm)	clay particle diameter
D_t (m)	settling column diameter	*d-value* (Å)	basal spacing
E' (MPa)	Young's modulus	$E^{'}$ (MPa)	storage modulus
E'' (MPa)	loss modulus	e_f	final sediment porosity
e_o	initial sediment porosity	F (96500 C/mole)	Faraday's constant
F_b ($kg.m/s^2$)	buoyancy force	F_d ($kg.m/s^2$)	drag force
F_g ($kg.m/s^2$)	gravitational force	F_R ($kg.m/s^2$)	resultant force on a section
F_s ($kg.m/s^2$)	elastic force	g (9.81 m/s^2)	gravitational acceleration
h (m)	sediment height	h_t (m)	height of settling column
h_{ts} (m)	sectional height of column	K (g/mg)	equilibrium constant
k_1 (g/mg.s)	adsorption rate constant	k_2 (1/s)	desorption rate constant
K_f	Freundlich constant	k_f	flux coefficient
K_l (g/mg)	Langmuir constant	K_{lf} (g/mg)	L-F constant
k_s (kg/s^2)	elastic constant	K_t	Temkin constant
m (g)	general term for mass	M_{ads} (g)	mass of adsorbed organic
M_{ash} (g)	mass of ash	m_c (g)	mass of clay
m_{co} (g)	initial mass of clay	m_{cp} (g)	mass of a single clay particle
m_{cr} (g)	dried mass of clay pellet	m_{cs} (g)	mass of clay in a section
meq	miliequivalents	M_o (g)	initial mass
$M_{org.Bt}$ (g)	mass of pre-existing organic on bentonite	$M_{org.sn}$ (g)	mass of organic in supernatant
$M_{org.total}$ (g)	mass of total organic	m_p (g)	mass of a single particle
M_{solid} (g)	mass of solid	Mt	montmorillonite
M_{water} (g)	mass of water	n	parameter of favourability
n_{cps}	number of clay particles in a section	n_f (moles)	number of moles in Nernst equation
n_{pt}	total number of particles in the system	N_s	number of column sections
P (kg/ms^2)	pressure exerted on a section	Q (m^3/s)	volumetric flowrate
R (8.314 J/mol.K)	universal gas constant	r_{cp} (μm)	radius of bentonite particle
Re_p	particle Reynolds number	R_t (s)	run time
T (°C)	temperature	t_{efflux} (s)	residence time of Ubbelohde tube
T_g (°C)	glass transition temperature	T_m (°C)	melting point
t_s (s)	settling time	t_{ss} (s)	Stoke's law settling time
V	general term for volume	V_{cp} (m^3)	volume of clay particle

V_f (ml)	final volume	V_o (ml)	initial volume
V_s (m/s)	settling velocity	V_{ss} (m/s)	Stoke's law settling velocity
V_{ts} (m^3)	volume of a section in settling column	x (m)	distance travelled by particles

Greek letters

α	Langmuir isotherm derivation constant	tan δ	loss factor
Δx	change in vertical distance	ε (%)	ultimate strain
ζ (V)	zeta potential	θ (^{o})	angle
λ (1.5406 Å)	wavelength of x-ray beam	μ (kg/ms)	general term for viscosity
μ_f (kg/ms)	dynamic viscosity of solution	μ_k (m^2/s)	kinematic viscosity
ρ (kg/m^3)	general term for density	ρ_{cp} (kg/m^3)	density of gelatin-treated bentonite
ρ_f (kg/m^3)	fluid density	σ (MPa)	tensile strength
σ_d	diffuse layer charge	σ_s	Stern layer charge
$\varnothing$	porosity	Ψ (V)	surface potential
Σ	sum		

Abbreviations

AAS	atomic absorption spectrophotometer	AFBR	anaerobic fluidized bed reactors
AFFR	anaerobic fixed film reactor	AFM	atomic force microscopy
AIPEA	International Association for the Study of Clays	Amine Bt	octadecylamine bentonite
ASTM	American Society for Testing and Materials	BET	Brunauer-Emmett-Teller
BOD (g O_2/m^3)	biological / biochemical oxygen demand	BSA	bovine serum albumin
BSE	bovine spongiform encephalopathy	CaBt	calcium bentonite
cBOD, $cBOD_5$ (g O_2/m^3)	carbonaceous BOD	CEC (mEq./g)	cation exchange capacity
COD (mg/m^3)	chemical oxygen demand	Cryo-SEM	cryogenic SEM
CTMAC	cetyl-trimetyl-ammonium chloride	DFM	dynamic mode atomic force microscopy
DSC	differential scanning calorimetry	EDS	energy dispersive spectroscopy
EPA	Environment Protection Authority	ESI-MS	electrospray ionization mass spectrometry
FE-SEM	field emission scanning electron microscope	FOG	fats, oils and greases
FTIR	Fourier transform infrared spectroscopy	GDP	gross domestic product
gdwt	gram dry weight	Ge2%	gelatin with C_o 2%
HDT (^{o}C)	heat distortion temperature	HE-TEM	high resolution transmission electron microscope
HPLC	high performance liquid chromatography	HRT (day)	hydraulic retention time

IEP (pH)	isoelectric point	IUPAC	International Union of Pure and Applied Chemistry
KCl	potassium chloride	L-F	Langmuir-Freundlich
MBR	membrane bioreactor	NaBt	sodium bentonite
NMR	nuclear magnetic resonance	NTP	Novatein Thermoplastic Protein
NTU	nephelometric turbidity unit	PA6	polyamide-6
PAM	polyacrylamide	PBS	phosphate buffer solution
PbS	polybutylene succinate	PCL	poly-ε-caprolactone
PDMS	polydimethyl siloxane	PEA	polyesteramide
PGA	polyglycolic acid	PHB	polyhydroxybutyrate
pKa	dissociation constant	PLA	polylactic acid
PP	polypropylene	pph_{BM}	part per hundred of bloodmeal
PU	polyurethane	PZC (pH)	point of zero charge
RH	relative humidity	SBR	sequencing batch reactor
SDS	sodium dodecyl sulphate	SDS-PAGE	sodium dodecylsulphate polyacrylamine gel electrophoresis
SDT	simultaneous DSC-TGA	SEM	scanning electron microscope
SS	sodium sulphite	SSA (m^2/g)	specific surface area
SW2%	stickwater with C_o 2%	TDS (mg/L)	total dissolved solids
TEG	tri-ethylene glycol	TEM	transmission electron microscope
TGA	thermogravimetric analysis	TS	total solids
UASB	upflow anaerobic sludge blanket	USDA	United States Department of Agriculture
UV	ultraviolet spectroscopy	UV_{280}	UV absorbance at 280 *n*m
XRD	X-ray diffraction		

CHAPTER 1

INTRODUCTION

1.1 Background

Value-added products from waste recovery have gained attention over the past few decades due to increasing environmental concerns. Examples include production of biodiesel from palm oil waste [33], solid fuel from municipal solid waste, plastic from feed stock based soy protein [34] and materials derived from paper mill sludge [35]. One of the driving forces behind this research is awareness against waste generation. From an industrial perspective, higher product utilization reflects increase of profit. Waste-generated products can be widely accepted if they can match the performance of conventional products [11]. Therefore, it is a win-win situation for producers, end-users and the environment.

New Zealand contributed about 5 % (611 million kg) to the world's beef-meat production in 2007 and 38 % (400 million kg) for sheep-meat, which translated into NZ$ 18.9 billion gross domestic product (GDP) [36-39]. In NZ, only 30 % of a whole slaughtered animal is used for human consumption due to dietary and cultural concerns. Thus, alternatives for producing value-added products from this waste are worth pursuing to prevent under-usage. Some research in this field includes extracting collagen from bone pellets [40], producing charred bones for heavy metal adsorption [41] and producing biodegradable plastic from bloodmeal [42, 43]. Another form of meat rendering waste which is often overlooked is stickwater. Both bloodmeal and stickwater are often dried and sold as low commercial value fertilizer or animal feed [44].

Stickwater contains gelatin which could serve as a cheap protein source for modification of composite fillers. The reinforcement of protein-modified fillers in bloodmeal plastics yield bio-composites and could potentially be developed as plant

pots and seedling trays for plant nursery and agricultural disposable tools such as weasand clips, nails and barbs.

The term "biodegradable" refers to the ability of a material to degrade by the enzymatic action of living microorganisms into carbon dioxide, water and biomass under aerobic conditions or into hydrocarbons, methane and biomass under anaerobic conditions [45, 46]. Depending on the application, biodegradability could be an advantage or disadvantage for bio-materials. Bioplastics generally are mechanically weaker than petroleum-derived plastics but can be improved by reinforcement.

1.2 Problem Statement

A medium-sized meat rendering plant in New Zealand can produce up to 30 000 L of stickwater per day [28]. Drying seems to be the most suitable and rapid process to evaporate moisture from stickwater but uses significant amounts of energy. Other alternatives like composting, land-filling and incineration are not sufficiently rapid to cope with daily production. Stickwater contains up to 5 % protein which could be a valuable resource if recovered [39, 47].

Adsorption is a separation process based on selective transfer of ions or molecules onto solid particles and is widely used in waste water treatment processes [48]. Stickwater is more complicated than some waste streams such as from pharmaceutical [5-8, 49], textile dye [50-52] and heavy metal [53-55] industries because it contains protein, organics, dissolved salts and fats which complicate the treatment process. Among the difficulties in applying adsorption to stickwater systems is to find suitable adsorption conditions with optimal adsorbent dosage as well as methods on how to deal with the spent adsorbent after treatment processes.

Bentonite is commonly used in adsorption and added into composites to improve their mechanical properties. Current research regarding bentonite is limited to adsorption or composite development only. As a bio-composite filler, bentonite has to be modified with organics to make it compatible with the matrix materials [11]. Modification with amine, bovine serum albumin (BSA), gelatin, alkylammonium and starch could be expensive. Using a waste source to modify bentonite for use in

nanocomposites could save cost and offer a value added proposition to a stickwater which is considered a waste.

1.3 Research Objectives

In previous work, the research group revealed the potential use of bentonite to treat stickwater by reducing the BOD. The bentonite was found to have good adsorption capacity for organic. However, due to the varying composition of stickwater, the results were not highly replicatable. Stickwater composition depends on the raw materials and the rendering methods used [24, 47]. Another branch in the research group deals with the development of bloodmeal-based plastics. Bloodmeal was successfully developed into bioplastic known as Novatein Thermoplastic Protein (NTP) [44].

In this work, as a first step, a model solution was used for adsorption and settling study. The objective was to predict the adsorption of gelatin onto bentonite under various conditions. Then, settling process was explored as an alternative for centrifugation to recover the adsorbed bentonite after treatment. Modelling was used to study the equilibrium adsorption isotherms, rate kinetics and particle settling. These were later verified on stickwater adsorption. The spent bentonite after adsorption was recovered and used in NTP reinforcement.

Experimental conditions in this work were kept as close to industrial process techniques, however, adaptation is still required for large-scale production.

In summary, the specific aims of this research were:

- to determine the optimal conditions for gelatin adsorption onto three types of bentonite: sodium, calcium and octadecylamine.
- to study the protein adsorption on bentonite by isotherm models and kinetics.
- to determine the extent of clay gallery intercalation or exfoliation by organics.
- to investigate the effectiveness of settling process for bentonite particles recovery from solution and to develop a settling model.
- to incorporate the unmodified and organically-modified bentonite into NTP via a conventional plastic production method and to study the effectiveness.

CHAPTER 2

MEAT RENDERING PROCESSES

2.1 Meat Industry

New Zealand has a sizeable meat processing industry which processes more than 5 million cows a year into food products [38]. Normally, only 30 % of the animal is utilized for human food. Due to economic demand, preferably all materials produced from the slaughter operation should be used profitably. High utilization of slaughtered animals is important to maximize profit. The animal parts that are not normally intended for human food are known as by-products. Figure 1 outlines the by-products produced in a meat rendering plant. They are processed into various low-cost products. Often the commercial value of these by-products is marginally higher than the sum of the meat plant operating cost [27, 41].

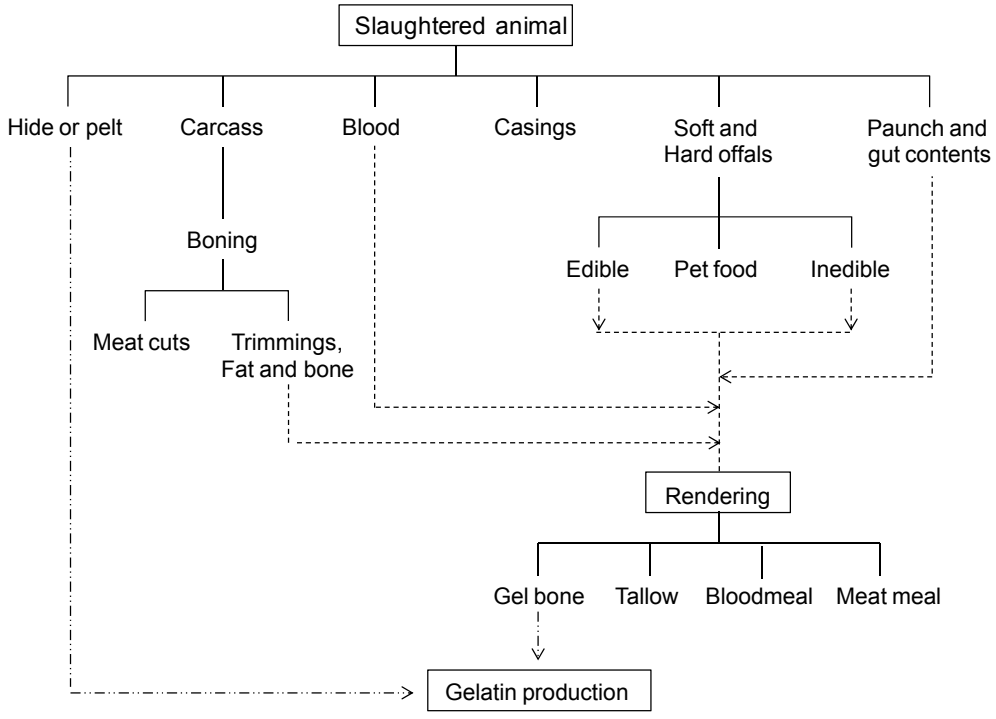

Figure 1: Flow diagram of products from a slaughtered animal [27, 40].

Offals or variety meats include the heart, liver, tongue, oxtail, kidney, brain, sweetbread (various glands), intestines, testicles and tripe. These represent up to 20 % of carcass weight [27]. There are sizeable demands for these by-products due to local diet preferences and a worldwide shortage of animal protein. The use of offals is limited depending on the country due to custom, religion, palatability and reputation of these products. As long as there is a demand for offals, the meat industry will supply them to maximize the use of these raw materials and also to keep the plant running cost manageable. Offals must always be processed hygienically for safe human consumption. Tripe, bone and skin can be used in collagen and gelatin manufacturing.

However, by-products are often not consumed by humans and therefore they are downgraded into pet foods because a profitable market does not exist [27]. The use of such biological wastes for livestock feeding is now becoming acceptable in modern society due to the concerns to reduce costs of animal farming and waste disposal, also to avoid competition with human consumption. This however, does not include animal waste blood due to consumer aesthetic concerns even though blood contains high concentration of protein [41]. When by-products are rendered, approximately one to two-thirds of the original weight of raw material is lost in liquid from the boiling process. This liquid waste is known as stickwater [27].

2.2 Rendering Processes

Rendering is the process of breaking scrap meat and other by-products into useful components through heat application [56]. It produces stable and hygienic products of commercial value from raw materials that are considered unsuitable for human consumption. The raw materials include offals (mostly), bone, tendons, sinew, meat scraps, cartilage and blood. Proteinaceous meat-based by-products are processed into nitrogen fertilizer and bone-based by-products are processed into phosphate fertilizer. Raw materials for rendering alone can represent up to 30-60 % of carcass weight. Depending on how the fat is removed, rendering process can be classified as wet or dry and can be operated in a batch, semi-continuous or continuous mode [27].

2.2.1 Wet Rendering

In wet rendering, raw materials are pre-ground and steam cooked at 380 to 500 kPa for 3 to 6 hours in a closed tank called a digestor, autoclave or cooker. At the end of the process, the pressure is released slowly allowing the solid and liquid to settle. The liquid-phase (liquor) is drained off and the solid is pressed or centrifuged to remove additional liquid (stickwater) prior to drying. The liquor and stickwater can be further processed to retrieve fines from the liquid and are recycled to the solid-phase [27, 57]. Floating fats are collected to remove residual water and fine particles using a disc centrifuge.

Wet rendering produces good quality fat compared to dry rendering and normally conducted in batch (Figure 2) or in a semi-continuous process (Figure 3). Batch processing is a very old method and less efficient than semi-continuous process. It requires long cook times, a large amount of energy, labour intensive and has significant loses with up to 25 % solids lost in stickwater [27].

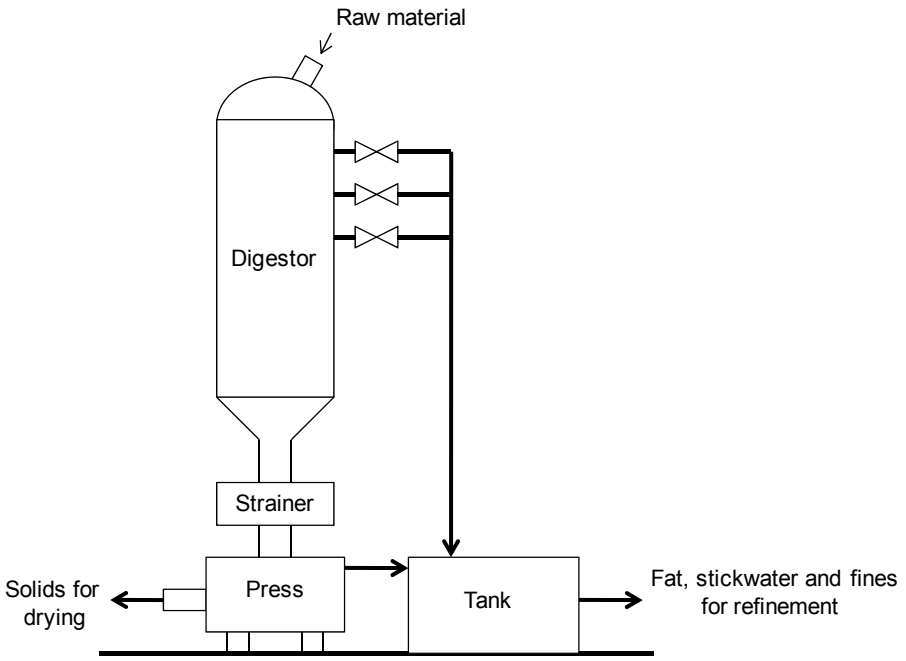

Figure 2: Batch wet rendering system [27].

The semi-continuous wet rendering process is a modern approach that uses a rendering cooker under pressure for a short time. Liquid waste including stickwater is dried in a continuous dryer and the concentrate is added to wet solids for further drying. The fat is separated from the liquor using a disc centrifuge. This system is more efficient than batch processing. It produces high quality of low-fat meal and uses less energy, however the capital and maintenance costs are high [27].

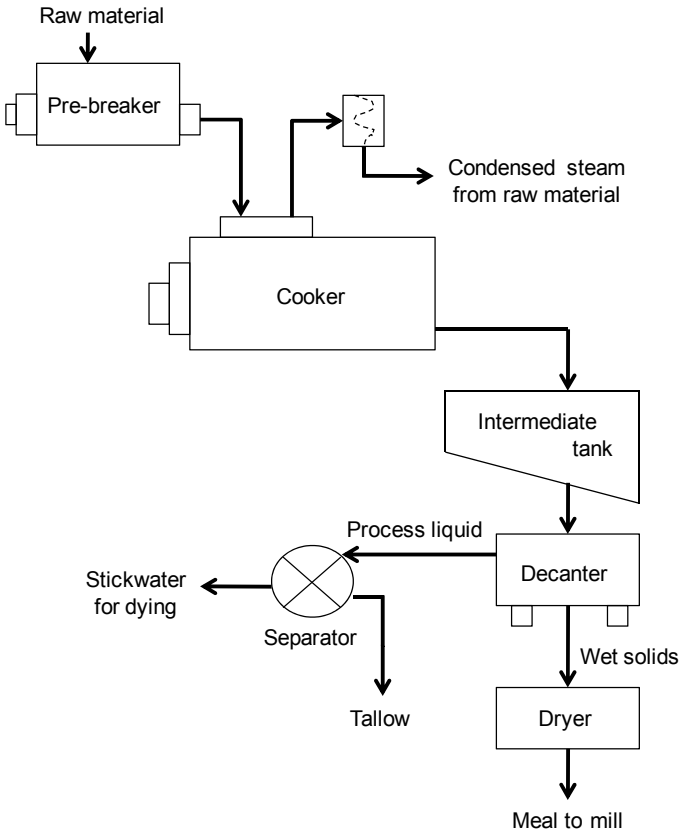

Figure 3: Semi-continuous wet rendering system [27].

2.2.2 Dry Rendering

Dry rendering does not refer to a dry process; in fact it has almost the same basis as in semi-continuous wet rendering system. The process can be operated in batch or continuous mode (Figure 4). Unlike wet rendering where the batch and continuous processes are completely different; in dry rendering processes, both operational modes utilize the same equipment. Pre-ground material is heated in a horizontal,

agitated and steam-jacketed vessel until most of the water has evaporated. The steam is usually condensed to recover useable heat and reduce atmospheric pollution. In batch mode, the material is cooked at 200 to 500 kPa until the hair and wool are hydrolyzed. The end temperature is often between 120 to 140 ^{o}C [27].

In continuous mode however, the cooking time depends on the feed-rate of the raw material. After hydrolyzing, the cooker content is transferred into a percolator to separate solid and fats. In continuous mode, the solid material is then pressed while in batch mode, it is centrifuged to remove additional fat. The meal is sent to a mill while fat is refined in disc centrifuges. There is no stickwater stream in Figure 4 because in dry rendering, stickwater is dried and sent to a mill after production [27].

In both wet and dry rendering processes, batch systems have less material loss and provide more flexibility in production because different cookers are assigned for different raw materials. However, batch processes use a lot of energy, are labour intensive and produce poorer fat quality that is associated with fines as a result of high temperatures use. Continuous dry rendering is better than batch dry rendering because it uses less labor and requires less space. The main disadvantage is sterilization cannot be done in continuous mode because the system cannot be pressurized continuously during operation [27].

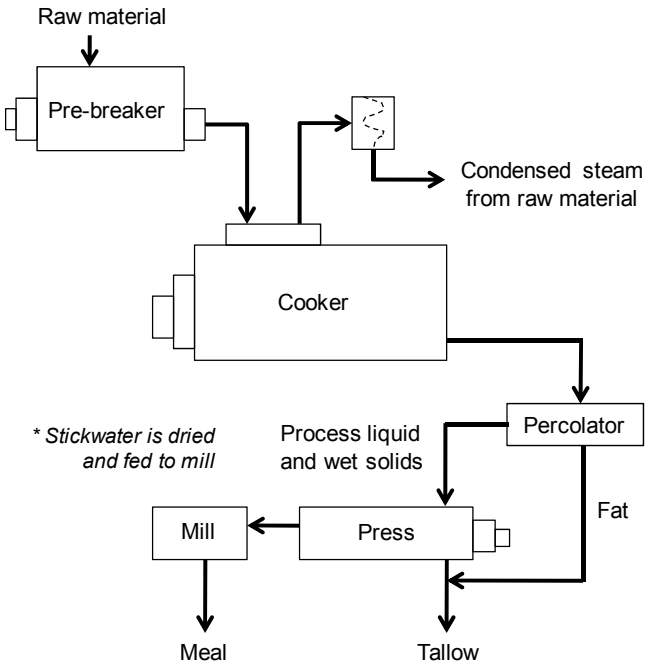

Figure 4: Dry rendering system (batch and continuous mode) [27].

2.3 Stickwater

Stickwater is a by-product from meat rendering plants and it contributes toward abattoir waste water as a whole. It has a brown to pale-grey appearance with a tangy rotten beef smell. It is an emulsion of water with dissolved fat, protein, minerals and organic matter. The volume of stickwater produced can be as high as 40 % of the total raw materials entering the rendering process due to fat, dissolved organics, mineral lost into waste water [27].

From Figure 2 and 3, stickwater is the liquid stream produced in the cooking step from meat rendering processes. During processing, the liquid is not termed stickwater because the product stream consists of a mixture of solid and liquid. After the liquid is physically separated from solids, it is termed stickwater and wet solids. Common equipment used to separate solids from stickwater includes strainers, decanters, centrifuges and screw-presses. Ideally, product loss in stickwater should be minimized to have a higher solid yield. Stickwater can be concentrated by ultrafiltration or evaporation by using recycled heat to remove more water before further drying in contact driers. Energy use is the main problem due to the considerable daily volume of stickwater generation [27].

The properties of stickwater are summarized in Table 1. The contents may vary according to animal species, rendering process and the desired end-product. Protein percentage in stickwater represents the loss of protein during the rendering process. It is important for the protein loss to be minimized without increasing the operating cost. The main protein in stickwater is denatured collagen (gelatin) [30, 58]. Stickwater is mainly dried with bloodmeal into particulates and sold as low-cost fertilizer. Some rendering plants dried and sold them separately for different applications such as for use in animal feedstocks. In edible rendering plant, stickwater fines are used as flavour enhancers in food industries [27, 57].

Table 1: Stickwater content [25, 27, 39, 40, 56].

Fats (%)	* Solid contents (%)	Protein (%)	$cBOD_5$ (g/l)	Organic-N_2 (g/m^3)
1-2	2-5	4-5	150	70-250

** Combination of organics loss (105 to 800 ^oC) and ash.*

2.4 Collagen

Collagen is a robust helical protein found in animal tissue including tendons, cartilage, skin and blood vessels. It makes up approximately 30 % of the total animal protein. In vertebrates, it provides strength and flexibility [59, 60]. A collagen molecule consists of three peptide chains, each approximately ~1011 amino acids long. About 75 % of the amino acids are hydrophobic while 160 (16 %) amino acids contain charged side groups that are distributed along its length [61]. The molecule has a rodlike shape with tropocollagen as the basic structure. It is made of three similar intertwined polypeptide α-chains as right-handed helix to form a three-strand rope or triple α-helix as illustrated in Figure 5. Each α-chain is about 1000 amino acid residues long with glycine occuring at every third residue for the whole length of the molecule. The molecular weight of collagen is about 100 and 200 kDa for α and β chains respectively [62]. The general sequence of the repeating triplet is glycine, X and Y with proline and hydroxyproline often make up X and Y. A sequence of repeating triplet represents one turn of the helix with dimension of 1.5 x 300 nm [40, 63].

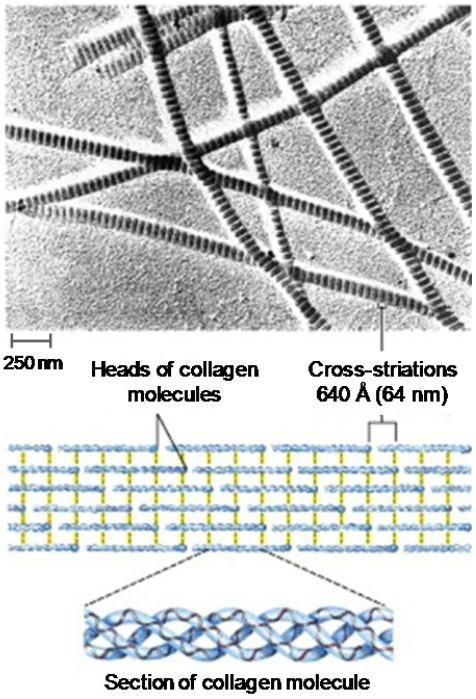

Figure 5: Structure of collagen [47].

There are several different collagens and each type has a different role. Type I collagen is the major collagen present in skin, tendons and bone. Type II collagen is specific to hyaline cartilage and has three identical chains. Minor collagen or type III is present in large blood vessels. Type IV is the collagen of basement membranes [40, 63].

Collagen is mainly used in food industry as gelling agent, protein additive and fat substitute that can give the same fat texture with different nutritional content. In dietary supplements, collagen is used to improve skin and fingernail appearance, maintain general health of joints and manage body weight. It is also used as an additive to cosmetic products like mascara and beauty lotions. Other applications include photographic film, medical skin grafting and biodegradable materials [40, 64].

2.4.1 Gelatin

Gelatin is an animal protein derived from hydrolysis of insoluble fibrous collagen found in skins and bones in meat rendering processes [34, 65]. It is a thermoreversible gel made up of broken collagen subunits and commercially produced from bovine, swine and fish sources. Fish-derived gelatin is relatively new to cater to specific dietary needs and less common. Research is increasing on fish gelatin due to consumer concern on bovine and porcine diseases such as bovine spongiform encephalopathy (BSE), foot and mouth disease, Japanese encephalitis and swine fever. Furthermore, cultural and religious concerns such as Halal (Islamic lawful slaughtering method), Kosher (Jewish-equivalent of Halal) and cows being sacred to Hindu make the use of commercial gelatin limited [40]. Agar or agar-agar is a vegetarian gelatin-substitute derived from red algae or seaweed. It is widely used in culinary, microbiology and motility assays [66].

By-products used for gelatin production include skins, bones, hides and cartilaginous meats of animal. The raw materials are pre-treated under an alkaline or acid process to remove impurities. Acid pre-treatment is faster than alkaline pre-treatment and takes around 10 to 48 hours. Pig skin collagen is simpler in structure because it has less crosslinks, therefore is suitable for a fast acidic process. Bovine skin collagen is more complex and it requires a longer alkaline process for up to a few weeks to break the crosslinks. The latest development in gelatin extraction is using enzymatic treatment which is faster and can give higher purity yield [67]. The pre-treatment process used determines the point of zero charge (PZC) of the gelatin. Gelatin produced from acid pre-treatment is known as type-A with PZC between pH 7-9 and alkaline-treated gelatin is called type-B with a narrower PZC range between pH 4.7-5.4 [34, 67]. For comparison, PZC of bovine serum albumin (BSA), chicken egg ovalbumin and porcine epimerace is at pH 4.8-5.2 [68, 69], 4.6 [70] and 5.75 [71] respectively.

Once pre-treated, gelatin is extracted by boiling in either water or acidic solution at a suitable temperature above the collagen melting point, T_m (39 ^{o}C, 29 ^{o}C and 16 ^{o}C for calf, shark and cod skin) to break the molecular bonds. Alkali pre-treatment can speed up the process, but it is not used in extraction step because it also promotes

degradation. The last step is recovery process and methods include evaporation, filtration, grinding and sifting. Both extraction and recovery processes are multi-stage processes to produce the desired final gelatin concentration [72].

Gelatin exists in gel or aqueous form when in solution at a temperature of about 40 ^{o}C and forms thermoreversible gels on cooling [30, 73]. Building blocks for gelatin are collagen molecules with α-chains (one polymer chain), β-chains (two α-chains covalently crosslinked) and γ-chains (three α-chains covalently crosslinked) [74]. During gelling, the chains undergo a conformational transition and tend to recover the collagen triple-helix structure. Thermal denaturation or physical and chemical degradation of collagen involves the breaking of the triple-helix structure to give gelatin a biodegradable, biocompatible and nonimmunogenic product. Once treated, the collagen is hydrolyzed to break hydrogen bond bridges that hold the triple α-chain structure. Denatured collagen has lost its triple helix structure and therefore lost its chemical resistance. This process changes collagen from insoluble form to soluble form [30, 72, 75]. A schematic diagram of the structure of gelatin is shown in Figure 6 and SEM images are shown in Figure 7.

Because gelatin is made of collagen subunits, it has similar amino acid composition to collagen. It contains mostly of glycine (Gly, 34 %), proline and hydroxyproline (Pro and Hyp, 16 %) and alanine residues (Ala, 10 %) as outlined in Table 2 [76]. The full sequence of collagen's amino acids and the number of residues are summarized in Table 41 (Appendix-1A) and Table 42 (Appendix-1B) respectively.

Table 2: Amino acid composition of gelatin (number of residues in 100 units).

Amino acid	Bovine [34]	Calf skin [67]	Pork skin [67]	Fish [34]	Bone [67]
Alanine	11.17	9.30	8.6	12.59	10.1
Arginine	4.64	8.55	8.3	5.12	5.0
Aspartic acid	4.55	6.60	6.2	4.29	4.6
Cystine	0.00	Trace	0.1	0.00	Trace
Glutamic acid	7.31	11.10	11.3	6.88	8.5
Glycine	33.79	26.90	26.4	34.91	24.5
Histidine	0.40	0.74	0.9	0.47	0.4
Hydroxylysine	0.49	0.91	1.0	0.82	11.9
Hydroxyproline	8.20	14.00	13.5	7.69	11.9
Isoleucine	1.09	1.70	1.4	0.77	1.3
Leucine	2.37	3.10	3.1	2.05	2.8
Lysine	2.47	4.50	4.1	2.28	2.1
Methionine	0.40	0.80	0.8	1.02	0.0
Phenylalanine	1.19	2.20	2.1	1.22	1.3
Proline	12.55	14.80	16.2	11.82	13.5
Serine	3.85	3.20	2.9	3.71	3.4
Threonine	3.26	2.20	2.2	2.41	2.0
Tryptophan	0.00	-	-	0.00	-
Tyrosine	0.40	0.20	0.4	0.28	0.0
Valine	1.88	2.60	2.5	1.67	2.4

Worldwide gelatin production is around 300 000 tonnes per year [40]. Gelatin has received much attention in research because it is biodegradable, environmentally friendly and possesses attractive commercial properties [65]. Gelatin is mainly used as gelling agent in food industry due to its stabilizing ability over a wide range of pH and its unique "melt at mouth temperature" characteristic [73, 75, 77]. In frozen food and dairy products, it is used as stabilizer or protective colloid against crystal formation [75]. It is also used as wound dressing in medicines because it is self-assembling, nonimmunogenic, nontoxic, biodegradable and inexpensive [78, 79].

In packaging industry, gelatin is used due to its film-forming ability, elasticity and effective oxygen barrier [22, 73, 80, 81]. Gelatin is unsuitable for forming plastics and films of any significant strength or durability without plasticization, crosslinking or reinforcement [30, 34, 81-84] and is a poor barrier against water due to its hydrophilic nature [22, 65, 81, 82]. But due to the number of side groups gelatin has, it easily undergoes chemical crosslinking [30]. Gelatin film can be stabilized by adding additives such as montmorillonite at dosage level as low as 3-10 wt% [80], chitosan [75]

and soy protein isolate [34]. Other applications of gelatin are in pharmaceuticals, photography, textiles, bio-films and cosmetics [30, 73, 85].

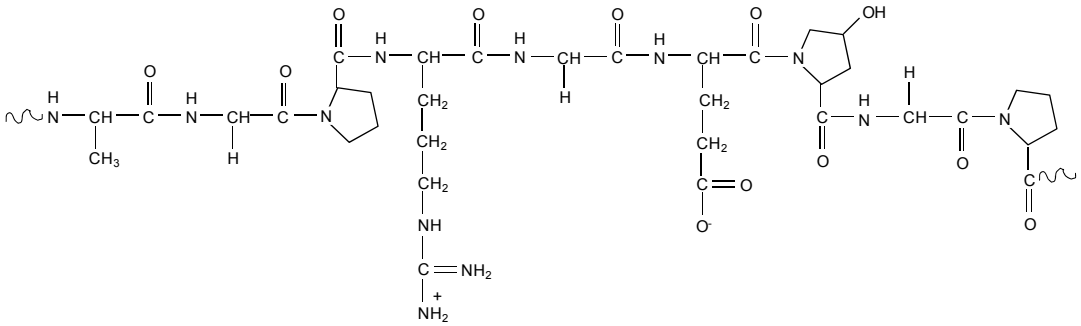

Figure 6: Schematic structure of gelatin [86].

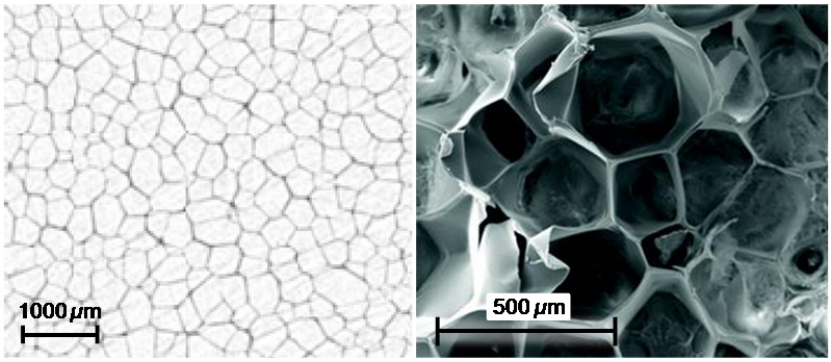

Figure 7: Images of gelatin structure viewed under cryogenic SEM [79].

2.5 Abattoir Wastewater and Stickwater Treatment Process

An abattoir is defined as a livestock processing facility that includes slaughtering animals and by-products processing such as tanneries, rendering of proteinaceous matter and fats; in order to produce hides, adhesives, gelatin, fertilizer, meat products and fleeces. Abattoirs utilize large amounts of water for animal processing, therefore generating significant amounts of waste water [26]. Generally, waste water from meat processing is extremely difficult to treat because of its specific characteristics, irregular discharge and content. The main pollutants such as organic matter, dissolved compounds and minerals result in pollution indices such as biological oxygen demand (BOD), chemical oxygen demand (COD), total dissolved solids (TDS), suspended solids, organic nitrogen, and fats, oils and greases (FOG) which are

significantly higher than the average domestic sewage. Direct disposal will bring adverse environmental effects, thus prior treatment processes are required [41].

There are some recommendations made by the Environment Protection Authority (EPA) to minimize abattoir waste such as 1) changing to better process equipment, 2) improving control process, 3) reducing the raw material inputs, 4) changing the composition of products to suit different needs, 5) improving maintenance and repair of equipment and 7) recycling waste internally or re-using waste on site [26]. Apart from waste minimization, finding alternative treatment processes for abattoir waste is necessary to cope with its high daily loading.

Three stages of abattoir waste water treatments are 1) primary - separation of floating and settling particles, 2) secondary - removal of organic matter and 3) tertiary - removal of nitrogen, phosphorus and suspended solids. Pre-treatments are normally conducted before the primary treatments. These include screenings, catch basins, floatation, equalization and settlers. Secondary stage could be anaerobic or aerobic treatments associated with various equipment, as outlined in Table 3 and Table 4. Compared to drying, the treatments outlined in Table 3 and Table 4 might have higher capital costs and require longer processing time. These methods normally utilize holding tanks or ponds to retain the waste water before disposal. Catering for sheer volume of stickwater production everyday means a plant has to employ many ponds which would be limited by site availability and cost. In the case of BOD and COD removal, most processes outlined in Table 3 and 4 can result in a very high percentage removal, well enough to meet the discharge consent of regulatory bodies (25 g O_2/m^3 for Hamilton [87]).

Table 3: Type of reactors used in anaerobic treatments with COD removal efficiency (cited by [41]).

Type of reactor	COD removal (%)
Anaerobic fluidized bed reactors (AFBR)	73
Upflow anaerobic sludge blanket (UASB)	77-91
Membrane bioreactor (MBR)	97
Anaerobic fixed film reactor (AFFR)	85-95
Fluidized bed	85
Anaerobic filter	30-85
	63-85
	37-77
Two-stage UASB	90
Anaerobic baffled reactor	75

Table 4: Aerobic digestion methods with COD and BOD reduction efficiency (cited by [41]).

Treatment method	Organic loading rate	HRT* (days)	BOD reduction (%)	COD reduction (%)
Fluidized bed biofilm reactor	305-602 mg BOD / L	8.8-30.8	71-93	-
Activated sludge	0.4-8 kg BOD / m^3.day	-	95	-
Sequencing batch reactor (SBR)	80-528 g BOD / m^3.day	1.5-5	$\geq$ 95	$\geq$ 95
	0.05-0.75 g COD / (gdwt)$^+$.day		99.6	98.1
SBR and reverse osmosis	0.15 g COD / (g TS^).day	12-36	99.5-99.6	96.9-97.3

**Hydraulic retention time, $^+$gram dry weight and ^total solid*

Stickwater has a very high BOD, is coloured and odorous which makes the treatment process expensive. Edible stickwater can be dried to retrieve flavour compounds for food addictives. Inedible stickwater is dried and processed into animal feed or fertilizer. Drying is expensive and the end-product is less valuable, therefore many small plants send their stickwater and bloodmeal to much larger plants for further processing [25, 27, 57].

Drying involves the removal of water and volatile compounds from solution to give solid products. In most cases, products are ready for packaging after drying. Feed to the dryer could be a liquid or solid from which the moisture is to be evaporated. Drying is widely used in industry and applications include the removal of moisture from 1) crystalline particles of inorganic salts and organic compounds to be free-flowing, 2) biological materials such as foods, 3) pharmaceuticals, 4) detergents, 5) paper and fibres, 6) dyes, 7) solid catalysts, 8) milk and 9) films and coatings [48].

Because drying involves vaporization of moisture, heat must be transferred to the feed. Commonly used modes of heat transfer are 1) convection from a hot gas in contact with the material, 2) conduction from a hot, solid surface in contact with the material, 3) radiation from a hot gas or hot surface in sight of the hot material and 4) heat generation within the material by dielectric or microwave heating. The selection of the suitable mode depends on whether the moisture to be removed is on the surface or / and inside the feed [48].

To date, drying is the most widely used method in meat rendering plants when it comes to stickwater and blood, especially when large amounts of moisture must be evaporated [24, 27]. Therefore, removing as much moisture as possible before drying is an added advantage. This could be done by mechanical means such as gravity, vacuum or pressure filtration and centrifugation. Examples of common drying equipment include direct-heat rotary dryers, tray and belt dryers, agitated dryers and tunnel dryers. There is no one device that performs absolutely better than the other. The equipment selection depends on the desired products [48].

Common operational modes for dryers are batch and continuous. Seader and Henley (2006) suggested that batch operation is generally applied when production rate is less than 230 kg per hour of dried solid, while continuous operation is preferred for production rate of more than 900 kg per hour. Depending on the size of a rendering plant and the scale of operation, a plant can produce up to 30 000 L of stickwater at up to 25 % solid (dissolved and suspended) [28]. Assuming 1 L stickwater equals to 1 kg, 7500 kg solids have to be dried per day or 22 500 kg moisture per day (937.5 kg / hour) to be evaporated. This is another reason of why the continuous batch mode rendering technique is preferred over batch mode.

Another treatment option is to send stickwater to waste water treatment facilities. In Hamilton, the cost to treat waste water is NZ$ 0.90 per kg BOD solids [29]. For 30 000 L of stickwater at 5 % dissolved solids, the company has to spend approximately NZ$ 1350 per day for the treatment process. In the US, butchers have to pay US$ 20 per barrel (119 L) for abattoir residual disposal which amounted to approximately US$ 10 million for 58 000 tonnes of waste from total national industry per day [56]. This is equivalent to NZ$ 0.23 per kg. Alternative treatment practices

used are composting, land filling, incineration and surface disposal. Problems associated with these methods are that they are time-consuming, space-filling, require stricter permits than municipal waste, bad odour, soil and water contamination by nutrients [41, 56].

Inorganic and organic flocculants had been used to treat agricultural waste especially from slaughterhouses to reduce $cBOD_5$, nitrogen, phosphorus and fine particles. The effectiveness of the flocculation depends on the composition of the waste water, temperature, rate of mixing and the order in which flocculants are introduced into the waste water [41, 88]. The main contaminants in abattoir waste are organic and protein. Removing these contaminants can potentially help in the treatment process.

Clays are widely used for waste water treatment via adsorption. Common clay types such as bentonite has a high specific surface area can be a suitable adsorbent for stickwater treatment. By extracting protein from stickwater, the treatment charges can be minimized due to a decrease in suspended solids and BOD. At 5 wt% protein concentration, stickwater can be a cheap source of valuable protein for clay modification [1, 89].

Protein adsorption onto bentonite can be studied by isotherm models. There are various isotherm models from literature. In the next chapter, four widely used isotherm models namely Langmuir, Freundlich, Langmuir-Freundlich and Temkin are discussed in terms of the assumptions made for adsorption and their advantages and disadvantages in research applications.

CHAPTER 3

ADSORPTION AND SEPARATION

3.1 Adsorption Process

Adsorption and ion-exchange are sorption processes in which certain components from fluid-phase are selectively transferred to insoluble, rigid particles suspended in a vessel or packed in a column [48]. The term sorption is believed to have been first introduced by Kayser in 1881 to describe condensation of gases on free surfaces which later used by J.W. McBain (prominent scientist in colloids and micelles) to describe selective molecules transfer to a surface and / or into the bulk of a solid or liquid. Adsorption refers to surface phenomena where accumulation of molecules or components take place on a surface of solid material for example water vapour is adsorbed by silica gel. Whilst absorption is a bulk phenomenon referring to penetration of molecules or components into a particle, for example water vapour is absorbed by calcium chloride [48, 90]. Though different, the words adsorption and absorption have often been used interchangeably due to similarities.

For porous solids, adsorption can occur within the pores provided that the size of solute molecules is comparable to the pore size. The concentration of the molecules is higher at the fluid-solid boundary than the bulk of fluid as outlined in Figure 8. In an adsorption process, adsorbed molecules (solute) are attracted to the active sites on the adsorbent surface (solid-phase) by weak intermolecular forces. Most adsorbents have heterogeneous surface which contain a wide range of energy sites, polarities and impurities arising from exposure to the environment. These factors characterize the adsorption which could be chemical or physical interaction [48, 89, 90].

Adsorption may occur physically (van der Waals adsorption) or chemically (activated adsorption or chemisorption) depending on the bond between solid-phase and solute molecule. Physical adsorption involves weak molecular interactions while chemisorption involves the formation of chemical bonds between solid-phase and

solute molecules on the surface. In both cases, the active separating agent (solid-phase) eventually becomes saturated with solute and must be regenerated or replaced periodically. Adsorbed molecules can detach from solid-phase or desorption through vigorous mixing, pH, temperature changes and from competition by other solutes. Desorption may be quite difficult for multimolecular solutes because solutes adsorb onto multiple points of the solid-phase [48, 90, 91].

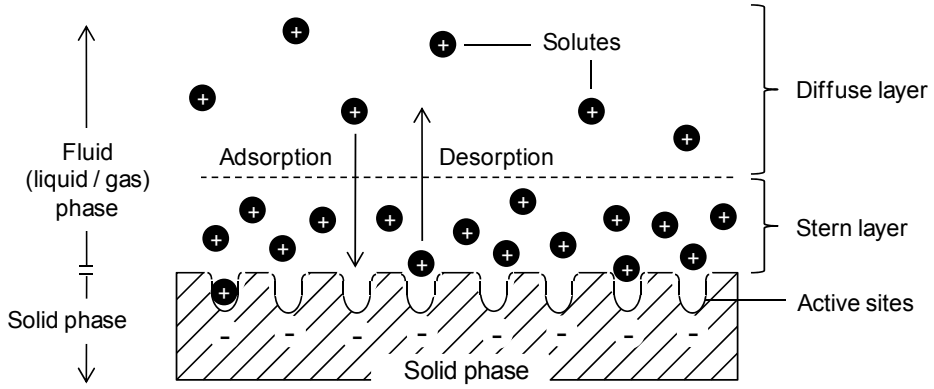

Figure 8: Adsorption and desorption process on solid surface [2, 89].

Generally, most solids are able to adsorb molecules from gases and liquids. For commercial application, a solid-phase having a large specific surface area per unit volume is desirable. This can be achieved by special manufacturing techniques that give solids a microporous structure. According to the International Union of Pure and Applied Chemistry (IUPAC), the pore diameter of a micropore is < 20 Å, a mesopore is between 20-500 Å and a macropore is > 500 Å (50 nm) [92]. The pore size correlates with adsorption capacity and kinetics. Commercial adsorbents include activated carbon, aluminium oxide, silica gel and synthetic sodium or calcium aluminosilicate zeolite (molecular sieves). The sieves differ from the other adsorbents in that they are crystalline and have pore openings of fixed dimensions, making them very selective. Commercial adsorbents rely on physical adsorption because the equilibrium is reached rapidly. Catalysis adsorbents rely on chemical adsorption due to specifically adsorbing solutes onto solid-phase with binding force much stronger than physical adsorption [48].

3.2 Ion-exchange

In an ion exchange process (Figure 9), ions in aqueous-phase replace dissimilar and displaceable ions of the same charge contained in a solid ion exchanger which encloses immobile, insoluble and permanently bound co-ions of the opposite charge. Generally the charged groups on the ion exchanger are associated with ions such as Na^+, Ca^{2+} and H^+ for cation exchange and Cl^- and OH^- for anion exchange. These ions will exchange for similarly charged groups of solutes in bulk fluid. The solute and counterions will exist in equilibrium between being "bound" to the ion exchanger and floating freely in the solvent. This process is reversible and does not cause any permanent change to the solid exchanger. Usually, only one type of exchange is used in adsorption at a time (either cation or anion), but in some instances, both types are used. An example of such processes is water softening where a cation resin exchanges H^+ for Ca^{2+} and Mg^{2+} prior to an anion resin for exchanging OH^- with SO_4^{2-}, $NO^{3-}$and Cl^- [48].

The column can be cleaned to be reused again for many times unless contaminated by organics. Column regeneration is usually accomplished by back-washing using a mild solution of sulfuric acid and sodium hydroxide for cation and anion resins respectively. Ion exchange resins are generally solid gels in spherical or granular form, which consists of 1) a three dimensional polymeric network, 2) ionic functional groups attached to the network, 3) counterions and 4) solvent [48].

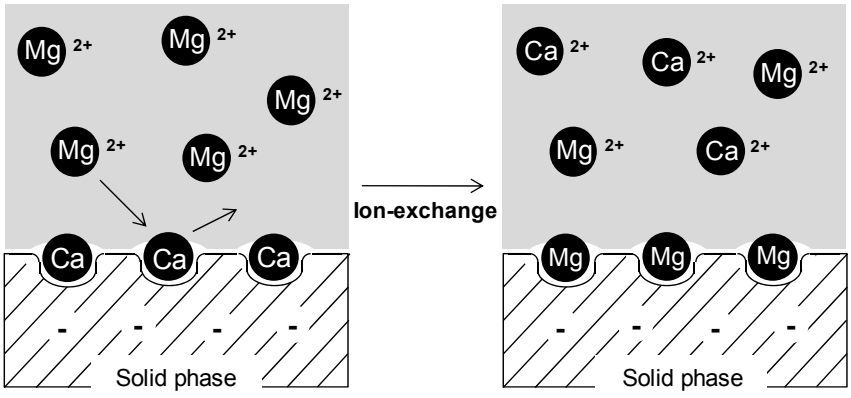

Figure 9: Ion-exchange mechanism.

Good sorbent criteria for adsorption and ion-exchange process are 1) high selectivity on the targeted solute, 2) high sorption capacity, 3) favourable kinetic and transport properties for rapid sorption, 4) chemical and thermal stability, including extremely low solubility in the fluid 5) good mechanical strength to prevent crushing and erosion, 6) a free-flowing to ease recovery, 7) high resistance to fouling, 8) inert to undesirable chemical reactions, 9) ease of regeneration and 10) relatively low cost; however very rarely is a single adsorbent optimal in all respects [48, 90, 93].

3.3 History of Adsorption

Ancient adsorption applications include Moses sweetening the bitter waters of Marah with a tree (Exodus, 15:23-26) (cited in [48]). Adsorption was mentioned in a Sanskrit manuscript about using charcoal to remove odour and taste from water (cited in [90]) and Aristotle observed that the dissolved salt in water is reduced when it penetrates through sand [48]. Milestones behind the modern application of adsorption include decolorizing solutions with charcoal (Lowitz, 1786), using activated carbon to adsorb toxins from water (Von Ostrejko, 1900) and the invention of synthetic zeolite, made famous for its high surface to volume ratio and widely used in various modern applications (Milton, 1959) [90].

In the processing industry, the importance of separation cannot be overstated with every process involving products and / or waste streams. Therefore, finding the best separation process either by improving existing processes or developing new technologies, is a continuous process. The scale of the development throughout the past century is massive owing to the complexities of the raw materials. Adsorption-based separation processes gained attention after their success in waste water treatment. Adsorption is now widely used in industry to purify and separate both gas and liquid components from fluid mixtures. The main reason behind its success is that adsorption is more economical than the traditional processes such as distillation [90].

3.4 Liquid and Gas Adsorption

3.4.1 Introduction

In gas adsorption, experiments can be conducted with pure gas or mixed gases in a confined space where a decrease in total pressure is the measure of adsorbed gas. Adsorption from a liquid is more complex to quantify experimentally because there are many more components involved in a solution than gas. When a liquid mixture is brought into contact with a microporous solid, adsorption of molecules in the mixture takes place on the surface and within the internal lattice of the solid-phase. Liquid adsorption starts with monolayer, followed by multilayer adsorption until capillary condensation occurs where pores are filled with solute. Thus, the adsorption capacity of a solid-phase is more related to the pore volume than the surface area [48, 90].

A common experimental approach to quantify solute adsorption from a liquid is to perform adsorption on a single solute component in a solvent. The adsorption with the solid-phase assumes the change of bulk concentration is entirely due to adsorption of the solute and adsorption of the solvent components is assumed not to occur. The maximum extent of adsorption at equilibrium depends on a set of experimental conditions and interaction between solute and solid-phases with different solutes exhibiting different adsorptive affinity toward the same solid-phase. In general, the higher the solute concentration, the higher is the adsorption of solute on the solid-phase [48, 90]. A summary of the forces involved in adsorption processes using a solid-phase in listed in Table 5.

Table 5: Forces of adsorption processes [2, 89].

Force	Description
Physical	van der Waals force as a result of short range dipole-dipole interactions at close proximity.
Hydrogen bond	Bond of which hydrogen atom acts as linkage such as between water molecules and hydroxyl group on clay lattice.
Hydrophobic bond	Bond resulted from nonpolar compounds competing for adsorption site such as polysaccharides exchanges water on clay surface.
Electrostatic bond	Attraction force due to electrical charge such as cation exchange reactions with negatively charged clay surface.
Ligand exchange	Solute with a stronger chelation capacity replaces a ligand.
Coordination reaction	The reaction between coordinate covalent bonding for example when a ligand donates electron pairs to a metal ion.

Interpretation of solid-gas adsorption isotherms was firstly made by Brunauer et al. in 1940. These authors classified isotherms into five categories. An additional isotherm (Type VI) was proposed much later which completed the IUPAC classification. Figure 10 depicts the adsorption isotherms where the shape of the curves indicates how the solid-phase becomes saturated with solutes. Type I and II isotherms are the desirable isotherms which correspond to unimolecular and multimolecular adsorption on microporous adsorbents. Type I is also known as Langmuir type while Type II is known as BET type [94]. Type III isotherm corresponds to multimolecular adsorption and is undesirable because the extent of adsorption is low except at high pressure. Type IV and V isotherms are the capillary-condensation or hysteresis versions of Type II and Type III isotherms respectively, indicated by the saturation reached before the maximum pressure point. Finally, Type VI isotherm represents an adsorption that occurs in stages. This classification has a deficiency for being incomplete because adsorption is assumed to be a function of pressure, resulting in the adsorbed solute increasing indefinitely with pressure [48, 95].

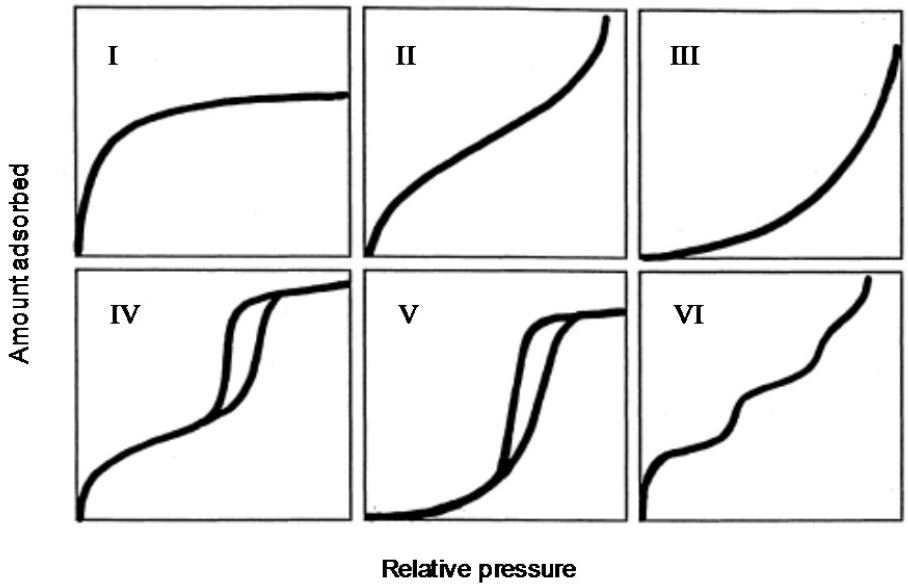

Figure 10: The IUPAC classification of adsorption isotherms [48, 94, 96].

3.4.2 Method of Adsorption Processes

In general, adsorption only requires a vessel containing adsorbent where the fluid is brought into contact (Figure 11). However, commercial approaches include contacting devices such as fixed beds, moving beds and fluidized beds operated in batch, semicontinuous or continuous mode. Normally, for liquid adsorption in batch mode, powder adsorbent is added into bulk liquid in an agitated vessel for a period of time until it forms a slurry. The adsorbent is removed from solution by sedimentation, filtration or centrifugation. Usually, adsorbent for the batch mode has a particle size of less than 1 mm [48].

The residence time required is determined by how fast equilibrium is reached. This could be done under a controlled lab experiment. Batch mode application is mainly for removal of a very small amount of dissolved solute with large molecules relative to water. Typically, the adsorbed particles are discarded because of the difficulty of desorbing large molecules from the surface [48]. An example of batch adsorption is dye pigments removal from water [50].

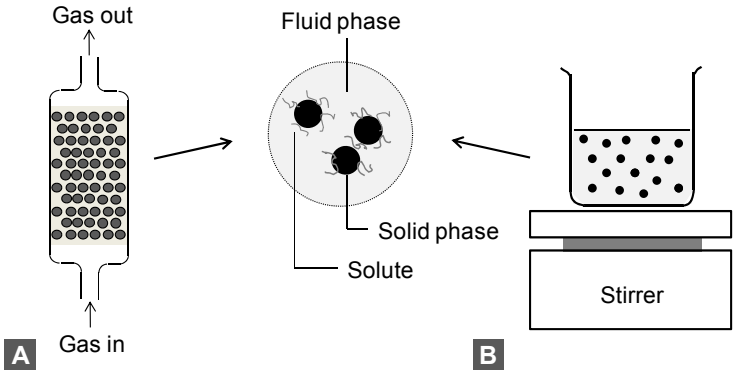

Figure 11: Common approach on A) gas and B) liquid adsorption.

The semicontinuous or cyclic-batch operating mode utilizes a fixed bed (also called percolation) and is widely used with both gas and liquid feeds. Fluid is continuously fed to and removed from the agitated vessel to be adsorbed on the fixed solid bed until the solid-phase is nearly spent. Adsorbent particle size ranges from 0.05 to 1.2 cm [48]. The optimal particle size is determined by measuring pressure drop across

the bed and solute transport rate; both decrease with increasing particle size. Downward flow is preferred in the bed to avoid fluidizing the bed during adsorption. The spent solid-phase can be regenerated at high temperature or discarded after adsorption depending on the extent of adsorption. Adsorption of organics from water is a suitable process for both batch or continuous processing [48].

Continuous adsorption is when the solute and solid-phase are continuously added to and removed from the agitated vessel. The slurry is assumed to be perfectly mixed by agitation. This is achievable by having a liquid depth to vessel diameter ratio of 1:2, proper agitation and sufficient axial flow to achieve complete suspension. Small particles can disperse better into liquid bulk than large particles. During agitation, small particles would move with the liquid because the relative velocity between small particles and liquid is low. Therefore, the rate of adsorption for small particles can be assumed to be regulated by external factors [48].

In liquid adsorption, pH is the most significant factor influencing the extent of adsorption processes [6, 68, 89, 90]. pH controls the ionization state of the solute in aqueous solutions and influence the electrostatic field (within the double layer) between the solution and the charged solute [90]. Solutes exhibit an overall negative charge when pH of solvent is above its point of zero charge (PZC) and an overall positive charge when solvent pH is below its PZC. At solution pH equal to PZC, the solute becomes neutral. Therefore, any adsorption process should be conducted in a polyelectrolyte solution to regulate the pH. For a strong electrolyte, ionization is nearly complete and therefore adsorption can be analyzed using an adsorption isotherm approach [90]. Weak electrolytes give incomplete ionization comprised of partially ionized and neutral species resulting in multi-component adsorption [90]. In the latter case, adsorption isotherm models have to consider the effect of competing ions and could be complicated.

In term of particle size, small porous adsorbents are preferred due to high pore volume and surface area. With good agitation and small particle size, the external resistance to mass transfer between bulk fluid and adsorbent surface is also small. Therefore, the rate of adsorption is rapid [48]. The particle size distributions of common industrial adsorbents are given in Figure 12. Activated carbon has a wider

range of pore sizes, indicating that it is more universal for much wider application. Zeolite is very selective by having a specific pore opening. Silica gel gives a good compromise between activated carbon and zeolite.

Other factors that affect adsorption are cation exchange capacity (CEC), nature of the solute to solid-phase interaction (Table 5), size and initial concentration of the solute molecules, salt competition in solution, mixing rate and system temperature [68, 89, 90]. However, the effect of temperature could be minimal as observed in BSA adsorption onto various clays at 5 to 25 ^{o}C [97].

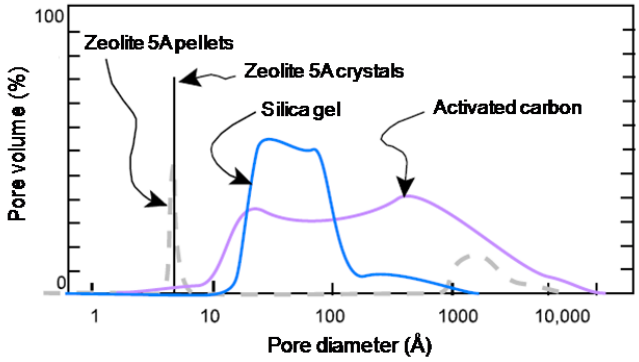

Figure 12: Pore size distribution of common adsorbents [93].

3.5 Adsorption Isotherm Models

An equilibrium isotherm is made by plotting the adsorption equilibrium data over a range of solute concentrations in a bulk solvent at time intervals. It reveals a limit on the extent to which a solute can adsorb on solid surface from a fluid mixture at a given set of conditions [48, 90]. Experimentally, isotherm models are derived from model solutions to simulate the real system. For example, BSA is used to model traces of protein in wine [70] and methylene blue is used to model dye pigment [51, 52]. The findings are then validated into the real system to investigate the model effectiveness.

Four commonly used isotherm models at different states are listed in Table 6 and summary of their application in various adsorption processes together with the analysis techniques involved are compiled in Table 7. To date, the best approach to

finding the right model and the adsorption rates is by means of conducting equilibrium adsorption studies and fit the data to various models [90, 98].

Table 6: Isotherm models at different states (Equation 1-12).

Isotherm model	Equilibrium	Linearized	Non-equilibrium	Ref.
Langmuir	$C_r^* = C_{rmax}\frac{K_l C_e^*}{1+K_l C_e^*}$	$\frac{1}{C_r^*} = \frac{1}{C_e^*}\left(\frac{1}{K_l C_{rmax}}\right) + \frac{1}{C_{rmax}}$	$\frac{dC}{dt} = -k_1 C\,(C_{rmax} - C_r) + k_2 C_r$	[5, 50, 99-104]
Freundlich	$C_r^* = K_f {C_e^*}^{\frac{1}{n}}$	$\log C_r^* = \frac{1}{n}\log C_e^* + \log K_f$	$\frac{dC}{dt} = -k_1 C^{\frac{1}{n}} + k_2 C_r$	[5, 50, 99, 104, 105]
Langmuir-Freundlich	$C_r^* = \frac{K_{lf} C_{rmax} {C_e^*}^{\frac{1}{n}}}{1 + K_{lf} {C_e^*}^{\frac{1}{n}}}$	$\frac{1}{C_r^*} = \frac{1}{{C_e^*}^{\frac{1}{n}}}\frac{1}{K_{lf} C_{rmax}} + \frac{1}{C_{rmax}}$	$\frac{dC}{dt} = -k_1 C^{\frac{1}{n}}(C_{rmax} - C_r) + k_2 C_r$	[90, 105-110]
Temkin	$C_r^* = B\,\ln(K_t C_e^*)$	$C_r^* = B\,\ln C_e^* + B\,\ln K_t$	$\frac{dC}{dt} = -k_1 C + k_2\, e^{\frac{C_r}{B}}$	[5, 50, 99, 103-111]

C_r* and C_r is the amount of solute adsorbed on solid-phase in equilibrium and non-equilibrium state (mg/g), C_e* and C is the protein concentration in solution at equilibrium and non-equilibrium state over time (mg/ml), C_{rmax} is the maximum clay protein concentration at saturation (mg/g), K is the equilibrium constant (g/mg) for Langmuir and Langmuir-Freundlich, (dimensionless) for Freundlich and Temkin (subscripts l = Langmuir, f = Freundlich, lf = Langmuir-Freundlich and t for Temkin), n is the parameter of favourability with $n > 1$ represents favourable adsorption.

The ratio of the adsorption and desorption rate constants, k_1 and k_2 (g/mg.s and 1/s for Langmuir and Langmuir-Freundlich, 1/s and 1/s for Freundlich and Temkin respectively) are expressed as:

$$K = \frac{k_1}{k_2} \tag{13}$$

The term B is is related to the heat of adsorption and is given by:

$$B = \frac{RT}{b} \tag{14}$$

where R is the gas constant (8.314 J/mol.K), T is temperature (K), b is a Temkin constant (J/mol).

3.5.1 Langmuir Isotherm

The Langmuir equation is the most widely used model for adsorption processes [6, 90, 112]. This isotherm provides a simple expression for gas and liquid adsorption (physical and chemisorptions) [7, 90, 112]. The Langmuir equation relates the coverage or adsorption of molecules on a solid surface to gas pressure or concentration of a medium at solid / liquid interface at a fixed temperature. The equation was developed by Irving Langmuir in 1916. The Langmuir model represents Type-I adsorption well [48, 90]. Assumptions made to this isotherm include a homogeneous surface of solid-phase, monolayer adsorption and that the forces of interaction between adsorbed solutes and solid-phase are negligible [7, 8, 48, 51, 90].

Langmuir isotherm has been successfully used in many adsorption systems for example, wine clarification [70, 113-115] and waste water treatment [6, 7, 100]. It was suggested that this isotherm can also be used for protein adsorption onto solid surface with an assumption of no intermolecular interactions between adsorbed molecules [103]. However, this could be erroneous because proteins are large amphoteric polymers that would result in multilayer adsorption on solid-phase.

The model was originally developed for physical adsorption of gases onto porous solids. However, it was found to model chemisorptions very well [48]. For Langmuir adsorption, Seader (2006) suggested that adsorption was due to chemisorptions, while Tien (1994) suggested it wass due to physical adsorption. The latter is characterized by adsorbates adhering weakly to solid surface and is relatively weaker compared to chemisorption. Strong adsorption systems are characterized by combinations of both which can be seen in adsorption of amoxicillin on activated carbon [6].

There are many approaches in deriving isotherms. The most common method is through a kinetic approach [90]. Consider the reaction below, where *S** is an empty active site on a solid adsorbent surface, *P* is the substrate and *SP* is the occupied binding site by the substrate molecule. The kinetic reaction can be expressed as:

$$S^* + P \overset{K}{\leftrightarrow} SP \tag{15}$$

The equilibrium constant, *K* is given by:

$$K = \frac{[SP]}{[S^*][P]} \tag{16}$$

Let ϕ be the fraction of the surface filled with adsorbate. Therefore, $(1-\phi)$ represents empty binding sites. Because the number of filled surface sites (*SP*) is proportional to ϕ, the number of unfilled sites (S^*) is proportional to $(1-\phi)$, the number of particles is proportional to the gas pressure or concentration *(P)* and α is the Langmuir constant. Equation 16 can be rewritten as:

$$\alpha = \frac{\phi}{(1-\phi)P} \tag{17}$$

Rearranging the equation gives:

$$\phi = \frac{\alpha P}{1 + \alpha P} \tag{18}$$

By incorporating a saturation term (C_{rmax}) and Langmuir constant (K_l), the isotherm model can be expressed as:

$$C_r = C_{rmax} \frac{K_l C_e}{1 + K_l C_e} \tag{19}$$

The C_e notation for equilibrium solute concentration can be replaced with the term "*p*" for partial pressure in gas adsorption.

A limitation of the Langmuir isotherm can be seen in ion-adsorption processes where the charges and affinity of the solid-phase are altered as ions are adsorbed. In the case of phosphate adsorption, the surface becomes more negative and adsorption weakens. The effect of ionic strength cannot be accounted by the Langmuir equation that assumes a constant ion-surface affinity. The isotherm will always predict that adsorption will increase until saturation. For salt competition adsorption, additional variables are required. But adding more terms complicates analysis and therefore, a more direct approach is always preferred such as analyzing just one solute component in solution [112].

3.5.2 Freundlich Isotherm

The isotherm was developed by Herbert Freundlich in 1909, originally used to represent the isothermal variation in gas adsorption empirically. It relates the quantity of adsorbed gas relative to the unit mass of solid-phase with pressure [48]. Assumptions made in this isotherm are multilayer adsorption, heterogeneous surface and nonuniform distribution of the heat of adsorption over the surface [7, 8, 51]. The expression of Freundlich isotherm is given by:

$$C_r = K_f \, C_e^{\frac{1}{n}} \tag{20}$$

The term *n* represents heterogeneity and cooperativity in adsorption which is a temperature-dependent constant, with $n > 1$ indicating favourable adsorption and $n > 10$ indicating the adsorption process is irreversible [7, 112]. For *n* equals to 1, the isotherm equation is reduced to Henry's law:

$$C_r = kC_e \tag{21}$$

According to Parfitt et al. (1983), this simple expression does not usually apply over the whole concentration range thus its validity is uncertain. He added that the isotherm is derived from consideration of heterogeneity of the surface when applied to gas adsorption on solids. Therefore, if data for liquid adsorption fit the equation, it is possible that the solid surface is heterogeneous, however this is not proven.

The limitation of the Freundlich isotherm is it has no saturation term. It fails at high pressure for gas adsorption. The reason for that is in gas adsorption, the adsorbed component, C_r varies directly with pressure until the saturation pressure is reached. Beyond this point, there should be no adsorption but the model would suggest C_r will keep on increasing. Similarly, for adsorption from solution, because the isotherm describes the C_r as a function of solute concentration (C_e), C_r always increases indefinitely with the solution concentration [105].

3.5.3 Langmuir-Freundlich Isotherm

Due to limitations of the Langmuir and Freundlich models, these isotherms can be combined into a single model to account for the weaknesses. The modified version of both isotherms is known as the Langmuir-Freundlich isotherm and is given by:

$$C_r = \frac{K_{lf}\ C_{rmax}\ C_e{}^{\frac{1}{n}}}{1 + \ K_{lf} C_e{}^{\frac{1}{n}}} \tag{22}$$

The logic for this isotherm is that it should cover the assumptions of both original isotherms. The Freundlich model suggests multimolecular adsorption on heterogeneous solid surfaces without considering the limited numbers of active sites while the Langmuir isotherm assumes single layer adsorption on homogeneous solid surfaces until saturation, with no intermolecular interaction. By incorporating both models, multiple-site adsorption can be represented cooperatively with the term C_r no longer increasing significantly with C_e [105]. Similar to Freundlich model, the term C_r is increasing with C_e but moderately with saturation trend could be obtained at equilibrium as can be seen from Figure 13.

Not all adsorption processes are well represented with this isotherm. Certain types of adsorption data such as hydrocarbon adsorption on activated carbon is better represented with either Langmuir or Freundlich equation alone [90].

3.5.4 Temkin Isotherm

The Temkin isotherm considers the influence of energy in adsorption. The energy is in the form of heat generated due to the exothermic nature of adsorption and the indirect interaction between solute and solid-phase [7]. Temkin assumes a uniform distribution of energies throughout the active sites on the solid-phase. The distribution of energies should depend strongly on the density and distribution of functional groups of both solute and solid-phase [50, 111]. The heat of adsorption of the solute on the surface decreases linearly with coverage [7]. Johnson and Arnold (1994) suggested that the model works well with chemisorptions (cited by [103]) and reversible protein adsorption [105]. The Temkin isotherm is given by:

$$C_r = B \ln(K_t C_e) \tag{23}$$

Sharma and Agarwal (2001) suggested that the isotherm is advantageous over the other models in explaining the heterogeneous nature of protein adsorption on complex adsorbents. In gas adsorption, Temkin isotherm always obeys Henry's law that states the solubility of a gas in fluid-phase is directly proportional with the pressure of the gas; which could be very important to predict chromatographic behaviour from equilibrium adsorption [105].

3.6 Product Recovery and Waste Treatment using Adsorption

One of the advantages of adsorption is it can perform separation at microscopic level which cannot be done by conventional techniques such as distillation and membrane separation. Therefore, this field has expanded rapidly as a unit operation to meet higher standards in environmental discharge and product recovery. Concurrently, the development of new adsorbents is increasing quickly to cater for new applications [93, 116]. Table 7 summarized recent adsorption applications, listing the types of absorbents and adsorbates, isotherm models and the analysis techniques used.

3.6.1 Selection of Adsorbents

The criteria for good adsorbents are mentioned in Section 3.2. Amongst them, compatibility and cost are the two main important factors in adsorbent selection. Compatibility covers the aspect of mode of adsorption such as physical or chemical and nature of solid-phase such as inertness and resistance to crushing. Cost on the other hand is important to make adsorption a persuasive separation process to existing techniques. However, the selection of adsorbent is often dependent on the application because every application requires different priorities such as low cost adsorbents are preferred in waste water treatment [48, 93].

Various adsorbents used in adsorption are listed in Table 7. For clay-based adsorbents, it can be seen that sodium bentonite is more commonly utilized than calcium bentonite. This is attributed to its abundant, very high specific surface area and cation exchange capacity. Besides, sodium bentonite is naturally occurring clay and therefore the cost could be relatively cheaper compared to calcium bentonite because no further modification is needed. Small size adsorbents are advantageous due to high specific surface area which can maximize the contact with solutes in solutions and lead to increase in adsorption rate.

3.6.2 Application of Isotherm Models

Recent adsorption applications (Table 7) show that the adsorbates used ranging from simple ions to complex protein molecules. They are categorized into proteins, polymers, heavy metals, dye pigments and traces of pharmaceutical and herbicide

waste. They could differ in the mode of adsorption on the solid-phase. For example many adsorbates rely on electrostatic force on negatively charged clay surface, however large adsorbates such as proteins and polymers can also adsorb via hydrophobic and hydrogen interactions. In addition, adsorption is very rapid for small adsorbates due to higher diffusion rate whereas larger molecules could take time and impose steric hindrance on the surface due to structural conformation. Therefore, when equilibrium data are applied to isotherm models, each model could differ based on the assumptions made. From Table 7, the Langmuir and Freundlich models are the most widely used isotherm models.

The Langmuir isotherm was developed originally for gas adsorption and now it is widely used to model adsorption of non-complex solutes considerably well, such as in the adsorption of chromium ions onto chitosan [54], amoxicillin and aniline by bentonite [6] and methylene blue by biotite hydrogel [51]. However, as the adsorption changes from single to multiple sites such as in protein adsorption, the Langmuir model failed due to number of reasons namely assumption of unilayer adsorption, homogeneous nature of adsorbent surfaces and no lateral and cooperative interactions between solutes-solutes in the liquid and on the solid-phase [105].

Nevertheless, a successful application of the Langmuir model on protein adsorption can be seen in wine clarification industries [70]. The reason is that the wine-protein molecules are present as short peptides. The proteins have less lateral interaction between them and one binding site on solid-phase could cater for a single solute. In the case of reactive blue adsorption onto fungal biomass, Langmuir was found unsuitable but Freundlich and Temkin fitted the adsorption data quite well [50].

For multiple binding site adsorption, such as for proteins, the Langmuir-Freundlich, Freudlich and Temkin are better because they are able to explain the cooperativity and binding heterogeneity in quantitative terms [105]. Even though the Freundlich model assumes multilayer adsorption, it may not always able to model multilayer adsorption data efficiently because there is no saturation term in the model equation. The calculated amount of adsorbed solutes would increase indefinitely with the solution concentration and therefore become unfit in certain cases such as in the adsorption of β-lactoglobulin onto calcium montmorillonite and calcium illite [117].

Having to incorporate both Langmuir and Freundlich assumptions, Langmuir-Freundlich has been used successfully in the adsorption of *E.coli* recombinant protein [107], BSA, chicken egg lysozyme and ovalbumin [105] onto immobilized metal ion gels. Protein solutes are relatively larger in size compared to metal ions and are amphoteric. Thus, the interactions between solutes in solvent and on solid-phase are likely with each protein molecule could occupy several binding sites on the solid-phase until saturation is reached.

In the case ovalbumin and BSA adsorption onto immobilized metal ion gels, the Langmuir model was unable to account for the data points by suggesting a linear correlation between C_r and C with disregard to the saturation point (Figure 13). This is a critical mistake because data points at the extremes provide the information on maximum adsorption capacity, $C_{rmax.}$ The Langmuir-Freundlich model however was found to represent the experimental data extremely well as depicted in Figure 13 with correlation coefficient > 0.99. More interestingly, it is able to model a sigmoidal adsorption pattern very well with $n > 1$, indicating a favourable adsorption or positive cooperativity. This means that the adsorbed macromolecular solutes interact in harmony on a heterogeneous surface [105].

For salt competition effect, ions present in aqueous solutions such as metal cations and inorganics anions often show the tendency to adsorb chemically on hydrous oxide solid-phase such as activated carbon [90]. This makes the extent of equilibrium hard to predict using conventional isotherm models such as Langmuir and Freundlich. The Temkin isotherm could be a suitable model based on its assumption that adsorption is characterized by a uniform distribution of binding energies on heterogeneous solid surface. As it was developed originally for gas adsorption on heterogeneous surface, the Temkin model is often found inadequate to model protein adsorption but could be better than the Langmuir model which assumes homogeneous surface.

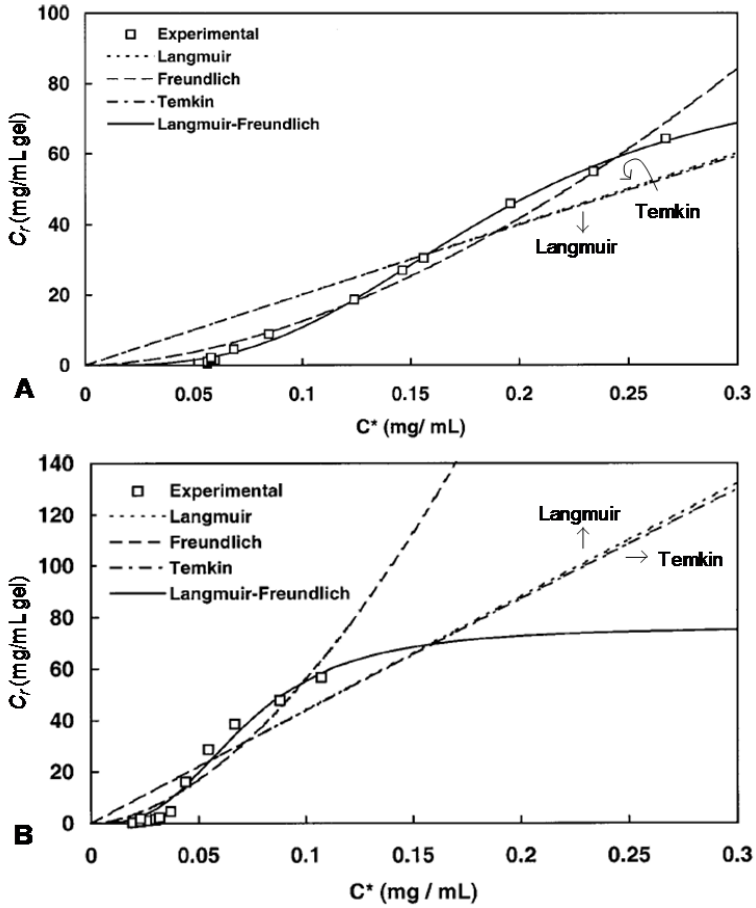

Figure 13: Adsorption isotherm models ploted along side the experimental data of adsorption of A) chicken ovalbumin and B) BSA onto Cu(II) immobilized metal ion gel [105].

3.6.3 Analysis Techniques on Solid-Phase

From Table 7, it shows that the analysis techniques become more diverse as the adsorption process expanded into more complicated system. X-ray diffraction (XRD) is widely employed to characterize the adsorbent before and after adsorption. It enables the determination of basal spacing (*d*-value) and crystallinity which are very useful to study the extent of adsorption. Bentonite has many characteristic diffraction peaks with two major peaks at 2θ of 2-10^{o} and 25-30^{o} [9]. Basal spacing is denoted by the first diffraction peak (d_{001}) and can be calculated using Bragg's law [2, 19]:

$$n\lambda = 2d\ sin\ \theta \tag{24}$$

where n is the order of diffraction, λ is the wavelength of x-ray beam, d is the basal spacing (Å) and θ is the angle of incidence (^{o}).

For treated samples after adsorption, solute intercalation into a clay gallery is indicated by an increase or decrease in d-value which are reflected by a left and a right shift of the d_{001} peak [7, 68, 118]. While exfoliation of clay layers is characterized by the absence of these peaks from its pristine condition [119]. Consider an example in Figure 14, Cloisite Na^{+} is unmodified sodium montmorillonite while Cloisite 20A and 30B are its organically-modified forms. They are modified with ammonium salt intercalation of dimethyl di(hydrogenated tallowalkyl) and bis-(2-hydroxyethyl) methyl (hydrogenated tallowalkyl) respectively [120, 121]. The XRD showed a left shift of d_{001} peaks indicating the expansion of clay galleries. Cloisite 20A resulted in a larger basal spacing compared to Cloisite 20B because of larger intercalated organic.

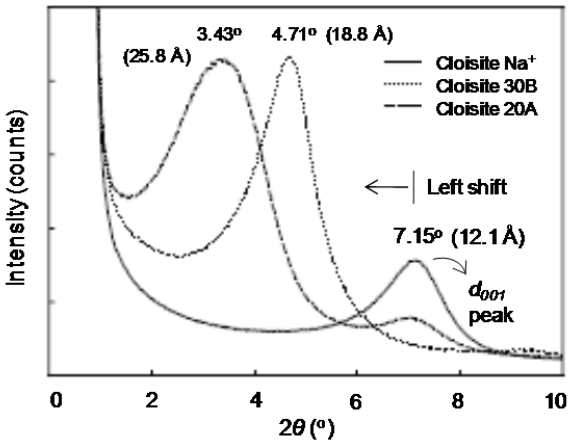

Figure 14: XRD patterns on three types of nanoclays [121].

From the compiled data (Table 7), XRD is employed mainly on protein and polymer adsorption. Overall, the average increase in d-value is larger in protein adsorption compared to polymers with up to six-fold increase can be observed for polyamines intercalation on sodium montmorillonite and mica. There is less research utilizing XRD for heavy metals, dye pigments and pharmaceutical traces possibly because the relative size of the adsorbates are small compared to the pre-existing ions on the solid-phase. Therefore, the knowledge on the change in basal spacing is less important.

Other analysis techniques used in adsorption work can be classified into characterization and validation. The former is significant to establish a thorough understanding on adsorbent before adsorption. It could give indications of the performance of the adsorbents in adsorption. Validation is used to compliment the adsorption isotherm studies for example XRD indicates solute intercalation and thermogravimetric analysis (TGA) quantifies the mass loss of sample by heating at high temperature to determine the composition breakdown. More information on the techniques with their functions is presented in Section 4.3.

The elaborate discussion and summary of literature so far suggest that the adsorption can be useful to capture organics from waste water. The process can be analyzed using equilibrium isotherm method and various models. However, despite showing efficiency in protein recovery, the application of adsorption onto stickwater is practically new. This process could potentially be an alternative treatment to the current approach that is drying.

Table 7: Adsorption application, isotherm models and analysis techniques used.

Adsorbent	Adsorbate	Model	XRD intercalation (Å)		Other analysis techniques and notes	Ref.
			Before	After		
	Proteins					
Bentonite	BSA, ovalbumin, lysozyme	Langmuir	-	-		[113]
Immobilized metal ion gels	Chicken egg proteins and BSA	Langmuir, Freundlich, Temkin and Langmuir-Freundlich	-	-		[105]
Hydroxiapatite-based metal ions gels	*E-coli* recombinant protein (containing His-tag)	Langmuir, Temkin and Langmuir- Freundlich	-	-	Bradford and SDS-PAGE	[107]
Na Mt from 3 origins	Chicken egg albumin	Langmuir	12.3, 13 and 11.8	-	CEC and BET	[70]
Na Mt	Albumin pH 4.0, 5.2 and 6.4	-	12.3	17-24.4	CEC	[68]
Mg Mt			15.4	15-16.2		
Na Mt	BSA	-	12	62	DFM	[118]
H Mt	(4/1 ratio BSA/Mt)		15	33		
POP modified Mt			53	61		
Na Mt	Polyamines	-	12.4	15-82	TEM	[122]
Mica			12.6	15-83.7		
Mt, illite and kaolinite	Catalase and β-lactoglobulin	Langmuir and Freundlich	15.7	29.4	FTIR and CEC	[117]
Na Mt	Poly-diamines	-	12.4	15-92	SEM	[19]
Na Mt	Agar	-	12.4, 18.8 and 25.8	18.3, 19.5 and 27.9	SEM, tensile test, water contact angle and resistance and antimicrobial activity	[121]
Mt	Gelatin	-	14.7	44.2	DSC, TGA and SEM	[20]
Na Mt	Gelatin	-	11.7	-	AFM, TGA and TEM	[80]
Na Mt	Gelatin	-	14.7	44.2	TEM and tensile test	[32]
Activated clays	Fish stickwater organics	-	-	-	Ashing and UV absorbance	[23]
Na Mt Ca Mt	Wine and juice, model solution (BSA and 1 g/L potassium bitartrate in Milli-Q water at pH 3.2)	-	-	-	Laser particle sizer, HPLC and turbidity	[123]

	Polymers					
Na Mt	POE (2000 g/mol)	-	12.4	19	TGA, CEC, SEM and TEM	[124]
	POP (2000 g/mol)		12.4	58		
Na Mt	Polymeric ammonium salts	-	9.6	14.26	TGA	[125]
Na Mt Ca Mt	Ethylene glycol, anionic polyacrylamide	-	12.8 12.4	16.7, 12.4, 16.7 and 12.2	FTIR and DTA	[126]
	Heavy metals					
Chitosan	Cr (VI)	Langmuir, Freundlich and Temkin	-	-	SEM	[54]
Bentonite Iron Oxide Bt/Iron oxide	Metal cations (Ni^{2+}, Cu^{2+}, Cd^{2+} and Zn^{2+})	-	14.3	-	BET, TGA, SEM and Mossbauer spectroscopy	[55]
Ca Mt and Sepiolite	Cu^{2+}, Zn^{2+}, Cd^{2+}, Co^{2+} and Pb^{2+}	Langmuir, Freundlich and Temkin	-	-	AAS, BET and SEM	[127]
Banana peels	Pb(II) and Cd (II)	Langmuir, Freundlich and Temkin	-	-		[53]
	Dye pigments					
Fungal biomass	Textile dye (reactive blue 4)	Langmuir, Freundlich and Temkin	-	-	SEM, FTIR, water content and contact angle	[50]
Cytosan-biotite hydrogel	Methylene blue	Langmuir and Freundlich	-	-	FTIR, thermodynamics study	[51]
Na Mt, Poly-ions modified Na Mt, Heated Na Mt	Methylene blue	-	12.6	-	ESI-MS, BET, SEM, EDS and FTIR	[52]

	Pharmaceutical, chemical traces and microorganisms					
Acid (H_2SO_4) activated Na Bt	Humic acid	Langmuir, Freudlich and Temkin	14.9	-	SEM and thermodynamics study	[5]
Activated carbon and bentonite	Amoxicillin	Langmuir and Freundlich	-	-	BET, SEM and FTIR	[6]
Fe^{3+}, Al^{3+}, Ca^{2+} and Na^{+}, K^{+} Mt	Herbicides	Freundlich	-	-	FTIR	[128, 129]
Kaolin, illite and smectite	Thiamin	Langmuir	-	-		[49]
Immobilized metal ion gels	Microorganisms	Langmuir, Freundlich, Temkin, Dubinin-Radushkevich, Redlich-Paterson, Sips, Khan, Radke-Prausnitz and Toth	-	-	A review paper FTIR, EDS and SEM	[104]
Cr Mt	Aniline	Langmuir, Freundlich, Temkin and Dubinin-Radushkevich	-	-		[7]
Cr Mt	4-hydroxyphenol	Langmuir, Freundlich and Dubinin-Radushkevich	-	-	Thermodynamics study	[8]

3.7 Settling Process and Modelling

3.7.1 Colloids, Flocculation, Coagulation and Sedimentation

The term colloids is defined as fine materials (discontinuous phase) uniformly dispersed in a medium (continuous phase). These include fogs (liquid droplets in gas), milk (fat in liquid) and slurries (fine solid particles in liquid). Colloids are sometimes known as lyophobic (hydrophobic) and lyophilic (hydrophilic). Multiple colloids refer to two or more colloidal systems exist together. There are no specific size limits for colloids but those having a size around 1 nm (10 Å) are usually presumed to behave similar to a molecular solution. Dispersion systems are said to be monodisperse for same size colloids and polydisperse for variable size colloids [130].

Flocculation is a formation of flocs (open aggregates) by colloids interacting and sticking together. For a denser floc, it is known as coagulation with the formation of coagulum. The floc may or may not separate out of solution. The aggregates can be separated out from solution either by sedimentation (when mass density of aggregates is larger than solution medium) or by creaming (when mass density of aggregates is lower than solution medium). Often the difference between flocculation and coagulation is ambiguous, therefore the terms flocculation and coagulation have been used interchangeably [92, 130].

Bentonite and activated carbon are some examples of adsorbents and flocculants used for waste water treatment such as removing traces of heavy metal [127, 131, 132], herbicide [128] and pharmaceutical [6]. Activated carbon is the preferred choice because of its high specific surface area and pore volume and its selectivity for small organic molecules. However, it is more expensive than other adsorbents which limits its application on large-scale. In waste water and water treatment, flocculation is mainly used for removal of colloids that cause colouration and turbidity. This process could work effectively for simple systems such as removal of organics to produce potable water but proves to be difficult for complicated systems [41, 51, 133].

Inorganic and organic flocculants have been used to treat agricultural waste especially from slaughterhouses reducing BOD by up to 80 % as well as reducing nitrogen, phosphorus and fine particulates. The effectiveness of the flocculation process

depends on waste water composition, organic concentration, pH, temperature, rate of mixing and the order in which flocculants are introduced into the waste water [41, 88]. This means for flocculation to work on stickwater, pre-treatments such as dilution, pH and temperature change need to be investigated.

3.8 Process Model

3.8.1 Stoke's Law Settling Model

Sedimentation of flocs in a settling tank or centrifuge is a simple separation process and is effective where settling is achieved when the mass density of flocs is higher than the solution. This phenomenon is explained by Stoke's Law. For a particle moving in a stationary fluid, there are three main forces acting the particle: gravity, buoyancy and drag. A particle's terminal velocity or settling velocity is reached when acceleration of the particle due to gravity in cancelled out by particle buoyancy and the increased frictional forces between the particle and solution [134, 135]. Stoke's Law found major applications in understanding natural science is such as settling of organisms in water and help to the understand about mist, snow and rain [136].

Stoke's law is valid for particles settling in laminar flow, therefore prior to model application, Reynold's number for particle (Re_p) should be calculated to characterize the fluid flow. The equation is expressed as:

$$Re_p = \frac{V_s \, D_{cp} \, \rho}{\mu} \tag{25}$$

where V_s is the particle settling velocity (m/s) relative to stationary fluid, D_{cp} is the particle's diameter (m), ρ is the solution density (kg/m^3) and μ is the dynamic viscosity (kg/ms) of the solution. The fluid flow is characterized as laminar for $Re_p <$ 0.3, transitional for Re_p between 0.3-500 and turbulent for $Re_p >$ 500. In laminar flow, the viscous forces are dominant in the system while inertial forces are dominant in a turbulent flow [137].

Assumptions made for Stoke's law include spherical particle, uniform size and material and no lateral interaction between particle / particle and particle / fluid. The Stoke's law settling velocity can be calculated by:

$$V_{ss} = \frac{2}{9} \frac{(\rho_p - \rho_f)}{\mu} g {r_{cp}}^2 = \frac{x_s}{t_{ss}} \tag{26}$$

where V_{ss} and t_{ss} is the Stoke's law settling velocity (m/s) and time (s), ρ_p and ρ_f is the density of particle and fluid (kg/m^3), g is the gravitational acceleration (9.8067 m^2/s), r_{cp} is the particle radius (m), x_s is the vertical distance travelled by the particles in the column (m) and t_{ss} is the time taken for the particles to settle (s).

By assuming the particles travelled a distance of the column height (0.4 m), Equation 26 is reduced to:

$$t_{ss} = \frac{0.1835\mu}{{r_{cp}}^2(\rho_p - \rho_f)} \tag{27}$$

Alternatively, a settling velocity can be determined by a laser sensor to measure the time taken for a particle to travel a predetermined distance in a glass tube. This way, the expression can be used in reverse to find the fluid viscosity.

3.9 Summary

Organic adsorption from stickwater is a multi-components adsorption, comprising of fat, protein, minerals and other organic matters. Since stickwater protein is mostly gelatin, model solution can be prepared from food-grade gelatin. Adsorption on model solution can be studied using four commonly used isotherm models to predict the extent of adsorption and for kinetic study.

After adsorption, various analysis techniques can be employed to verify adsorption results. For example, XRD is used to show protein intercalation into clay galleries, TGA is used to quantify the organic mass loss, and SEM is used to determine surface elements as well as microscopic observations. Sedimentation or settling of particles after adsorption could possibly be achieved at certain conditions. Therefore, particle settling in gelatin solution should be conducted at various conditions especially at different solution pH.

Nanoclays could be suitable adsorbents attributing to their desirable properties such as high specific surface area, cheap and abundant, nontoxic and inert in solution. The optimum adsorbent dosage and adsorption conditions can be investigated on model solution prior to validation on stickwater.

Although some clay types could be advantageous at organic adsorption, the downstream process for separation from solution could be complicated due to swelling nature of clays especially smectites. This characteristic leads clays to gel in solution forming a stable network of clay platelets and it was reported that the structure remained stable even at high dosage of flocculants [133].

Proceeding in the next chapter is a discussion about clay origin, properties and potential. Nanoclays are used in nanocomposites but require modification to improve compatibility in biopolymer matrices and are often modified with organics. Therefore, adsorbing organic from stickwater can be beneficial for waste water treatment and clay modification. Priority in this research was to find the right balance between adsorption capacity and settling ability of bentonite in solution as well as utilizing the organically-modified bentonite for bioplastic reinforcement.

CHAPTER 4

CLAY MINERALS AND NANOCOMPOSITES

4.1 Clay, Clay Mineral and Bentonite

The International Association for the Study of Clays (AIPEA) defines clay as a material composed primarily of fine-grained minerals in soil or sediment while clay minerals (also known as phyllosilicates) are hydrous layered aluminosilicates which harden upon drying or firing [9]. Clay minerals form the major constituents of the colloidal fraction of soils. Nanoclays refer to clay minerals with particle size ranging between 1 to 1000 nm. They are made of aggregated sheets of approximately 8-10 units with dimension of 100 x 100 x 1 nm for each sheet. These include koalinite, micas and smectites [1, 2, 9, 138, 139].

The name of montmorillonite was given to smectite clay found in Montmorillon area in France while bentonite was suggested by Knight in 1898 for smectite clay from Fort Benton, Wyoming [1]. Bentonite (Bt) belongs to smectite group and mainly composed of montmorillonites (Mt) with other minerals such as feldspar and quartz [1, 9, 138, 139]. The following definition of bentonite proposed by Ross and Shannon (1926) (cited by [1]) has been widely quoted in literature: "Bentonite is a rock composed essentially of a crystalline clay-like mineral formed by the devitrification and the accompanying chemical alteration of a glassy igneous material, usually a tuff or volcanic ash". These authors further stated that, "the characteristic clay mineral has a micaceous habit and facile cleavage, high birefringence, and a texture inherited from the volcanic tuff or ash, and it is usually the mineral Mt, but less often beidellite". Technically, the term bentonite and montmorillonite refer to the same type of clay which is smectite, and they are used interchangeably.

Montmorillonite deposits were formed by the alteration of volcanic material [1, 139]. They are widely available and can be found almost everywhere except Antarctica [139]. Montmorillonite is categorized as 2:1 clay consists of 2 tetrahedral

sheets of Si-O separated by an octahedral sheet of Al–O–OH (Figure 15). Trivalent Al^{3+} and divalent Fe^{2+} or Mg^{2+} sometimes can be found replacing the tetravalent Si^{4+} in the tetrahedral sheet. This substitution by almost-similar sized ions is termed isomorphous substitution. Exchange with higher charge cations is more common [9]. Comparison between the size and charge of the replacing ions is illustrated in Figure 16. It was suggested that the selectivity preferences for cations exchange is Ca>Mg>K>Na but is not always valid and depended on the type of adsorbing surfaces [140]. The charge difference from cations exchange (for example Al^{3+} and Mg^{2+}) renders part of the oxygen coordination incomplete, resulting in negative surface charge [9, 89]. This gives the clay an amphoteric characteristic allowing positive ions such as Ca^{2+} and Na^{+} to adsorb on the Mt basal plane via ionic interaction [1, 2, 70, 126, 141]. Smectites contain cations that are easy to exchange such as Ca^{2+}, Na^{+} and Mg^{2+} which other transition metal cations can also be found in octahedral layers such as Fe (II), Fe (III), Ni (II), Zn (II), Mn (II), chromium and titanium [9]. General formula for smectites is $Na_{0.7}Al_{3.3}Mg_{0.7}Si_8O_{20}(OH)_4.nH_2O$ [133].

New Zealand is an active volcanic region with bentonites have been found in many places [1]. Bentonite is a national mining commodity in New Zealand with up to 1613 metric tonnes being mined in 1994 at Greymouth Inspectorate generating NZ$ 32 260 or equivalent to NZ$ 20 per tonne [31]. Local bentonite mining peaked at 6154 metric tonnes in 2007 and the demand weakened in following years [142]. Naturally occurring bentonite in New Zealand is more commonly found in the form of sodium bentonite than calcium bentonite [143].

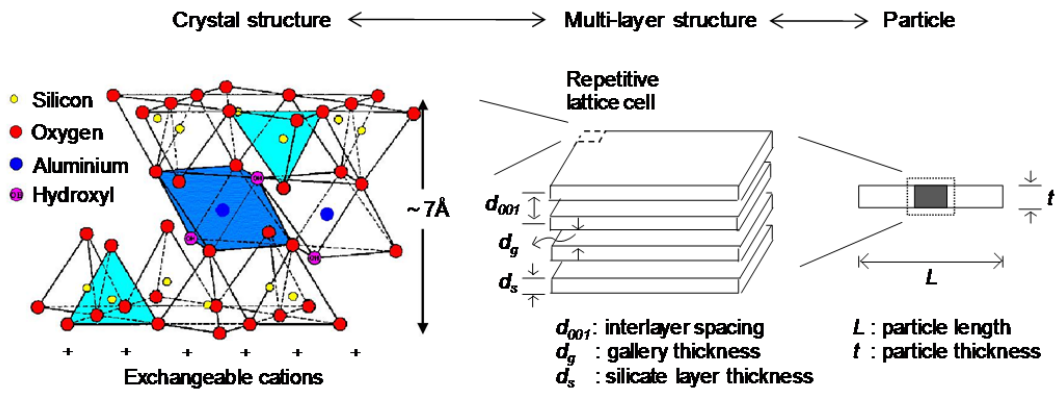

Figure 15: Structure of montmorillonite [144, 145].

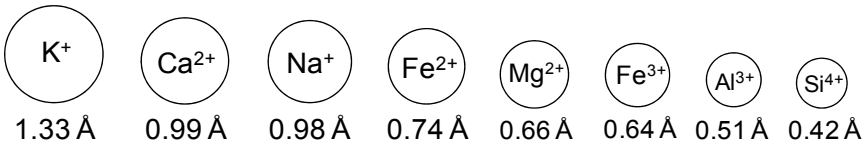

Figure 16: Relative dimensions and charges of ions commonly found in soils [2, 9].

4.2 Bentonite Charges, Surface Potential and Point of Zero Charge

4.2.1 Bentonite charges

Isomorphous substitutions (Si^{4+} with Al^{3+} and Al^{3+} with Mg^{2+}) give a net permanent negative charge on the clay surface [1, 2, 89]. At the platelet edge there is a condition called "broken bonds" where the terminal mineral elements do not bind to any mineral. Therefore, charge components exist at the edge. These charge components are known as variable charges because they are pH-dependant and readily react in electrolyte solution. If the surface charge of clay is weak (kaolinite and talc), charges at the edges will dominate the particle overall charge. However, in the case of highly charged surfaces such as smectites and mica, the variable charge at the edges make only minor contribution toward the overall charge [140].

In solution, the dissociation of alumina and silica elements as well as the hydroxyl (OH) groups at the edge determines the overall charge. Aluminium has point of zero charge (PZC) at pH 7 and silica's PZC is about ~pH 4. At high pH, the hydrogen of these groups dissociates into H^+ ions in solution, leaving O^- ions on the clay lattice, contributing toward the overall negative charge. At low pH, aluminium and silica are positively charged while OH_2^+ forms on the surface, giving bentonite an amphoteric characteristic [89].

Two types of adsorbing ions are charging ions which can adsorb on any neutral or charged surface and non-charging or indifferent ions which can only adsorb when the surface is charged. The charged ions are of two types; if they are components of the solid-phase and / or the solvent (e.g. H_3O^+ and OH^- in oxide systems) then they are known as potential determining ions. If the ions are not components of solvent and solid-phase, they are known as specifically adsorbing ions. Both types of ion can alter the surface charge [112]. The association and dissociation of protons from clay lattice in electrolyte system can be illustrated as follows:

In an alkaline medium: —Al–OH + OH^- ↔ —AL–O^- + H_2O

In an acidic medium: —Al–OH +H^+ ↔ —Al–OH_2^+

Because H+ and OH- ions are part of the solid / solvent phase and contributing significantly to the development of particle charges, they are known as potential determining ions [2].

4.2.2 Surface Potential

In adsorption systems, opposite charge ions from solution that adsorbed on a solid-phase is said to exist in a solid / liquid phase. When the opposite charged ions are attracted to each other, an electrical potential is developed at the inter-phase or also known as surface potential, ψ (Figure 17). A potential gradient would be established with a high cation concentration at or near the surface and decreasing with the distance from the surface. The solid / liquid layer of which the solute or positive counterions interact with the solid-phase is called the electric double layer [2, 89]. The first layer (Stern layer) is on the solid-phase where the solute molecules occupy the active sites. The second layer (diffuse layer) is the liquid-phase containing evenly distributed solutes that are attracted to the solid-phase. These two layers will come to an equilibrium with a net distribution of ions [2].

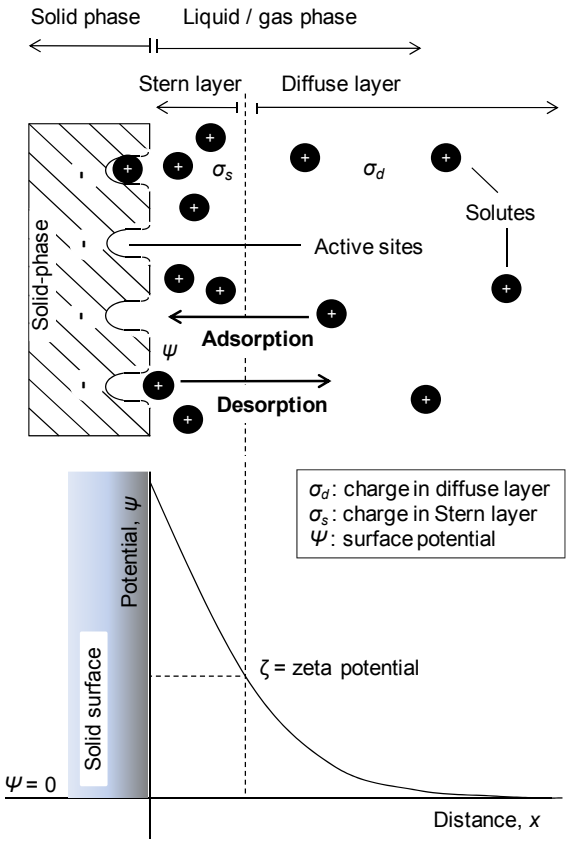

Figure 17: Surface potential in relation to adsorption and desorption process [2].

The Nernst equation is probably the most widely used equation to quantify the magnitude of surface potential [2, 112]. The Nernst equation relates the activity of potential determining ions in solution to the electrostatic potential of the surface, ψ. The magnitude of the surface potential given by Nernst equation is expressed as [2, 89]:

$$\psi = \frac{RT}{\mathrm{nF}} \ln \frac{(\mathrm{H}^+)}{(\mathrm{H}^+)\mathrm{PZC}} \tag{28}$$

where R is the universal gas constant (8.31 volt.coulomb/mol.K), T is the temperature (K), n is number of moles of exchanged electrons during electrochemical reaction (moles) and F is the Faraday's constant (96 500 coulomb/mol).

When ψ is measured in volts and potential determining ions in aqueous electrolyte solutions are at 25 ^{o}C, changing into common log gives [2, 112]:

$$\psi = 0.059\ (\mathrm{PZC} - \mathrm{pH}) \tag{29}$$

A limitation of the Nernst equation is it assumes constant surface potential at any given pH. This is not true for the case of specific adsorbing ions where they can adsorb at any pH and or the case of amphoteric surfaces [2, 89]. The equation proves useful to describe a simple system with a single electrolyte. However, it is not suitable for a system of mixed electrolytes at various concentration ranges. For example, when used for systems with weak acid dissociation characteristics (e.g. silica), it may lead to gross errors. Colloidal systems that can be described with the above equations are said to show a Nernstian behaviour [112].

There are many other theories to describe the electrical potential layer on the surface. Helmholtz, Guoy-Chapman and Stern theories described the electric double-layer while Yates et al. (1974) proposed the Triple-Layer theory [2]. Stern double-layer theory is widely used in literature to describe the surface potential. Stern layer adsorption is usually described by the Langmuir isotherm which assumes a monolayer adsorption.

4.2.3 Point of Zero Charge

Researchers are divided in the definitions of PZC and isoelectric point (IEP). According to IUPAC, PZC is the pH at which the summation of the positive and negative charges in a system is zero while IEP is defined as the pH at which the sum of the charges due to adsorption of potential determining ions is zero [112]. Both terms indicate the same pH point for an individual species such as clay and gelatin when the charges balance out as neutral. Both terms are often used interchangeably although under certain circumstances they could be different. When they exist together in an adsorption process, PZC is the most widely used generic term to mark the pH when the overall summation of charges exist in the system equals to zero. At this condition, the diffuse layer charge (σ_d) is zero. This phenomenon happens when the adsorbed potential determining ions and specifically adsorbing ions become part of the solid-

phase which equalize the potential gradient at the solid / liquid interface (Figure 17) [89, 112].

These definitions are not fully agreed among researchers. Kim (1992) suggested that PZC and IEP are the same as both points mark the pH at which the net surface charge becomes zero [2]. Theng (1980) stated that when both of the conditions exist at the same time, the condition is called pristine point of the zero charge [112]. This is a unique characteristic of the solid-phase that does not depend on the nature of the electrolyte. The IUPAC definitions of PZC and IEP are adopted in this research.

There are few methods to determine the charge and streaming potential of a solution as outlined in Table 8. The streaming potential technique is the most direct approach to determine the PZC. Streaming potential is an electric voltage that exists in electrolyte system when aqueous ions are driven by pressure through a charged channel wall [146]. To determine the PZC, acidity and alkalinity of a solution is adjusted until a zero potential is reached. The pH corresponds to this condition is taken as PZC. This technique is good for homogeneous solution such as protein solution but is unsuitable for a solution consisting of suspended particles.

Table 8: Examples of techniques available to measure the electro-potential of particles [89].

Technique	Conditions	Procedure
Streaming potential	Static interface	Mix liquid and measure potential
Electro-osmosis	Static interface	Apply potential and measure liquid motion
Sedimentation potential	Moving interface	Sediment particles and measure potential
Electrophoresis	Moving interface	Apply potential and measure particle motion
Primary electroviscous effect	Moving interface and liquid	Measure suspension viscosity
Ultrasonic vibration	Moving interface and liquid	Apply ultrasound and measure potential

4.3 Characterizing Bentonite

Knowing the properties of bentonite is fundamental to understanding how it behaves in colloidal systems. Some important properties include overall charge, point of zero charge, particle size, basal spacing and mineral contents. Table 9 lists common clay characterization techniques with their functions and Table 10 summarizes the properties of CaBt and NaBt found in literature.

The morphology of bentonite has been extensively studied using electron microscopy. The word morphology refers to the observations and descriptions of form, colour and coatings of parts that make up the whole unit [140]. Single crystallites of smectite-type clay exist in a few shapes as outlined in Figure 18.

Clay particles in distribution could be a combination of few shapes. Lath and fibre particles are relatively smaller than the rest of the shapes and would have higher surface area for the same amount of mass. This could enhance the adsorption processes by maximizing contact with the solute. However, sedimentation is harder to achieve compared to their counterparts because small particles have higher tendency to form stable suspensions due to their light weight. In terms of composite fillers, small particles are preferred because a higher degree of dispersion in the matrix materials can be achieved with relative ease.

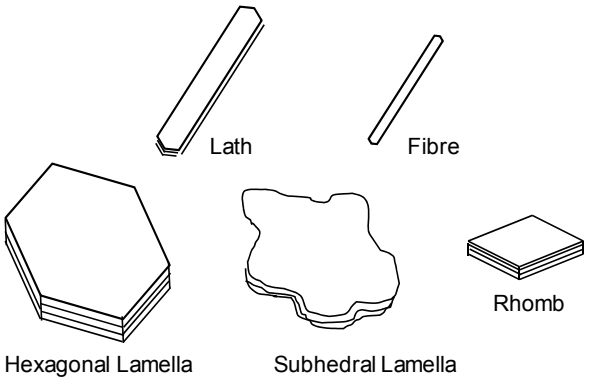

Figure 18: Common forms of bentonite single crystallites [89].

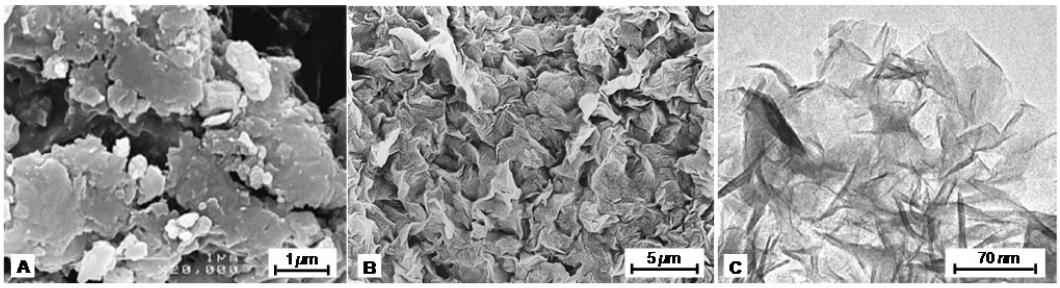

Figure 19: Morphology of A) sodium bentonite from SEM [6], B) sodium bentonite in water from cryo-SEM [147] and C) ethanol-treated magnesium montmorillonite from TEM [148].

In field emission scanning electron microscopy (FE-SEM), a flux of secondary and backscattered electrons resulting from electrons bombarding the clay surface is used to create very clear two-dimensional images with minimum resolution of 0.01 μm as depicted in Figure 19A [9]. From the figure, the particles are observed to have layered structure with majority of the platelets have hexagonal and subhedral lamella shapes. The mean particle size can be calculated from SEM images using image-analysis software. Energy dispersive spectroscopy (EDS) can be used to estimate the elemental composition of the clay minerals. FE-SEM analyzes dry samples under high voltage and vacuum environment [89].

Cryogenic SEM or cryo-SEM can be used to study morphology of liquid or semi-liquid specimens. The technique utilizes a constant feed of liquid nitrogen to provide a cryogenic environment in FE-SEM unit. This technique prevents loss of volatiles from aqueous and non-aqueous systems such as gels, emulsions and biological samples. From a cryo-SEM image of sodium bentonite (Figure 19B), it can be seen that the platelets are possibly exfoliated as indicated by relatively small particle size to the one determined from FE-SEM (Figure 19A). Some difficulties in using cryo-SEM are no proper standard and inadequate tools for cryogenic sample preparations. These issues create further problems during operation such as large frozen sample is difficult to fracture and to make it fit into a standard sample holder. With few available references in the literature, the findings could not be validated with other workers [149, 150].

In TEM, electrons are bombarded through the samples to generate “black and white” shadowy images such as in Figure 19C. It has greater magnification compared to

SEM with a common range of 2 *n*m to 1 μm [94]. Its black and white images can be used to study clay particles size, dispersion and exfoliation in composites [119].

Small particles have high specific surface area (SSA) which is desirable to maximize the contact with solutes during adsorption. For example SSA for sodium bentonite and activated carbon is 92 and 1093 m^2/g respectively. The latter was found to adsorb amoxicillin solutes four times better than the former [6]. A method called Brunauer-Emmer-Teller (BET) is widely used to determine the SSA of known mass particles by physical gas adsorption. It is called N_2-BET when nitrogen gas is used [9]. When clay particles are in solution, laser analysis can be used to estimate the average diameter and SSA of swollen clay particles. However this technique could be erroneous because it assumes either spherical or cylindrical shapes of particles in the algorithm calculations [89, 94].

Determination of clay charge is perhaps one of the most important characterization aspects. The charges on the solid-phase can influent the electrostatic interaction with solutes. The overall clay charge can be determined from potassium chloride (KCl) solution test. The charge quantity is normally expressed as cation exchange capacity (CEC). It reflects the total amount of positive charges that any particular type of clay can hold. High CEC with high SSA is desirable in adsorption to increase the yield of adsorbed solutes. CEC is dependent on pH and charge of clay [2, 112, 140].

It is clear from Table 10 that, sodium bentonite has a significantly higher CEC and SSA compared to calcium bentonite. This indicates that sodium bentonite has high affinity toward anions and greater contact with solutes. This explains the preference for sodium bentonite over calcium bentonite in adsorption processes as listed in Table 7. The use of calcium bentonite could have an advantage in separation processes attributed to its relative large particles. Therefore, it should be easier to sediment out from solution after treatment processes.

XRD analysis is commonly used in clay characterization to determine the inter-gallery distance or basal spacing (*d*-value) and mineral cystallinity. An illustration of clay gallery thickness, basal spacing and layer thickness is given in Figure 15. Table 10 shows that calcium bentonite has a higher *d*-value than sodium bentonite,

implying the interlayer adsorption could potentially be enhanced over sodium bentonite. However, Ca^{2+} ions might limit adsorption by imposing a stronger interlayer force that holds the platelet layers tighter relative to Na^{+} of sodium bentonite.

TGA is an effective method to analyze thermal stability and often used to quantify the binding energy of water associated with clay minerals. Associated water includes surface moisture and lattice hydroxyl groups that are lost with increasing temperature. The change in mass at increasing temperature is measured by TGA to help characterize the minerals. The two major TGA degradation regions of clay occur at 0-200 ^{o}C and 200-600 ^{o}C, corresponding to loss of surface water and low molecular organic, and intercalated organic and hydroxyl water respectively [9]. Solid content is the sum of organic and residual solid mass or ash. Previously, either mass loss or temperature change can be monitored at a time using TGA and DSC respectively. Nowadays, both criteria can be recorded simultaneously using a simultaneous DSC-TGA or also known as SDT [151].

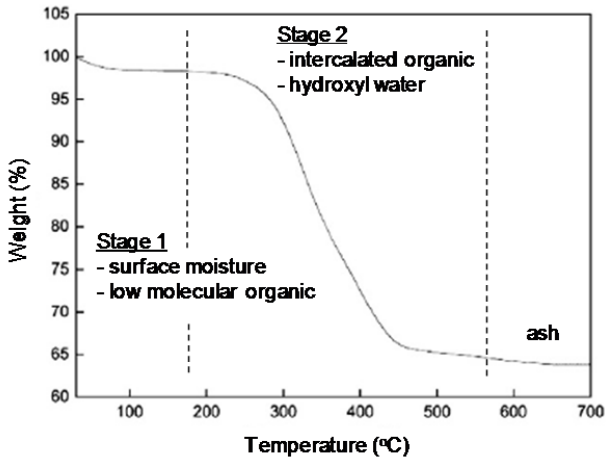

Figure 20: TGA curve of octadecylammonium montmorillonite [152].

Table 9: Common characterization techniques used for clay minerals [2, 9, 94, 151].

Quantification criteria	Characterization tools	Function
Particle size and morphology	SEM	2D images at resolution as small as 0.01 μm. EDS technique can be used to determine the elemental composition.
	TEM	Shadow images of clay particle with greater magnification than SEM. High resolution TEM (HE-TEM) has a resolution of < 2 nm.
	AFM	Observation of individual atoms on mineral surfaces and their bonding.
Surface area	BET	Based on the amount of adsorbed inert gas at monolayer coverage of powder sample.
	Laser	Laser beam is shined to particle dispersion in water and the refracted beam is counted at collector. The value reflects the surface area of swollen particles.
Charge	CEC	This is a measurement of the total positive charges.
	Δ pH	The change in pH of clay solution in 1M KCl and distilled water. It reflects the overall charge of particle.
Powder diffraction	XRD	Order of diffraction, basal spacing and crystallinity.
Thermal analysis	TGA	Thermal degradation analysis to quantify the binding energies of water and hydroxyl in clay matrix.
	DSC	Heat flow rate to a sample is monitored against temperature in a programmed heating.
	DTA	Endothermic and exothermic events are observed.
	SDT	Simultaneous TGA and DSC or TGA and DTA.
Structure, dynamic of clay minerals and clays in sorption system	NMR	Characterization of clay minerals and their organic interaction, monitoring the crystallization mechanism of clays and determining the interlayer cations distribution. For gel-clay interface, NMR helps to determine the orientation, interaction and mobility of interlayer sorbed organics.
	Infrared (IR)	Does not normally apply to clay minerals unless they contain organic molecule because IR is less sensitive to differences in clay structures than methods such as XRD and NMR.

Table 10: Summary of bentonite properties from literatures (references in brackets).

Properties	Value	
	Calcium bentonite	Sodium bentonite
Ion size (Å)	0.99 [2]	0.98 [2]
Particle size (μm) *	2 [153]	75 [125], 40 [32]
N_2-BET surface area (m^2/g)	30-50 [9, 117, 154]	750-860 [69, 97, 118, 155]
	80-94 [9, 132]	500 [156]
CEC (mEq./100g)	73-78 [117, 153, 157]	115-130 [46, 118, 122, 124, 159]
	88-105 [70, 132, 158]	90-95 [80, 121, 125, 156, 159]
Point of zero charge (pH)	~7 [89, 160]	~7 [89, 160]
Basal spacing (Å)	12.8 [126]	12-12.5 [68, 118, 121, 122, 126]
	15-15.3 [132, 158]	9.6 [125, 153, 161]

**Can be manipulated by physical processes, the values can vary significantly and are rarely reported.*

4.4 Applications of Bentonite

The diversity of bentonite uses is connected to its abundance, low-cost, well-understood characteristics and the wide possibilities of modification in terms of physical, rheological and sorption properties [116]. Today, bentonite has found various applications as outlined in Table 11. The following paragraphs discuss several selected applications with respect to the properties.

Bentonite has high degree of swelling in water, enabling it to retain large amount of water compared to other types of clays. For that reason, bentonite is used as adhesives, construction materials, drilling slurry, agriculture and wet-mash type animal feeds [1, 3, 126].

Due to its surface negativity and non-toxic, bentonite is utilized for neutralizing agent for radioactive disposals, bedding for animal litter, pelletizing aid for animal feed pellets, pharmaceutical drug carriers and detoxing aid in human and ruminant diet [1, 3, 162]. The characteristics above coupled with small particle size made it a good dispersing agent in adhesives, greases, inks and cosmetic products [1, 3]. Bentonite helps in the food industry to stabilize emulsion by acting as intermediate between oil and water [1]. In waste water treatment processes, bentonite is used to adsorb contaminants and in some applications, it can form flocs after adsorption and settle to the bottom [89]. This makes the recovery of spent adsorbent less complicated.

In the wine industry, clarification process is used to remove dissolved protein that causes a hazy appearance. Bentonite is preferred as adsorbent in wine solution because of its negatively charged surface, low-cost and inertness. The latter characteristic gives minimal impact on the taste and flavour of the wine. Since wine proteins exist in a simple form of protein molecule, the spend bentonite after treatment can be removed from the solution by sedimentation [70].

Clays were long used in construction and material fabrications such as buildings and potteries. Modern industries use bentonite as additives to composites due to various unique characteristics. In nanocomposites, bentonite is used because the particles can disperse well at nano-scale and together with its surface negativity; bentonite platelets can interact with various organics to form bio-nanocomposites. It is non-toxic and is suitable for bio-based applications such as reinforcement materials to bioplastics. The use of bentonite has been shown by many workers to improve the mechanical properties of composites [14, 80, 119, 163, 164]. However, as bio-composite filler, bentonite has to be modified with organics to increase compatibility with the matrix [9, 11].

Even though there are extensive work done on clay-based adsorption for waste water treatment but there is very little research conducted on utilizing nanoclays for gelatin recovery from stickwater. The closest research done so far was using activated clay to clarify fish stickwater as listed in Table 7. By adsorbing organics from stickwater using bentonite, two aims could be met namely; cleaning the waste water and organically modifying bentonite into bio-composite filler.

Table 11: Application of bentonite.

Applications	Function	Ref.
Adhesives	Gelling and binding chemicals and organic liquids.	[1]
Agriculture	As a soil mix because of its retention capacity for water and fertilizers and contains traces of elements for plants.	[1]
Animal bedding	Absorbing and deodorizing animal waste.	[1]
Animal feed	Bonding agents in pelletizing animal feed.	[1]
Radioactive disposal	Absorbing the isotopes and fixing them against leaching.	[1]
Catalyst	Stable solid support for polymer catalysts.	[125]
Cement, mortar and aggregates	Reducing aggregate segregation, improving workability and impermeability.	[1]
Construction	Stabilizing the structures.	[3]
Clarification of wines	Reducing protein and iron content.	[1, 70]
Drilling fluid	Thickening and thixotrophic agent for colloidal dispersions.	[3, 126]
Floor adsorbents	Reducing shrinkage and removing filament adherence.	[1]
Food emulsion and stabilization	Mixing agent in oil / water systems and suspending agent for solid particles in liquid.	[1]
Foundry and casting	Optimizing the foundry consistency due to its binding capacity, high fusion temperature and high dry strength.	[157]
Gene and cell therapy	Bio-material interacts well with proteins and nucleic acids.	[118]
Greases	Stabilizing the gel properties of greases.	[1]
Ink	Controlling consistency and penetration during printing.	[1]
Iron ores and fuels	Pelletizing finely ground ore concentrate.	[1]
Medicines, pharmaceuticals and cosmetics	Stabilizing antibiotics into bentonite pastes; medicinal use due to its antidotal effect; improving barium sulphate suspensions for radiological tests; and purifying and concentrating of vitamins.	[1, 3]
Motor vehicles	Reinforcement material for nanocomposites.	[12, 144]
Paint	Suspending and thickening agent in water-based paints; emulsifying agent in water and oil-based paints; improving pigment suspensions, viscosity, thixotropy control, brushability and spraying.	[1, 3, 126]
Paper	Preventing the agglomeration of fine particles of pitch, tar, waxes and resinous material which cause defects; increasing the pigments; improving the pigment distribution; dispersing and adsorbing pigment particles.	[1, 126]
Pesticides	Thickeners, carriers and diluents in pesticide preparation.	[1, 3]
Petroleum derivatives	Recovering the chemical derivatives.	[4]
Rubber	Thickener and stabilizer for latex.	[1]
Smectite-organic complexes, hybrid and bio-materials	Forming complexes and hybrid materials by various reactions with organics and polymers. Improving mechanical property of composites.	[14, 46, 120, 121, 124, 165]
Soaps, cleaning and polishing compounds	Partial replacement for fatty-acid due to its emulsifying action, affinity for carbon particles, detergent effect, dispersing agent and water softening action.	[1]
Water clarification	Dispersing, absorbing and adsorbing pollutants from water as outlined in Table 7. The use of alum can flocculate the clay to gather and collect the colloidal materials.	[1, 6, 7, 55, 132, 155]
Water impedance	Impeding the movement of water through earthen structures and retard similar movement through cracks in rock and concrete structures.	[1]

4.5 Composites

4.5.1 Introduction

Materials that are made up by two or more constituents with significant difference in physical and chemical properties are known as composites. The constituents retain their properties and do not dissolve or merge into one another in the composite form. Often, a strong component known as additive or filler is present in an abundant and softer constituent known as the matrix. Examples include filler materials such as graphite, carbon and tungsten are used to strengthen metal matrix such as aluminium, magnesium and copper; polymer matrix such as polyesters and vinyl esters; and ceramic matrix such as zirconia, alumina and aluminium nitride [166, 167].

On the other hand, bio-composites are composite materials comprising of bio-derived constituents. Common additives used include plant fibres such as cotton, flax, hemp and wood; animal fibres such as wools and chicken feathers; and mineral particles such as natural clays. The matrices for bio-composites may be polymers and proteins ideally derived from renewable sources such as vegetable oils and starches [11, 168]. Unlike composites, fillers and matrix polymers interact with each other in bio-composites [11].

The term composite is used as the generic term to represent all composite subcategories. They are designed to display combinations of the best characteristics of each of the component materials. The introduction of additive into a matrix changes the composite characteristics such as morphology, mechanical, viscoelastic and thermal stability properties [11, 167].

4.5.2 Petroleum-Based Plastic and Bioplastic Composites

For the past few decades, research has been going on to find a better alternative for petroleum-based plastics (petroplastics). Petroplastics are non-biodegradable, generate waste in production and is a major cause of marine hazards [11]. Bio-based plastics are the new generation materials that have attracted much attention due to environmental concerns, the awareness of petroplastic hazards and the availability of sustainable raw materials [11, 46, 169]. Examples of new environmentally friendly

materials are poly-ε-caprolactone (PCL), polyesteramide (PEA), polylactic acid (PLA), polybutylene succinate (PbS) and polyhydroxybutyrate (PHB) [119, 151, 170]. Amongst these, PLA which is a corn-derived thermoplastic polyester is the most widely used bioplastic in the market [11, 171]. Lately, more attention has been directed to using waste sources such as agricultural and meat processing waste to avoid competition that bioplastics have with food production [21, 22, 34, 46].

Bio-materials are highly appreciated due to multifunctionality and biodegradability. Biodegradable term refers to the ability of a material to degrade by enzymatic action of living microorganisms into carbon dioxide, water and biomass under aerobic conditions or into hydrocarbons, methane and biomass under anaerobic conditions [45, 46]. Biodegradability is important for the environment especially for greener disposal of single use and short-life plastic packaging.

Although bioplastics have achieved significant commercial success, its high cost relative to conventional plastics is the main inhibitor for vast application. Relative to the petroplastic industry, bioplastics represent only a small portion of the overall plastic industry [171]. However, future demand for bioplastics looks strong with market acceptance is forecast to grow rapidly as illustrated in Figure 21. This is attributed to large technical innovations toward enhancing the properties of bioplastics. The demand for bioplastics in the US is projected to soar at a 20 % growth rate through 2016 to 250 000 tonnes, valued at US$ 680 million. Increase in production will reduce prices and enables bioplastics to compete with its petroleum-based counterpart more effectively [171].

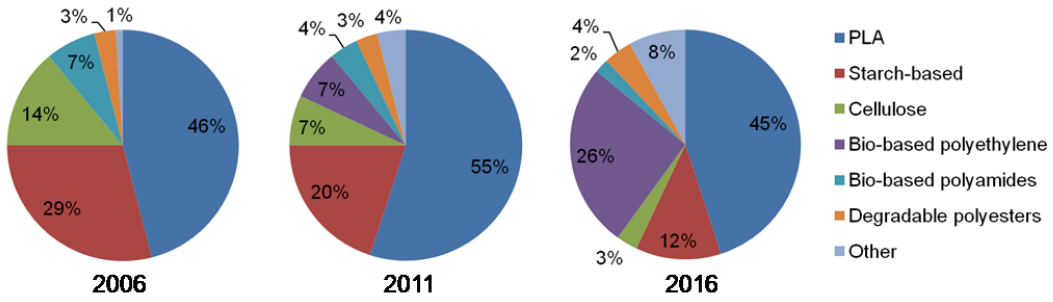

Figure 21: Breakdown of commercial bioplastics based on demand in the US. Study done by The Freedonia Group Inc. (cited by [171]).

Disadvantages of many recent bio-materials are 1) they do not dissolve in water but have high water uptake capacity or swelling, 2) they are prone to bacterial degradation (disadvantage of biodegradability) and 3) they are generally weak and have unsatisfactory mechanical and processing properties if prepared without reinforcement fillers [11].

Bioplastics are commonly made from natural sources such as proteins, carbohydrates and cellulose. Proteins are good barriers against oxygen and aromas at low relative humidities, but are poor barriers against water due to their hydrophilic nature [22, 34]. These could be improved by incorporating nano-fillers such as bentonite. The main purpose of bioplastics is not to replace petroplastics entirely, but to focus usage in applications where biodegradability and / or sustainability of natural resources are advantageous [46].

4.5.3 Bentonite Reinforced Polymers

Numerous materials have been added into bioplastics to improve properties such as heat resistance and mechanical strength or to limit properties such as electrical conductivity and permeability to gas and water vapour. Stiff particles such as fibre and silica are added to improve mechanical strength. Compared to fibres, use of clay in composites is relatively new with incorporated particles being 1000 times smaller than fibres in conventional composites. Incorporation of nano-fillers into composites yields nanocomposites. Organically-modified bentonites are preferred in bio-composite production because they can promote strong interactions with the matrix polymers [11, 172].

Unlike the common clay minerals such as talc and mica, smectite clays such as bentonite can be exfoliated and dispersed as individual layers in polymers, each at ~1 *n*m thick. The exfoliated form of nanoclay has specific surface area of ~750 m^2/g and the aspect ratio of greater than 50 [10]. For that reason, bentonites nowadays are routinely used as additives in plastics to improve or change the mechanical properties [12-17]. As reinforcements, bentonites give unique qualities such as high strength and stiffness, good barrier properties against gases such as oxygen and nitrogen, good flame retardation and acceptable processibility [11, 80]. Because bentonite particles are

very small, they also offer extra benefits like low density, transparency, good flow, better surface properties and improved dimensional stability [11]. In addition, a great improvement in elongation at break of the composite has also been observed with bentonite reinforcement. It was reported that the elongation at break of PLA nanocomposites was increased by 36 % with just 4 wt% addition of montmorillonite (cited by [164]).

Difficulties in using unmodified bentonite in polymer composites include ensuring good separation between platelet layers and good interfacial adhesion between the polymer and the bentonite's surface [15, 122]. In many cases, bentonite is only partly dispersed during mixing resulting in aggregate formation. This causes little or no improvement compared to unfilled polymers [11]. Therefore, bentonite needs to be modified, for example with organics to increase their dispersity and compatibility with polymers [14, 122].

Sodium and calcium bentonite typically consist of layered flat sheets with a spacing of about 1.2-1.5 nm between sheets, resulting in a filler with a very high aspect ratio when exfoliated and well-mixed with polymer [15, 173]. When completely exfoliated, bentonites can be used to produce nano-composites that have improved properties compared to composites formed using micron-scale fillers [15, 46, 161]. Exfoliation is necessary because clay layers stack together in nature, meaning most of the layers are stuck in the inside and are unable to interact with the matrix [144].

The addition of small amounts of bentonite can increase the strength of the material significantly. For example, the addition of 5 wt% of smectite to a koalinite clay increased the strength from 1931 to 5033 kN/m^2 [1] and the incorporation of 4.2 wt% of exfoliated Mt into polyamide-6 (PA6) increased the Young's modulus by a factor of 2.1 [119]. In foundry industry, clay is mixed with sand to provide bonding strength and plasticity to moulding sands [1]. Back in 1980's, the world's famous car manufacturer, Toyota pioneered the commercial use of nanoclays as additive to polymers to improve strength [144, 174]. They found that by adding as little as 5 wt% montmorillonite, the strength of ordinary nylon-6 increased remarkably [144]. A similar finding was reported on PA6-clay nanocomposites. At a clay additive level of 2-5 wt%, the nanocomposites showed a significant improvement on mechanical

strength, thermal stability and improved barrier properties especially with application of exfoliated clays (Table 12).

Microscopy validation such as TEM can be used to confirm the exfoliation hyphothesis such as in the case of PA6 reinforced with nanoclays (Figure 22). The nanoclays used in this example were Cloisite Na^+, Cloisite 10A and Cloisite 30B. They are sodium montmorillonites in pure form, organically-modified with di-methylbenzyl (hydrogenated tallowalkyl) ammonium and bis-(2-hydroxyethyl) methyl (hydrogenated tallowalkyl) ammonium respectively [175]. Reinforcement with unmodified clay resulted in very little or no exfoliation with low level of filler dispersion in the PA6 matrix (Figure 22A). The filler particles are large due to stacking of several platelets together. The condition was significantly improved at reinforcement with organically-modified clays as shown in Figure 22B and C. The filler dispersions are more homogeneous and well-oriented in a specific direction. This is because of the smooth flow of fillers within the matrix as a result of improved interaction. Therefore, when shearing forces such as extrusion are applied, the fillers are aligned according to the processing material's flow [175].

Table 12: Properties of PA6-clay nanocomposite [10].

PA6 blend	Clay amount (wt%)	Tensile strength (MPa)	Young's modulus (GPa)	Charpy impact strength (kJ/m2)	HDT* (^oC) at 145 MPa
PA6	0	69	1.1	2.3	65
PA6 with exfoliated nanoclay	4.2	107	2.1	2.8	145
PA6 with nonexfoliated nanoclay	5.0	61	1.0	2.2	89

**Heat distortion temperature*

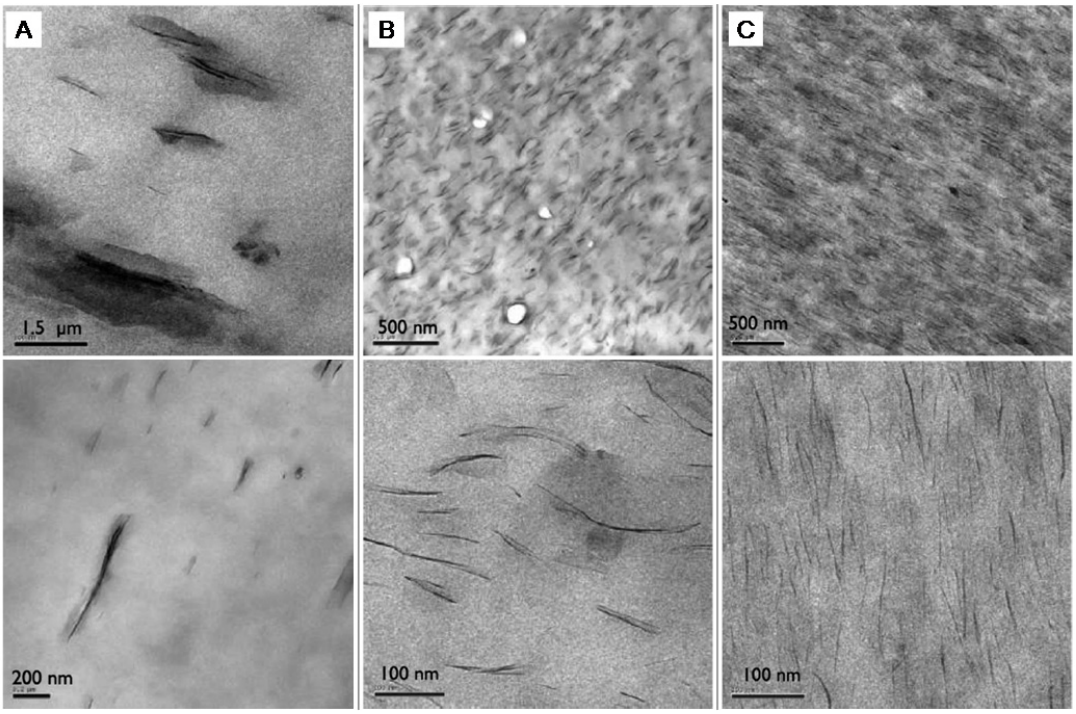

Figure 22: TEM images at low and high magnifications of PA6 nanocomposites reinforced with A) Cloisite Na^+, B) Cloisite 10A and C) Cloisite 30B [175].

4.5.4 Novatein Thermoplastic Protein

Meat rendering plants in New Zealand processed more than 5 million cows into food products per year [38]. This produces high volume of raw blood to be treated due to environmental concern. For economic reason, this by-product is often dried into bloodmeal and sold as low-cost fertilizer. Raw blood contains 80% water, 18% protein and 2 % fats and minerals. Upon drying at more than 100 ^oC for a period of time, bloodmeal yields 90 % protein which is utilized as a precursor for renewable thermoplastic called Novatein Thermoplastic Protein (NTP) [43, 44].

There are three main steps in NTP formation, namely breaking the existing covalent crosslinks between protein chains, evaporating processing water and formation of new interactions. Chemical additives such as urea, water, sodium dodecyl sulphate (SDS) and sodium sulphite (SS) are added during production to reform the structure. Tri-ethylene glycol (TEG) is added as plastizer in addition to water. Previous work done suggested that SS is responsible for breaking the covalent bonds, SDS and urea are used to disrupt the protein-protein interactions and water functions as

plasticizer [43, 44]. The mechanical properties of NTP at various formulations of the additives were investigated for optimization. Mechanical properties of NTP and other widely used biopolymers are summarized in Table 13.

In comparison with other biopolymers, conditioned NTP scored moderate tensile strength (σ) and Young's modulus (E). No data was available on ultimate elongation (ε) of NTP but based on the average values of σ and E, it can be expected the ultimate elongation could be comparable to PLA. With suitable reinforcement, the mechanical properties of NTP can potentially be improved.

Table 13: Mechanical properties of NTP in comparison to other bioplastics.

	σ (MPa)*	E (GPa)*	Toughness (MPa)	ε (%)	Ref.
NTP					
Unconditioned	6.5 ± 0.58	0.24 ± 61.3	0.92 ± 0.21	-	[43]
Conditioned (23 °C, 50 % RH, 7 days)	21.1 ± 1.8	1.48 ± 83.4	0.18 ± 0.04	-	[43]
PLA	21-60	0.35-350	-	2.5-6	[176]
	-	3.4 ± 0.1	-	2.0 ± 0.2	[11]
Linseed oil PU	57	1324	-	6	[11]
PGA	60-99.7	6-7	-	1.5-20	[176]
PCL	20.7-42	0.21-0.44	-	300-1000	[176]
PHB	40	3.5-4	-	5-8	[176]

* Abbreviations: polyurethane (PU), polylactic acid (PLA), polyglycolic acid (PGA), poly-ε-caprolactone (PCL) and polyhydroxybutyrate (PHB).

4.5.5 Nanocomposite Production

Three main approaches to produce clay-based nanocomposites are polymerization, melt compounding and solution blending. In the polymerization method, monomers are mixed with clay to produce exfoliated nanocomposites. The melt compounding method requires heat application and often clay is mixed with polymer in a heated extruder. Solution blending consists of mixing a polymer and clay in a solvent and removing the nanocomposites from the solvent afterwards [11]. Melt-processing with a variety of shear devices such as extruders, mixers and ultrasonicators result in high level of clay exfoliation and dispersion. Among these devices, twin-screw extruders are the preferred choices due to effectiveness [177].

When clay is mixed with liquid, the liquid molecules penetrate between the clay layers resulting in layers being swollen, exfoliated or unaffected as depicted in Figure 23. These behaviours depend on the type of clay. For example in water, smectites swell or exfoliate due to high ionic charge, talc is unaffected because it is neutral and has no inter-gallery space and mica layers are impenetratable by water molecules due to its high concentration of intermolecular cations; making the binding between layers too strong for water to enter [11]. Exfoliation of clay layers into individual layers happens when the clay swells beyond the point that they are no longer organized into stacks [144].

Once swollen, the interlayer cations are exchanged with organic molecules as illustrated in Figure 24. There are three modes of filler formations in the matrix during mixing process namely phase-separation, intercalation and exfoliation. The latter is more desirable to ensure better dispersion with high volume ratio to the polymer matrix. The presence of organic molecules lowers the ionic bond strength between the layers and renders it compatible with biopolymers [11, 178].

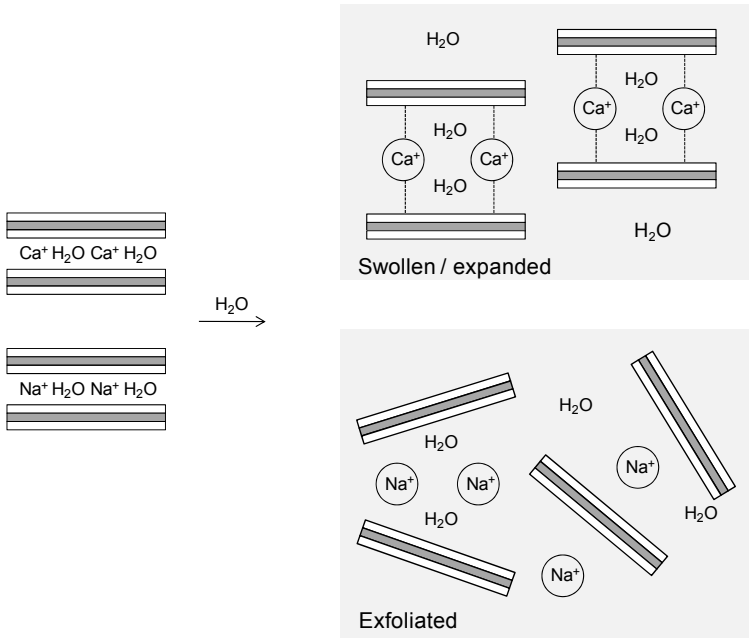

Figure 23: Swelling of calcium bentonite and exfoliation of sodium bentonite layers in water.

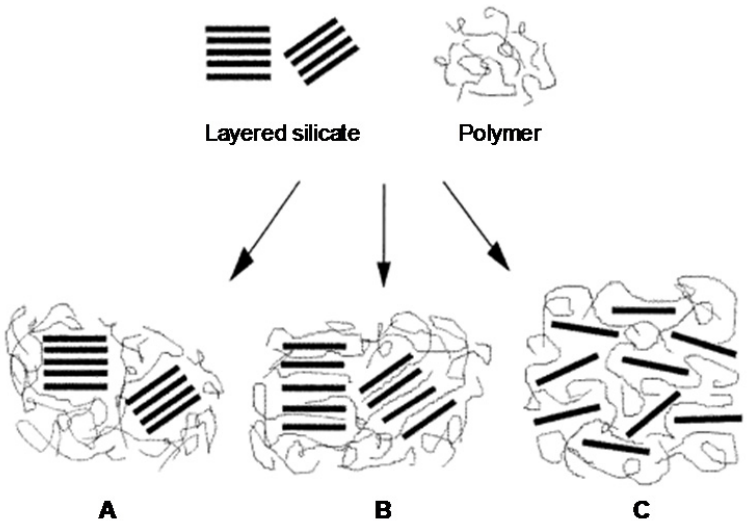

Figure 24: Schematic diagrams of A) phase-separated (microcomposite), B) intercalated or expanded (nanocomposite) and C) exfoliated (nanocomposite) clay layers in polymer matrix [178].

4.6 Summary

There is an abundance of work done on clay application for adsorption (Table 7) and its potential use as filler (Table 11). So far, the application of clay has been limited to only adsorption processes or as filler. As a reinforcement material, clay has to be purchased at considerable cost. For example, research grade organic-modified montmorillonite costs NZ$ 104.5 per 500 g [179]. For bioplastic reinforcement, fillers have to be modified with organics to increase the compatibility with the polymer matrix. Therefore, by modifying bentonite using organics from stickwater can potentially fill this gap. It is a dual-functional process, reducing stickwater's BOD and producing bio-based fillers.

Exfoliation of bentonite could potentially be achieved from organic adsorption. The modified bentonite after treatment can be used as filler in NTP to produce bioplastic composites. The modified filler could improve the mechanical properties of NTP by promoting various interactions as well as enhancing the dispersion of particles in the matrix. Bloodmeal and stickwater are meat rendering by-products and bentonite is a natural clay that exists in abundance. By combining them, a new bio-composite material can potentially be developed from what has been traditionally considered as waste.

CHAPTER 5

EXPERIMENTAL

5.1 Introduction

Experimental work in this thesis is divided in three parts; 1) gelatin and stickwater adsorption using bentonite, 2) settling of bentonite from gelatin and stickwater solutions and 3) production of NTP reinforced with bentonite. Prior to these, raw materials were characterized for morphology, particle size, charge, PZC, SSA, basal spacing and thermal degradation.

The first step was commenced by finding the suitable dosage of adsorbent and equilibrium treatment time for adsorption on model solution. Gelatin solution was used as model solution because stickwater's protein is primarily gelatin. The adsorption was conducted using calcium, sodium and octadecylamine bentonite. Experimental data was fitted to models for equilibrium isotherms and kinetic study. The model parameters were used to predict organic recovery from stickwater and were compared to experimental data from stickwater adsorption.

In the second part, sedimentation or settling of treated bentonite in gelatin solution was investigated using a settling column. Adsorptions at selected conditions were scaled-up into 1.2 L volume. The equilibrium solutions were transferred into a settling column and the change in turbidity was recorded over time. Experimental data on the conditions that gave settling were used to build a particle settling model. This was then tested on stickwater solution. Treated bentonite after adsorption and settling experiments were recovered for use in bio-composite development.

The final stage is the reinforcement of NTP with various bentonite samples. Extrusion and injection moulding were used to fabricate the composite specimens and were characterized further to study the change in properties. The equipment and materials used are summarized in Table 14 and Table 15 respectively.

Table 14: List of equipment used.

Equipment	Manufacturer and model
BET surface analyzer	Quantachrome Instruments- Nova 2200e
Centrifuge	Sigma centrifuges- 6-15
	Eppendorf- Minispin Plus
Charge detector	Mutek- PCD03
Conditioning chamber	Llyod Instruments
Desiccator	Jencons
Dynamic mechanical analyzer	Perkin-Elmer- DMA 8000
Fan oven dryer	Contherm- Thermoter 2000
FE-SEM	Hitachi- S-4700
Fine balance	Sartorius- CP225D
Fridge	Elba
Food processor	Kenwood multipro
Freeze dryer	Labconco- Freezone 2.5
Freezer	Kelvinator
Furnace	Jetflow
Grinder	Ika- MF10
Injection moulder	BOY- 35A
Laser particle sizer	Malvern Instruments- Mastersizer 2000
Magnetic stirrer	Chiltern Scientific- MM31
Microtome	Reichert-Jung- Ultracut
pH meter	Eutech Instruments- CyberScan 100
Settling column	Waikato Glass Blower
TEM	Philips- CM 30
Tensile tester	Instron- 33R-4204
TGA	TA Instrument- SDT 2960 DTA-TGA
Tri-blade granulator	Castin machinery
Turbidity meter	Hach- 2100P
Twin-screw extruder	Thermo Prism TSE-16-TC
Ubbelohde tube	Cannon Instrument- 1B M423
UV spectrometer	Pharmacia Biotech- Ultrospec 2000
Water bath	Grant- GD120
Water pump	Little Giant Pump Co.- 2E-38NY
X-ray machine	Philips- X'Pert

Table 15: List of materials used.

Materials	Supplier	Grade	Additional notes
Adsorption			
Calcium and sodium bentonite	Transform Minerals	Industrial	Volcanic origin [1]
Octadecylamine bentonite	Sigma-Aldrich Chemicals	Research	25 % octadecylamine ($CH_3(CH_2)_{17}NH_2$) and 75 % sodium Mt [179]
Gelatin	Davis Gelatin	Food	Bovine origin. pH 5.4 at 5 wt% in distilled water at 30^oC
Stickwater	Local meat rendering plant	Non-food	Bovine origin. pH 5.2-5.4 at 20 ^oC
Chemicals			
Na_2HPO_4 (s), NaH_2PO_4 (s), NaCl (s), HCl (aq) and KCl (s)	Ajax Finechem	Analytical	
NaOH (s)	Scharlau	Analytical	
NTP composites			
Bloodmeal	Local meat rendering plant	Industrial	Bovine origin. ρ 1300 kg/m^3
Urea	Ajax Finechem	Analytical	CON_2H_4
Sodium dodecyl sulfate (SDS)	Merck	Technical	$C_{12}H_{25}NaO_4S$
Sodium sulfite (SS)	BDH Lab	Technical	Na_2SO_3
Tri-ethylene glycol (TEG)	Orica Chemnet	Technical	$C_6H_{14}O_4$

5.2 External Lab Analysis

Approximately, 300 g of raw stickwater was sent to SGS Laboratory in Auckland to analyze for protein, fat and nitrogen content. For carbonaceous biochemical oxygen demand ($cBOD_5$) analysis, gelatin and stickwater at 2 % protein concentration were treated with calcium and sodium bentonite (CaBt and NaBt) at 3 g bentonite / 100 ml solution under native solution pH (~pH 5.2). The equilibrium solutions were centrifuged at 4000 rpm for 20 minutes and 500 g supernatant was sent to Hill Laboratory, Hamilton.

5.3 Solution Preparation

5.3.1 Phosphate Buffer Solution

Phosphate buffer solution (PBS) stock of 1 L was prepared at 0.1 M concentration by mixing 10.9 g Na_2HPO_4, 3.2 g NaH_2PO_4 and 90 g NaCl with distilled water on a magnetic stirrer. The PBS was adjusted to different pH using 1 M hydrochloric acid (HCl) and 1 M sodium hydroxide (NaOH). It was filtered using Whatmann filter

paper (100 μm) to remove suspended materials. Dilutions were made with distilled water into 0.02 M concentration prior to use.

5.3.2 Gelatin Solution

As the first step, protein standard curves were prepared by measuring UV absorbance at 280 nm (UV_{280}) for gelatin solutions between 0 to 25 mg/ml. Four separate curves were prepared at pH 3, 5.23, 7 and 9. The absorbance data and plotted graphs of "UV_{280} absorbance vs. protein concentration" are presented in Table 43-46 (Appendix-2A) and Figure 77 (Appendix-2B) respectively. The curves were used to calculate the protein concentration in gelatin solution. PBS solutions at respective pH were used as baseline solutions to zero the UV spectrophotometer.

Gelatin powder was weighed using a fine balance and mixed into 100 ml PBS solution in a Schott bottle. The mixture was placed in a water bath at 37 ^{o}C to dissolve the gelatin. Gelatin solutions of 100 ml were made at different concentrations of 4, 5, 6, 10, 15 and 20 mg/ml in 0.02 M PBS at pH 3, 5.23, 7 and 9. Solution pH was adjusted using 1 M HCl and NaOH. The pH range was designed to be at different ionization states of gelatin and bentonite at below and above the PZC.

Gelatin concentration of 2 % (Ge2%) was chosen because that is the highest gelatin concentration in solution that can be analyzed using UV_{280} without dilution. This was done to minimize human errors related to dilution.

5.3.3 Stickwater at 2% Protein Concentration

Frozen stickwater was thawed in a water bath at 37 ^{o}C and diluted with distilled water into 2 % protein concentration. The solution was adjusted to pH 3, 5.23, 7 and 9 using 1 M NaOH and HCl. The solution was incubated in a water bath at 37 ^{o}C prior to use. Stickwater was diluted to 2 % protein concentration (SW2%) to replicate the gelatin concentration in the model solution.

5.4 Properties of Bentonites, Gelatin and Stickwater

5.4.1 Particle Size Distribution and Specific Surface Area

For dry particle, untreated samples of calcium, sodium and octadecylamine bentonite in powder form were examined directly under SEM. From SEM images, the mean diameters of few hundreds bentonite platelets were determined using CorelDraw and Microsoft Excel software. Due to irregular shape of bentonite platelets, diameter measurement was taken as the length of the longest chord within each particle.

For hydrated or swollen bentonite, laser analysis was used to determine the particle size and SSA. Bentonite powder of 3 g was added into Mastersizer machine and water vortex mixing was applied. Laser light was then emitted across the solution and the scattered light was measured by a sensor. An average value of three replicates was calculated. Octadecylamine bentonite is a hydrophobic substance that forms clumps in water. Thus, it was not directly added into the Mastersizer machine but the clay was mixed with distilled water using magnetic stirrer for 4 hours and left overnight to let most of the clumps settle to the bottom or top. The supernatant which contains suspended particles was used for the size analysis.

For adsorbed samples, equilibrium solution of gelatin treated with calcium and sodium bentonite at equilibrium (60 min) were used for particle size analysis instead of powder sample.

5.4.2 BET Surface Area

Surface area of dry adsorbents was determined by nitrogen adsorption using a BET analyzer. Known weight of powder adsorbents were degassed at vacuum condition at 150 ^{o}C for 24 hours. Nitrogen adsorption was measured across five points of relative pressure (P/P_o) for 6 hours. Mean value of BET surface area was determined using Multi-Point BET method from the list of calculation techniques available from the analysis software.

5.4.3 Overall Bentonite Charge

The net charge of bentonite was determined using a technique developed by the United States Department of Agriculture and Soil Survey (USDA) (cited by [2, 112]). Bentonites at different weight concentrations were mixed with 30 ml of 1 M KCl solutions and distilled water in 100 ml beakers. The mixtures were stirred on magnetic stirrers for 10 minutes before recording the final pH. The difference between the two final pH values was calculated using the formula:

$$\Delta pH = pH_{H_2O} - pH_{KCl} \quad (30)$$

A positive value for ΔpH indicates negatively charge bentonite and a negative ΔpH indicates positively charged bentonite.

5.4.4 Point of Zero Charge

A particle charge detector was used to measure the streaming (electrical) potential across a solution. Stickwater and gelatin solutions were prepared at different concentrations in deionized water and incubated at 37 ^{o}C in a water bath.

Electrolyte solutions of 0.5 M HCl and NaOH were used to adjust the streaming potential until it reached 0 mV (equal number of positive and negative charges in the solution). The solutions were then measured for pH. Solution and electrolyte were added slowly into the sample holder to avoid turbulence and bubble formation.

This technique was unsuitable for suspended particles such as bentonite in solution. Bentonite settled at the bottom and the measured streaming potential reflected the value of the solution not the particles. The PZC of bentonite was taken from literature.

5.4.5 Surface Morphology and Mineral Contents

Bentonite surface morphology was studied using a field emission scanning electron microscope (FE-SEM). Energy dispersive spectroscopy (EDS) was used to identify elements on bentonite surface. Bentonite samples before and after adsorption

(at initial gelatin concentration of 2 %) were dried overnight at 105 ^{o}C in an oven, ground and sieved at 250 μm using a benchtop grinder and re-dried for overnight at 105 ^{o}C. The temperature was chosen to remove the surface moisture because water evaporates at 100 ^{o}C. The samples were stored in a desiccator for at least overnight at 20 ^{o}C prior to analysis and composite reinforcement.

Powder samples were lightly scattered on carbon tape on aluminium stub holders. They were sputter-coated with platinum to improve conductivity and enhance image quality. The SEM was operated at 5 to 20 kV.

In order to minimize the change in surface morphology due to heat application and grinding, selected samples of treated CaBt and NaBt in gelatin 2 % were frozen in a refrigerator for 2 days and freeze-dried for another 5 days. Unlike powder samples in FE-SEM, chunks of freeze-dried samples were analyzed using a similar method.

5.4.6 Surface Morphology in Liquid State

In cryogenic SEM (Cryo-SEM), a cryogenic preparation chamber was assembled to the main SEM machine and liquid nitrogen was circulated to stabilize the system for two days prior to the experiment. The equilibrium solutions were centrifuged at minimum speed and time to increase the pellet viscosity to enable the sample to be transferred onto the standard sample holder (stub). It was then instantly frozen using liquid nitrogen and transferred into the vacuum system. The subsequent steps are similar to FE-SEM except liquid nitrogen must be constantly replenished to keep all areas of the SEM cold.

The ideal sample preparation of entirely cryogenic systems (Figure 25) is proved to be unattainable due to reasons outlined in Section 4.3. The difficulties in cryo-SEM analysis include sample preparation and lack of standardization as reported by other workers [149, 150].

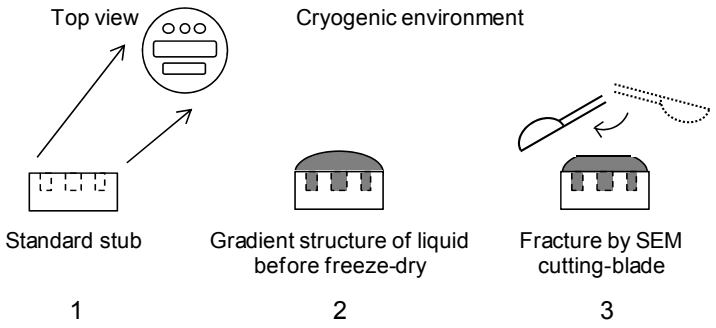

Figure 25: Ideal steps of cryo-SEM sample preparation.

5.4.7 Basal Spacing of Bentonite

Basal spacing (*d*-value) was determined using X-ray diffraction (XRD). XRD was carried out at low angle configuration of $2\theta = 2^{o}$ to 12^{o}, a scanning rate of $2\theta = 2\ ^{o}$/min, operating current of 40 mA, a voltage of 40 kV using $CuK\alpha_1$ radiation with a wavelength of 1.540598 Å. Basal spacing was calculated using Bragg's law (Equation 24 in Section 3.6.3). A silicon standard was used to calibrate the deflection positions. Sample preparation was outlined in Section 5.4.5.

5.4.8 Thermalgravimetric Analysis

A 10 mg sample was placed in a ceramic crucible and heated side by side with a reference sample (empty identical crucible) using a simultaneous DTA-TGA analyzer. The samples were heated from 20 to 800 °C at a heating rate of 10 C/min with air flowing at 150 ml/min. Sample preparation was outlined in Section 5.4.5.

5.5 Gelatin Adsorption

5.5.1 Bentonite Dosage

Previous work showed that 0.04 – 0.05 g bentonite / g stickwater was a suitable dosage for recovering protein from stickwater [24]. This was further examined for a model gelatin solution using calcium bentonite. A dosage of 1, 3 and 6 g of bentonite was added into 5 and 20 mg/ml gelatin solution. The mixture was stirred using a magnetic stirrer for 1 hour. Equilibrium solution was analyzed for protein concentration by UV spectrophotometer at a wavelength of 280 nm.

5.5.2 Adsorption from Model Solution

Gelatin solution of 100 ml was transferred into 120 ml beaker and mixed with 3 g of bentonite. The mixture was stirred on a magnetic stirrer at room temperature until equilibrium. The equilibrium time is reached when the UV_{280} reading reached a plateau. Three 1.5 ml samples were taken at 5, 10, 20, 40, 60 minutes and placed into 1.5 ml centrifuge tubes. The samples were centrifuged at 14 500 rpm for 2 minutes using a mini centrifuge. The supernatant was collected and analyzed for protein content. Bentonite pellets after 60 minutes treatment with an initial gelatin and stickwater concentration of 2 % were collected for SEM, TGA and XRD analysis.

5.5.3 Protein Concentration in Model Solutions

Gelatin is the only organic present in model solution, therefore protein and organic concentration refers to the same entity. Standard curves of UV_{280} absorbance vs. protein concentration were made prior to the adsorption experiments (Figure 77, Appendix-2B). Protein concentration during adsorption was calculated by recording the UV_{280} absorbance of the solution and converted the readings into concentration values using the standard curve equations. Protein recovered and absorbed were calculated using Equation 31 and 32 respectively [54]:

$$\text{Percentage recovery (\%)} = \frac{C_o - C_e}{C_o} \times 100 \tag{31}$$

$$C_r \text{ (mg / g)} = \frac{V\,(C_o - C_e)}{m} \tag{32}$$

where C_o and C_e is the initial and equilibrium protein concentration (% or mg/ml), C_r is the amount of protein adsorbed on bentonite at equilibrium (mg/g), V is the solution volume (ml) and m is the bentonite mass (g). Percentage (%) was used as the unit of protein concentration unless stated otherwise (1 % equals to 10 mg/ml).

5.5.4 Adsorption Isotherm Models and Kinetics

Experimental data from gelatin adsorption was fitted into linearized forms of Langmuir, Freundlich, Langmuir-Freundlich and Temkin isotherms (Table 6, Section 3.5) in Microsoft Excel. Model parameters were calculated using the equations obtained from curve fitting. The best fit model was also used in kinetic study.

The adsorption rate, k_1 (g/mg.s) was determined by fitting the non-equilibrium form of the L-F isotherm to bentonite gelatin concentrations measured at 5 minute intervals. Desorption rate, k_2 (1/s) was calculated using the equation below:

$$k_2 = \frac{k_1}{K_{lf}} \tag{33}$$

The adsorption isotherm and kinetics were studied separately at pH 3, 5.23, 7 and 9. The calculated isotherm constants and rate kinetics were used to predict protein recovery from stickwater in a single stage adsorption process.

5.5.6 Adsorption from Stickwater

Calcium and sodium bentonite at 3 g were added into 100 ml stickwater 2 % in a 120 ml beaker and stirrer for 1 hour using a magnetic stirrer. For model solutions, three 1.5 ml samples were centrifuged for UV_{280} absorbance. This method did not work for stickwater due to its murky appearance even after high speed centrifugation. Samples were ashed to quantify the organics adsorbed onto bentonite.

A benchtop centrifuge was used instead of mini centrifuge to separate pellet and supernatant. Three 15 ml stickwater / bentonite samples (at equilibrium) were transferred into preweighed centrifuge tubes and centrifuged at 4000 rpm for 20 minutes. The centrifuging time was increased to achieve the same sedimentation as with using faster centrifuge in Section 5.5.2. The mass of wet pellet and supernatant were recorded and samples were kept for analysis.

5.5.7 Protein Quantification after Adsorption from Stickwater

Ceramic crucibles (75 ml-size) were heat-treated at 650 ^{o}C for 2 hours, cooled in desiccators overnight and weighed prior to use. Known masses of pellet and supernatant from the stickwater adsorption experiments were transferred into separate crucibles. The samples were dried overnight in an oven at 105 ^{o}C to determine moisture content and ashed in a furnace at 650 ^{o}C for 20 minutes to determine the organic content. Mass of crucible with sample, before and after every step was recorded for mass balance calculations. The procedure was conducted in triplicate.

A mass balance was applied over the entire system (centrifuging, weighing, drying and ashing steps) to account for the mass loss at every stage. A process flow diagram and mass balance equations used are illustrated in Figure 26. The unit used throughout the process was gram (g).

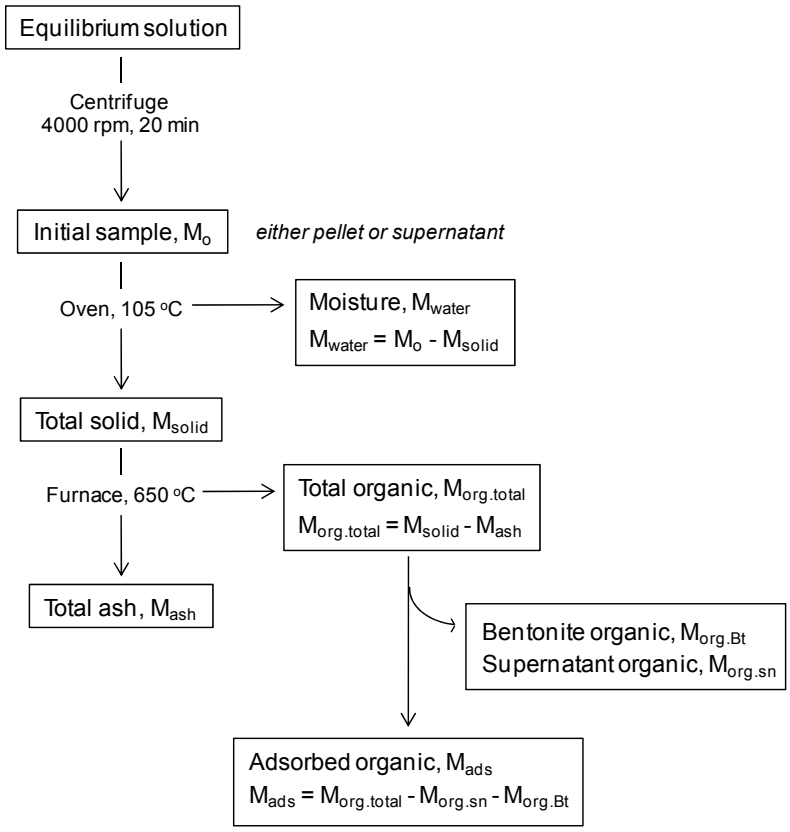

Figure 26: Ashing flow diagram for treated bentonite with stickwater (Equation 34-36).

5.6 Settling of Bentonite from Solution

5.6.1 Settling Column Fabrication

A high quality boron silicate 1200 ml cylinder from Duran was modified with five sampling outlets as depicted in Figure 27. A 5 ml syringe was used for sampling through silicon septums to reach the solution in the settling column. Different syringes were used at different outlet points and sampling was done in order of outlet 1 to 5. Silicon septums were replaced occasionally to prevent leakage.

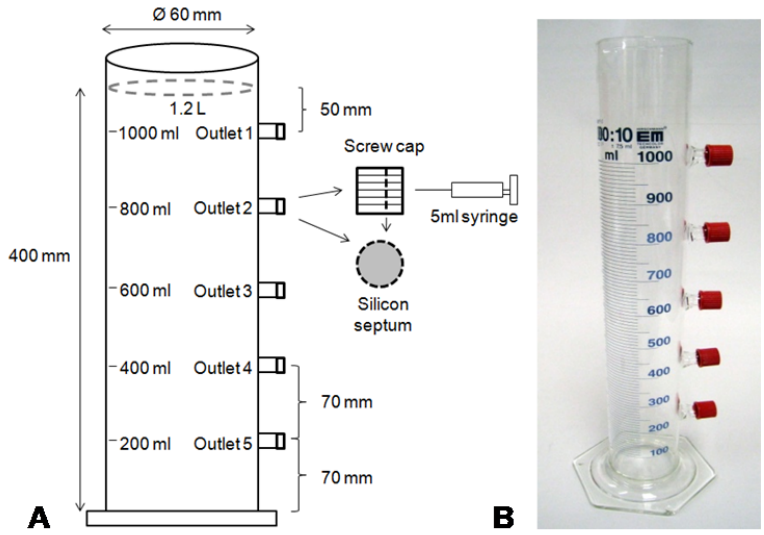

Figure 27: A) technical diagram and B) fabricated product of the settling column.

5.6.2 Bentonite Settling from Gelatin Solution

The adsorption experiments were repeated at 1200 ml volume for 0 (in PBS only) and 2 % gelatin concentration. The initial turbidity and UV_{280} were recorded prior to adsorption. A 36 g bentonite (0.03 g/ml concentration) was added to the solution on a magnetic stirrer and stirred for 1 hour. Equilibrium solution was transferred into a settling column and placed in a holding tank with heated water circulation. A water bath was used to heat water to 38.3 ^{o}C to maintain water circulation in the holding tank at 37 ^{o}C (due to heat loss to surrounding). A water pump was used to circulate water in a closed-system. The settling experiment was conducted isothermally to avoid gelling of solution. The process diagram is presented in Figure 28.

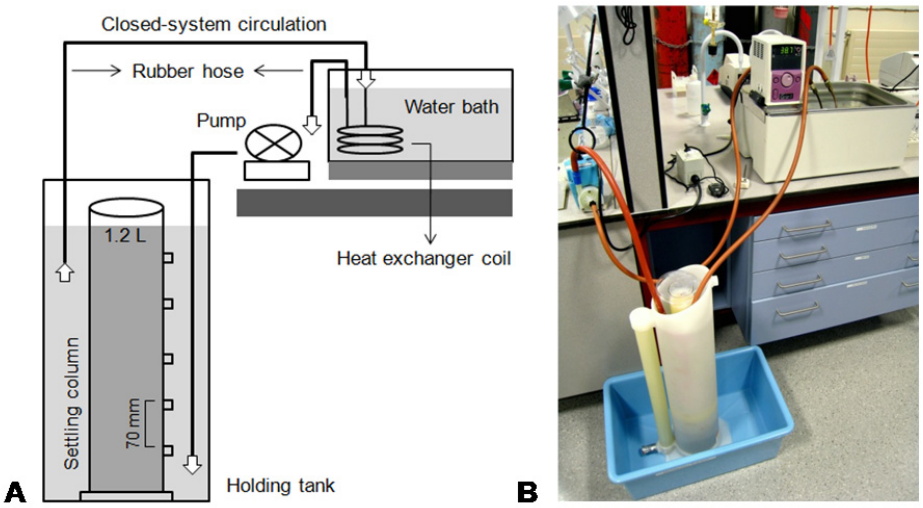

Figure 28: A) technical diagram and B) laboratory setup of a closed-system water circulation for settling experiment.

5.6.3 Bentonite Settling in Stickwater

Equilibrium stickwater / bentonite solutions from adsorption were transferred into three 15 ml clear test tubes, covered with parafilm and incubated at 37 ^{o}C in a water bath for overnight. The conditions that showed settling were repeated according to Section 5.6.2.

5.6.4 Analysis of Settling Experiments

Turbidity standard curves were prepared for calcium and sodium bentonite by measuring turbidity of bentonite solution using a turbidity meter. For model solutions, four standard curves were prepared at pH 3, 5.23, 7 and 9 by adding bentonite at 0 to 22 mg into 15 ml of 0.02 M PBS. For stickwater, 0 to 15 mg of bentonite was added into diluted stickwater at 0.02 % concentration at pH 3. The recorded turbidity for gelatin solution is tabulated in Table 47-50 (Appendix-3A) and the graphs of "turbidity (NTU) vs. bentonite concentration (mg/ml)" are presented in Figure 78 (Appendix-3B) whereas the data and graphs for stickwater solution can be referred from Table 51 (Appendix-4A) and Figure 79 (Appendix-4B).

Samples of 5 ml (1 ml for stickwater) from settling experiments were withdrawn at 10, 30, 60, 90, 120 and overnight at five outlet points using separate syringes. The samples were analyzed for turbidity. The height of the pellet formation at the bottom

of the column was recorded at every sampling interval when visible. The overnight pellet was processed according to Section 5.4.5 for analysis and composite reinforcement.

5.6.5 Viscosity Measurement

Gelatin solutions at 0, 10, 20, 30, 40 and 50 mg/ml at pH 3, 5.23, 7 and 9 were prepared according to sample preparation for the adsorption experiment (Section 5.3.2). Relative viscosity was measured using a Ubbelohde tube (Figure 29). The tube was filled with 15 ml gelatin solution and placed in a water bath at a pre-set temperature. The time taken for the solution to travel the predetermine distance (shaded area in Figure 29) or efflux time, t_{efflux} (s) was measured in triplicate at 20, 30, 40, 50, 60, 70 and 80 ^{o}C. It should be noted that the experiment was carried out at one specific concentration over the entire range of temperatures before changing to a new concentration and pH. The procedure was repeated for stickwater solutions.

Ubbelohde tube measures viscosity of solution relative to water's dynamic viscosity of 1 mPa.s or 1 cP at 20 ^{o}C. Kinematic viscosity, μ_k (mm^2/s) is given by:

$$\mu_k = t_{efflux} \times C_u \tag{37}$$

Gelatin dynamic viscosity, μ_f (kg/ms or Pa.s) is obtained by:

$$\mu_f = \mu_k \times \rho_f \tag{38}$$

where C_u is the Ubbelohde tube constant (0.05108 mm^2/s^2) and ρ_f is the solution density (g/ml).

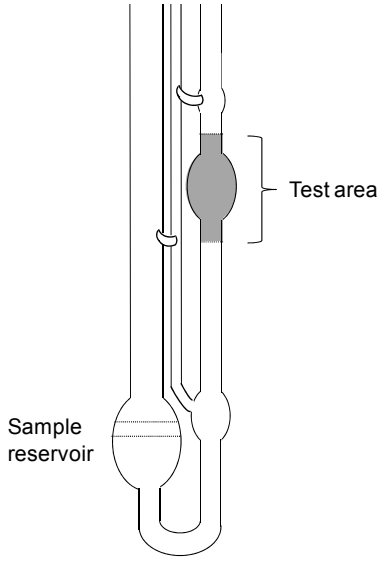

Figure 29: Ubbelohde tube for kinematic viscosity measurement.

5.6.6 Density Measurement

For gelatin solution, density measurement was carried out parallel to viscosity measurement in Section 5.6.5. A 1 ml solution was transferred into a pre-weighed 1.5 ml centrifuge tube and weighed using a fine balance. For stickwater, 20, 50 and 100 ml of stickwater were transferred into pre-weighed volumetric flasks and weighed.

For density of bentonite pellets, adsorption experiments as outlined in Section 5.5.2 and 5.5.6 were repeated at 300 ml volume. The equilibrium solution was transferred into four 50 ml centrifuge tubes, centrifuged at 4000 rpm for 20 min. The pellets were recovered, dried and the masses were recorded, m_{Cr} (kg). Three identical 50 ml measuring cylinders were filled up with 40 ml tap water as the initial volume (V_o) and placed on a fine balance. The reading was zeroed and a random amount of bentonite pellet, m (kg) was added into the measuring cylinder and the final volume of water, V_f (ml) was recorded. Density, ρ (kg/m^3) was calculated using Equation 39 below and was done in triplicate.

$$\rho = \frac{m}{V_f - V_o} \tag{39}$$

5.7 Preparation and Evaluation of Bentonite Reinforced Bloodmeal

5.7.1 Formulation of NTP Composites

Ingredients in Table 16 were weighed into a beaker and water was added. The mixture was stirred and heated between 50 to 60 ^{o}C until visibly clear. Bloodmeal powder was sieved, weighed and transferred into a food processor. The hot solution and bloodmeal were blended for 5 minutes and TEG was added. The mixture was further blended for 5 minutes to obtain a homogeneous mixture. For NTP composites, bentonite was added at 0.25, 0.5 and 1 part per hundred parts bloodmeal (pph_{BM}) into pre-weighed bloodmeal in a food processor prior to the hot solution. The powder formulations were kept in zip-lock bags and stored in a fridge overnight prior to extrusion and injection moulding.

Table 16: Standard recipe of NTP [43, 180].

Ingredient	Amount	
	Mass (g)	pph_{BM}
Bloodmeal	200	100
Urea	20	10
Sodium dodecyl sulfate (SDS)	6	3
Sodium sulfite (SS)	6	3
Tri-ethylene glycol (TEG)	40	20
Distilled water	80	40

5.7.2 Fabrication of NTP Composites

The prepared composite formulations in Section 5.7.1 were extruded using a twin-screw extruder, palletized using a tri-blade granulator at 4 mm mesh and moulded into dog-bone shape specimens according to ASTM D638-03 standard using an injection moulder. Figure 30 illustrates the composite fabrication process and Table 17 outlines the parameters used. Details of the processing zones of the twin screw extruder in shown in Figure 31.

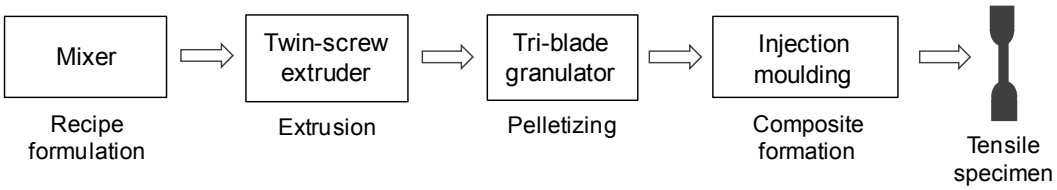

Figure 30: Process diagram of NTP composite production.

Table 17: Temperature profile of extrusion and injection moulding [180-182].

Extrusion	Injection moulding
Temperature profile (°C)	
Feeding zone: 70 Mixing zone 1: 100 Mixing zone 2: 100 Mixing zone 3: 100 Mixing zone 4: 100 Die: 120	Feeding zone: 100 Mixing zone 1: 115 Mixing zone 2: 120 Mixing zone 3: 120 Nozzle: 120 Mould: 70
Other parameters	
Screw speed: 150 rpm Torque: 50-60 % (12 Nm per screw maximum)	Screw speed: 200 rpm Injection pressure: 150 bar Back pressure: 2 bar Residence time in mould: 40 s

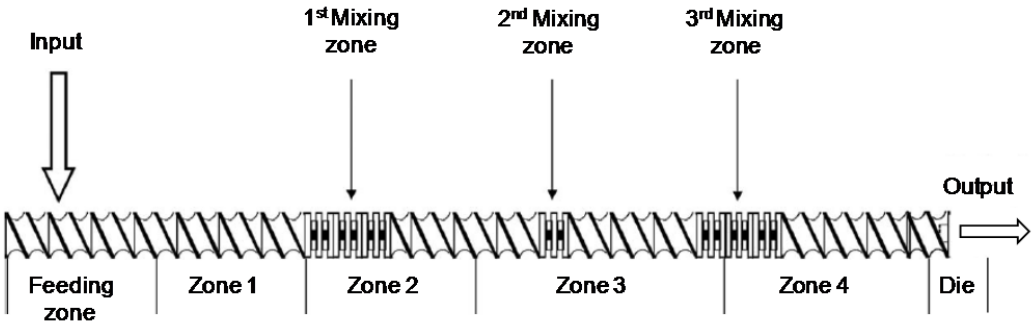

Figure 31: Extruder screw configuration [183].

5.7.3 Composite Tensile Testing

Injection moulded specimens were conditioned at 23 °C and 50 % relative humidity (RH) for 7 days prior to tensile testing. The tensile strength, Young's modulus and elongation at maximum break were analyzed according to ASTM D638-86 method using a tensile tester, fitted with a 5 kN load cell and with a cross head speed of

5 mm/min. A 50 mm extensometer was attached to the middle part of test specimen to measure strain. Load vs. extension data were obtained from the machine-interface software. All tensile properties values reported were machine-generated except for Young's modulus that was determined by re-plotting the "stress-strain" curves and a secant modulus was calculated between 0.0005 to 0.0025 strain. At least five samples were tested for each composition at room temperature of 20 ^{o}C and RH of 50 %.

5.7.4 X-Ray Diffraction, Thermalgravimetric Analysis and Scanning Electron Microscopy

Conditioned test specimens from injection moulding were cut into smaller pieces for XRD and were ground and sieved into powder for TGA analysis. The XRD and TGA methods were outlined in Section 5.4.7 and 5.4.8. Fracture surfaces from selected tensile specimens were cut and placed on carbon tape on aluminium stub holders. They were sputter-coated with platinum and analyzed under SEM at 5 to 20 kV.

5.7.5 Dynamic Mechanical Analysis

A sample with the approximate dimensions of 12.8 x 6.5 x 3.5 mm was analyzed using the single cantilever bending system at a temperature range of -60 to 150 ^{o}C, 1 Hz frequency and 0.03 mm dynamic displacement. The sample was cooled using liquid nitrogen and heated at 2 ^{o}C/min. The storage modulus ($E^{'}$), loss modulus ($E^{''}$) and loss factor (tan δ) were recorded. Glass transition temperature (T_g) was determined from the peak of tan δ curves.

5.7.6 Transmission Electron Microscopy

Selected unused tensile specimens were microtomed to less than 100 *n*m thickness using a diamond knife at room temperature. A colour interference card was used to determine the true section thickness after sectioning. The cut section was carefully transferred onto a standard 200-mesh copper grid from a water bath. The access water on the grid was wicked off with a wedge of filter paper and the grid was kept in a petri dish and stored in a desiccator at room temperature prior to analysis. TEM photographs were taken at accelerating voltage of 100 kV.

CHAPTER 6

CHARACTERIZATION AND ADSORPTION

6.1 Introduction

As the first step toward gelatin adsorption, the adsorbents or the solid-phases were characterized according to methods outlined in Section 5.4. Some important properties are particle size, specific surface area and overall charge. Adsorbate solutions were characterized for composition, density and viscosity. These properties influence adsorption and settling, therefore a thorough understanding is important.

The point of zero charge of gelatin was determined to find suitable pH conditions for adsorption. Then optimum adsorbent dosage and equilibrium treatment time were determined from gelatin adsorption at different starting protein concentrations. After the optimum conditions were established, adsorption of model and stickwater solutions were conducted in a similar condition on all adsorbents. By doing so, the adsorption results from model solution are comparable to stickwater.

Adsorption data was recorded at specific time intervals until equilibrium was reached. The adsorption data was fitted to isotherm models to investigate the maximum extent of gelatin adsorption onto bentonite at different conditions. The recovered solid-phases were analyzed for changes to investigate the effect of protein adsorption on bentonite layers.

6.2 Properties of Bentonite, Gelatin and Stickwater

6.2.1 Physical Properties of Calcium, Sodium and Amine Bentonite

Bentonite properties determined from experiments are summarized in Table 18. For particle size determined by laser analysis, it should be noted that the values of mean diameter represent hydrated bentonite while size determined by SEM corresponds to dry particles. Laser sizing could result in a discrepancy due to the assumption of cylindrical shape particle whereas bentonite comprises of platelet sheets. Therefore,

the mean size distribution provided from laser analysis is a collective measurement of the length of platelet edges and surfaces. Examples of full size particle distributions are presented in Figure 80 (Appendix-5).

Compared to SEM, laser analysis gave a smaller average particle size for CaBt and NaBt as the layers were possibly exfoliated in water. When hydrated, NaBt registered a 73 % decrease in particle size compared to 33 % for CaBt. Platelet layers of CaBt are held more tightly because of the divalent charge (Ca^{2+}), therefore less exfoliation compared to monovalent (Na^{+}) charged NaBt. Amine Bt had the smallest particle size from SEM but gave a two-fold increase in size when hydrated. This is due to its hydrophobic nature that caused the particles to form clumps or aggregates to minimize the contact with water molecules.

Bentonite is composed of silica and alumina sheet-like units arranged in a way that smectites are essentially books of sheets or laths. The charge interaction between sheets is somewhat diffuse as a result of isomorphous substitutions in the octahedral layer. The individual sheets are loosely held together and during adsorption, the cations are easily substituted with organics or large amounts of water can enter between the sheets, separating them apart (exfoliate). As a consequence, smectite clays are readily dispersed in water into extremely small particles, resulting in a high surface area beneficial for adsorption [1, 9, 39].

Table 18: Properties of bentonite.

Bentonite type	Diameter (μm)		N_2-BET surface area (m^2/g)	Specific mass (g/cm^3)	pH in distilled water at 10 wt%
	Dry (SEM)	Hydrated (laser)			
Calcium	21.09	14.16	60.31	2.70 [143]	10.8
Sodium	15.09	4.01	88.98	2.70 [143]	9.6
Amine	12.03	26.08	208.25	-	4.3

Table 19: Difference in pH of bentonite in distilled water and KCl solution.

Bentonite type	Dosage (g / 30 ml)	ΔpH
Calcium	150	0.86
	300	1.06
	450	1.07
Sodium	150	0.61
	300	0.68
	450	0.71
Amine	150	-0.34
	300	-0.22
	450	-0.17

The overall charge of bentonite determined according to Section 5.4.3 is summarized in Table 19. It can be seen that CaBt and NaBt had an overall negative charge as indicated by positive ΔpH and the opposite was observed for amine Bt. The difference in charge of amine Bt compared to CaBt and NaBt is attributed to its amine composition. Dissociation of amines in electrolytes dictates the overall charge of the particle and the process is pH-dependent. Amine bentonite was observed to disperse well in KCl solution but not in water, further emphasizing its hydrophobic nature.

From the result in Table 19, it is expected for CaBt and NaBt to give better protein adsorption compared to amine Bt because CaBt and NaBt have a negative charge. Sodium bentonite is potentially a better adsorbent than CaBt because of its small particle size and high SSA (Table 18). However, CaBt is advantageous over NaBt by having a divalent ion (Ca^{2+}) compared to monovalent ion (Na^{+}) of NaBT. Even though BET analysis indicated amine Bt has a very high surface area, this alone will not give a high adsorption capacity because protein molecules are amphoteric and large. Therefore, proteins can form multi-layers on a solid-phase. In addition, adsorption is also significantly influenced by whether the solid-phase is hydrophilic or hydrophobic. Amine Bt could result in poor adsorption compared to the rest but it would serve as good comparison to study the effect of hydrophobicity and organic modification of bentonite in adsorption system.

6.2.2 Properties and Composition of Gelatin and Stickwater Solutions

Biochemical oxygen demand ($cBOD_5$) analysis was conducted to investigate the effectiveness of bentonite to remove organics from the solutions. Protein content was determined for stickwater in order to make dilution prior to adsorption because stickwater's organic content is not entirely protein unlike the model solution where the organic presence can be attributed solely to gelatin. The reports provided by the external labs are summarized into Table 20 and presented in Figure 81, 83 and 84 (Appendix-6A, B and C).

From Table 20, the stickwater had significantly lower $cBOD_5$ than values from the literature (150 000 O_2/m^3) [25]. Comparing the value to stickwater produced from the same local rendering plant, the $cBOD_5$ obtained was higher than what was reported at 59 000 g O_2/m^3 [87]; this further emphasises the variation of the content and the need of model solution for isotherm study.

The discharge consent for the rendering company is 50 kg BOD per day. At its stickwater daily production volume of 2000 m^3, the allowable discharge amount is only 25 g O_2/m^3 (compared to 66 000 g O_2/m^3 produced). Thus, without a proper treatment process, stickwater cannot be directly discharged [87]. From Table 20, at 2 % protein concentration in stickwater (SW2%), treatment using CaBt and NaBt at 0.03 g clay / ml solution gave 18 and 35 % decrease in $cBOD_5$ respectively from 34 000 g O_2/m^3. In comparison to decrements of 50 and 64 % obtained for the same treatment in model solution. Reduction in $cBOD_5$ suggests the potential use of bentonite to remove organics from the solutions.

From Table 21, undiluted stickwater had 6.67 wt% solids, which is 45.3 % higher than reported in literature (3.65 %) even though they were produced at the same plant. Stickwater 2 % was prepared by diluting stickwater on the basis of protein concentration. Therefore, the rest of mass compositions were not necessarily changed proportionally with dilution. At 2 % protein concentration, stickwater had 3.57 wt% organics, meaning that not only protein (gelatin) but other components such as fat and volatile solids also contributed to the overall organic content. For the model solution, the total 2 % organic was attributed to gelatin alone. It is apparent that at the same

protein concentration, the properties of model solution and stickwater are somewhat different.

In terms of rheological properties, stickwater has a lower density but higher viscosity compared to gelatin solution. The fat in stickwater reduced the overall density of the solution while viscosity is increased due to the suspended solids. Gelatin solutions were found to gel at a specific concentration and temperature while stickwater solutions did not gel across all conditions tested (Table 52, Appendix-7). This may be attributed to gelatin in stickwater being comprised of short-chain molecules as the result of high temperature and pressure used in the rendering plant (Chapter 2). On the other hand, commercial gelatin was produced by boiling the materials at minimal temperature only sufficient for bond breaking but not too high to degrade the gelatin. Upon cooling, gelatin molecules in model solution undergo a conformational transition to recover the collagen triple-helix structure and form a gel [34, 67].

Table 20: External lab analysis results (literature values in bracket).

Sample	$cBOD_5$ (g O_2/m^3)	Protein (%)	N_2 (%)	Fat (%)
Gelatin 2 % (Ge2%)	14100			
Ge2% treated with CaBt	7100			
Ge2% treated with NaBt	5100			
Raw stickwater	66000 (150000) [25] (59000) [39, 87]	3.5 (4-5) [25] (3.7) [47]	0.57 (0.6) [47]	1.6 (0.37) [39, 87]
Stickwater 2 % (SW2%)	34000			
SW2% treated with CaBt2	28000			
SW2% treated with NaBt	22000			

Table 21: Summary of adsorbate properties (literature values in brackets).

Properties	Stickwater	Stickwater 2%	Gelatin 2%
Solid content (wt%)	6.67, (3.65) [39, 87]	4.10	1.78
Protein content (wt%)	3.5	2	2
Moisture content (wt%)	93.33	95.90	98.22
Ash content (wt%)	0.90, (0.67) [47]	0.53	0.06
Organic content (wt%)	5.79	3.57	1.73
Native pH	5.2-5.5 (4.2) [87], (5.23) [24]	5.2-5.5	5.1-5.3
Density (kg/m^3)	1006, (910) [39]	1004	1336
Viscosity @ 37^{o}C (cP or mPa.s)	2.591 (1.095) [87]	1.196	1.001

The analysis was conducted on solutions in their native pH.

6.2.3 Point of Zero Charge

From titration, gelatin had an average PZC at pH 5.23 (Table 22), similar to results reported by other workers [24, 184]. This is attributed to the carboxyl, amino and guanidine groups on the side chain of gelatin [185]. However, Johlin showed that gelatin had two PZCs at pH 4.68 and 5.23 while Hitchcock and Zheng found only one at pH 4.86 and pH 5.05 respectively [20, 184, 186]. This was further explored by calculating the overall charge of gelatin across a wide pH range based on its amino acid composition (Table 42, Appendix-1B). The finding is summarized into Figure 32.

From Figure 32, gelatin is completely positively charged at pH below than 4 and negatively charged above pH 12. In between these two extremes, the overall gelatin charge is a combination of positive and negative charges. The graph also suggests that gelatin is becoming more negatively charged at increasing pH. However, due to its amphoteric nature, one should remember that large positive and negative regions could still exist even when they are balanced to give an overall neutral charge (PZC).

PZC of bentonites was taken from literature as pH 7 [2, 24, 160]. However, it was suggested that alumino-silicate clays such as bentonite have two PZCs arising from silica (PZC < pH 3) and alumina (PZC at pH 7) [89, 94, 160]. Recall that, bentonite is a 2:1 clay consisting of 2 tetrahedral sheets of Si-O separated by an octahedral sheet of Al–O–OH. The silica resides at the surface while alumina at the edge [1, 2, 89, 138]. From isomorphous substitution, bentonite surface is always negatively charged and the edge is positively charged. This amphoteric characteristic allows adsorption of cations and anions to occur regardless of pH.

Table 22: Titration summary of gelatin PZC.

Solution	Protein concentration (%)	pH at 0 mV potential		
		Run 1	Run 2	Run 3
Gelatin	2	5.22	5.27	5.32
	5	5.17	5.20	5.21
		Average PZC = 5.23		

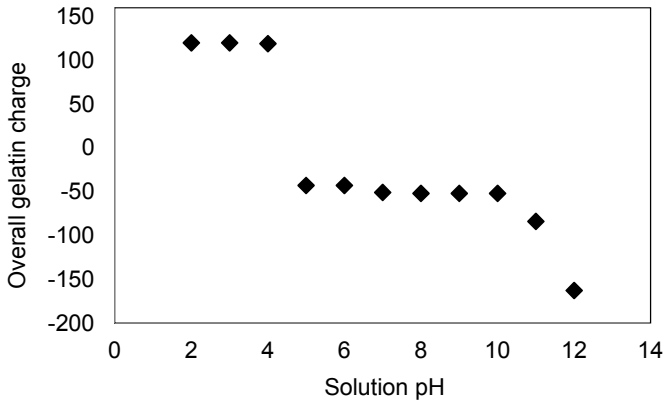

Figure 32: Overall gelatin charge with pH, based on amino acid composition (Table 42, Appendix-1B).

6.3 Gelatin Adsorption onto Bentonite

6.3.1 Selection of pH and Temperature for Gelatin Adsorption

Phosphate buffer solution (PBS) is a polar solvent containing ions such as Na^+, PO_4^-, Cl^-, H^+ and OH^-. It was used in gelatin preparation instead of water to normalize solution pH. Depending on concentration, gelatin dissolves in polar solvents at certain temperature to form polyelectrolyte solution. Early experimental work showed that a 20 mg/ml (2 %) gelatin in PBS solution dissolves at 30 ^oC (Table 52, Appendix-6). At this stage however, interaction between gelatin molecules and PBS solvent is dominant. At higher temperature when there is sufficient activation energy, the conformation of the gelatin molecules is minimally disturbed by solvent / gelatin interactions and the molecules exist in more random coil forms. A temperature of 37 ^oC was chosen for adsorption to ensure the gelatin is fully dissolved into aqueous solution.

Gelatin adsorption was done at pH 3, 5.23, 7 and 9. The pH were chosen based on gelatin and bentonite overall charge. Gelatin is positively charged at pH 3, equal number of positive and negative charge at pH 5.23 (PZC), negatively charged at pH 7 and 9 (Figure 32). Above pH 12, gelatin is fully negatively charged and was observed to precipitate out of solution. The precipitation happened because gelatin became more hydrophobic and repulsion was very high between molecules. Bentonite has an overall positive charge at pH 3 and 5.23, neutral at pH 7 (PZC) and negative charge at

pH 9. However, the platelet surface is always negatively charged. Gelatin was expected to adsorb best when it carries the opposite charge to bentonite.

6.3.2 Adsorbent Dosage

Previous work showed that 0.04 – 0.05 g bentonite / g stickwater was a suitable dosage for recovering protein from stickwater [24]. This was further examined for a model gelatin solution using CaBt. From Figure 33, increase in bentonite loading resulted in higher recovery of protein from solution. For example, at initial gelatin concentration of 0.5 % (C_o 0.5%), a 75% recovery was obtained using 6 g of bentonite in 100 ml model solution. However, the yield of gelatin adsorbed per gram bentonite, C_r (mg/g) was the lowest. A similar trend was observed in C_o 2%. Therefore, a dosage of 0.03 g bentonite / ml solution was selected as it gave a good compromise between adsorption yield and recovery. Similar findings were obtained in methylene blue adsorption using biotite [51] and aniline adsorption [7] on chromium bentonite where the recovery percentage increased but adsorption capacity decreased at increasing adsorbent loading.

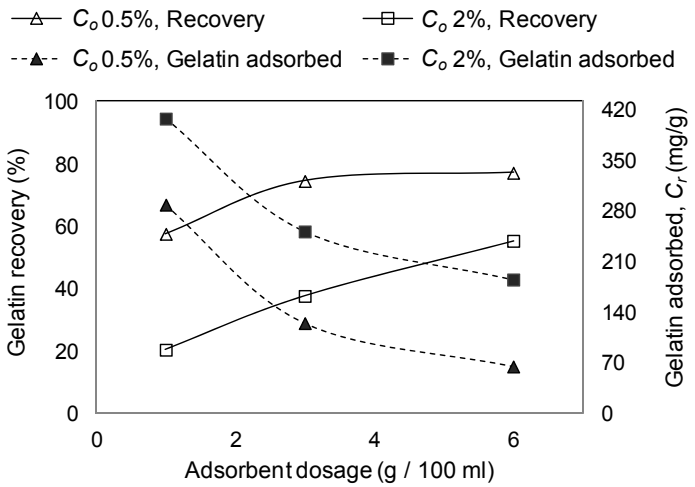

Figure 33: Relation between adsorbent dosage, gelatin recovery and amount of gelatin adsorbed (calcium bentonite, pH 7). Datapoints are mean values of three replicates.

6.3.3 Adsorption Equilibrium

Gelatin adsorption onto bentonite is a type-I isotherm as depicted in Figure 34 and Figure 35. Adsorption started immediately after mixing with bentonite until equilibrium. Gelatin adsorption on bentonite was very rapid with equilibrium being reached within 20 minutes (Figure 34). Rapid adsorption was also reported in other clay-based adsorption processes such as adsorption of amino acids from distilled water [156], protein traces from model wine [70], aniline from aqueous solution [7] and amoxicillin from distilled water [6]. From Figure 35, C_r generally increased with C_o. It was clear that the bentonite saturation was not obtained for some pH conditions and bentonite types.

A summary of gelatin adsorption at C_o 2% is given in Table 23. It can be seen that the maximum saturation of amine Bt for the conditions tested was at pH 9. At this pH, gelatin has an overall negative charge which suggests adsorption was based on hydrophobic interactions. However, TGA results (Table 31) showed no net increase in organic matter (discussed later on) suggesting very little adsorption. Amine has a dissociation constant or pKa of 10, so it is possible that the octadecylamine had a lower affinity for the bentonite at higher pH and was more readily displaced by the gelatin. XRD revealed an increased in *d*-value confirming the exchange reaction had occurred (Table 31).

Sodium bentonite had the highest C_r at pH 3 and 5.23 and the lowest at pH 7. At pH 3, adsorption is attributed to combination of electrostatic (negatively charged bentonite surface and positively charged gelatin) and hydrophobic interactions (positive bentonite edges and positively charged gelatin). Adsorption was possibly a direct exchange between Na^+ ions and the charged groups on gelatin. As pH increased, the number of positively charged groups on gelatin decreased (Figure 32) possibly due to the abundance of OH^- ions and hence adsorption was lower at pH 7.

Similar adsorption patterns were observed for BSA and hemoglobin adsorption on montmorillonite [69, 70, 97], bovine serum albumin adsorption onto electrostatic microspheres [103] and chicken egg ovalbumin adsorption onto montmorillonite [70]. Hedges and Hare (1987) showed that sodium montmorillonite was not only good at adsorbing positively charged amino acids, but was also able to absorb uncharged

amino acids [156]. Arai and Norde (1990) noted that protein adsorption on a sorbent was sometimes enhanced with increasing protein hydrophobicity which suggests that there is less electrostatic repulsion occurring between protein molecules [187].

There was a drop in adsorption for CaBt and NaBt at pH 7, while the solution gelled at pH 9 for NaBt, making it impossible to analyze the gelatin concentration via UV absorbance. At pH 9, hydrophobic interaction between gelatin molecules was the highest compared to all pH tested due to large region of negative charges on gelatin. This interaction and the increase in crosslinking between gelatin and exfoliated NaBt layers could have increased the solution viscosity and led to gel formation.

Amine Bt and CaBt did not gel because they had a much larger particle size than NaBt in solution (Table 18). Sodium bentonite has more particles in solution than CaBt and amine Bt for the same amount of mass, making it easier for gelatin to crosslink the particles. Hydrophobic interaction between gelatin molecules possibly had predominated at higher pH, increasing the solution viscosity and for this reason a gel was formed. If this hypothesis is true, the recorded values of protein concentration for NaBt at high pH might have not reflected the true values in the solution. The recorded UV readings were possibly higher than the actual values because of cloudy solutions and resulted in higher final protein concentrations, thus a smaller yield, C_r.

Calcium bentonite showed the highest adsorption at pH 7 and 9 (Figure 35). At low pH, gelatin is positively charged, resulting in ion exchange reaction and electrostatic repulsion of same charged gelatin molecules. However, as pH increased, more side groups on the gelatin became negatively charged, so adsorption became a combination of ion exchange, electrostatic and hydrophobic interaction. It is possible that either the positively charged groups on gelatin displaced the calcium ions on the bentonite, the calcium ions having a 2^+ charge formed crosslinks between the negatively charged groups on the gelatin and the particles, and / or between the negatively charged groups on the gelatin. This hyphothesis can be supported by work done on CaBt flocculation in water by polyacrylamide (PAM), in which the author postulated that the flocculation could be attributable to crosslinking of divalent Ca^{2+} ions and PAM [126]. Lowest gelatin adsorption for CaBt was obtained at the PZC of gelatin, pH 5.23. Adsorption of catalase onto Fe (III)-montmorillonite showed similar

trend where the minimum adsorption was obtained at pH close to PZC of catalase and he also noted that adsorption of catalase can occur regardless of pH [117].

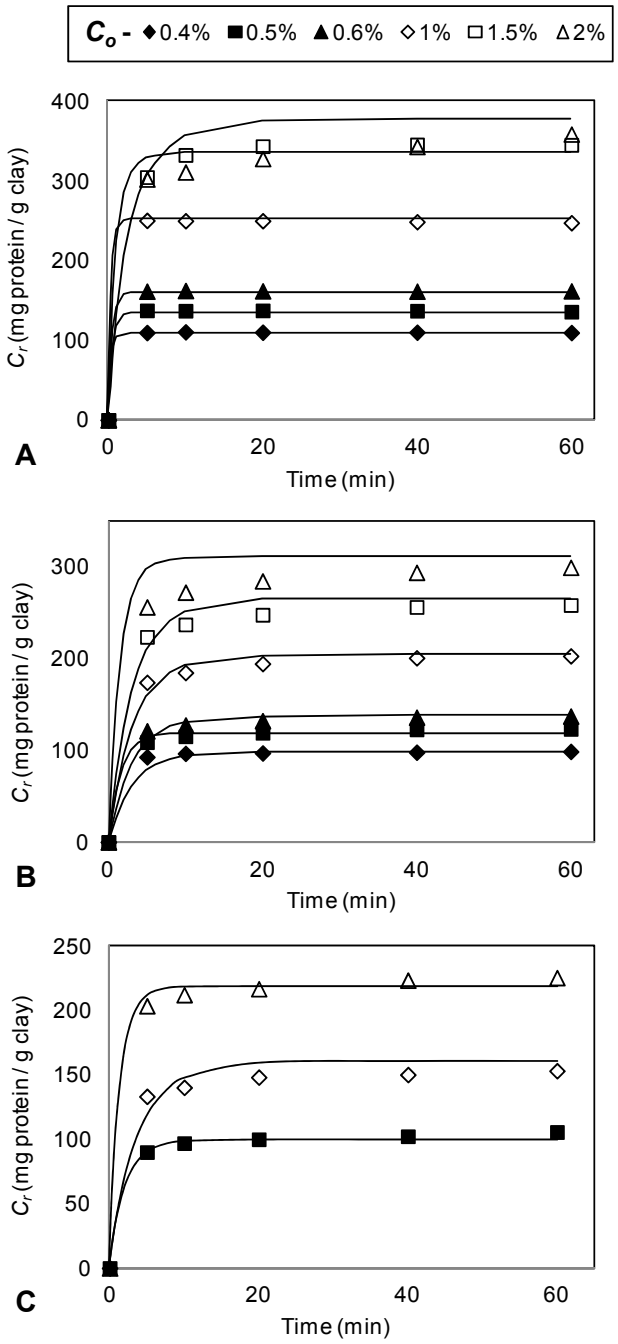

Figure 34: Equilibrium time for gelatin adsorption at pH 3 using A) calcium, B) sodium and C) amine bentonite. Lines indicate Langmuir-Freundlich models. Datapoints are mean values of three replicates.

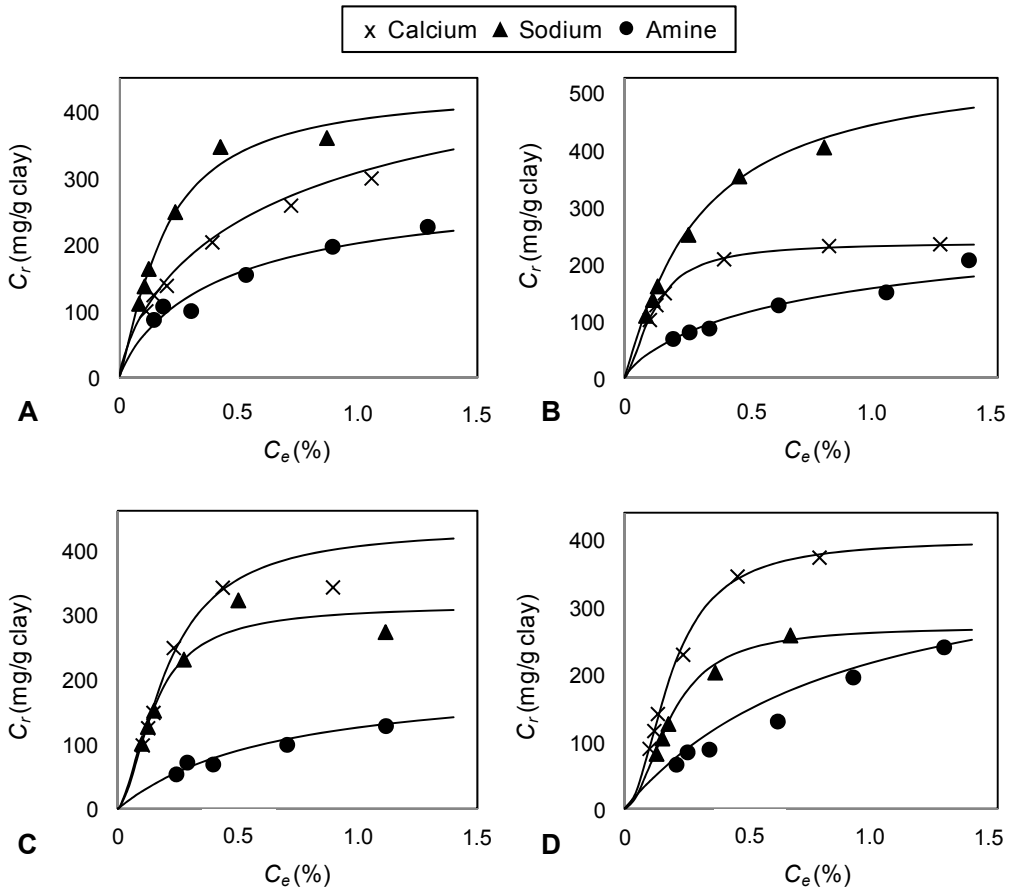

Figure 35: Gelatin adsorption equilibrium isotherms for calcium, sodium and amine bentonite and fitted Langmuir-Freundlich models (lines) at pH A) 3, B) 5.23, C) 7 and D) 9. Datapoints are mean values of three replicates.

Table 23: Equilibrium data for gelatin adsorption at C_o 2%.

Bentonite type	pH	C_e (%)	C_r (mg/g)	Recovery %
Calcium	3	1.05	298.31	45.94
	5.23	1.26	235.37	35.87
	7	0.89	342.49	53.48
	9	0.78	371.98	58.85
Sodium	3	0.87	359.07	55.44
	5.23	0.80	404.85	60.37
	7	1.11	273.41	42.41
	9	gel	-	-
Amine	3	1.32	225.54	33.50
	5.23	1.38	207.36	30.49
	7	1.54	154.39	21.13
	9	1.28	239.23	28.53

6.4 Adsorption Isotherm Models and Kinetic Study

6.4.1 Langmuir, Freundlich, Temkin and Langmuir-Freundlich Models

Some examples of linearized adsorption models are given in Figure 36 and all isotherm constants and regression coefficients are summarized in Table 24. Best fit linearized equations from curve fitting of adsorption data for all the isotherm models are given in Table 53 (Appendix-8). It is clear from Table 24 that the Langmuir and Langmuir-Freundlich (L-F) isotherms gave very good fits for gelatin adsorption on bentonite. This could be traced back to the principal concepts underlying the model. Langmuir assumes mono-layer adsorption with saturation whilst Freundlich assumes multi-layer adsorption with no saturation term. In the model gelatin system, multi-layer adsorption is highly possible due to multi-charges and large molecular structure of gelatin. Combining the models made L-F the most suitable model for the adsorption system.

Overall, the experimentally determined C_{rmax} are much lower than calculated theoretically using Langmuir and L-F models (Table 24). The difference could be because the models do not account for desorption of bound gelatin from solid-phase that might happen during centrifugation and steric hindrance from gelatin molecules. The latter could have resulted from structural restriction of gelatin molecules when adsorbing on the surface. In protein adsorption on immobilized metal ion gels, the author suggested “steric crowding effect” at the center of binding pores by multi-site protein solutes that resulted in much higher theoretical C_{rmax} compared to experimental values [105]. The Freundlich isotherm gave excellent fits for amine Bt, but did not represent the data well when CaBt and NaBt appeared to be saturated because it does not have a saturation term like the Langmuir and L-F isotherms.

The Temkin isotherm gave good fits for all bentonites across all pH except for NaBt at pH 7. Unfortunately, to achieve overall good fits for the Temkin model, calculation of C_r yielded negative values at solution equilibrium concentrations, C_e below ~0.1 %, which suggests the Temkin model is not suitable for describing type-I isotherms, and would only be suitable for predicting bentonite adsorption at C_e above 0.1 %.

For CaBt and NaBt, it appears that the term *n* (L-F) decreases with increasing pH. A higher value of *n* suggests favourability of adsorption at low pH. The *n* factor is useful to represent calcium displacement by gelatin, which if equilibrium dependent, the displacement is more likely to occur at higher gelatin concentrations. At pH 3, gelatin was fully positively charged, so it competed more successfully with calcium for binding sites on bentonite, leading to more favourable adsorption at low pH for CaBt and NaBt.

From Table 24, generally the constant terms for Langmuir (K_l) and L-F (K_{lf}) models appear to be higher for conditions where bentonite has a low C_{rmax} and lower for a high C_{rmax} which suggests there was some competition occurring between gelatin and the desorbed Na^+ and Ca^{2+} for binding sites on bentonite. If Na^+ or Ca^{2+} ions in solution were measured and combined with the pre-existing amount of Na^+ or Ca^{2+} on the bentonite, a competitive Langmuir isotherm could be used where k_2 (Table 25) is multiplied by $1+ [K(_{Na^+ \text{ or } Ca^{2+}}) \, . \, C(_{Na^+ \text{ or } Ca^{2+}})]$ to account for the competition between the ions and the gelatin. The competitive isotherm can remove the need to have the *n* factor because both the behaviour of the gelatin and ions could be accounted for.

For the amine Bt, the adsorption was found to be more favourable at low pH as indicated by high *n* values from L-F model. At higher pH, *K* is lower (much lower than for CaBt and NaBt) suggesting the rate of desorption is higher, possibly due to the overall negative charge of gelatin, reducing the interaction between the bentonite and gelatin. The model findings are in contrast to experimental data in Table 23 that shows amine Bt adsorbed best at pH 9. The reason being the models did not consider the effect of hydrophobicity of solid-phase on adsorption.

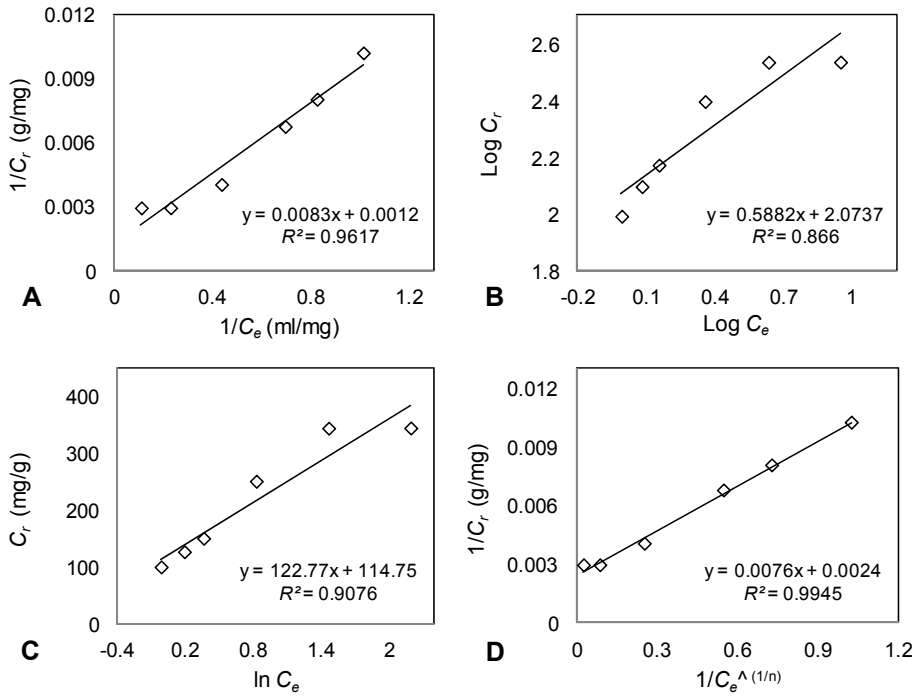

Figure 36: Linearized isotherm models for CaBt at pH 7 for A) Langmuir, B) Freundlich, C) Temkin and D) Langmuir-Freundlich. Datapoints are mean values of three replicates.

Table 24: Isotherm model parameters and regression coefficients for gelatin adsorption on bentonites.

Model parameters	Calcium bentonite				Sodium bentonite				Amine bentonite			
	pH 3	pH 5.23	pH 7	pH 9	pH 3	pH 5.23	pH 7	pH 9	pH 3	pH 5.23	pH 7	pH 9
Langmuir												
C_{rmax} (mg/g)	357	286	833	1111	556	625	455	588	227	233	192	357
K_l (g/mg)	0.35	0.63	0.15	0.10	0.33	0.26	0.32	0.14	0.42	0.21	0.17	0.11
R^2	0.99	0.98	0.96	0.97	0.99	0.99	0.96	0.97	0.86	0.96	0.93	0.96
Freundlich												
K_f	101	109	118	108	142	134	123	80	74	49	36	41
n	2.10	1.46	1.70	1.46	1.96	1.70	2.29	1.52	2.31	1.91	1.90	1.46
R^2	0.99	0.90	0.87	0.94	0.92	0.97	0.81	0.96	0.94	0.98	0.97	0.98
L-F												
C_{rmax} (mg/g)	556	238	435	400	435	556	313	286	302	300	200	400
K_{lf} (g/mg)	0.21	0.76	0.30	0.37	0.46	0.31	0.51	0.32	0.26	0.17	0.15	0.11
n	1.30	0.60	0.60	0.50	0.80	0.90	0.60	0.50	1.12	1.24	0.97	0.97
R^2	0.99	1.00	0.99	0.99	0.99	1.00	0.99	0.99	0.94	0.92	0.96	0.92
Temkin												
K_t	2.78	9.75	2.55	2.04	3.63	2.62	4.48	1.86	2.49	1.35	1.18	0.90
B	86.8	52.1	123	143	113	136	83.1	104	62.3	63.8	50.5	91.4
b (J/mol)	28.1	46.8	19.8	17.1	21.6	17.9	29.3	23.5	39.1	38.2	48.2	26.7
R^2	0.99	0.95	0.91	0.99	0.96	0.99	0.80	0.99	0.94	0.93	0.96	0.94

6.4.2 Kinetics

Using the L-F isotherm parameters obtained, k_1 was determined by fitting the non-equilibrium form of the isotherm to bentonite gelatin concentrations measured at 5 minute intervals. The models (solid lines, Figure 34) appear to fit well with the lower starting concentrations of gelatin, but at the higher concentrations there appear to be diffusion effects slowing the rate of adsorption, which could be due to the high loading of gelatin on the bentonite surface resulting in steric hindrance and possibly multilayer adsorption. Summary of adsorption and desorption rates for all conditions are shown in Table 25.

Adsorption rate, k_1 for CaBt and NaBt decreased with increasing gelatin concentration for most pH. The extent of the decrease appeared to be dependent on solution pH with the greatest decrease for CaBt was at pH 5.23 and 7. For NaBt, the largest decrease was at pH 3 and 7, while no decrease was observed at pH 5.23. Rate constants for amine Bt were consistent at all conditions. Unfortunately, this could not be explored further due to the equilibrium being reached within 5-10 minutes in many cases that limits the experiments for not being able to measure gelatin concentration rapidly enough to explore what was occurring within the first 5 minutes.

Table 25: Summary of rate kinetics from the Langmuir-Freundlich isotherm.

Bentonite type	C_o (mg/ml)	k_1 10^{-5} (g/mg.s) Solution pH				k_2 10^{-5} (1/s) Solution pH			
		3	5.23	7	9	3	5.23	7	9
Calcium	4	2.0	3.0	2.0	2.0	8.4	3.8	6.3	6.1
	5	2.0	1.2	2.0	2.0	8.4	1.5	6.3	6.1
	6	1.5	1.0	1.0	2.0	6.3	0.5	3.2	6.1
	10	1.5	0.4	1.0	2.0	6.3	0.5	3.2	6.1
	15	1.5	0.3	0.2	1.0	6.3	0.4	0.6	3.0
	20	1.5	0.2	0.2	0.8	6.3	0.2	0.6	2.4
Sodium	4	3.0	2.0	3.0	2.0	6.5	6.4	5.9	7.0
	5	3.0	2.0	3.0	2.0	6.5	6.4	5.9	7.0
	6	3.0	2.0	3.0	2.0	6.5	6.4	5.9	7.0
	10	3.0	2.0	3.0	0.7	6.5	6.4	5.9	2.4
	15	1.0	2.0	1.0	0.7	2.2	6.4	2.0	2.4
	20	0.5	2.0	0.5	-	1.1	6.4	0.9	-
Amine	5	2.0	2.0	2.0	1.0	7.7	11.6	13.5	9.1
	10	2.0	2.0	2.0	1.0	7.7	11.6	13.5	9.1
	20	2.0	2.0	2.0	1.0	7.7	11.6	13.5	9.1

6.4.3 Estimation of Gelatin Recovery

Gelatin recovery (Table 26) was estimated for a single stage adsorption process using the L-F isotherm constants (Table 24) and Equation 31. Calcium bentonite showed the best recoveries for pH 7 and 9 while NaBt had the best recoveries for pH 3 and 5.23. Amine Bt had poor recoveries overall, less than 61 % of CaBt and NaBt at their best recoveries on C_o 2%. For comparable recoveries, almost twice as much amine Bt would need to be used. Due to poor protein recoveries, amine Bt was discarded for stickwater adsorption experiments.

Table 26: Predicted gelatin recovery from Langmuir-Freundlich isotherm and kinetic data.

Bentonite type	pH	Predicted gelatin recovery (%) at starting concentrations (% protein)					
		0.4	0.5	0.6	1.0	1.5	2.0
Calcium	3	74	71	69	61	52	46
	5.23	76	75	74	62	45	36
	7	75	76	76	75	69	59
	9	74	75	76	76	68	58
Sodium	3	81	80	80	76	68	58
	5.23	80	80	79	76	69	62
	7	76	76	76	71	58	47
	9	67	68	68	65	53	40
Amine	3		59		48		33
	5.23		48		38		27
	7		39		31		22
	9		52		47		38

6.5 Gelatin Adsorption Mechanism

Figure 37 depicts the repulsion and attraction forces involved in bentonite / gelatin system. Gelatin and bentonite are positively charged at pH 3 (Figure 37A) and the overall repulsion force in the system is high. The repulsion force decreases with increasing pH (Figure 37B) and is minimal at PZC of gelatin and bentonite (pH 5.23 and 7). At pH 9, gelatin and bentonite are predominantly negatively charged and this causes the repulsion force to increase. However due to multiple charges of gelatin and bentonite, gelatin attraction towards the solid surface can still occur with combination of interactions from gelatin-gelatin and gelatin-bentonite.

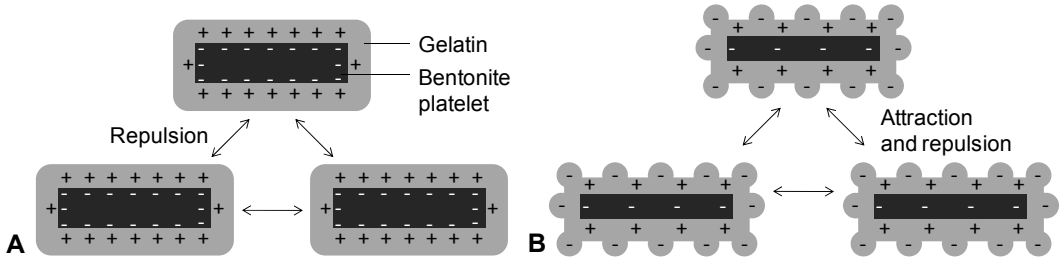

Figure 37: Repulsion and attraction forces of gelatin adsorption on bentonite at A) low pH (below 3) and B) higher pH (above pH 3).

In the model solution, aqueous ions in PBS solution are readily adhered to a surface as depicted in Figure 38. Competition for binding sites occurs when gelatin molecules are present. During adsorption, trains (molecule turns on the surface) attach to the bentonite surface while loops (molecules turns away from the surface) and tails of gelatin molecules point out into solution (Figure 39). Gelatin molecules displaced the adsorbed salts on solid-phase based on affinity and size difference. The process could take time because gelatin adsorption involves "multi-point" attachment and slow surface motion due to gelatin's structural restriction or steric hindrance [89].

At low gelatin concentration, positive and negative parts of gelatin attract the opposite charge of PBS ions. At this stage, gelatin chains are in an expanded configuration because gelatin-salts interaction is more dominant than gelatin-gelatin interaction due to few gelatin molecules in the solution. When bentonite is added, gelatin / salt mixtures adsorb on the surface and also within the interlayer matrices. Bridging is suggested for low solute concentration due to the expanded protein chain structure [89]. The bridging behaviour may also occur for a polymer when a high molecular weight substance is added to a dilute solid-phase dispersion [130].

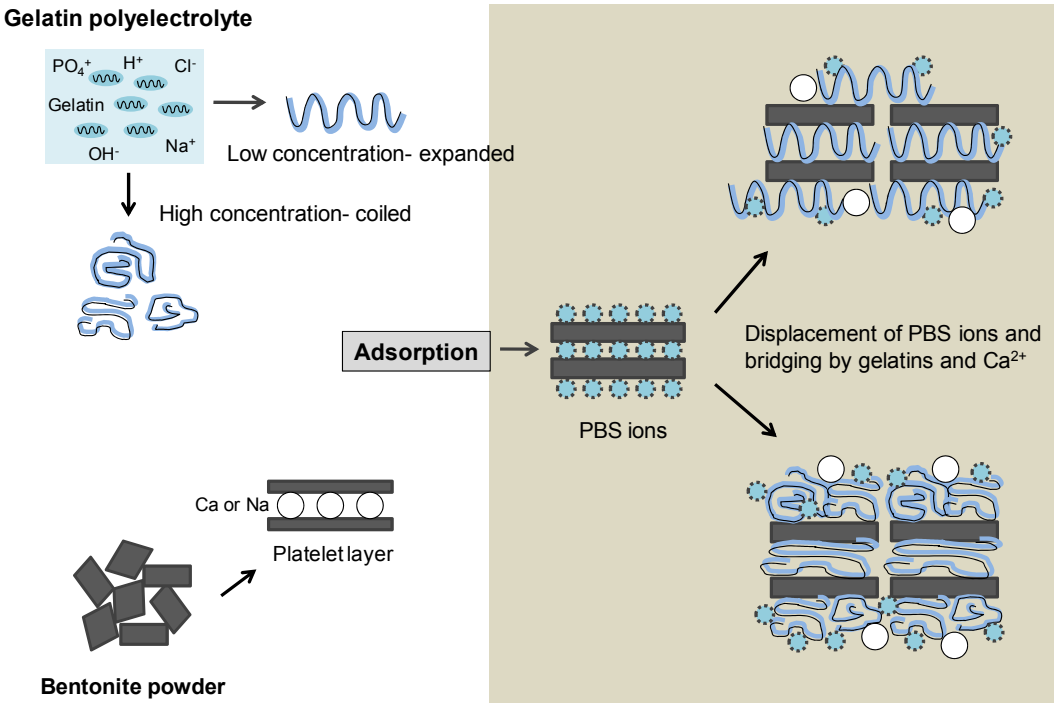

Figure 38: Proposed gelatin adsorption mechanism based on bridging mechanism [89, 130].

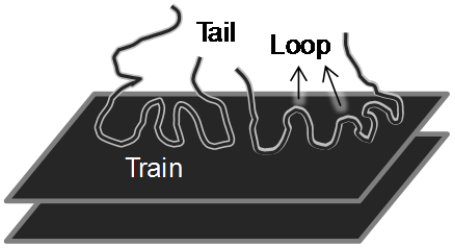

Figure 39: Gelatin molecules on bentonite surface [89, 98].

As the concentration increases, gelatin molecules become "space-filling" due to internal bondings as explained by Flory-Huggins theory (Figure 40). The theory illustrates a filled cubic lattice with solvent molecules surrounding the polymer chains. The lattice must be fully occupied and the solvent molecular size is assumed equal to the polymer chain segment size. At high concentration, the distance between polymer molecules is less, therefore polymer-polymer interaction is more dominant making the chains more tangled and coiled [89]. This hypothesis agrees with a work done on cryogenic gelatin structure (Figure 7) where it was observed that the gelatin pore size decreased with increasing concentration due to increased molecular interactions [79].

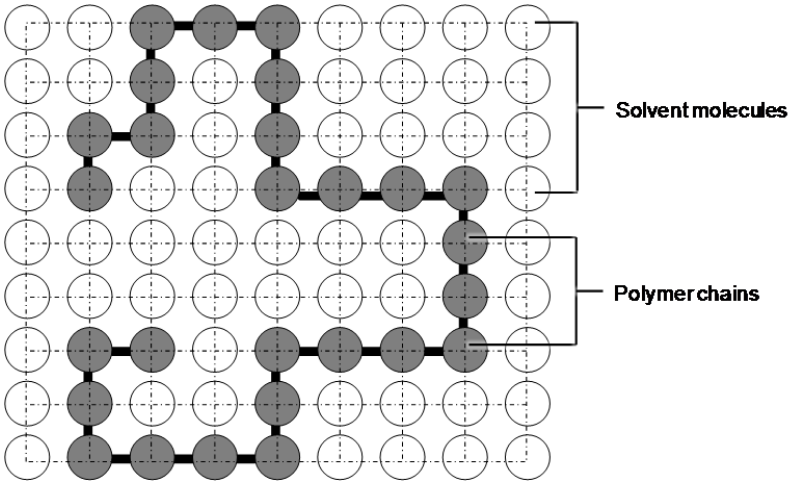

Figure 40: Flory-Huggins theory of polymer solutions [89].

6.6 Stickwater Adsorption onto Bentonite

6.6.1 Preliminary Test

Adsorption on stickwater was conducted in a similar manner to the experiment with model solution as outlined in Section 5.5.6. However, a different method for protein measurement was used. Centrifuged bentonite / stickwater solution had a muddy appearance with three visible layers which are fat, stickwater and bentonite (Figure 41). For this reason, UV measurement for protein analysis was not possible without a significant dilution. Also, the suspended organics in stickwater gave variable readings. Therefore, ashing in a furnace was used to determine the total organics adsorbed on bentonite. The values were then corrected with the pre-existing organics on bentonite. Unlike UV absorbance, this method is not very sensitive and prone to human-errors. Hence, extra care was taken during measurement such as using a desiccator for transporting and storing samples, recording the mass at every step to keep track of the mass balance and using the same ashing crucibles and furnace for consistency.

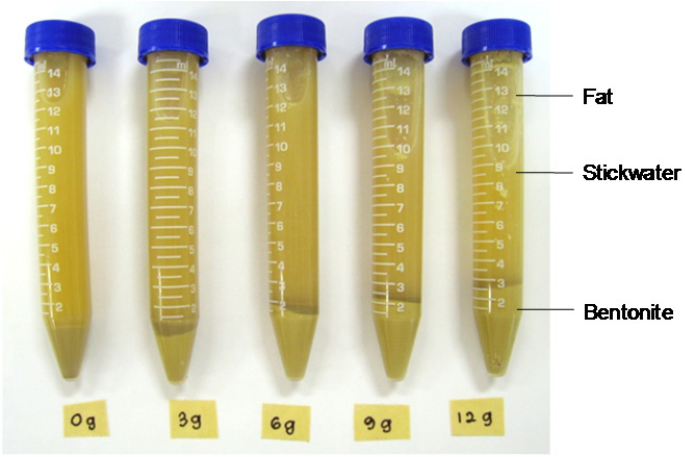

Figure 41: Centrifuge stickwater / bentonite solutions at different adsorbent loadings.

6.6.2 Adsorption Equilibrium and Kinetics

As can be seen from Figure 42, adsorption from stickwater was very rapid with equilibrium being reached within 5 to 10 minutes, similar to gelatin adsorption. From equilibrium adsorption data (Table 27), it should be noted that the values of C_e is attributed to the final organic concentration in the solution instead of protein concentration alone, unlike in the case of model solutions. As stated in Section 6.2.2, at 2 % initial protein concentration, stickwater contained 3.57 % organics which is a combination of protein, fats and volatile solids.

Table 27: Equilibrium data for stickwater adsorption at C_o 2%.

Bentonite type	pH	C_e (%)	C_r (mg/g)	Recovery (%)
Calcium	3	1.42	245.92	61.00
	5.23	2.05	158.18	43.64
	7	2.16	149.00	40.78
	9	2.02	175.51	44.69
Sodium	3	1.52	234.42	58.25
	5.23	1.75	213.78	52.04
	7	1.84	204.32	49.54
	9	2.14	174.50	41.28

No gel formation was observed in any of the stickwater adsorption systems compared to NaBt that gelled at pH 9 in model solution. Figure 42 shows that the adsorption pattern did not replicate the adsorption of model solution. Overall, the adsorbed

organic, C_r for stickwater was a lot less than gelatin solution (Table 27). The highest adsorption for both types of bentonite occurred at pH 3, contrary to the gelatin adsorption where it was found that CaBt and NaBt adsorbed best at pH 9 and pH 5.23 respectively. The organic recovery from stickwater was calculated to be between 41 to 61 % using CaBt and the recovery for NaBt was at 41 to 58 %. These recovery percentages are within 5 % with the gelatin recovery from model solution (Table 23). The C_r difference from gelatin and stickwater adsorption is the highest at pH 7, corresponds to a 53 % difference.

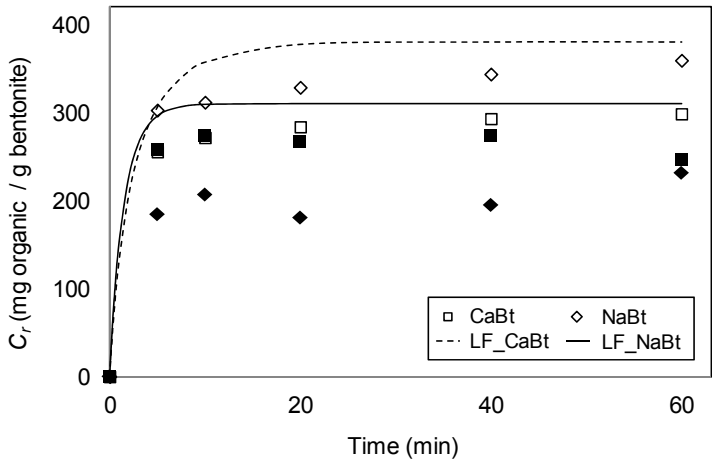

Figure 42: Equilibrium time for stickwater adsorption (solid dots) at pH 3 using CaBt and NaBt with gelatin adsorption (open dots). Lines indicate L-F models. Datapoints are mean values of three replicates.

The L-F model was found to be inadequate to model stickwater adsorption data. It is hard to quantify for just protein adsorption in stickwater without undertaking a total protein concentration for the supernatant for each solution at equilibrium (which was beyond the means of the project at the time). The adsorption was a combination of proteins, fats and minerals, therefore competition between the solutes for the binding sites on the solid-phase must have occurred. To compensate this, competition terms for fats and minerals were introduced into Equation 32:

$$C_r = \frac{\left(K_P C_P^{\frac{1}{nP}} C_{rpmax}\right) protein}{1 + \left(K_P C_P^{\frac{1}{nP}}\right) protein + \left(K_F C_F^{\frac{1}{nF}}\right) fat + \left(K_M C_M^{\frac{1}{nM}}\right) mineral} \quad (40)$$

where C_r is the amount of adsorbed organic on bentonite (mg/g); K_P, K_F and K_M are L-F equilibrium constants (g/mg) corresponding to protein, fat and mineral; C_{rpmax} is the maximum amount of protein yield at saturation (mg/g); C_P, C_F and C_M are equilibrium concentration of protein, fat and mineral; nP, nF and nM are the parameters of favourability with values greater than 1 signify favourable adsorption.

The fitted L-F curves for stickwater adsorption (Table 28) did not give a very good fit as determined from low regression coefficient, R^2 compared to gelatin solution (Table 24). When fitting the model to the stickwater adsorption data (Table 28), the parameters of K_P, nP and C_{rpmax} were taken from gelatin adsorption (Table 24) and the organic content left in solution at equilibrium was used for C_P instead of gelatin concentration. It was assumed that the fat and mineral content did not adhere on the solid-phase, therefore the mineral and fat concentrations used were assumed to be the same as the starting diluted concentration of the fat and mineral content. Excel Solver was used to estimate the parameters K_F, nF, K_M and nM by minimizing the residual sum of squares between experimental data and model data.

The calculated parameters for both calcium and sodium bentonite are shown in Table 29. The model results showed that fat adsorption had no affect on organic adsorption onto CaBt. In this case, K_F was zero indicating that no competition between fat and protein for binding sites on the solid-phase. The mineral adsorption parameters for CaBt were found to be K_M of 1.51 and n_M of 488 039. When mineral concentration was raised to the power of 1 / 488 039, the value of C_M became 1. Therefore, organic adsorption is independent of mineral concentration but dependent on the mineral equilibrium term, K_M. Thus for CaBt, Equation 40 is reduced to:

$$C_{r\,(caBt)} = \frac{\left(K_P C_P^{\frac{1}{nP}} C_{rpmax}\right)}{1 + \left(K_P C_P^{\frac{1}{nP}}\right) + K_M} \quad (41)$$

For NaBt, a similar result was achieved for the mineral adsorption parameters, but there was a dependency on fat concentration as the K_F value was 0.6 and the nF was 0.89. Therefore Equation 40 can be reduced to:

$$C_{r\,(NaBt)} = \frac{\left(K_P C_P^{\frac{1}{nP}} C_{rpmax}\right)}{1 + \left(K_P C_P^{\frac{1}{nP}}\right) + \left(K_F C_F^{\frac{1}{nF}}\right) + K_M} \tag{42}$$

The independence of both calcium and sodium bentonite organic adsorption on stickwater mineral content can be explained by the fact that there is a thousand fold greater molar quantity of mineral molecules in stickwater compared to gelatin molecules (assuming gelatin has a similar molecular weight to an intact α-chain collagen strand of 100 000 g/mol [62] and the mineral has a similar molecular weight to NaCl of 58 g/mol). The independence of CaBt organic adsorption on fat content can be explained by the CaBt platelets expanded rather than exfoliated in solution (Ca^{2+} holds the layers stronger than Na^{+}), therefore fat would have to diffuse inside the layers as well as attach on a highly charged surface, of which both are unlikely due to fat's hydrophobic nature. Sodium bentonite exfoliated and could have provided a much larger surface area for adsorption and therefore it was possible for fat adsorption to occur by associating with the hydrophobic regions of adsorbed gelatin on the solid-phase.

Both models would need to be tested in the future to confirm the above hypothesis by assessing the equilibrium concentrations of protein and fat in both the solution and solid-phase. Protein concentrations in both phases could be assessed by carrying total protein analysis while fat concentration could be done by Soxhlet extraction. The calculated values from competitive L-F models are graphed into Figure 43 alongside the experimental data.

Table 28: Summary of stickwater adsorption data used for competitive L-F model calculation based on adsorption at pH 3.

C_o (%)	C_P (%)	C_F (%)	C_M (%)	Theoretical yield, C_{rt} (mg/g)	Experimental yield, C_{re} (mg/g)	$(C_{rt}-C_{re})^2$
Calcium bentonite						
4	0.144	0.183	0.103	55.28	67.47	148.57
5	0.360	0.229	0.129	101.63	59.15	1804.58
6	0.438	0.274	0.154	114.78	90.87	571.37
10	0.604	0.457	0.257	138.99	135.84	9.88
15	0.920	0.686	0.386	175.34	202.95	762.06
20	0.161	0.914	0.514	230.27	245.92	245.19
				$R^2 = 0.9028$		3541.66
Sodium bentonite						
4	0.228	0.183	0.103	52.03	46.88	26.51
5	0.252	0.229	0.129	56.37	75.33	359.55
6	0.447	0.274	0.154	98.99	75.76	539.33
10	0.556	0.457	0.257	110.08	147.30	1385.48
15	1.235	0.686	0.386	192.11	161.50	937.04
20	1.723	0.914	0.514	222.42	234.42	143.99
				$R^2 = 0.8686$		3391.89

Table 29: Calculated L-F paramaters for stickwater adsorption at pH 3 using constants from gelatin adsorption (underlined).

Clay type	$\underline{C_{rmax}}$ (mg/g)	$\underline{K_P}$ (g/mg)	K_F (g/mg)	K_M (g/mg)	$\underline{nP}$	nF	nM
CaBt	556	0.21	0	1.51	1.3	2.82	488039
NaBt	435	0.46	0.60	7.30	0.8	0.89	488040

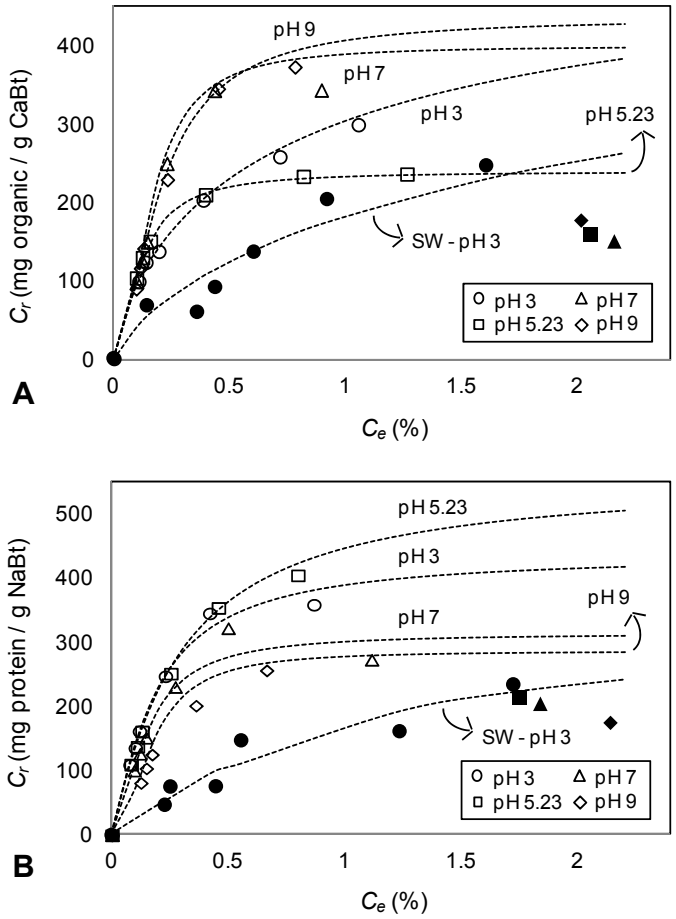

Figure 43: Stickwater adsorption isotherms (solid dots) of A) calcium and B) sodium bentonite in comparison with gelatin adsorption (open dots). Lines indicate L-F models. Datapoints are mean values of three replicates.

6.7 Analysis of Gelatin and Stickwater-Modified Bentonite

6.7.1 Basal Spacing and Thermal Degradation

Powder samples of adsorbates and adsorbents were analyzed for basal spacing and thermal decomposition using XRD and TGA. Bentonite basal spacing (*d*-value) was calculated from XRD data using Bragg's law (Equation 24). The mass loss curves of bentonite over temperature are depicted in Figure 45 and summarized into Table 31. The percentage mass loss was calculated at 200 ^{o}C temperature intervals up to 800 ^{o}C, corresponding to percentage loss of water, surface organics, hydroxyl water, intercalated organics and low volatility compounds.

It can be seen from Table 30 that the basal spacing of raw CaBt is 20 % larger than NaBt because Ca^{2+} ions are larger than Na^{+}. Amine Bt has the largest basal spacing at 21.8 Å corresponding to an increase of 43 % over NaBt (its original form) attributed to the intercalated octadecylamine. Compared to the raw forms, *d*-value for oven-dried samples decreased 28 % and 26 % for CaBt and NaBt respectively. This suggests that the presence of water in the samples can expand the basal spacing. Amine Bt did not exhibit this behaviour because it adsorbed very little water due to its hydrophobic nature.

The swelling of bentonite is resulted from a negative charge on the surface that is balanced by soluble cations in the electrolyte solution. Bentonite consists of platelets that are 1 nm thick; upon hydration, water penetrates between the layers and the negative charge of the surfaces repel each other and cause the clays to swell [89]. On drying, the layers collapse to the original basal spacing. Research conducted by others showed that air-dried and oven-dried CaBt samples had similar *d*-values [117]. Mpofu et. al. (2005) stated that smectite layers can swell up to 100 % of the original basal spacing (from 10 to 20 Å) due to the uptake of four layers of water on both the external and interlayer surfaces. This phenomenon is termed as crystalline swelling. Above 20 Å, osmotic swelling may also occur and result in complete separation of layers or exfoliation [133].

From Table 30, *d*-value of PBS-treated (gelatin 0 %) CaBt and NaBt are about ~10 Å, corresponding to a decrease of 27 % for CaBt and 4 % for NaBt from their oven-dried forms. The decrease in *d*-value for CaBt is attributed to isomorphous substitution between intercalated Ca^{2+} with smaller size Na^{+} ions from the solution. A small change in *d*-value of NaBt was due to an exchange with similar size ions. The PBS ions may not be able to substitute for octadecylamine molecules on amine Bt due to large difference in size and charge. It is possible that those ions were trapped in the octadecylamine interstices which could increase the basal spacing as shown in Table 30 where there is a 16 % increase in *d*-value for PBS-treated amine Bt.

It is interesting to see that the *d*-value for all untreated bentonite ashes are about ~10 Å after heat treatment in a furnace at 650 ^{o}C (Table 30). The organics on the adsorbents degraded after 650 ^{o}C as indicated by equilibrium being reached from

mass loss curves (Figure 45). Calcium bentonite and amine Bt were derived from NaBt, during ashing, the layers collapsed and assumed the original NaBt layer formation. This indicates that the basal spacing is collapsible to a limit once the interlayer water and organics are completely removed.

Table 30: Summary of basal spacing for untreated and treated bentonite.

Sample	2θ (^{o})			*d*-value (Å)		
	CaBt	NaBt	Amine Bt	CaBt	NaBt	Amine Bt
Raw	5.69	7.15	4.05	15.5	12.4	21.8
Oven-dried	6.51	8.51	4.11	13.6	10.4	21.5
Ash	8.95	8.61	8.35	9.9	10.3	10.6
Gelatin-treated						
pH 3- 0% (PBS)	8.97	8.81	3.53	9.9	10.0	25.0
0.4%	5.05	5.43	-	17.5	16.3	-
0.6%	5.07	5.15	-	17.4	17.1	-
1.0%	5.13	4.55	-	17.2	19.4	-
1.5%	5.05	4.65	-	17.5	19.0	-
2.0%	4.97	4.43	3.05	17.8	19.9	28.9
pH 5.23- 2.0%	4.69	4.03	3.39	18.8	21.9	26.0
pH 7- 2.0%	4.45	3.83	3.17	19.8	23.1	27.9
pH 9- 2.0%	4.43	4.13	2.99	19.9	21.4	29.5
SW-treated						
pH 3- 0.4%	6.17	5.57	-	14.3	15.9	-
0.6%	6.35	5.45	-	13.9	16.2	-
1.0%	5.67	5.37	-	15.6	16.4	-
1.5%	6.07	5.33	-	14.6	16.6	-
2.0%	6.17	5.63	-	14.3	15.7	-

In the presence of gelatin (prepared in PBS solution) at all concentrations, the *d*-value had increased as shown in Table 30, indicating that the intercalation is independent of solute concentration. From XRD diagrams in Figure 44, untreated CaBt and NaBt gave sharp d_{001} peaks at 2θ of 6.5^o and 8.5^o, corresponding to *d*-value of 13.6 Å and 10.4 Å respectively. The d_{001} peaks for gelatin treated bentonite shifted to lower angles indicating an expansion of the clay gallery by gelatin intercalation. The peaks are broader than the untreated bentonite which implies a decrease in perfection of clay gallery stacking [9]. This trend is more visible on treated amine Bt (apart from PBS-treated) suggesting that the layers were becoming poorly ordered as the pH increased. In a work done on montmorillonite / gelatin film, the d_{001} peaks were

observed to become broader and even started to disappear at increasing pH above PZC of gelatin [32].

The emergence of additional reflection peaks can be seen for treated amine Bt (Figure 44). These multiple basal reflections are attributed to the intercalation of foreign molecules. Overall, no exfoliation of bentonite was observed based on the presence of d_{001} peaks for all conditions, which if otherwise was obtained, the first reflection peak would have disappeared.

Gelatin-treated NaBt at pH 7 had the largest increase in *d*-value at 122 %, suggesting that the NaBt layers were only weakly bonded together allowing greater gelatin intercalation. Calcium bentonite had the highest increase in *d*-value of 46 % at pH 9, much lower than NaBt because the increased interaction between silica layers due to Ca^{2+} holding the layers together more strongly compared to Na^{+}. At pH 9, amine Bt had the highest increase in *d*-value of just 37 %, due to the exchange of comparable sized molecules between octadecylamine and gelatin, whereas gelatin exchanged for much smaller ions (Na^{+} and Ca^{2+}) for the previous cases. These findings were also observed in albumin adsorption onto sodium and magnesium montmorillonite where the *d*-value increased from 12 Å to between 17-24 Å (41.7 to 100 % increase) for sodium bentonite, but magnesium bentonite showed little change [68]. In another work, Lin et al. (2007) observed an increase in basal spacing of up to 62 Å for BSA adsorption onto sodium montmorillonite [118].

Stickwater treated bentonite had a smaller *d*-value than their gelatin counterparts. At 2 % protein concentration, stickwater-modified CaBt and NaBt only gave an increase in *d*-value of 5 % and 51 % compared to their initial oven-dried forms. This is attributed to relatively shorter chain length of intercalated organics from stickwater compared to gelatin molecules in model solution (previously discussed in Section 6.2.2). For adsorption of solute with a long molecular chain, it was reported that greater clay layer separation can be achieved as evidence from adsorption of long-alkyl chain ammonium onto montmorillonite [18].

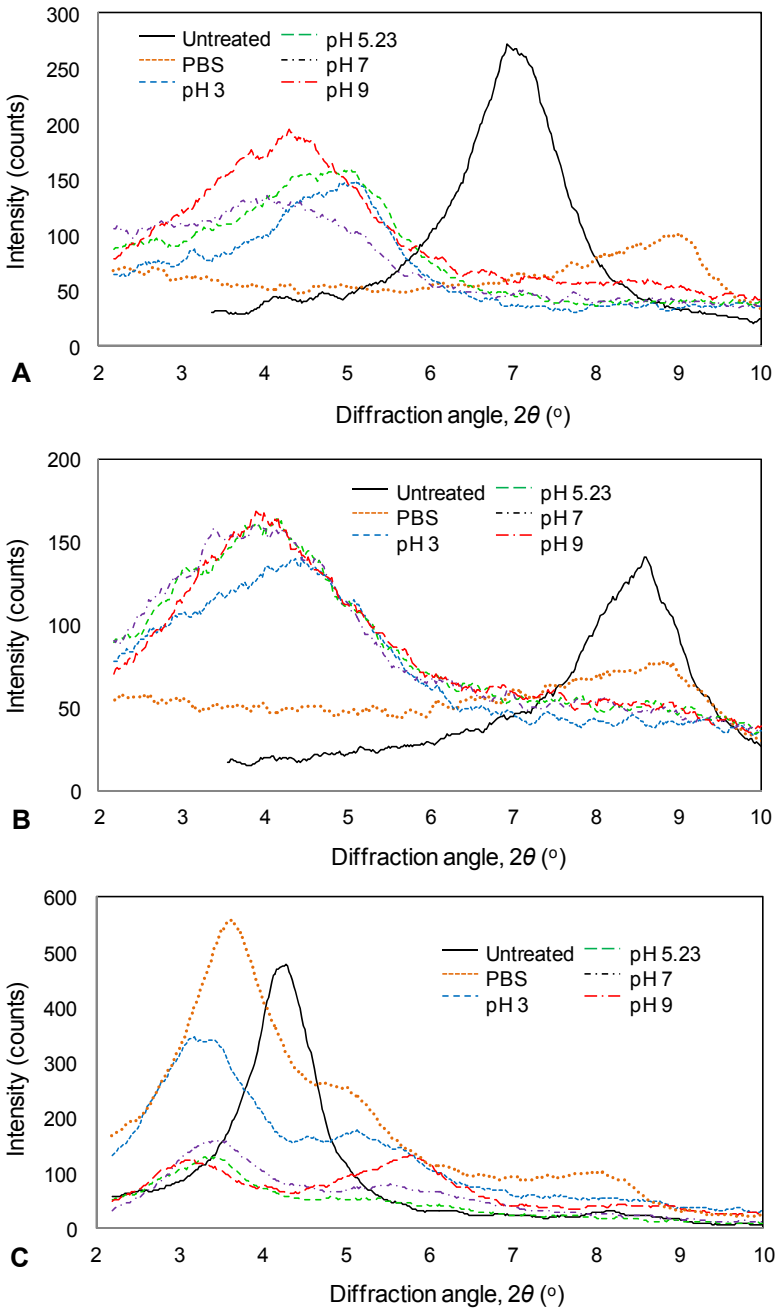

Figure 44: XRD diagrams of untreated and gelatin-treated at C_o 0% (PBS) and 2% for A) calcium, B) sodium and C) amine bentonite.

TGA summary in Table 31 shows that there are significant amount organic present on gelatin-treated CaBt and NaBt compared to their untreated forms, confirming the organic adsorptions. A small change in organic content is obtained for amine Bt due to the exchange between bound octadecylamine molecules and gelatin from the solution. The findings are in agreement with XRD (Table 30) where *d*-values increased significantly for CaBt and only minor for NaBt and amine Bt.

From Table 31 and TGA curves (Figure 45A and B), the percentage organics for PBS-treated CaBt and NaBt are slightly higher than the raw forms. The PBS organics could be originated from phosphate (PO_4) content in solution formulation. Untreated and PBS-treated amine Bt gave almost similar mass loss percentage below 200 ^oC, indicating there was no bound water on the surface due to its hydrophobic nature. Treatment with PBS only resulted in 2 % organic difference compared to the original form, implying that there was no exchange between PBS ions with octadecylamine molecules. The finding is in-line with the literature that suggests the substitution is effective only with similar or larger size and charge ions [2, 9].

From Figure 45, decomposition curves of untreated and PBS-treated CaBt and NaBt occurred in two stages at 0-200 ^oC and 400-600 ^oC. While gelatin-treated CaBt and NaBt had three decomposition stages at 0-200 ^oC, 200-400 ^oC and 400-650 ^oC corresponding to surface water, surface organics and intercalated organics. Three stages of degradation were also observed for amine Bt but at different temperature intervals that are at 200-400 ^oC, 400-600 ^oC and above 600 ^oC.

All curves had reached the equilibrium at 800 ^oC except for stickwater and amine Bt. Therefore, the amount of ash was possibly over estimated while the amount of organic was under estimated for stickwater and amine Bt. Stickwater and gelatin have similar thermal degradation pattern with gelatin had 3 % higher organic than stickwater. But the organic of stickwater could be higher if the TGA temperature was increased. Thermal degradation curves for CaBt and NaBt were also depicting identical patterns. Sodium bentonite had approximately 1 % higher organic content than CaBt. This could be explained by NaBt had larger specific surface area which could contain more organics at the same mass of CaBt. TGA curve of amine Bt does

not resemble its origin of NaBt, suggesting that the octadecylamine molecules must have displaced the interlayer sodium ions during adsorption.

Generally for clay, from room temperature (~20 ^{o}C) to 90 ^{o}C, surface water is lost at defects or broken bond sites on the clay surface which accounted for a mass loss of 1 wt%. Interlayer water and low molecular mass compounds are lost at 100 to 200 ^{o}C. The interlayer water is associated with interlayer cations in smectites as monolayers (2.5 Å) or bilayers (5 Å). Between 200 to 400 ^{o}C, surface organics are lost and degradation of particles occurred. Dehydroxylation and loss of intercalated organics take place between 400 to 600 ^{o}C. Finally, low volatility organic compounds degraded at 600 to 800^{o}C. The mass of ash left after the treatment corresponds to the calcined clay residue [9, 80]. Overall, bentonite was found to be thermally stable until 500 ^{o}C as shown in Figure 45 (also suggested by [20]).

Gelatin treated CaBt and NaBt showed a decrease in water content from the average value of 11.2 wt% to 6-8 wt%, an increase in surface organics from 1.3 wt% to 10-12 wt% (showing some gelatin had been adsorbed on the surface), an increase in hydroxyl water and intercalated organics from 4.3 wt% up to 20 wt% and an increase in low volatility compounds from 0.7 wt% to 1.5-6 wt%. This indicates that adsorption was a combination of surface adsorption and intercalation. Calculated organics absorbed from TGA data (Table 31) were within the same range as calculated from gelatin adsorption equilibrium (Table 23). The highest organics from TGA for both CaBt and NaBt correspond to the highest C_r obtained from gelatin adsorption.

TGA data is expected to give slightly higher values than the real adsorption because of organic matter in solution was trapped within the interstices and between bentonite particles when the solution was centrifuged. Sodium bentonite could have overstated the amount of C_r more because NaBt swells more and may experience even greater centrifugal compaction than CaBt.

TGA curves for CaBt indicated increased thermostability with increasing pH and the onset of intercalated organic decomposition shifting from 430 ^{o}C at pH 3 to 530 ^{o}C at pH 9. Unlike NaBt, the onset was independent of pH and occurred at 530 ^{o}C

(Figure 45). Calcium bentonite had the highest adsorption at pH 7 and 9, and it is possible that the free calcium ions were stabilizing the system by forming crosslinks between gelatin molecules. Sodium bentonite did not exhibit this because sodium ions have only a single positive charge.

PBS and gelatin treated amine Bt showed similar TGA curves with its unmodified form, showing no increase in organic content, but from the equilibrium isotherm data (Table 23), there was an increase in *d*-value, confirming the hypothesis that the adsorption was a direct exchange between gelatin and octadecylamine molecules.

Table 31: Summary of thermal degradation of untreated and treated bentonite.

Sample	pH	TGA composition * (%)				Organic (wt%)	Ash (wt%)
		A	B	C	D		
		0-200°C	200-400°C	400-600°C	600-800°C		
CaBt							
Untreated +		10.87	1.44	3.80	0.52	5.76	83.26
PBS	3	4.39	1.31	4.68	3.96	9.96	85.65
Ge2%	3	8.28	11.38	16.30	2.61	30.28	61.44
	5.23	7.31	9.96	17.94	1.56	29.45	63.24
	7	6.38	10.92	19.39	3.44	33.75	59.87
	9	6.45	11.13	18.70	5.93	35.76	57.79
NaBt							
Untreated +		11.53	1.10	4.74	0.84	6.68	81.80
PBS	3	2.35	1.15	4.66	4.19	10.00	87.65
Ge2%	3	7.66	11.42	19.90	3.95	35.28	57.07
	5.23	7.72	11.80	19.33	5.46	36.58	55.70
	7	7.73	11.02	18.65	5.47	35.14	57.13
	9	7.82	11.50	19.02	4.55	35.07	57.11
Amine Bt							
Untreated +		1.49	14.30	10.35	10.01	34.66	63.84
PBS	3	1.15	14.18	12.19	5.90	32.27	66.58
Ge2%	9	1.90	15.72	12.74	6.27	34.73	63.37
Gelatin		13.25	41.18	38.04	6.78	86.00	0.75
Stickwater		10.47	51.74	23.64	7.60	82.99	6.54

***** A: Surface/pore water and low molecular mass compounds; B: Surface organics and degradation of particles; C: Hydroxyl water and intercalated organics; D: Low volatility organic /compounds [24, 80];

+ Oven-dried raw bentonite powder at 105 °C for overnight.

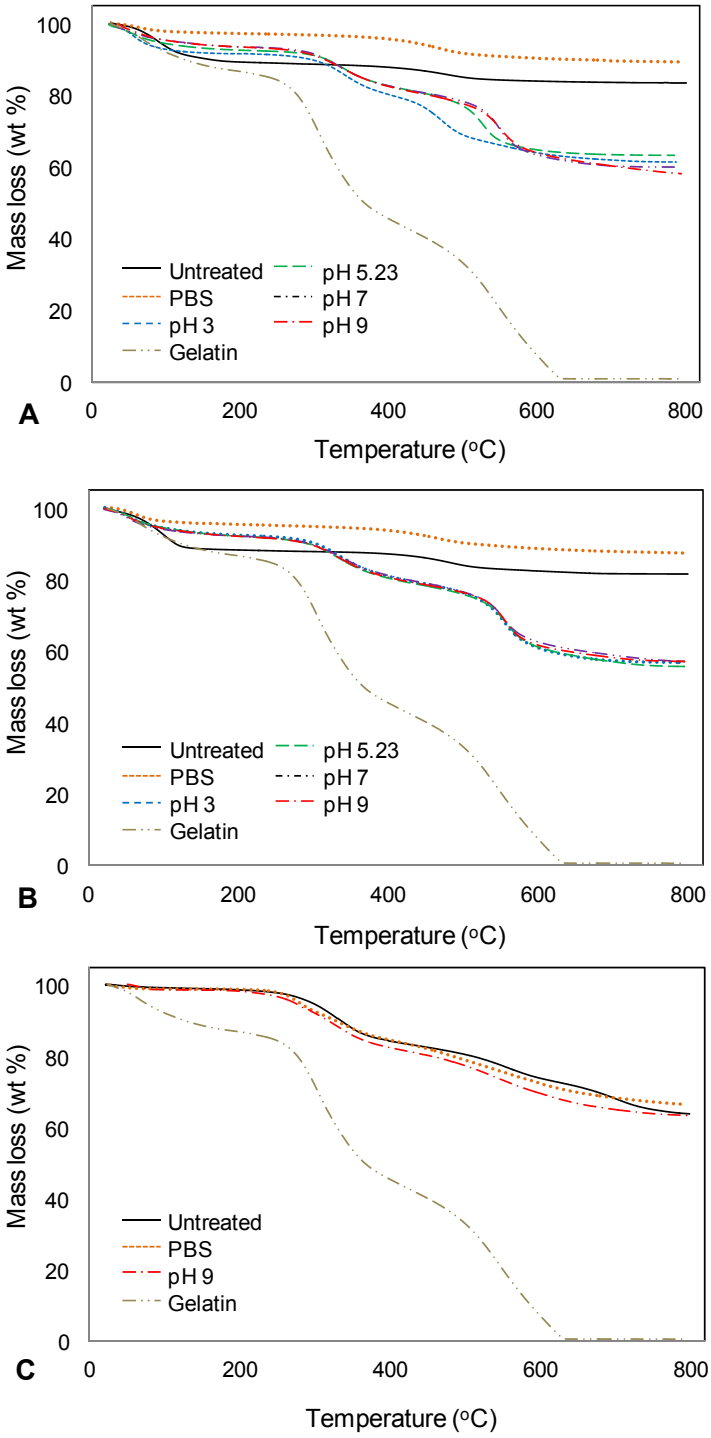

Figure 45: TGA curves of gelatin, untreated and gelatin-treated (0 and 2 %) A) calcium, B) sodium and C) amine bentonite.

In summary, organic intercalation within the bentonite gallery had been achieved as indicated by the increase in basal spacing. The intercalation was found to be independent of protein concentration (0.4 to 2 % concentration) but dependent on protein molecular size (between organic from gelatin and stickwater) as listed in Table 30. Basal spacing for PBS-treated CaBt and NaBt decreased while their organic-treated forms showed increased basal spacing which corresponds to isomorphous substitution. Amine Bt had almost similar basal spacing at treatment with PBS and gelatin solution, stressing the point made about similar size or charge ions are needed for the exchange. The size of octadecylamine molecules could be comparable to gelatin while PBS ions are much smaller.

However, XRD alone is inadequate to investigate the extent of adsorption because the adsorbed solutes on the surface cannot be accounted for from the diffraction peaks. Therefore, TGA was employed to study the thermal degradation of the adsorbents before and after adsorption. The change in mass loss at a specific temperature interval could reflect the amount of certain substances presence.

Thermal degradation analysis confirmed the presence of organics on the surface and within the interlayer gallery as indicated by the mass loss percentage between 200 ^{o}C to 400 ^{o}C and 400 ^{o}C to 600 ^{o}C. High amount of organics was observed for CaBt and NaBt complementing the findings in XRD and adsorption experiment (Section 6.3.3) where the increased basal spacings and adsorbed gelatin, C_r correspond to high percentage of organics from TGA. Amine Bt had a small change in TGA organics and basal spacing, but adsorbed up to 239 mg gelatin / g of clay which can be attributed to the isomorphous substitution between bound octadecylamine molecules on solid-phase and gelatin from solution.

6.7.2 Mineral Content

Energy Dispersive Spectroscopy (EDS) revealed an increase in N and C elements for treated CaBt and NaBt indicating gelatin presence on the clay surfaces as summarized in Table 32. EDS for amine Bt indicated no N element, but this could be because the N peak was too small and was masked by the C peak which was much larger compared to other bentonites because of substitution of Na^{+} with octadecylamine.

Gelatin adsorption did occur on amine Bt as showed from adsorption experiment in Figure 35.

However, the analysis only revealed the presence of salt minerals on the surface. Therefore, elemental increase or decrease can only be attributed to the presence of salt minerals on the surface not within the interlayer. Treated CaBt and NaBt showed a decrease in Ca and K an increase in Na elements (Table 32). This implies that the interlayer Na had been substituted with Ca and K during adsorption as they possess higher cation exchange preferences (Ca>Mg>K>Na) as discussed in Section 4.1.

The adsorption was a combination of gelatin and dissolved salts as illustrated in Figure 38 (Section 6.5). Competition for binding sites must have occurred with aqueous salts diffusing at a very fast rate and must have occupied the binding sites on solid-phases initially, until gelatin molecules displaced the ions. The ions later could have 1) attached to free unbound gelatin molecules in solution, 2) trapped within the conformational structure of adsorbed gelatin on bentonite layers or 3) combination of both, as suggested for protein polymer adsorption using clay [89].

Table 32: EDS analysis of bentonites before and after adsorption.

Sample		Element											
		C	N	O	Na	Mg	Al	Si	Cl	K	Ca	Ti	Fe
Na raw	% wt	9.87	-	41.4	2.93	0.85	9.09	25.3	0.60	0.40	0.99	0.96	8.48
	% err	1.29	-	0.61	0.10	0.08	0.18	0.24	0.09	0.05	0.08	0.10	0.38
Na treated	% wt	17.8	4.69	40.5	3.50	0.78	5.95	17.1	2.64	0.16	0.66	0.89	5.88
	% err	1.12	1.71	0.74	0.15	0.08	0.14	0.18	0.10	0.04	0.06	0.89	5.88
Ca raw	% wt	16.7	-	45.4	-	0.91	6.99	18.3	-	0.19	0.86	1.09	9.68
	% err	1.04	-	0.65	-	0.09	0.15	0.21	-	0.03	0.11	0.13	0.41
Ca treated	% wt	20.3	6.62	41.6	0.93	0.65	6.23	16.6	0.55	0.27	0.24	0.95	7.05
	% err	1.13	1.71	0.81	0.09	0.08	0.16	0.21	0.07	0.05	0.05	0.12	0.38
Amine raw	% wt	30.4	-	39.3	-	1.36	7.80	20.0	0.28	-	-	0.28	1.17
	% err	1.06	-	0.78	-	0.07	0.17	0.23	0.05	-	-	0.09	0.19
Amine treated	% wt	29.7	-	37.2	6.88	1.01	5.01	14.2	5.58	-	0.25	-	0.98
	% err	0.91	-	0.71	0.15	0.09	0.13	0.18	0.13	-	0.05	-	0.15

6.7.3 Surface Morphology of Bentonite

SEM images of the surface of powder particles before and after gelatin adsorption are presented in Figure 46 and Figure 47. Untreated and treated bentonite particles indicate a plate-like characteristic of clay layers. This shape resembles a subhedral lamella form in Figure 18, one of the common bentonite platelet shapes. Fine mineral deposits, possibly traces of gelatin and salts can be seen on the surface. It should be noted that for treated samples, SEM was performed mainly to analyze the mineral content using EDS and the images shown are less significant, because the particles morphology could have been modified by grinding during sample preparation.

In order to minimize the structural change on morphology due to oven-drying and grinding, the treated samples were freeze-dried and chunks were used for SEM instead of ground powder. For freeze-dried samples, gelatin can be seen acting as bridges to crosslink the CaBt agglomerates (Figure 47A) while NaBt platelets were completely covered by gelatin and the particles appear to have remained individual rather than aggregates (Figure 47B). From the scale bar provided in Figure 47b, it can be seen that the size range for treated NaBt is between 2 to 5 μm, in-line with laser sizing result (Table 18). In addition, the finding agrees to the adsorption data where NaBt had better adsorption capacity than CaBt at pH 3 (Table 23) due to high specific surface area when in solution.

The difference in SEM images between Figure 46 and Figure 47 reveals the effect of drying mechanisms used. Oven drying uses heat while freeze drying uses vacuum. Since gelatin is heat-sensitive, its structure could significantly be affected when moisture is evaporated at high temperature. The structural change can be minimized by removing moisture without heat application such as using freeze drying. Gelatin was found to have a scaffold structure in cryogenic environment as shown in Figure 7 (Section 2.4.1) and this structure collapses at high temperature [79].

After gelatin adsorption, it can be seen from Figure 47 that the particles were modified into intercalated and exfoliated forms for CaBt and NaBt as suggested from the literature (depicted in Figure 24). Exfoliation of clay is desirable to enhance adsorption and as reinforcement, it can improve the mechanical properties of composites via various interactions and improved dispersion in the matrix.

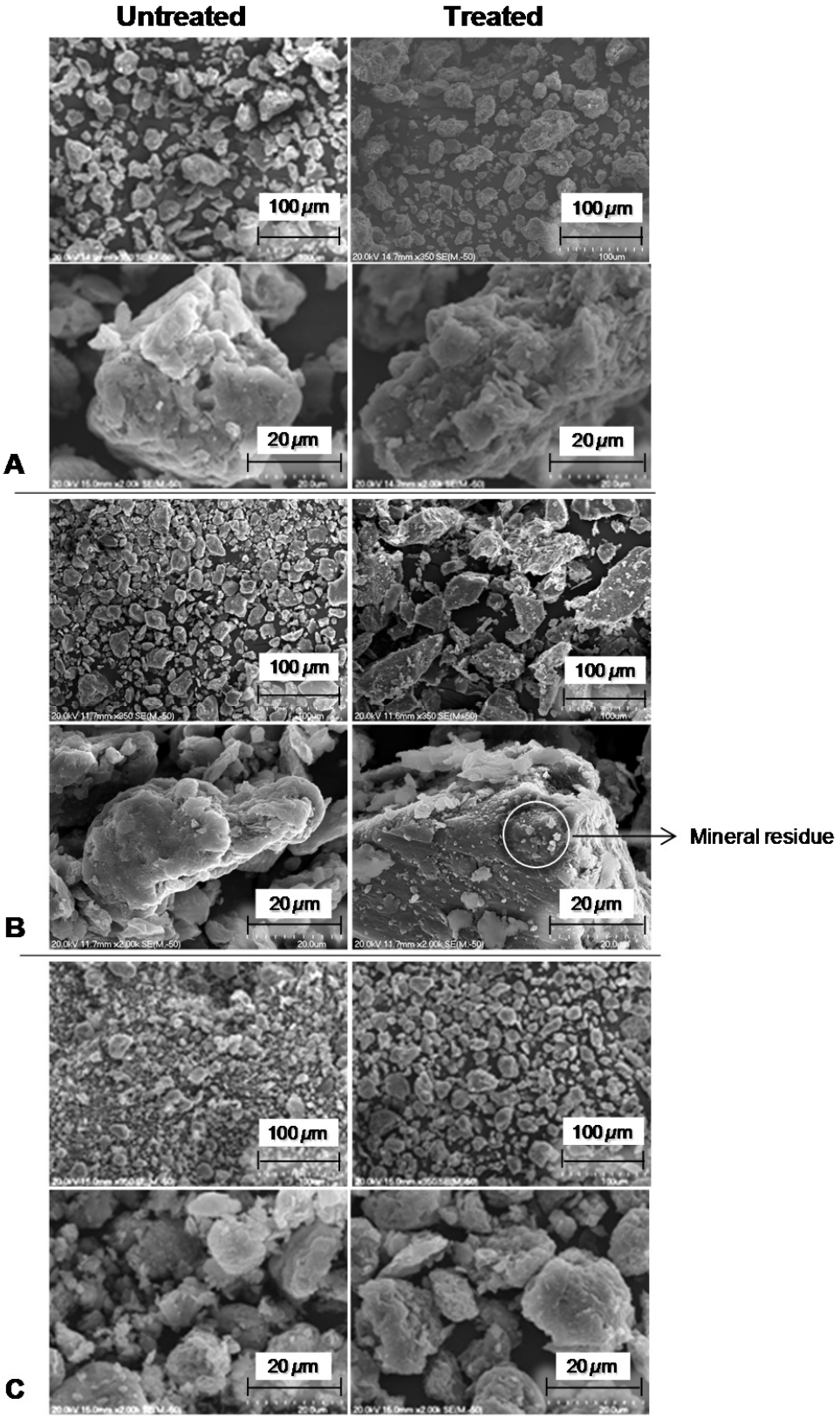

Figure 46: SEM images of oven-dried samples of untreated and treated A) calcium, B) sodium and C) amine bentonite. Treatment with gelatin 2 % at pH 3.

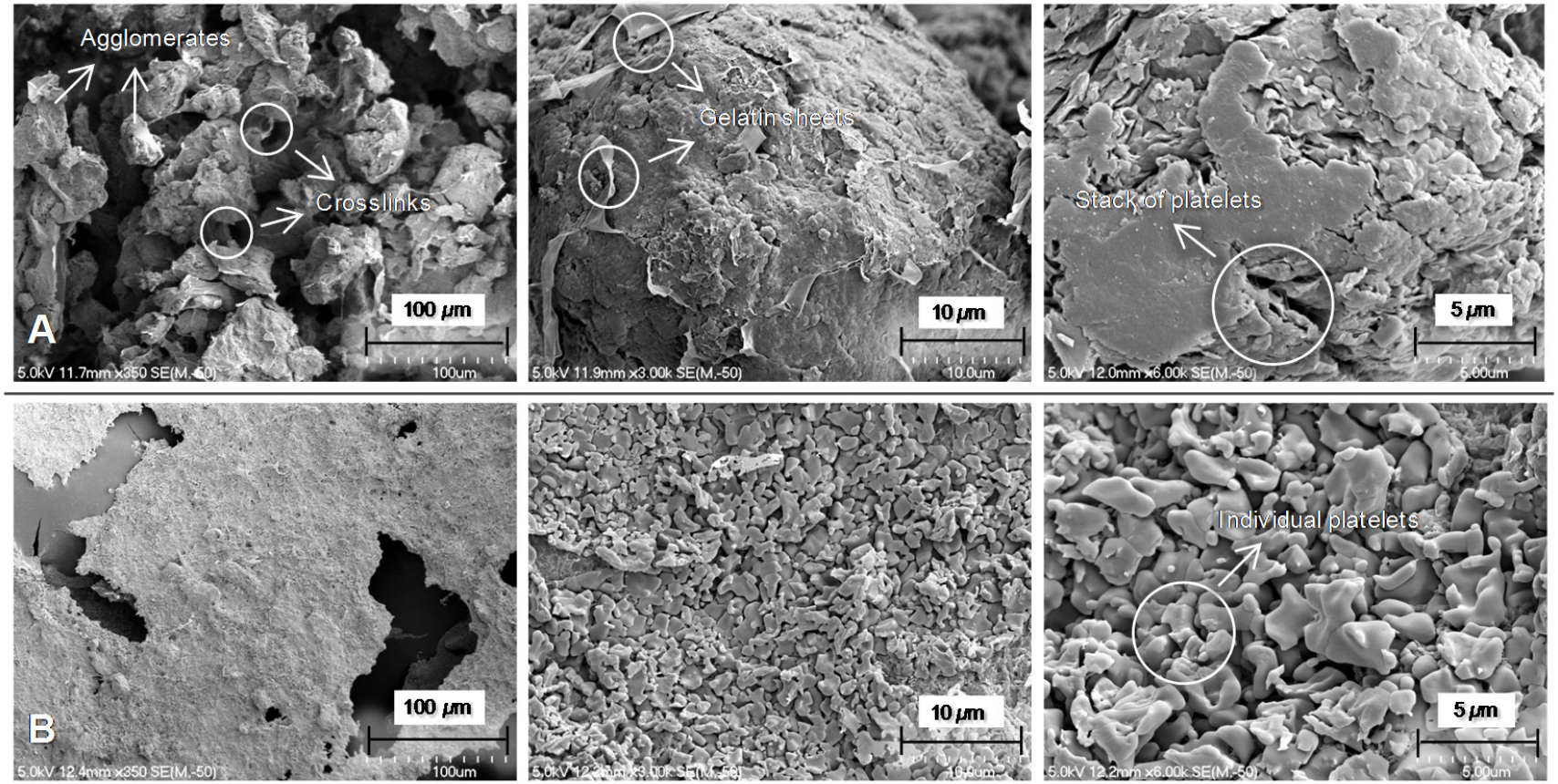

Figure 47: SEM images of freeze-dried A) calcium and B) sodium bentonite treated with gelatin 2 % at pH 3.

6.7.4 Liquid-State Surface Morphology of Bentonite in Gelatin Solution

From cryo-SEM images in Figure 48, it should be noted that the images were obtained from centrifuged samples. Therefore, in real suspension system (without centrifugation), it can be expected that the particles are more sparsely apart than what being shown. The centrifugation was employed to increase the solution viscosity in order to prepare the sample according to Section 5.4.6.

It appears from the cryo-SEM images that NaBt exfoliated while CaBt swollen in solution. Comparing with SEM images of untreated bentonite (Figure 46), gelatin molecules appear to have enveloped the platelets and acted as connecting bridges or crosslinks between particles as shown in Figure 48. This observation has similarities to the freeze-dried SEM (Figure 47) in terms of bridge formations, particles are covered by gelatin molecules, agglomeration of CaBt and exfoliation of NaBt. The CaBt seemed to have more compact pellet with less moisture trapped in the particle / gelatin network. Sodium bentonite showed stable suspensions with particles were connected by long gelatin chains. Exfoliated NaBt had higher specific surface area compared to agglomerated CaBt and therefore NaBt gave higher gelatin adsorption (Table 23).

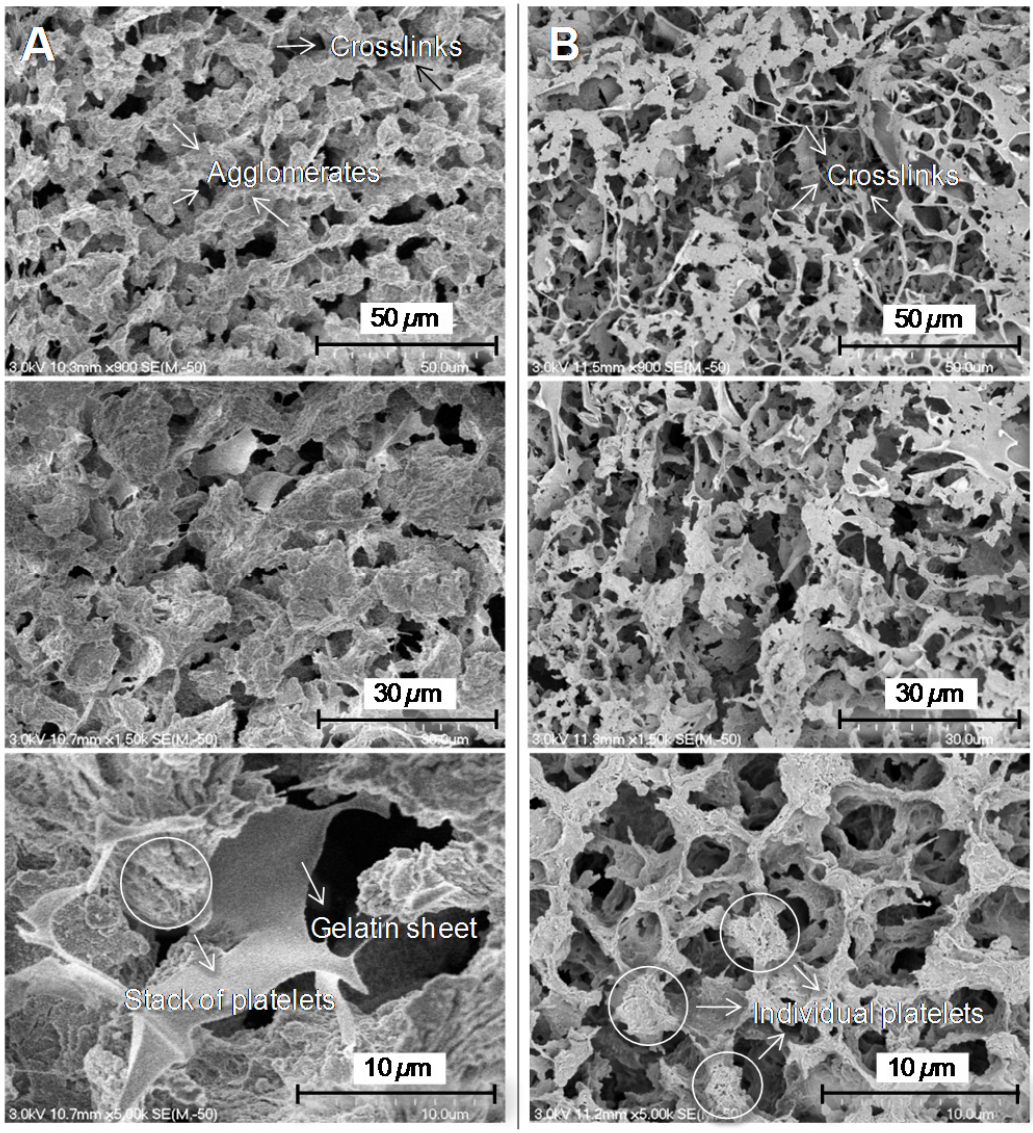

Figure 48: Cryo-SEM images on pellets of A) calcium and B) sodium bentonite at equilibrium treated with gelatin 2 % at pH 3.

6.8 Adsorption Summary

Bentonite was found to have considerable potential for protein adsorption as demonstrated from gelatin and stickwater solutions, coupled with its relative abundance and low-cost would make it even more attractive than conventional adsorbents such as activated carbon and silica gel.

If maximum protein recovery is the priority, adsorption can be performed at pH 9 for CaBt and pH 5.23 for NaBt. Sodium bentonite with high SSA could give a better

protein adsorption but the use of CaBt might be advantageous for subsequent sedimentation process due to its divalent cation, Ca^{2+} compared to Na^{+} for NaBt. However, it has been shown that protein adsorption can occur at any pH conditions due to the amphoteric characteristics of gelatin and bentonite.

The isotherm models used had potential to be used in adsorption analysis. Amongst all models tested, the Langmuir-Freundlich was found to fit the experimental data well for gelatin solution. However, stickwater adsorption resulted in considerable differences than model solution, owing to solute competition for binding sites and possible fouling from stickwater's fat and minerals content. To improve protein quantification from stickwater adsorption, a new parameter such as fat can be introduced into the model solution and analyzed using a competitive form of L-F model.

The analysis from XRD and TGA revealed the extent of adsorption and the results are in harmony with the adsorption findings. It was found that CaBt and NaBt adsorbed best at pH 9 and 5.23 respectively which correspond to large increase in basal spacing from XRD and high amount of organic from TGA. Amine Bt was observed to have noticeable gelatin adsorption but no significant enhancement in basal spacing and organic amount which points out the direct substitution between gelatin and octadecylamine molecules. Microscopy analysis corroborated the above findings by depicting the morphological states of bentonite in gelatin solution. Sodium bentonite with a better adsorption capacity revealed an exfoliated form of particles while CaBt showed formations of platelet stacks.

In terms of composite filler, the treated bentonite was produced in the form of phase-separated (expanded) layers for CaBt and exfoliated layers for NaBt. The latter is highly desirable for its ability to improve the mechanical properties of composite when it is used as reinforcement material. As far as nanocomposite production is concern, producing organically-modified bentonite is essential and maximum protein recovery is an added advantage. Therefore, treated NaBt could be better at composite reinforcement because of high organic content and exfoliation.

CHAPTER 7

PARTICLE SETTLING PROCESS

7.1 Introduction

After gelatin adsorption, spent adsorbent has to be separated. For lab scale experiments, a centrifuge can be used, however due to cost (more in Section 7.8), large scale clay recovery from solution needs other alternatives such as settling tanks, screw presses and sieving. Screw presses saw major use in sewage treatment plants to thicken the final sludge product with 70 % water removal and it is suitable for continuous operation [188]. Most modern meat rendering plants in New Zealand are semi-continuous processes and could potentially use screw presses for clay recovery. However, the solid content in solution has to be high for the screw press to be effective [188]. This makes this approach unsuitable for a clay recovery process unless the clay has settled into a thick slurry.

In this chapter, the settling behaviour of bentonite in gelatin solution was studied. The settling was investigated by placing the gelatin and betonite solution in a settling column and recording the change in solution turbidity in the column at different heights over time. The turbidity readings were converted into clay concentration in the solution using standard curves in Figure 78 and Figure 79 (Appendix-3B and 4B). Then, settling profile graphs were plotted at various conditions. Other parameters recorded include the height of pellet formation and visual observation.

To help understanding the settling process at different pH conditions, viscosity profiles of gelatin and stickwater solutions were developed. Stoke's Law was used to predict settling velocity based on solution viscosity, density and particle size. A settling model was later developed in Matlab based on various assumptions.

7.2 Viscosity Profile of Gelatin and Stickwater

Gelatin solution could be a Newtonian or non-Newtonian liquid depending on the concentration of solute and temperature. It changes from visco-elastic liquid at high temperature to Bingham plastic when cooled to a gel. When heated in solution, it loses its triple helix structure and behaves like a viscous liquid. It flows in the direction of the stirring force but when the force is stopped, the flow slows down and reverses before stopping due to its elasticity. When in gel-form, gelatin behaves as a solid in the absence of stress and flows like a liquid at high stress, like toothpaste [189]. Graphs of viscosity profiles of gelatin and stickwater were developed at different pH, protein concentration and temperature to be used in settling model. The term viscosity refers to dynamic viscosity unless stated otherwise.

Figure 49 shows that the viscosity of gelatin solution increases with gelatin concentration but decreases with temperature, typical for a Newtonian fluid. Higher gelatin concentration increases the frequency of molecular crosslinkings to form a large network. This reduces the molecular diffusivity of gelatin in the solution and increases the tendency of gel formation. As temperature increases, the molecules gain more energy to move faster, causing the viscosity to decrease. Also, the boundary layer between the solution and the Ubbelohde tube wall becomes thinner at high temperature creating a more streamline flow. This is shown by the difference between solution viscosities across all concentrations were within 275 % at 20 ^{o}C and reduced to 130 % at 80 ^{o}C. All viscosity profiles of solutions are presented in Figure 84 (Appendix-9).

Raw stickwater had a much higher viscosity than 4 % gelatin, even though it contained only 3.5 % protein (Table 20 – Section 6.2.2) because of its organic and fat content. Dilution of stickwater to 2 % protein concentration reduced the viscosity by over 60 % which might be an advantage for adsorption (Figure 49). There were no data points for viscosity of gelatin solution at 2 % and 4 % concentration (Figure 49) at 20 ^{o}C because gels were formed. This is in contrast to stickwater solutions that remained in liquid-form across all temperature tested, attributable to shorter-length gelatin molecules in stickwater because the meat by-products were heated at high temperature for a long time, causing some thermal degradation of the gelatin.

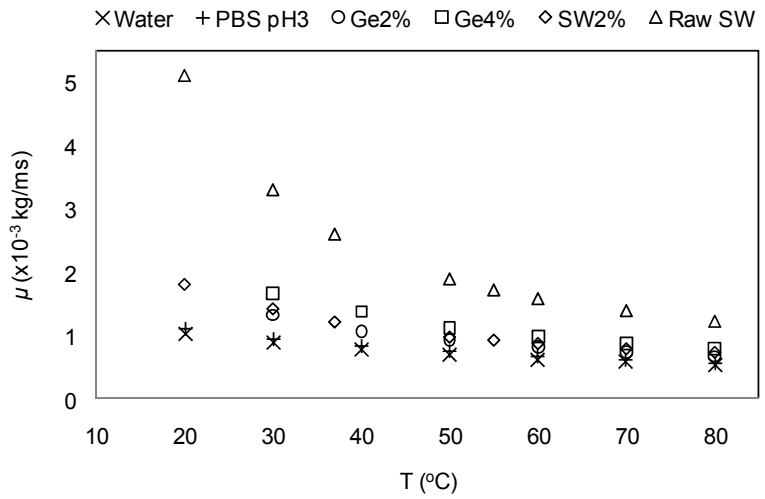

Figure 49: Viscosity profile of gelatin and stickwater solutions at various concentrations and temperatures ($1x10^{-3}$ kg/ms = 1 mPa.s). Datapoints are mean values of three replicates.

7.3 Reynold's Number for Particle

By applying the experimentally determined viscosities, μ (Figure 49), particle diameter, D_{cp} (Table 33) and settling velocity (V_s) (Figure 52) into Equation 25 (Section 3.8.1), Reynold's numbers (Re_p) were calculated for the conditions that had resulted in settling and summarized in Table 34. The Re_p values are well below 1, indicating a laminar flow or the system is said to be in the Stoke's region [137].

Table 33: Particle size of treated samples with gelatin 2 % as determined from laser analysis.

Treated sample	Solution pH	Particle diameter, D_{cp} (μm)
CaBt	3	35.72
	5.23	35.68
	7	18.62
	9	9.21
NaBt	3	20.54
	5.23	17.88
	7	9.51
	9	5.89

Table 34: Reynold's number of bentonite particle in settling system.

Bentonite type	Settling condition	V_{ss} (x 10^{-5} m/s)	μ (x 10^{-3} kg/ms)	Re_p
CaBt	Ge2%, pH 3	1.94^{+}	1.22	0.00056
	SW2%, pH 3	4.35^{+}	1.20	0.00128
NaBt	SW2%, pH 3	$1.78^{\wedge}$	1.20	0.00048

Settling velocity at $^{+}$85% and ^ 60% clay recovery.

7.4 Stoke's Law Particle Settling Velocity

Equation 26 (Section 3.8.1) was used to find the Stoke's law settling velocity, V_{ss} of bentonite particles in gelatin and stickwater solutions using experimentally determined data such as viscosity in Figure 84 (Appendix-9); density (Table 36) and particle size (Table 33). To determine settling time, the column height (400 mm) was divided by the settling velocity. It can be seen from Table 35 that the Stoke's law gave high settling times for CaBt at pH 7 and 9, and for NaBt at pH 5.23, 7 and 9, implying the particles would require a long period of time to settle or not settle at all. Based on experiments, settling was obtained only at pH 3 and 5.23 for CaBt in model solutions at conditions of relatively high V_{ss} and low t_{ss} (Table 35). However, CaBt settling at pH 5.23 was marginal compared to pH 3 (Figure 51A and B).

Validation on stickwater 2 % was done at pH 3, corresponding to the best settling conditions from model solutions. It was found that the V_{ss} and t_{ss} for stickwater are comparable to its gelatin counterparts. At 2 % protein concentration, stickwater had higher solution density and viscosity compared to gelatin 2 % due to the organic content. From the Stoke's law equation, V_{ss} is decreasing at increasing ρ_f and μ which explains the lower V_{ss} obtained for stickwater (Table 35).

Experimentally determined settling velocities were smaller than theoretical values (Table 35). For example, the settling velocity for CaBt in gelatin 2 % solution at pH 3 is 1.94×10^{-5} m/s (at 85 % removal) compared to an average calculated value of 20.1×10^{-5} m/s from Stoke's law. This suggests that the Stoke's law over predicted the settling velocity for clay in gelatin solution because it does not consider the interactions between particles-gelatin and particles-particles.

In the following section, the clay settling velocity profiles were constructed based on the experimental data for comparison with the Stoke's model. Later, a model was developed by considering the physical forces involved in the settling process to predict the clay concentration in solution over time.

Table 35: Stoke's law settling velocity, V_{ss} and time, t_{ss} of bentonite particles in gelatin solutions.

Solution	Settling velocity, V_{ss} (x 10^{-5} m/s)		Settling time, t_{ss} (hr)	
	CaBt	NaBt	CaBt	NaBt
Ge2% - pH 3	20.10	4.78	0.55	2.32
pH 5.23	15.02	0.44	0.74	25.49
pH 7	8.91	0.08	1.25	132.53
pH 9	1.19	0.36	9.31	30.58
SW2% - pH 3	19.60	4.15	0.57	2.68

7.5 Bentonite Settling Experiment

7.5.1 Particle Settling in Gelatin Solution

Flocs are formed when fine suspended solids or colloids stick together. When floc density is larger than the surrounding solution they start to settle. In this work, the term pellet was used to refer to the solid mass of gelatin-treated bentonite recovered after centrifugation. Without centrifugation, the term sediment is used to refer to the settled solid mass via gravity.

Experimental results on settling experiments are listed in Table 36, and shown in Figure 50 and Figure 51. Particle settling patterns in Figure 50 suggest that bentontite settling in gelatin solution is strongly influenced by solution pH. It can be seen from Figure 51 that the treated CaBt gave good settling at pH 3, marginally settled at pH 5.23 and did not settle at pH 7 and 9. There was no settling observed for treated NaBt at all conditions. Large volumes of floc with clear solutions can be observed for unsettled conditions while small volumes of sediment with muddy solutions were obtained for settled conditions (Figure 51, CaBt- A and B).

For conditions that gave settling, the clay concentrations in solutions were decreasing over time across all outlets (Figure 50) and flocs were observed to form compact sediments at the bottom of the settling column. These observations are in agreement to the increase in clay recovery percentage during settling (Figure 85A and B, Appendix-11A). Where clay did not settle, there was little change in clay concentration at all outlets due to a stable particle dispersion of a "sponge-like" structure known as hydrogel (Figure 51). The stability of this structure depends on the temperature, pH and the ionic strength of the solution [130, 133].

XRD performed on solid particles recovered after settling experiments showed that the basal spacings of bentonite before (Table 30) and after (Table 54, Appendix-10) settling were similar, indicating that there was no desorption of solutes from the interlayer gallery. The values of density, ρ and mass of dried recovered pellet, m_{Cr} were recorded from the overnight settling and it was assumed that the readings remained unchanged after 2 hours of settling.

Table 36: Summary of bentonite settling.

Treated sample	Gelatin 2 %					Stickwater 2 %		
	Settling	m_{Cr} (g)	ρ (kg/m^3)	h* (mm)		Settling	h (mm)	
				2 hr	overnight		2 hr	overnight
CaBt								
pH 3	Yes	42.44	1353.9	31.0	38.0	Yes	148.0	90.0
pH 5.23	Yes/No	42.07	1329.7	nv$^+$	134.5	No	-	-
pH 7	No	53.25	1120.7	nv	283.0	No	-	-
pH 9	No	54.30	1123.5	nv	294.5	No	-	-
NaBt								
pH 3	Yes	56.56	1092.3	nv	283.0	Yes	135.0	92.0
pH 5.23	No	58.44	1046.5	nv	317.0	No	-	-
pH 7	No	60.02	1054.1	nv	331.0	No	-	-
pH 9	No	59.92	1070.7	nv	nv	No	-	-

** sediment height, $^+$ not visible.*

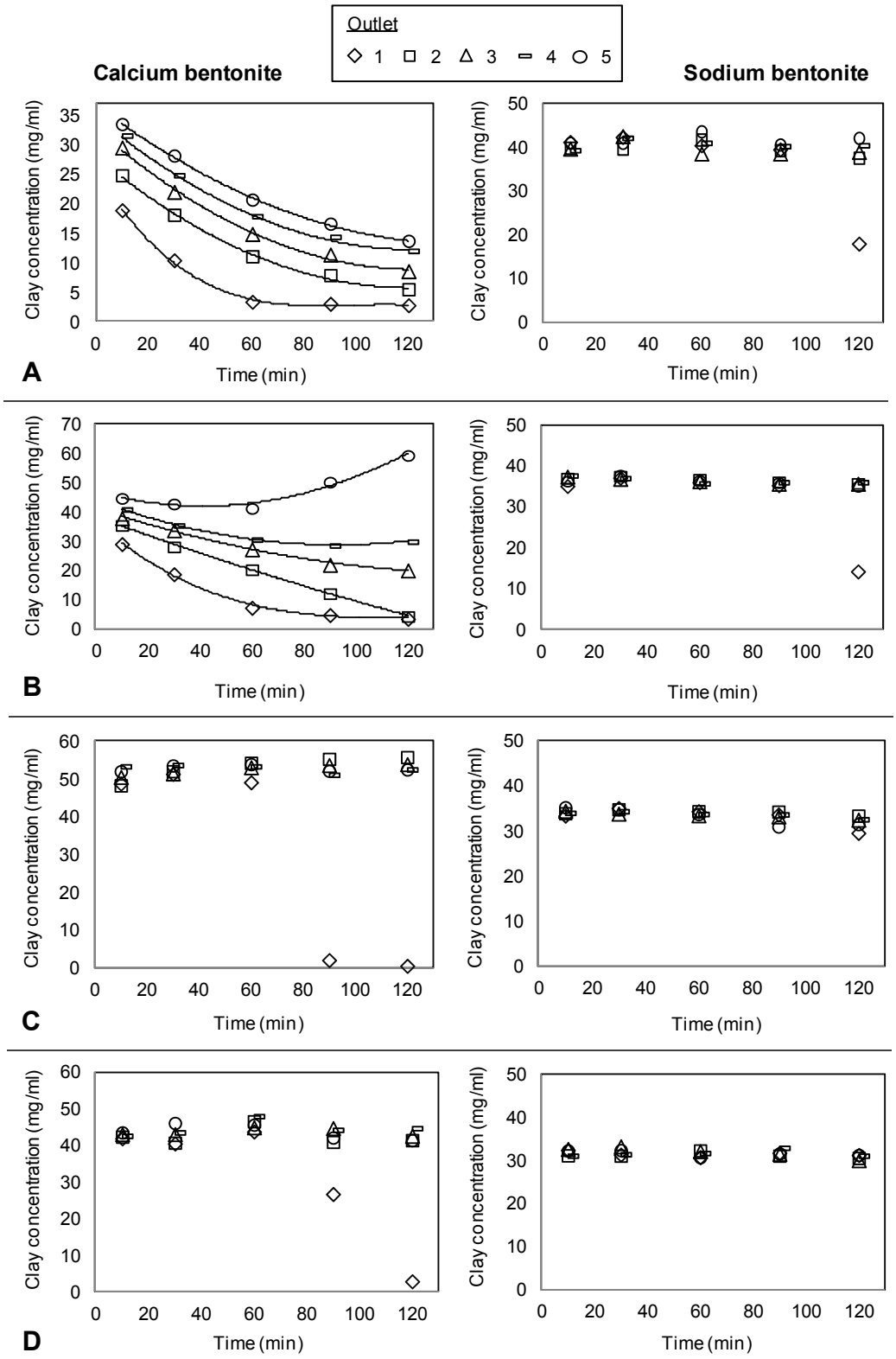

Figure 50: Bentonite settling over time in Ge2% for CaBt and NaBt at pH A) 3, B) 5.23, C) 7 and D) 9. Outlet 1 is at the top and 5 is at the bottom (Figure 27). Datapoints are mean values of three replicates.

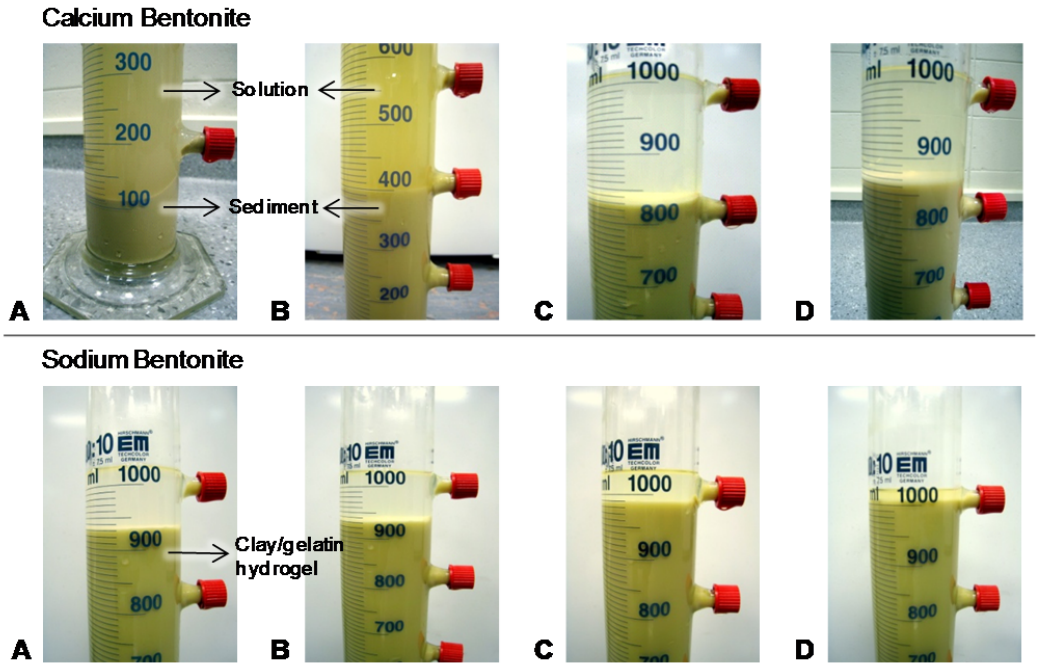

Figure 51: Particle settling after overnight in gelatin 2 % solution for CaBt and NaBt at pH A) 3, B) 5.23, C) 7 and D) 9.

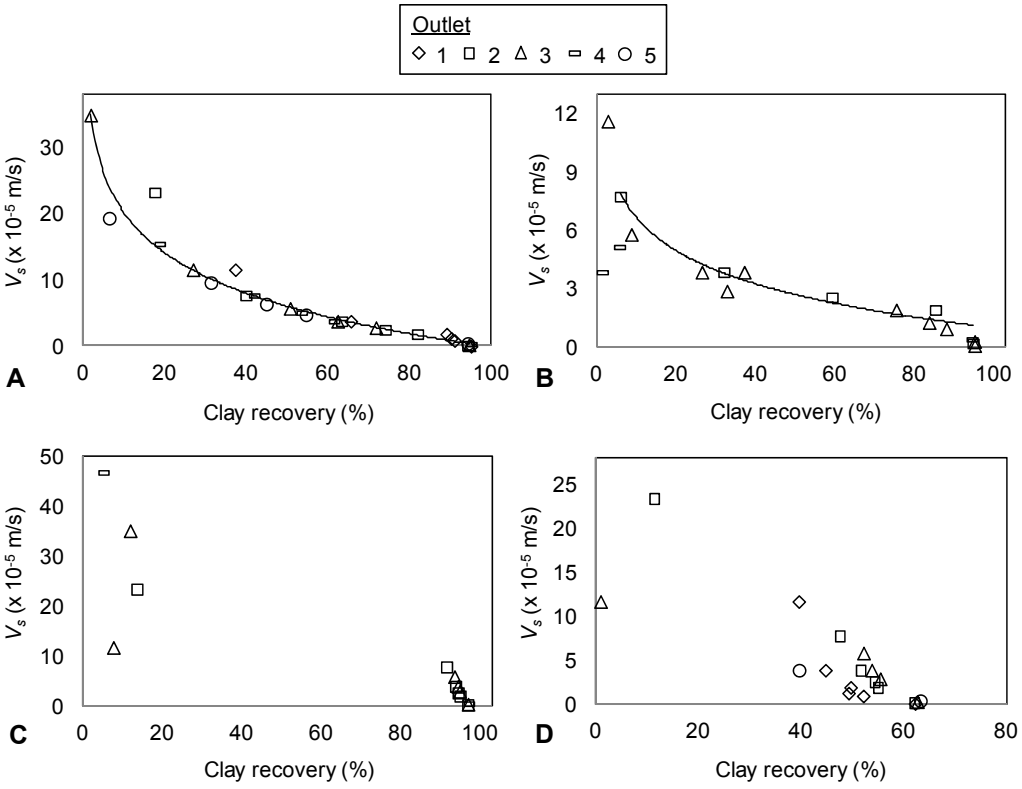

Figure 52: Profiles of overflow settling velocities of up to 2 hours for CaBt in gelatin 2 % solution at A) pH 3, B) pH 5.23, C) stickwater 2 % at pH 3 and D) NaBt in stickwater 2 % at pH 3.

From the calculated percentage removal of organics (Table 56, Appendix-12), the profiles of the overflow settling velocity (Figure 52) were graphed by calculating settling velocity for each outlet position and time and plotting that against percentage removal. Figure 52 indicates the required overflow settling velocity to achieve a specific percentage of organic removal. The negative values of removal obtained (Table 56, Appendix-12) resulted from sediment rising above the sampling outlet as well as increasing suspended particle concentration in the early stages of settling. Any negative values were excluded from Figure 52.

Treated CaBt had the highest pellet densities at pH 3 and 5.23, however the amount of adsorbed gelatin, C_r and mass of dried recovered pellets, m_{Cr} were the lowest. This can be explained by larger particle size of CaBt at pH 3 and 5.23, which is at around 36 μm compared to others (Table 33). The CaBt particles were not exfoliated in solution at pH 3 and possibly at pH 5.23 (as evidenced from cryo-SEM images in Figure 48) therefore had a lower specific surface area leading to a lower adsorption of gelatin, C_r. At pH 5.23 (Figure 50B), outlet 5 shows clay concentration for CaBt at 60 minutes onward is increasing. This is attributed to sediment height rising above the sampling point which can be seen from the overnight sedimentation in Figure 51B for CaBt. This trend was absent at pH 3 because the sediment was more compact and settled below the sampling outlet.

Adsorption using CaBt was high at pH 7 and 9 which corresponded to small particle sizes, but no settling was observed. Small particles have higher specific surface area and can enhance adsorption. High C_r implies more opportunities for crosslinks between gelatin and bentonite to form an expanded and stable low density network, therefore no sedimentation. This resulted in lower CaBt pellet densities at pH 7 and 9.

Sodium bentonite exfoliated in solution and had higher SSA and C_r. Similar to CaBt at high pH, the high degree of crosslinking between platelets and gelatin could be a reason for the stable particle dispersion and therefore did not settle. For treated NaBt at all conditions, the differences in ρ and m_{Cr} were within 4.4 % and 6.1 % respectively. The consistent values suggest that NaBt could have a similar binding affinity toward gelatin regardless of solution pH. This hypothesis supports the idea made earlier regarding the discrepancy in C_r measurement on NaBt due to gelling at

high pH (from pH 3 to pH 9). If this was the case, C_r values for NaBt should have been a lot higher than what were obtained (Table 23).

In the settling process, the two types of forces involved are physical and chemical forces. Physical forces include gravitational, buoyancy and drag while chemical forces refer to the molecular interactions in the system as listed in Table 37. The ionic interaction could be the main force influencing the settling. In a stable particle dispersion, the forces are in balance and settling of bentonite does not occur unless there are external forces disturbing colloidal stability. Some chemical interactions in Table 37 are affected mainly by solution pH. It was suggested that in the case of charge-stabilized dispersion (ionic interaction due to charge deficiency), often an addition of electrolyte leads to gelation rather than flocculation due to the increased interactions with the aqueous ions and solutes. Gelation can be viewed as continuous phase flocculation which can be disturbed by changing the electrolyte concentration [130].

Calcium bentonite adsorbed best at pH 9, implying a strong interaction between the clay and gelatin. This interaction weakened as pH decreased. At pH 3, both bentonite and gelatin had an overall positive charge. Repulsion force between gelatin molecules was greater at pH 3 than at any other pH. This means more energy was needed to bring gelatin molecules together rather than keeping them apart. The gelatin molecules adhered to the bentonite surface by weak electrostatic forces. This had decreased the free energy of activation needed for bonding solutes onto the solid-phase. As a consequence, the stable colloidal state of clay particles weakened and the particles started to settle. Therefore at low pH, the particles are more likely to fall freely in the solution due to gravity.

Calcium bentonite only showed partial settling at pH 5.23 (gelatin PZC) because the overall charge of gelatin is a combination of positive and negative charges. Thus, electrostatic interactions between negatively charged bentonite surface and gelatin had increased. At the same time, the repulsion force between gelatin and solution viscosity increased, leading to a stable particle dispersion. It is expected for this behaviour to intensify as the solution pH increases.

Table 37: Interactions of clay and gelatin molecules in solution [2, 9, 89].

Interactions	Details
Electrostatic	Between positively and negatively charged regions on bentonite platelets and gelatin, platelet edge and surface and inter/intra molecular of gelatin.
van der Waals	Adsorption of neutral molecules onto external surfaces.
Hydrogen bond	Water molecules and amino acids of gelatin molecules.
Hydrophobic	Water-dislike regions on gelatin molecules.

7.5.2 Particle Settling in Stickwater

Settling experiments of bentonite in stickwater were done according to the method outlined in Section 5.6.3. Settling was only observed at pH 3 for CaBt and NaBt. From Figure 53, it can be seen that the clay concentration increased over time at outlet 4 and 5 for CaBt and NaBt. They both settled at almost similar settling rates and formed comparable sediment heights (Table 36). Figure 53 shows that CaBt had lower clay concentration in solution after 2 hours, indicating better settling and more compact pellet (Figure 54A). This agrees with the previous work done on stickwater organic recovery using CaBt and NaBt where the former was found to form a denser sediment [24]. This is also the main reason for using CaBt for wine clarification because it produces a more compact lees (clay / wine organics sediment) that could be advantageous in downstream processing [70, 123].

Unlike in previous experiments using gelatin-treated bentonite, both CaBt and NaBt settled at pH 3 in stickwater instead of just CaBt. From the stickwater adsorption data (Table 27), the settling corresponded to the conditions with the highest organic adsorption (230 - 240 mg/g), whereas for gelatin solution, CaBt settled at the lowest gelatin adsorption (230 - 300 mg/g) (Table 23). It is clear that in both model and stickwater solutions, the settling occurred at conditions with almost similar C_r, therefore the solution pH had a higher influence on settling than the amount of adsorbed gelatin.

At pH 3, gelatin had a positive charge and formed crosslinks between clay particles leading to sedimentation. This trend was diminishing at increasing pH as the gelatin was becoming more negatively charged; increasing the electrostatic interactions and the solution viscosity. Therefore, the settling of bentonite in gelatin solution was poor

at high pH. The situation is different for stickwater because the organics are in the form of short-chain molecules (shown by smaller *d*-value in Table 30). Stickwater was unable to form a gel across all temperatures tested because collagen had lost its triple-helix structure, reduced molecule size and/or the presence of fats and other organic matters could have hindered the gel formation. It is also possible that the organics were in expanded configuration rather than coils. During adsorption, bridging and particle network formation can occur between the stickwater organics and platelets. However, the particle dispersion network could be less stable compared to bentonite in gelatin solution, making the system very sensitive toward pH changes.

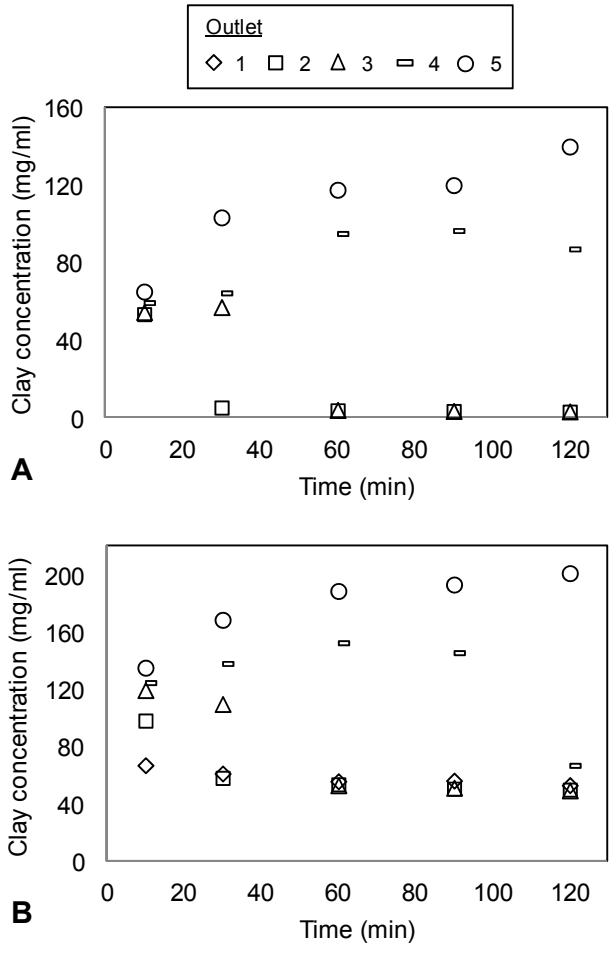

Figure 53: Particle settling over time in stickwater 2 % solution at pH 3 for A) CaBt and B) NaBt. Datapoints are mean values of three replicates.

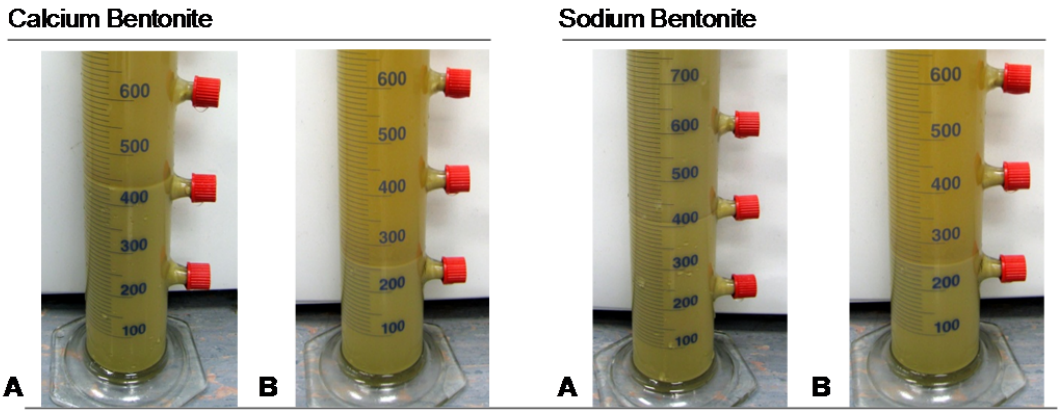

Figure 54: Particle settling of CaBt and NaBt in stickwater 2 % solution at pH 3 after A) 2 hours and B) overnight.

7.6 Particle Settling Mechanism

From earlier discussion, bentonite platelets consist of silica surfaces (permanently negatively charged) and alumina edges (charge is pH-dependent). The point of zero charge (PZC) of bentonite is a combination of the PZC of silica (< pH 3) and alumina (~pH 7). The negative charge accounts for 95 % of the total surface area and is balanced out by cationic adsorption [112, 156].

In solution, the bentonite layers swell because of water uptake. At decreasing pH, the alumina edge is becoming more positively charged resulting in an "edge-face" interaction, leading to a "house of cards" structure (Figure 58). Many authors had hypothesized the role of this structure for gelation of smectites at low pH and low electrolyte concentration. The formation is largely influenced by electrostatic forces. In aqueous solution, the gel can be formed at as low as 2 wt% clay dispersion [130, 133]. The gel is a three-dimensional network of clay and in the presence of gelatin, the house structures are interconnected by gelatin molecules into a large network of card houses which are larger and denser than individual platelets. This formation had resulted in settling of CaBt at pH 3 where the particles were shown to have larger particle size (Table 33).

The card-house formation can be disrupted by changing the solution pH. For example, as pH increases, the edge charge shifts from positive to negative, causing the face-edge electrostatic interaction to weaken. The house of card formation

eventually collapses into the original forms of stacks of individual platelets at pH above the PZC of bentonite [130]. It was suggested that the flocculation can be achieved at this stage by adding anionic copolymer such as polyacrylamide (PAM) [133]. When the bentonite is in gelatin solution however, flocculation could be hard to achieve because the faces of these individual platelets are covered with gelatin molecules resulting in a stable suspension. The particles were possibly exfoliated in solution at high pH as shown by small particle sizes especially for CaBt at pH 9 and NaBt at pH 7 and 9 (Table 33).

Apart from pH, the degree of smectite gelation and swelling can be reduced by increasing the electrolyte concentration such as by adding multivalent cations. The cations would occupy the binding sites on the surface and help to suppress the electric double layer (a reference diagram of surface potential is given in Figure 17, Section 4.2.2). An example of such cases can be seen in bentonite settling in water where at higher surfactant loading, the gel formation changed to voluminous flocs. In stronger electrolytes, there will be less water uptake by the platelets and therefore less swelling [190]. Stickwater has a high aqueous salt content than gelatin solution as evidenced from a high ash content obtained from TGA (Table 21), so it is possible that there was some exchange of Ca^{2+} or Na^{+} for monovalent or multivalent cations in stickwater, leading to the similar settling behaviour of CaBt and NaBt in stickwater.

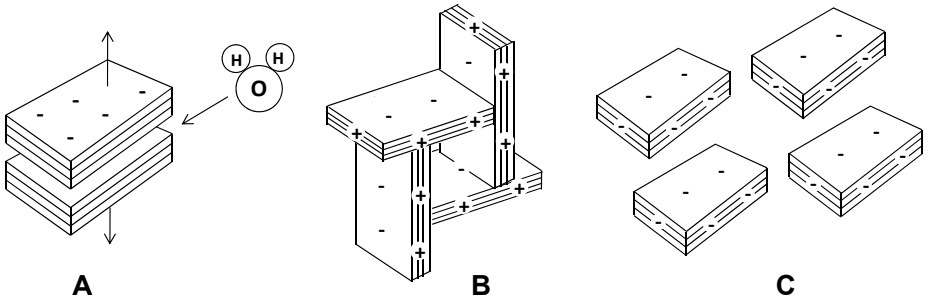

Figure 55: Bentonite structure in solution A) swelling upon hydration, B) "house of card structure" at low pH (below 7) and C) platelets dispersion at pH above 7 [191].

Gelatin molecules adsorb on the surfaces and also within the interlayers. Flocculation or coagulation can happen via two mechanisms; bridging and / or "charge-patch" [89]. For relatively large ratio of solid-phase size to solute molecules, charge-patch is highly likely to take place while bridging is most effective if the particles are small and concentrated. A collagen molecule is relatively small (1.5 nm x 300 nm) compared to bentonite (less than 36 μm, Table 33). However, gelatin molecules can form large intertwined networks in solution especially at high concentration. In adsorption, gelatin molecules can be seen enveloping entire bentonite particles and also crosslinking the particles (as viewed under cryo-SEM, Figure 48). This finding ruled out the charge patch possibility.

Unlike in adsorption, there was no stirring mechanism applied for settling. Without this external force, platelets started to attract and repel each other depending on the solution pH. At pH 3 and 5.23, CaBt had positive edges and thus assumed the card-house structure. This form of bentonite had less total surface area compared to individual platelets. During adsorption, gelatin would adsorb on the surface of the card-house structure, restricting access to the internal surfaces, thus resulting in lower C_r. The card-houses were connected via bridging by gelatin molecules to form larger and denser flocs that settled as compared to bridging of gelatin with individual platelets at high pH which did not settle (Figure 56).

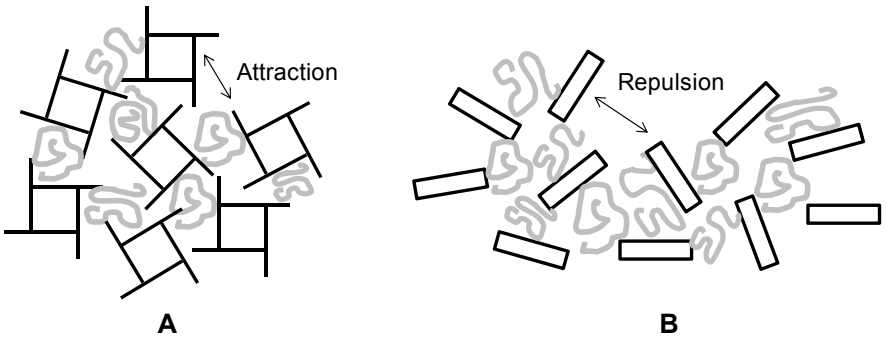

Figure 56: Bridging mechanism between gelatin molecules and bentonite in the forms of A) "house of card" at low pH and B) individual platelets at high pH.

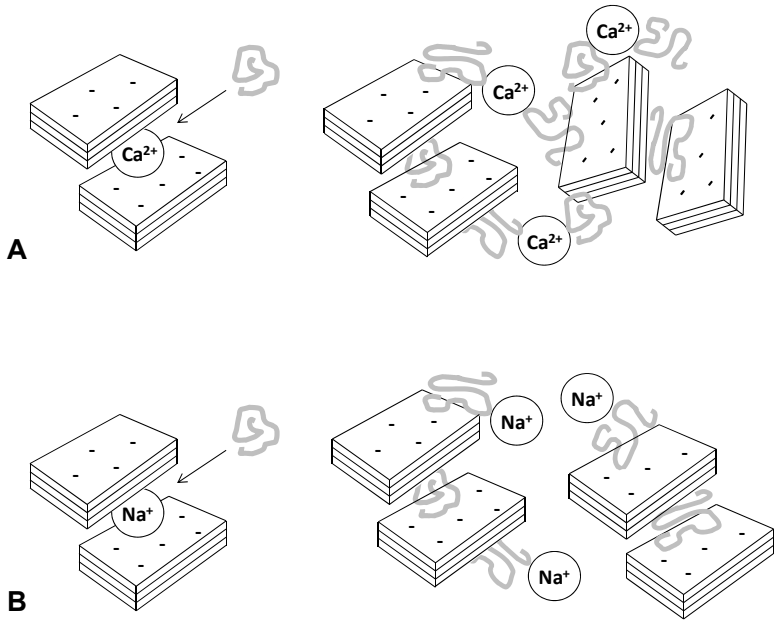

Figure 57: Effect of element's valency on gelatin adsorption on A) calcium and B) sodium bentonite.

Above pH 7, the house card structure collapsed into individual platelets, with both face and edge were negatively charged (Figure 55). Because the bentonite existed in individual platelets, the total surface area increased and gave better gelatin adsorption but no settling. One could assume settling is directly related to the amount of gelatin adsorbed because the adsorbed particles are presumably heavier and would settle. However, experimental findings showed that as the adsorption yield increased, the tendency for the solution to form a stable suspension also increased. This is attributed to the increase in repulsion force and high tendency of bridging between platelets and gelatin molecules.

Apart from pH, the valency of the ions is important because the coagulating power of an ion increases rapidly with its valency for example Ca^{2+} coagulates more than Na^{+} as depicted in Figure 57 [89]. The Ca^{2+} can easily bridge two counterions from gelatin molecules compared to just one for Na^{+}. This is shown by polyacrylamide (PAM) adsorption using bentonite in water where PAM had a flocculation effect with CaBt and deflocculation effect with NaBt [126]. Therefore, application of CaBt for settling process could be advantageous over NaBt due to bridging flocculation by Ca^{2+} compared to Na^{+}.

In term of clay type, the flowability of clay dispersion is related to the mineral composition and the following order was suggested from literature, CaBt > illite > koalinite > NaBt [1]. Overall, the stability of a bentonite dispersion in solution is a function of bentonite type, concentration of solid-phase and absorbate, agitation, solution pH and temperature.

7.7 Development of Settling Model for Bentonite in Gelatin Solution

To model the settling process, assumptions were made covering as many interactions as possible. The interactions and the model considerations are depicted in Figure 58. The assumptions made for the model are:

1) Spherical shape and uniform size particles.
2) Gelatin treated bentonite is assumed to behave as a fluid while travelling the column length due to its size (very small particles flow with the liquid).
3) The bentonite particles are evenly dispersed in solution with a uniform coating of gelatin.
4) Laminar settling of particles with a constant settling velocity across the width of the column.
5) Particle mass and size does not change because gelatin concentration on bentonite has reached equilibrium.
6) The entire particle system behaves as a crosslinked sponge with a large interconnected network structure with open pores for water to flow through.
7) No mixing of particles occurs between sections.
8) Negligible interaction of the mixture with the column wall because of very high aspect ratio (column diameter, 0.06 m divided by particle diameter, 3.572×10^{-5} m).

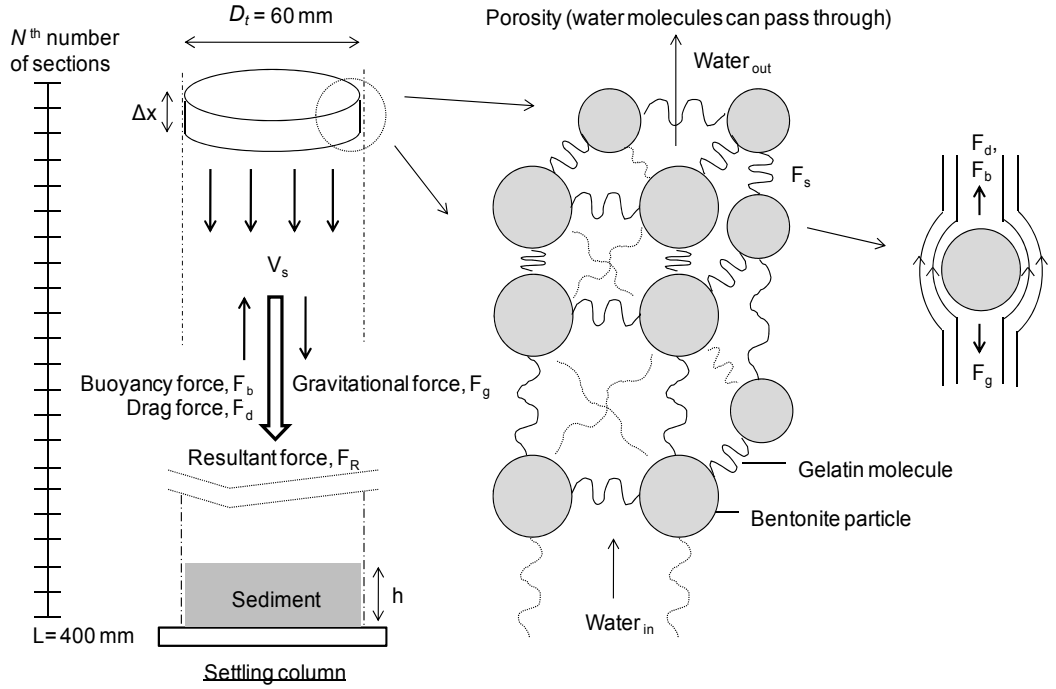

Figure 58: Free-body-diagram of bentonite particles in quiescent gelatin solution.

Assumption number four is justified through the Reynold's number calculation where solution flow around the particles in gelatin and stickwater solutions is laminar. For assumption number five, basal spacing of CaBt after settling overnight (Table 54, Appendix-10) are within 10 % (± 2 Å) to that from adsorption (Table 30) and C_r was within 5 % from 20 to 60 minutes (Figure 34), indicating the system was at or close to equilibrium. The final assumption can be supported by a simple ratio calculation:

$$Aspect\ ratio = D_t : D_{cp} \tag{43}$$

where D_t and D_{cp} are the diameter of settling column (m) and clay particle (m). Substituting the values from Table 38 gives an aspect ratio of 1680 to 1. This correlation is important when the ratio of column to particle diameter is less than 50 to 1, at which wall effects become significant [192]. Therefore the wall effect is negligible for bentonite settling in this work.

Assumption number six can be supported by examining the microporous structure of gelatin / clay mixtures. At 2 % gelatin solution, the system was observed under cryo-SEM to have a microporous network (Figure 48), with gelatin-treated CaBt having pore sizes ranging from 10 to 20 *u*m. A crude calculation of distance between particles in a suspended solution (36 g bentonite in 1200 ml solution with an average particle diameter of 36 *u*m) showed that there was approximately 87 *u*m distance between particles and when settled, the distance was reduced to approximately 20 *u*m between particles. A similar observation was reported in cryo-SEM performed on pure gelatin solution where it was shown to have a pore diameter of 147 μm at 5 wt% concentration and reduced to 70 μm at 15 wt% concentration [79]. It is therefore reasonable to assume that the bentonite / gelatin suspension behaves like a crosslinked sponge.

The settling column was divided into number of sections, N_s (400) along the tube height, h_t (400 mm) to give tube sectional height, h_{ts} of 1 mm. The cross sectional area, a_{ts} (m^2) and volume of a single section, V_{ts} (m^3) can be calculated by:

$$a_{ts} = \frac{\pi {D_t}^2}{4} \tag{44}$$

$$V_{ts} = a_{ts}.h_{ts} \tag{45}$$

where D_t is the tube diameter (m). Initially, 36 g of bentonite (m_c) was added and mixed into the solution; therefore, each section contains an equal mass of bentonite clay. The mass of particles in a section, m_{cs} (kg) and an individual particle mass, m_{cp} (kg) were determined from:

$$m_{cs} = \frac{m_c}{N_s} \tag{46}$$

$$m_{cp} = V_{cp}.\rho_{cp} \tag{47}$$

where m_{co} is the initial mass of bentonite added (kg), V_{cp} and ρ_{cp} are the volume (m^3) and density (kg/m^3) of an individual gelatin-treated bentonite particle. By assuming spherical shape particles, Equation 47 becomes:

$$m_{cp} = \frac{4}{3}\pi {r_{cp}}^3 . \rho_{cp} \tag{48}$$

where r_{cp} is the average particle radius (m). The total number of particles in a section, n_{cps} was calculated using:

$$n_{cps} = \frac{m_{cs}}{m_{cp}} \tag{49}$$

To find the modelling parameters, experimentally determined values were substituted into Equations 44-49 and the calculated values are summarized in Table 38.

From Figure 58, there are several physical laws governing the settling process. For each clay particle, there are four forces acting on it; gravity, drag, buoyancy and elastic force. The elastic force is generated by the gelatin molecules acting as springs between particles. By taking a column section as a system, the gravitational force, F_g (kgm/s^2) acting on a section can be expressed as [193]:

$$F_g = m_{cs} . g \tag{50}$$

where g is gravitational acceleration (9.8067 m/s^2). The buoyancy force, F_b (kgm/s^2) is expressed as [130, 135]:

$$F_b = \rho_f . g . V_{cp} . n_{cps} \tag{51}$$

where ρ_f is the density of gelatin solution (kg/m^3). The gravity and buoyancy force were considered to be constant throughout the settling process.

Table 38: Parameters of settling process model for CaBt in gelatin 2 % at pH 3.

Modelling parameters	Values
Column dimension	
Diameter, D_t	0.06 m
Height, h_t	0.4 m
Height of a section, h_{ts}	0.001 m
Number of section, N_s	400
Calculated values	
Cross-sectional area of column, a_{ts}	0.002827 m^2
Volume of a section, V_{ts}	2.827 x 10^{-6} m^3
Volume of a single particle, V_{cp}	2.3863 x 10^{-14} m^3
Mass of a particles in a section, m_{cs}	9.0 x10^{-5} kg
Mass of a single particle, m_{cp}	3.2309 x10^{-11} kg
Total number of particle in a section, n_{cps}	2785627
Final sediment porosity, e_f	0.75252
Experimental data	
Initial mass of bentonite added, m_{co}	0.036 kg
Diameter of bentonite particle, D_{cp}	35.72 x 10^{-6} m
Radius of bentonite particle, r_{cp}	17.86 x 10^{-6} m
Density of gelatin-treated bentonite, ρ_{cp}	1353.9 kg/m^3
Density of gelatin, ρ_f	988.654 kg/m^3
Dynamic viscosity of gelatin, μ_f	0.0012171 kg/ms
Constants	
pi, π	3.1416
Gravitational acceleration, g	9.8067 m/s^2
Elastic constant, k_s	0.22 kg/s^2
Flux coefficient, k_f	0.000002

Another force acting in the opposite direction (Figure 58) is the drag force, F_d (kgm/s^2) and can be calculated using [130, 135]:

$$F_d|_{n,t} = 6\pi.\mu_f.r_{cp}.V_s|_{n,t} \quad (52)$$

where μ_f is the gelatin viscosity (kg/ms) and V_s is the settling velocity (m/s) which is dependent on section, n (or height) and time t. At $t = 0$, $V_s = 0$, thus the initial $F_d = 0$.

Finally, the spring force, F_s (kgm/s^2) is represented by Hooke's Law and is dependent on element position and time [194]:

$$F_s|_{n,t} = k_s.\Delta x|_{n,t} \quad (53)$$

where k_s is the spring constant (kg/s^2) and the initial value was estimated based on gelatin elasticity obtained from literature (Figure 86, Appendix-13) [195]. This value was adjusted to find the best fitted curve relative to the experimental curves in Figure 50. The term Δx is the change in sediment height formation at a given time and is expressed:

$$\Delta x|_{n,t} = h_{ts}|_{n,t=0} - h_{ts}|_{n,t} \tag{54}$$

In cases where $h_{ts}|_{n,t} > h_{ts}|_{n,t=0}$, $\Delta x|_{n,t} = 0$. This was to prevent negative values where section height had increased larger than the initial section height (i.e. spring under tension) which increased the total force being applied on a section.

The resultant force, F_R (kg.m/s^2) can be summarized as:

$$F_R = Downward\ forces - upward\ forces \tag{55}$$

$$F_R|_{n,t} = F_g - F_b - F_d|_{n,t} \tag{56}$$

Because F_s is only acting as an opposing force in the section of interest only, it is excluded from the F_R calculation and introduced in the following calculation for pressure. Because the system was model based on a "crosslinked sponge" structure, the stacking of each layer section on top of another resulted in a pressure acting on a section at a given height, P (kg/ms^2) and can be determined by:

$$P|_{n,t} = \frac{\left(\sum_{n=1}^{n-1} F_R|_{n,t}\right) - F_S|_{n,t}}{a_{ts}} \tag{57}$$

As the sediment is settling and compacting, the porosity is decreasing as solution is pressed out from between the particles. The porosity, e can be calculated from:

$$e|_{n,t} = 1 - \left[(V_{cp} \,.\, n_{cps}) \,/\, V_{ts}|_{n,t} \right] \tag{58}$$

Volumetric flowrate, Q (m^3/s) of solution leaving the element at a given time is:

$$Q|_{n,t} = \left(\frac{k_f}{h_{ts}|_{n,t}} \right) . a_{ts} . e|_{n,t} . \left(P|_{n,t} - P|_{n-1,t} \right) \tag{59}$$

where k_f is the flux coefficient and the initial value used was 0.000002. The volume of a given element at a given time is:

$$V_{ts}|_{n,t+\Delta t} = V_{ts}|_{n,t} - \left(Q|_{n,t} + Q|_{n+1,t} \right) \Delta t \tag{60}$$

At the top of the column or n=1, because solution is migrating to the top element:

$$V_{ts}|_{n,t+\Delta t} = V_{ts}|_{n,t} + Q|_{n+1,t} \Delta t \tag{61}$$

and at the base of the column or n=N_s:

$$V_{ts}|_{n,t+\Delta t} = V_{ts}|_{n,t} - Q|_{n,t} \Delta t \tag{62}$$

The height of a section or element can be calculated by:

$$h_{ts}|_{n,t} = \frac{V_{ts}|_{n,t}}{a_{ts}} \tag{63}$$

The concentration of a section or element is given by:

$$C|_{n,t} = \frac{m_{cs}}{V_{ts}|_{n,t}} \tag{64}$$

Modeling was done in Matlab where a programmer within the research group set up the workfile (the m-file is presented in the Appendix-14). The column was divided into 400 sections (N_s). Total simulation settling run times were two hours at time intervals, Δt of 0.05 seconds, a total of 144 000 time steps. During settling, each section size is changing with time. Therefore, the element position relative to a sampling point in the settling column is also changing. At each time step, the position or height of the element was determined by summing all the section heights underneath it. Then the clay concentration was determined by finding the elements corresponding to the outlet heights of 70, 140, 210, 280 and 350 mm. The model output is presented as clay concentration over time at five outlets (Figure 59) and was used to compare with the experimental results for CaBt settling in gelatin 2 % at pH 3 (the best settling condition).

Initially a large time interval was used in the simulation, but it was found that very small time intervals were required for the model to be stable. The memory demand for the simulation was around 5 gigabytes. Initial compiling of the code in Matlab took three to four hours, after which each simulation took 15 minutes. The constants k_f and k were adjusted to obtain a model result that approximated the experimental data best. This proved difficult to do because the model results and stability were extremely sensitive to these constants. A high k_f resulted in the model sediment settling too quickly while a high k resulted in the model not settling at all.

The model gave a similar decreasing trend of clay concentration compared to experimental findings (Figure 59). However, the model overpredicted the clay concentration in the solution at the different heights. Regression coefficient, R^2 was calculated from clay concentration data of the graphs (between Figure 59A and B). The R^2 seems to improve with settling distance from top to bottom (outlet 1 to 5). These values can be improved by reducing the time step in model and adjusting k_f and k to obtain comparable values to the experimental data. However the extent to which k_f and k could be adjusted and model remained stable was dependent on the time step which seemed to be limited by the computer resources. A smaller time step would increase the number of iterations and cause the computer to run out of memory and crash.

Another limitation of the model is it assumes a constant particle size (Table 18) whereas for more precise modelling, a particle size distribution should be considered. From the size distribution, larger particles should settle faster than smaller particles, making the modelling assumption of particle settling as crosslinked layers invalid. For particles with variable sizes, crosslinking structure maybe less stable and particles would settle individually rather than in sections.

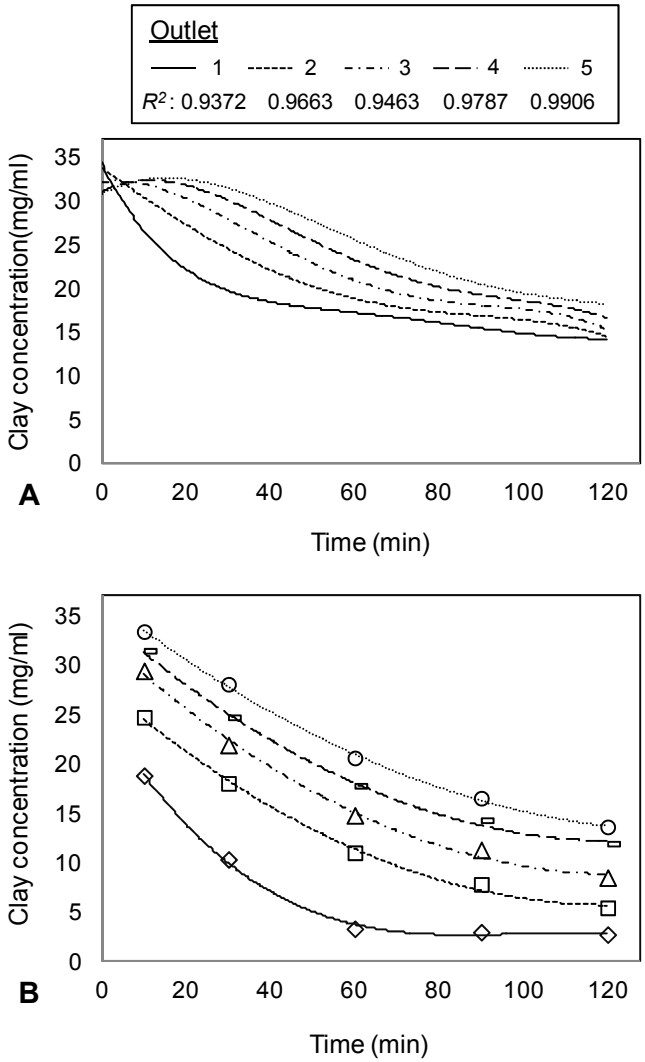

Figure 59: Settling profile of CaBt in gelatin 2 % at pH 3 based on A) Matlab modelling and B) experimental data. Open dots indicate the measured data from experiments.

7.8 Cost Analysis

From Figure 52A, settling velocity corresponding to 85 % CaBt removal from gelatin solution is 1.94 x 10^{-5} m/s. Assuming 8 hours treatment period for 30 000 L of stickwater, daily volumetric flowrate of stickwater is 0.001042 m^3/s. Dividing the flowrate by the settling velocity gives the area of the required settling tank and a round tank ($A = \pi r^2$) yields a diameter of 8.3 m. The purchase cost of the clarifier is NZ$ 129 996 while an equivalent sedimentation centrifuge costs NZ$ 133 149 (Figure 87, Appendix-15) [196]. This shows that equipment cost using sedimentation tanks is 2.4 % less than centrifuge but such small difference is not very promising to propose an alternative treatment process. In addition, a settling tank has a bigger footprint at 8.3 m diameter compared to a centrifuge and the treatment process is much slower.

However, stickwater treatment using sedimentation tank could be advantageous due to low operating cost in terms of electricity, labour requirement and maintenance. Furthermore, the adsorption process and settling can be performed in the same tank compared to a centrifuge where adsorption has to be conducted elsewhere prior to centrifugation. The choice of treatment process would be dependent on the desired product. For example adsorption should be performed if clays are intended for organic modification. Otherwise, a centrifuge could be suitable to dewater the stickwater prior to drying. More comprehensive cost analysis study should be performed covering all potential treatment processes and equipments. This should also include the prospective aspect of product development and the cost needed to adhere to environmental regulations.

7.9 Settling Summary

The setting of bentonite in gelatin solution was achieved with CaBt at pH 3 while for stickwater, both CaBt and NaBt settled at pH 3. These conditions did not always correspond to specific conditions of high or low gelatin adsorption, indicating the effect of solution pH is more dominant in settling compared to the amount of adsorbed protein. Hydrogel formation can be attributed to the gelatin network and the crosslinked particles while settling behaviour corresponded to the collapse of this structure. This clay / gelatin suspension is pH-sensitive and can be brought down by reducing the pH to 3. Sedimentation in stickwater at pH 3 could due to smaller gelatin molecules in stickwater compared to in model solution.

At conditions where settling was observed, graphs of clay recovery percentage from solutions were plotted (Figure 85, Appendix-11A). These graphs complement the settling trend obtained in Figure 50A and B and Figure 53. After 2 hours of settling, the highest clay recovery at outlet 4 in gelatin solution was obtained for CaBt at pH 3 (60 %) while in stickwater solution, NaBt at pH 3 gave the best particle recovery at 39 %. The recovery improved significantly after settling overnight as indicated by up to 94 % and 96 % recoveries for CaBt in gelatin and stickwater solution at pH 3 (Table 55, Appendix-11B). This suggests that a longer sedimentation time is needed for maximizing the clay recovery after adsorption treatment.

The Stoke's law predicted high settling velocities for conditions where settling did occur. However, it only assumes that the settling is a result of the particle's mass when the other forces balance each other. Hence, the settling velocity predicted from this expression is significantly higher than the experimental values. A settling model developed based on the physical interactions in the system showed reasonable comparison to experimental data, but further development is needed to improve the model fit as well as exploring methods to reduce memory use and simulation run time.

In the following chapter, the recovered sediments were incorporated into bloodmeal plastic to investigate its potential use as renewable bio-composite fillers. This would add value to the treated bentonite instead of just for stickwater treatment.

CHAPTER 8

BENTONITE NANOCOMPOSITES

8.1 Introduction

Clay minerals are known to improve many properties of polymers even at very low reinforcement dosage [10]. A considerable number of studies have been conducted using various types of layered silicates to enhance properties such as mechanical strength, thermal stability and flame retardation [177, 178]. Clays are modified with organics to increase the compatibility with polymers; the key to nanocomposite assemblies is the molecular interactions such as electrostatic, hydrophilic, hydrophobic, hydrogen bonding and van der Walls interactions [9, 11, 86].

In this chapter, bentonite was incorporated into Novatein Thermoplastic Protein (NTP) which is a bio-derived plastic from bloodmeal. The standard formulation of NTP is given in Table 16 (Section 5.7.1) and the mechanical properties from literature suggest that NTP has a tensile strength of 21 MPa, comparable to polylactic acid (PLA) and poly-ε-caprolactone (PCL) (Table 13, Section 4.5.4). The incorporation of bentonite into NTP could potentially yield a nanocomposite with improved mechanical properties as demonstrated in bentonite-reinfoced PLA [164], polydimethyl siloxane (PDMS) [172] and polypropylene (PP) [177]. The term composite is used as the generic term instead of nanocomposite to refer to the fabricated products of reinforced NTP because the formation of nanocomposites is yet to be proven.

The fillers (calcium and sodium bentonite) were organically-modified with gelatin and stickwater adsorption (Chapter 6) and prepared according to Section 5.4.5. Composite reinforcement was investigated using different bentonite types, intercalants and dosage amount while processing parameters and composition of the matrix polymer remained unchanged. The filler dosage was added on the basis of parts per hundred of bloodmeal (pph_{BM}).

Various characterization techniques were used on the composites to ascertain the effectiveness of bentonite reinforcement. The characterizations were performed in parallel to NTP in its pure forms for comparison. The sequence of the tests conducted and the abbreviations used for the composites is given in Table 39 and Table 40 respectively.

The injection moulded specimens were first characterized for their mechanical properties using tensile testing. Selected fractured specimens were viewed under SEM to assess their morphology. Viscoelastic properties were investigated using DMA to study the change in glassy and rubbery state of the composites. XRD was used to determine the intercalation or exfoliation of bentonite layers in the composites as well as the percentage crystallinity. The composites were finely ground into powder to be analyzed in TGA for thermal degradation properties. Finally, selected specimens were microtomed and viewed under a TEM to determine the state of filler dispersion (non-exfoliated or exfoliated) in the matrix polymer.

Table 39: Sequence of analysis techniques for bloodmeal composites.

Technique	Characterization parameters
Tensile testing	Tensile strength (σ), Young's modulus (E), toughness and strain (ε).
SEM	Morphology of fracture surfaces.
DMA	Glass transition temperature (T_g), storage ($E^{'}$) and loss ($E^{''}$) modulus.
XRD	Crystallinity, clay layers intercalation or exfoliation.
TGA	Moisture, organic and ash content.
TEM	Particle distribution in the matrix and clay layers exfoliation.

Table 40: Abbreviations for composites.

Designations	Filler type	Filler dosage (pph_{BM})
NTP	-	-
NTP-CaRaw0.25	Unmodified calcium bentonite	0.25
NTP-CaRaw0.5	Unmodified calcium bentonite	0.50
NTP-CaRaw1	Unmodified calcium bentonite	1.00
NTP-CaGe0.25	Gelatin-modified calcium bentonite	0.25
NTP-CaGe0.5	Gelatin-modified calcium bentonite	0.50
NTP-CaGe1	Gelatin-modified calcium bentonite	1.00
NTP-CaSW0.25	Stickwater-modified calcium bentonite	0.25
NTP-CaSW0.5	Stickwater-modified calcium bentonite	0.50
NTP-CaSW1	Stickwater-modified calcium bentonite	1.00
NTP-NaRaw0.25	Unmodified sodium bentonite	0.25
NTP-NaRaw0.5	Unmodified sodium bentonite	0.50
NTP-NaRaw1	Unmodified sodium bentonite	1.00
NTP-NaGe0.25	Gelatin-modified sodium bentonite	0.25
NTP-NaGe0.5	Gelatin-modified sodium bentonite	0.50
NTP-NaGe1	Gelatin-modified sodium bentonite	1.00
NTP-NaSW0.25	Stickwater-modified sodium bentonite	0.25
NTP-NaSW0.5	Stickwater-modified sodium bentonite	0.50
NTP-NaSW1	Stickwater-modified sodium bentonite	1.00

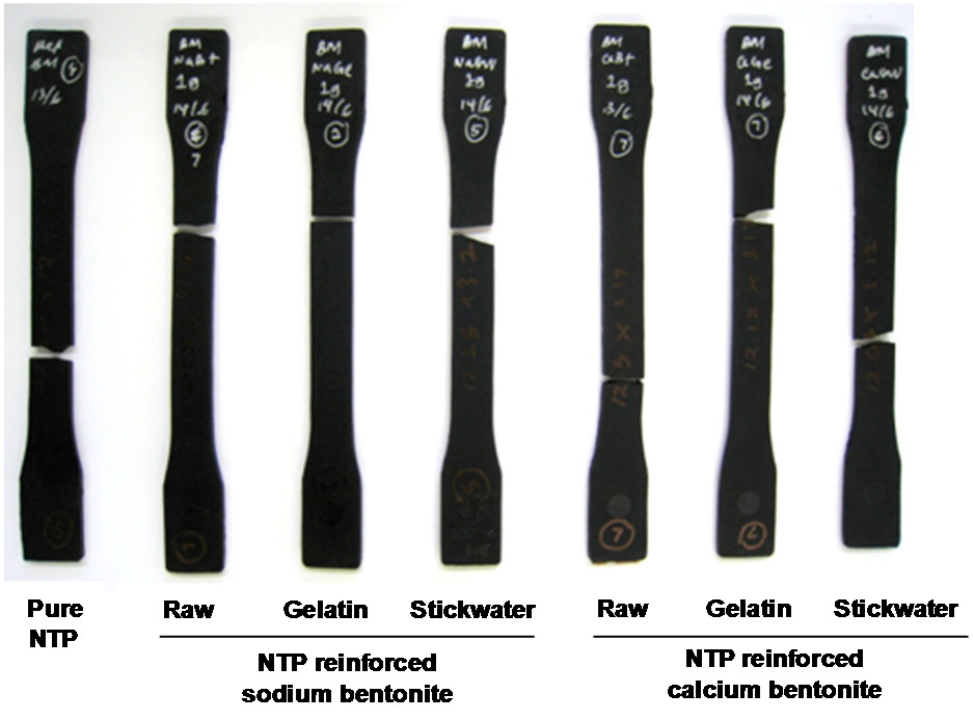

Figure 60: Visual observations on fractured specimens after tensile testing (1 pph_{BM} filler dosage).

8.2 General Observations

Pure NTP and composites of different blends have a sharp and pungent smell. The tensile specimens produced with and without fillers were identical in terms of physical appearance such as colour, smell and smooth surface finish. This could mean that the unmodified and organically-modified bentonite fillers compounded efficiently with NTP, but further tests need to be conducted to verify this. The appearance could also be unaffected because of the small amount of filler used (0.25, 0.5 and 0.1 pph_{BM}). Fractured samples from tensile testing revealed that the samples could be brittle as evidenced from the lack of necking (Figure 60).

Based on practical experience during specimen production, composite processability was slightly reduced at higher dosage of unmodified fillers (CaRaw and NaRaw). Although the raw materials were able to be extruded well, product formation during injection moulding was problematic at the beginning. It was noticed that the first few specimens did not form properly at the highest dosage of 1 pph_{BM}. At no adjustment in the processing parameters, subsequent specimens produced started to improve and were comparable to the rest of the composites. Therefore, initial samples were discarded. Poor processability at high filler loading was also observed for mica [197] and glass fibres [198] in polypropylene matrix.

This trend diminished with the presence of organics. NTP formulations with gelatin and stickwater-modified bentonite extruded and injection moulded very well. Based on this alone, it is reasonable to say that organically-modified bentonite can improve the processability of composites compared to its pure form. The same premise was drawn by other workers who observed improvements in mouldability using organically-modified clays in various polymer matrices [119, 120, 199].

8.3 Mechanical Properties

The mechanical properties were assessed at different filler contents to investigate the microscopic effect of clay-based reinforcement in NTP. The effect of sample conditioning was investigated by performing the mechanical tests on conditioned and unconditioned specimens. The results on tensile strength (σ), Young's modulus (E) and toughness are presented in Figure 61 and Figure 62 while elongation at break (ε)

is given in Figure 63. Each bar represents an average value of a minimum of five tested specimens. The tabulated data for mechanical properties of conditioned and unconditioned specimens are summarized in Table 57 (Appendix-16A) and Table 58 (Appendix-16B).

8.3.1 Unconditioned vs. Conditioned Specimens

Comparing Figure 61 and Figure 62, it is clear that the conditioned composites had better mechanical properties than their unconditioned counterparts. Overall, tensile strength obtained was above 8 MPa for conditioned and 1.5 MPa for unconditioned samples. Large difference can also be seen in Young's modulus where high values between 400 to 700 MPa was achieved for conditioned samples compared to between just 25 to 55 MPa for the unconditioned samples. A similar trend was observed for toughness where average values of greater than 3 MPa were obtained for conditioned samples while all unconditioned samples resulted in less than 0.5 MPa. These huge differences indicate that the conditioned samples were significantly stronger and stiffer compared to unconditioned samples, mainly as a result of the evaporation of water during conditioning.

In terms of elongation at break, the values obtained for unconditioned samples were generally more consistent than the conditioned samples (Figure 63) as indicated by smaller errors (except for NTP-CaRaw1). Conditioned samples improved the elongation at break for reinforcement with raw and gelatin-modified bentonite for most cases, while the elongation was overall decreased at using stickwater-modified bentonite. Between conditioned and unconditioned pure NTP, it can be seen that the latter has slightly higher elongation at break with 73.6 % elongation compared to 72 % for conditioned NTP.

The difference in tensile properties between these two conditions can be attributed to the conditioning process. During seven days of conditioning (23 ^{o}C and 50 % RH), water was evaporated, reducing moisture content of the samples. In composites, water can act as a plasticizer to assist the polymer chains mobility. At reduced water content, specimens are more brittle because of the increased in restriction of chain movements [183]. Therefore, it is easy to assume that all conditioning samples would

result in relatively more brittle materials compared to without conditioning. However, that is not entirely true based on the results shown in Figure 63. It is apparent from these results that the differences between conditioned and unconditioned samples were less than expected after the incorporation of fillers. The effect of chain restriction is clearly just as important as the plasticizing effect of water when it comes to elongation at break.

Significant changes observed on the mechanical properties are attributed to the filler's reinforcement. At maximum dosage of 1 pph_{BM}, it is far less than what were observed in many works which showed that higher filler dosage was required for such improvements. For example, 5 wt% of organically-modified sodium montmorillonite was required to increase Young's modulus of polypropylene-ethylene octane polymer by 21 % [177] compared to 17 % increase demonstrated at reinforcement of just 0.5 pph_{BM} (< 0.5 wt%) stickwater-modified NaBt in NTP (Figure 61).

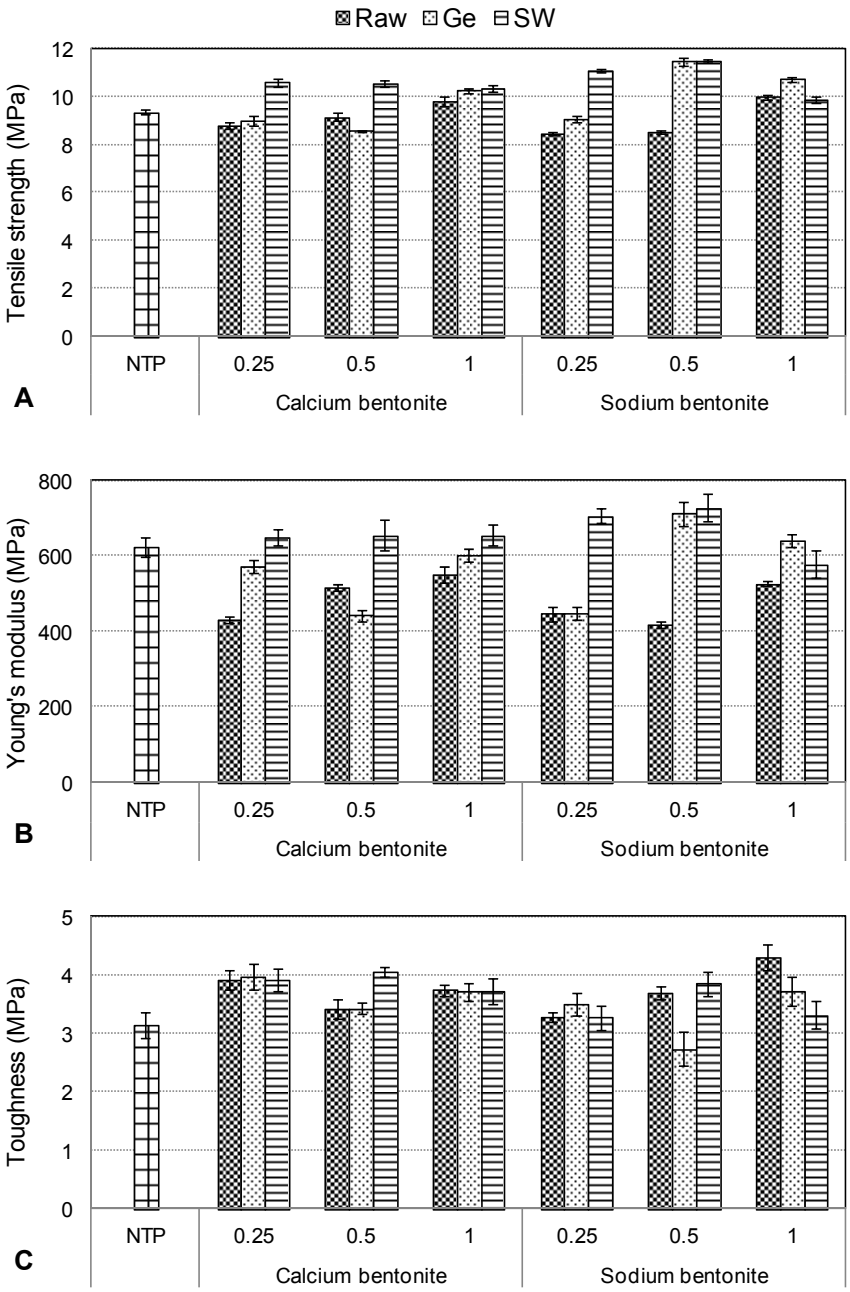

Figure 61: Mean values of A) tensile strength, B) Young's modulus and C) toughness of conditioned composites. Error bars indicate standard error of the mean values.

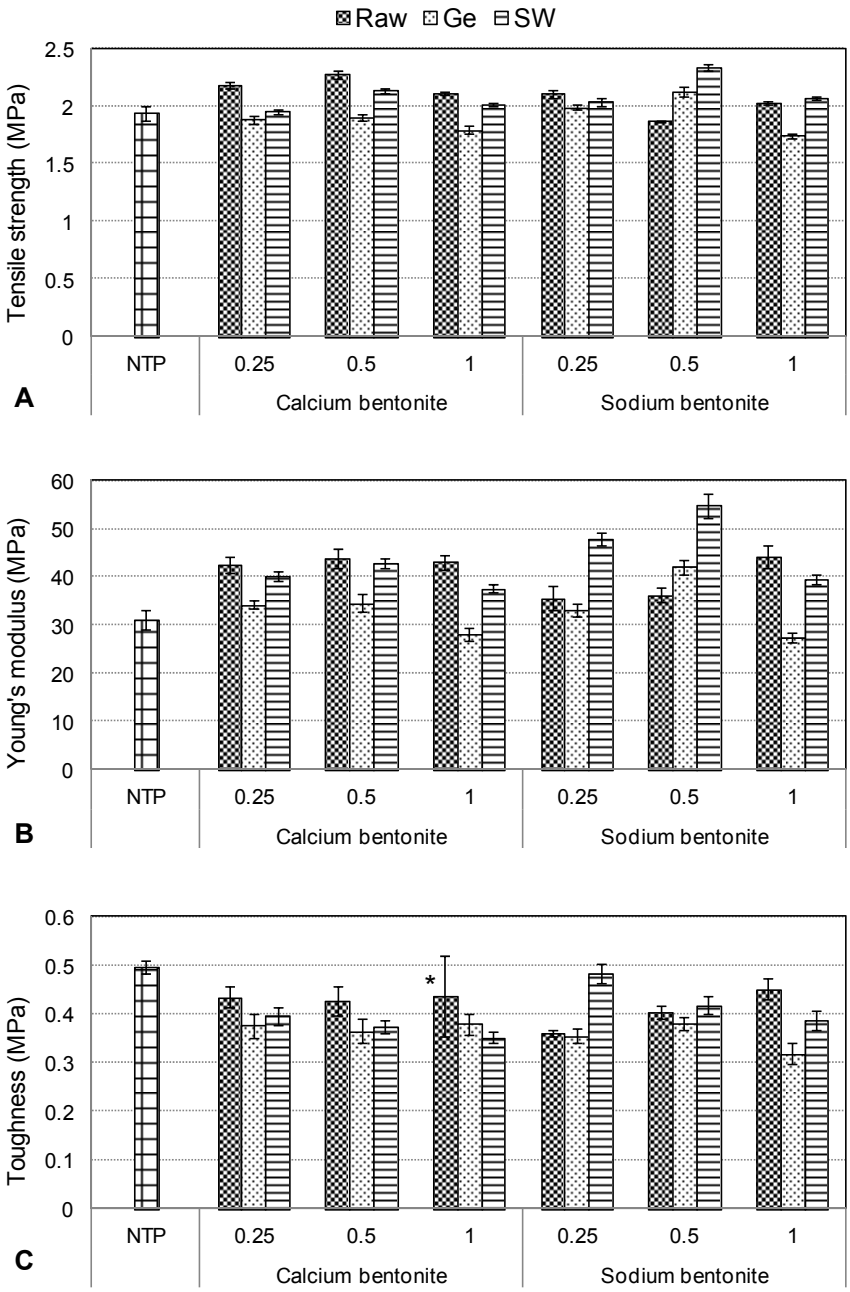

Figure 62: Mean values of A) tensile strength, B) Young's modulus and C) toughness of unconditioned composites. Error bars indicate standard error of the mean values. Only three specimens were tested for '*'.

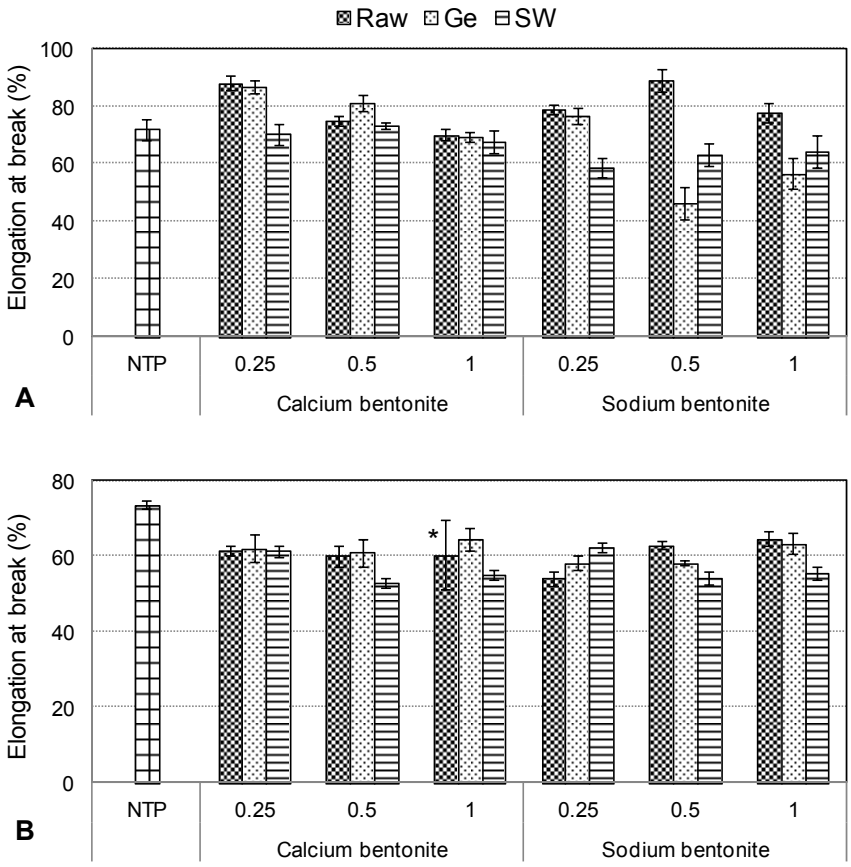

Figure 63: Elongation at break for A) conditioned and B) unconditioned composites (error bars indicate standard error of the mean values). Only three specimens were tested for '*'.

8.3.2 Tensile Strength of Conditioned Specimens

Results depicted in Figure 61A revealed that stickwater-modified CaBt and NaBt improved the tensile strength (σ) of composites the most at all filler dosage. Reinforcement with gelatin-modified fillers gave mix results, enhanced tensile strength for CaGe1, NaGe0.5 and NaGe1; and decreased for the remaining compositions. Raw bentonite did not increase the tensile strength except at 1 pph_{BM} which corresponds to about 6 % increase. The highest improvement overall was obtained at using gelatin and stickwater-modified NaBt at 0.5 $pph_{BM,}$ increasing strength about 23 % from 9.34 MPa of pure NTP.

It is clear that the organically-modified bentonite led to a distinct improvement in σ. This could mean that the compatibility of filler with the NTP matrix was increased by organically modifying bentonite. If otherwise was true, a decrease in σ should been

expected as shown by the unmodified bentonite. Bentonite particles act as rigid fillers in the matrix, assisting the stress transfer and with good dispersion, the fillers can induce energy dissipation in the matrix [164]. Organically-modified bentonite is more advantageous than raw bentonite due to improved interfacial bonding between fillers and matrix polymers by various physical and chemical interactions which gave an overall increase in σ.

Increase in filler loading of pure clay has been reported to improve the tensile strength of many polymer matrices until saturation, beyond which it started to decrease such as for polyimide reinforced with organic montmorillonite where σ reached the optimum values at 5 wt% filler content [178]. In this work, the trend can be seen at application of unmodified bentonite where σ was increased with filler loading (overall σ is lower than pure NTP except at 1 pph_{BM}). This is expected because fillers act as load bearers in the matrix and an increase loading implies stronger composites.

Tensile strength of organically-modified bentonite was not proportional to the loading dosage even though the σ was overall increased. Gelatin-modified CaBt showed significant improvements in σ at 1 pph_{BM} and similar observations obtained for NaBt at 0.5 and 1 pph_{BM}. Distinct improvements are apparent for stickwater-modified bentonite at all filler levels. The difference in σ shown between modified bentonite with gelatin and stickwater could be related to the molecular size of the organics. Stickwater organics with shorter chains had possibly dispersed better in the matrix and imposed less steric hindrance compared to more complex structure of gelatin molecules.

Sodium bentonite generally gave better σ than CaBt particularly at organic modification. As theorized by many researchers, the size of filler is very important to improve the mechanical properties of composites. The filler dispersion in the matrix could be enhanced with decreasing filler size. At the best adsorption condition, it was determined that the average particles size for treated NaBt was 17.88 μm (pH 5.23) and for treated CaBt it was 9.21 μm at pH 9 (Table 33, Section 7.3). These did not reflect the idea stated earlier where good σ should correspond to the smaller size particle. However, as it was discussed in Section 7.5.2, C_r measurement for NaBt could have been erroneous due to gelling at high temperature. Comparing at the

smallest size of NaBt (5.89 μm at pH 9) to CaBt particles in gelatin solution, the particle size of NaBt is 56 % smaller than CaBt which complements greater improvement of σ (Figure 61).

8.3.3 Young's Modulus

From Figure 61B, the addition of raw bentonite at all dosage decreased the Young's modulus (E) between 13 to 48 %. For gelatin-modified bentonite, increment in E was obtained for NaBt at 0.5 and 1 pph_{BM} loading while the rest of the blends resulted in lower E than pure NTP. Improvement in stiffness can be seen for all stickwater-modified bentonite except at 1 pph_{BM} NaBt. For stickwater-modified CaBt, consistent increase in E was obtained across all filler concentration. The highest improvement was achieved at using NaSW at 0.5 pph_{BM}, reflecting a 17 % increase from pure NTP.

These results are attributed to interfacial adhesion between fillers and the matrix. Addition of bentonite increased the stiffness of the polymer because the dispersed fillers are not only constraining the movement of polymer chains but could also act as stress concentrators. Organic modification of bentonite improved the load bearing ability by promoting a strong filler / matrix bond via various possible interactions, resulting in an increase of σ and E. However, this pattern is not directly related to the amount of organic retained by the filler. For example, sodium bentonite with overall higher σ and E had high C_r from gelatin adsorption (Table 23) but not on stickwater adsorption (Table 27). If the the composite's load bearing capacity increases with organic loading, stickwater-modified CaBt should have resulted in better improvement of σ and E as it adsorbed more organics in stickwater than NaBt.

This finding could further strengthen the point made where in bentonite nano-filler preparation, modification with organics is more important than the amount of organic adsorbed by the fillers in order to improve the mechanical strength. Coupled with small filler size, the strength could be enhanced even more as demonstrated by NaBt fillers. Sodium bentonite fillers with small particle size resulted in better improvement in E than CaBt because it had higher specific surface area and could have dispersed better in the NTP matrix, increasing the molecular interactions and adhesion. Although CaBt had relatively larger size, it might be advantageous by

carrying 2^+ ions which could improve the intermolecular interactions. However, these charges must have been electrostatically shared with adsorbed organics and therefore the matrix did not benefit from these charges, as shown by the overall lower performance in σ and E of CaBt than NaBt fillers.

Improved in σ and E of NaBt can also be referred to XRD where basal spacings for treated NaBt fillers had larger increased than CaBt. This could potentially have increased the filler / matrix interactions within the clay gallery because matrix polymers could have gained easier access to the NaBt gallery. In addition, Na^+ charge had weaker hold of the platelet layers compared to Ca^{2+}, further facilitating the interlayer interactions.

8.3.4 Toughness

Toughness indicates the ability of the composite to absorb energy up to fracture and is measured by the area under stress-strain curve [166]. From Figure 61C, improved toughness can be seen for all composites except for gelatin-modified NaBt at 0.5 pph_{BM}. There is no obvious effect of organic modification on bentonite as indicated by the average toughness of 3.60 MPa for composites with organic fillers compared to 3.57 MPa for composites with unmodified fillers.

Higher toughness signifies improved shock-absorbing ability of the composites, leading to a better fracture resistance which could potentially enhance the elongation at break. However, the condition of the highest toughness (NaRaw at 1 pph_{BM} with a 37 % increase) did not correspond to the condition of high σ and E as well as elongation at break, ε. The reason is because tough materials are not necessarily strong (high σ and E) as stiffer composites maybe more brittle, have shorter stress-strain curves, thereby yielding smaller areas under the curves.

8.3.5 Elongation at break

Addition of raw montmorillonite at a very small loading has previously been shown to increase the elongation at break (ε) of many polymer composites such as PLA [164], polysiloxane [172], polyamide-6 [175] and polypropylene [14]. It was suggested that organic clays can enhance ε due to the plasticizing effect of the fillers where the

organics contribute to the formation of dangling chains between filler / matrix interface. This is by far not exclusive since equal amount of work showed ε decreased with increasing organic clays reinforcement [175].

In this study, composites displayed an overall increase in ε with unmodified bentonite, a combination of results for gelatin-modified bentonite and a decrease for stickwater-modified bentonite (Figure 63A). Generally, unmodified NaBt had higher elongation at break than CaBt possibly due to better dispersion in the polymer from smaller size fillers. This trend is however reversed with organic modification where CaBt revealed higher ε than NaBt. It is speculated that because NaBt exfoliated in solution and with good coverage of organics on the surfaces (as observed from cryo-SEM, Figure 48), had led to increased interactions with the matrix and the composites and therefore stronger (high σ and E) but had lower ε.

The highest ε was recorded for unmodified NaBt, corresponding to a 23.5 % increase from pure NTP. At 0.5 pph_{BM}, this increment is considerably high compared to a 36 % increase in PLA with 4 wt% montmorillonite and a 60 % increase in PLA with 4 wt% nanotitania coated with PCL [164].

Composites with CaBt fillers showed a dependency on the filler loading where ε is inversely proportional to filler content for raw and gelatin-modified CaBt. Apart from these, no general relationship between ε and filler loading can be seen for the others.

The increase in elongation is attributed to debonding of matrix polymers during extension. In the presence of fillers, the rearrangement of polymer chains became restricted by dispersed fillers. Unmodified fillers had higher ε because of fewer interactions between the filler and matrix. Organically-modified fillers showed improved interfacial bonding from various filler / matrix interactions making the composites stiffer and therefore failed earlier (low ε).

Figure 64 resembles typical stress-strain curves of ductile materials. The curves main features are i) yield point, ii) ultimate tensile strength, iii) elastic point, iv) plastic region and v) fracture region as depicted in Figure 64A. The yield point was established by constructing a straight line parallel to the elastic portion of the stress-

strain curve at specified strain of 2 %. The line intersection corresponded to stress was taken as the yield point [166].

The curves show less pronounced yield points at around 4 % elongation followed by a period of strain softening in the plastic region. It can be said that the curves are sensitive to filler concentration because even at low filler dosage (0.25 to 1 pph_{BM}), the changes on the stress-strain curves are noticeable. The presence of organics on the NaBt fillers can be seen to cause earlier fractures than unmodified NaBt (Figure 65A) but it was unobserved for modified CaBt (Figure 64B).

It is also interesting to note that the curves show no sudden dip after the yield stress as exhibited by many plastics such as PLA [164, 200]. The dip is caused by a sudden change in the cross sectional area of the sample due to necking. This trend was absent from Figure 64, indicating that the cross sectional area of the composites was almost unchanged until fracture, a characteristic of brittle material. All conditioned composites were observed to fracture with noticeable shatter noise and displayed flat fracture surfaces (Figure 60), attributed to a loss of plasticizer (water) during conditioning. Based on these observations, the composites can be said to exhibit a combination of ductile and brittle properties.

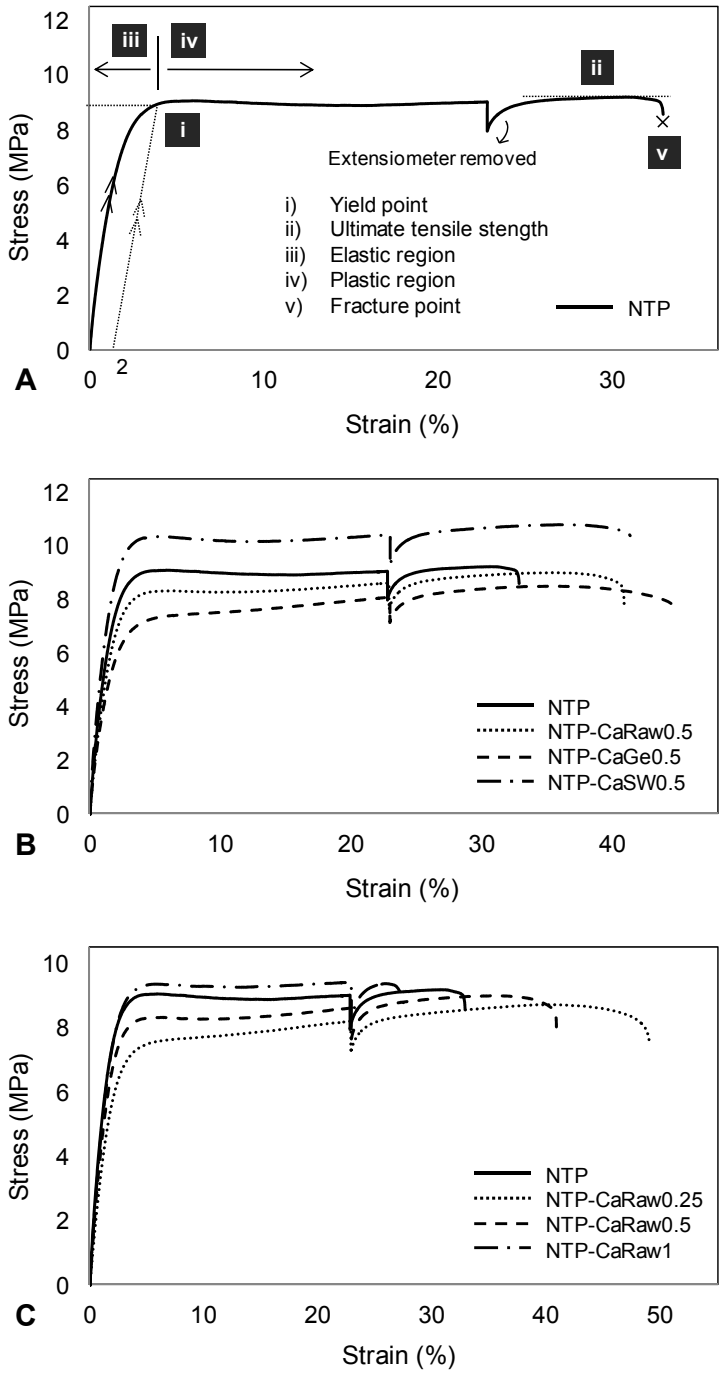

Figure 64: Tensile "stress vs. strain" curves of A) NTP and composites with CaBt fillers at B) 0.5 pph_{BM} for all types and C) increasing filler dosage for unmodified type. The extensiometer was removed at 23 % strain as indicated by the sharp drop.

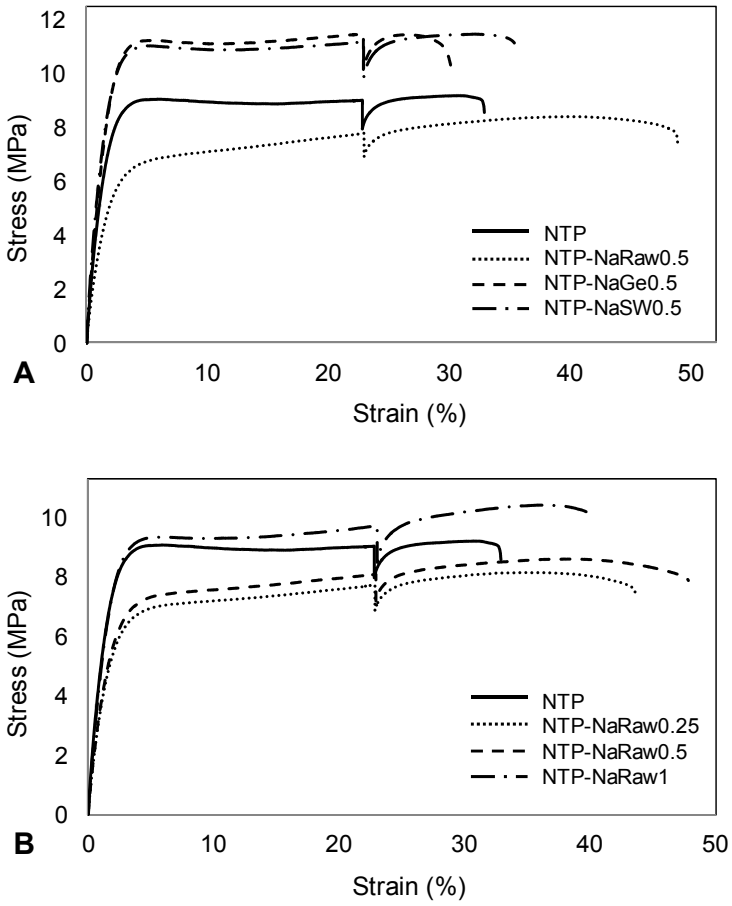

Figure 65: Tensile "stress vs. strain" curves of NTP composites with NaBt fillers at A) 0.5 pph_{BM} for all types and B) increasing filler dosage for unmodified type.

8.4 Morphology and Fracture Surface

Images obtained on tensile fractured surfaces at different magnifications are presented in Figure 66. Overall, there is no clear indication of the presence of fillers on the surfaces. The appearance of NTP is still fairly consistent throughout the test specimens. This could suggest the particles were exfoliated and dispersed at nano-scale beyond the SEM magnification or the fillers were completely covered by the matrix into a singular visible unit. Moreover, at such low filler content and with good dispersion, the fracture surface would resemble that of the matrix. For large size fillers, large voids on the fracture surface can be seen with SEM. This is typically caused by a sudden reinforcement pull-out as reported for PLA reinforced with impact modifier [164].

From Figure 66, the fractures normally initiated at the edge of the specimens and travelled toward the middle part. This process was amplified by the presence of microscopic flaws, cracks, voids and scratches. The surfaces revealed a combination of brittle and ductile fracture characteristics. The former is indicated by rapid crack propagation in the direction perpendicular to the applied stress and yielded a relatively flat fracture surface while ductile fracture is indicated by a pulled-out mark corresponding to a long plastic region on stress-strain curve (Figure 64 and Figure 65). The fracture surface in general can be said more inclined toward brittle fracture such as epoxy rather than PLA. An absolute brittle fracture is said to be unique with each material and would show a distinct pattern unlike appearance of pulled-plastic for a purely ductile material [166].

XRD analysis revealed that the NTP composites had on average of 23 % crystalline and 77 % amorphous (more on this in later section). It is reported that for amorphous materials, brittle fractures yield a relatively shiny and smooth surface while crystalline materials show crack propagation pattern along specific crystallographic planes [166]. The fracture images obtained revealed the former feature the most because the composites were highly amorphous. The latter feature was less visible possibly because of the insignificant crystal boundary in the composites due to small filler concentration and particle size.

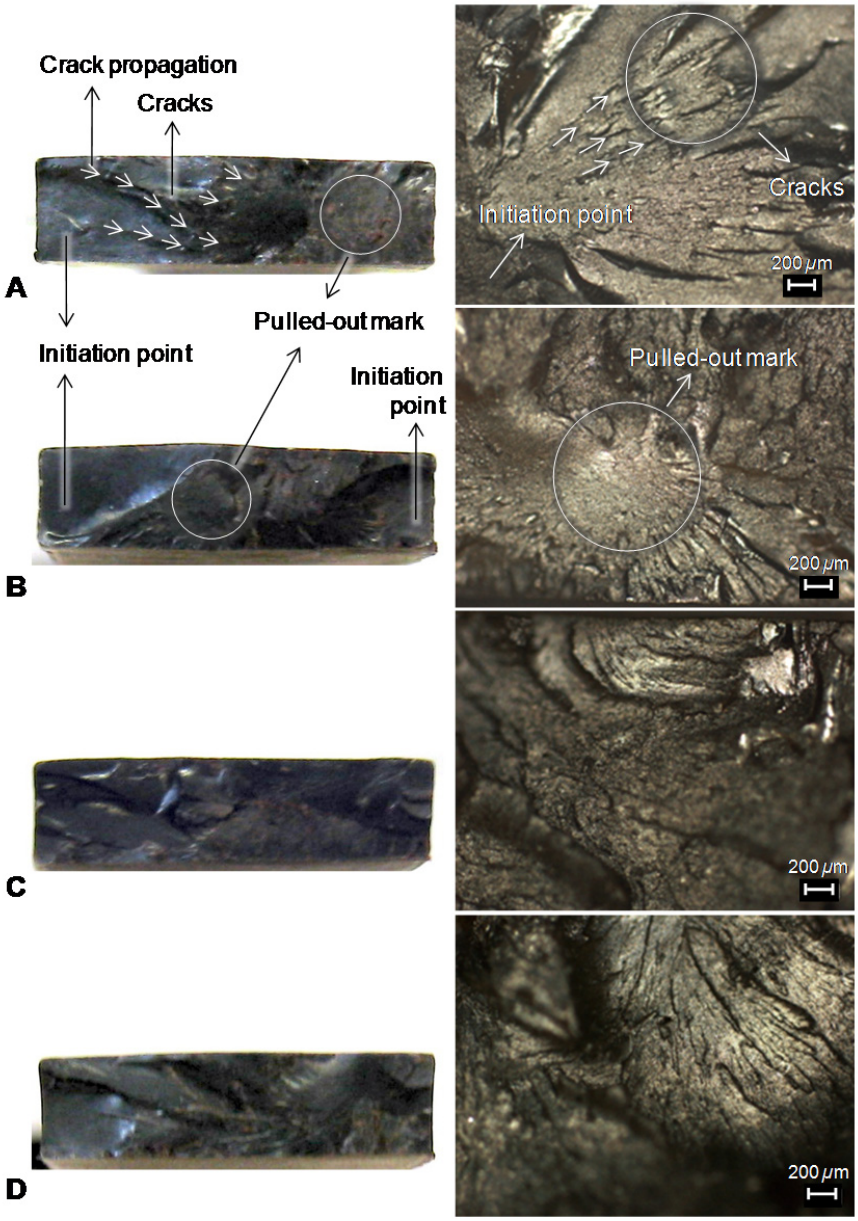

Figure 66: SEM images of tensile fractured surfaces of A) NTP, B) NTP-CaRaw, C) NTP-CaGe and D) NTP-CaSW at 0.5 pph_{BM} dosage. Similar results were observed for NaBt fillers.

8.5 Thermo-Mechanical Properties

Storage modulus ($E^{'}$) and tan δ of composites are presented as a function of temperature and filler types in Figure 67 to Figure 69. The overall shapes of the graphs are mostly similar with only a small shift relative to NTP. From Figure 67A and Figure 69A, three typical viscoelastic regions can be identified; glassy (less than 0 ^{o}C), transition (0 to 100 ^{o}C) and rubbery region (above 100 ^{o}C). A sharp drop in $E^{'}$ was observed between 40 to 80 ^{o}C, associated with the glass transition temperatures (T_g). Reinforcement with fillers resulted in the storage modulus was unaffected in the first region, shifted upward in the transition region and were mostly similar in the rubbery region.

In the glassy region, the composites were very stiff and brittle due to the low temperature. As the temperature increased, the polymer chains gained more energy causing the chains to move. Filler addition resulted in various interactions within the matrix, making the composites stronger as shown from tensile testing. Therefore, higher energy was needed to overcome the molecular interactions as indicated by the upward shift in *E'* peaks. Enhancement in *E'* could signify better structural stability at high temperature.

At high temperature, there was sufficient energy to transform the composites from brittle to ductile solids. With so much energy available due to heat, the presence of fillers in relatively small contents was not enough to cause any significant change. This explains the small difference (within 5 %) in *E'* in the rubbery region.

From Figure 67B and Figure 69B, the peaks in tan δ shifted to the right indicating higher values of T_g for reinforced composites. Figure 70 shows that the T_g for all composites increased between 5 to 22 % compared to pure NTP at 61.8 ^{o}C. This implies that higher temperatures were needed to allow polymer chains to slide past each other because the dispersion of fillers in the matrix restricted the polymer chain movement. Summary of T_g for all composites with the percentage increase is given in Table 59 (Appendix-17).

Generally, modified bentonite gave lower T_g, possibly because the embedded organics within the polymer matrices increased the spacing and free volume allowing

the chains to move at relatively lower temperatures. Whereas, raw bentonite fillers were rigid and contained no organics to assist in chain entanglement.

The increase in filler dosage caused little effect on $E^{'}$ (Figure 68B) and T_g (Figure 70) with no overall increasing or decreasing pattern observed. High filler content was suggested to increase both quantities due to increase in stiffness [164]. However, the trend was not observed here because the amount of fillers used in NTP was very small.

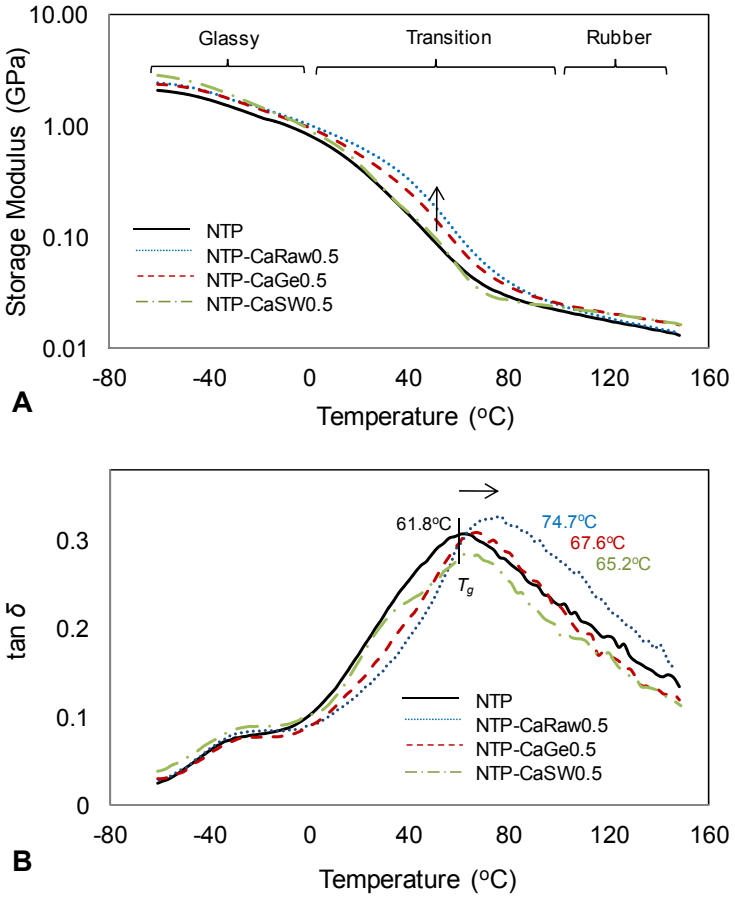

Figure 67: A) Storage modulus and B) tan δ curves for conditioned composites with CaBt fillers at 0.5 pph_{BM} dosage.

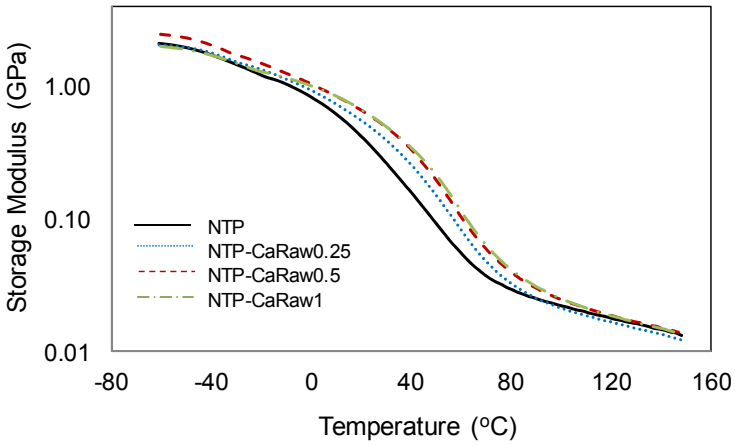

Figure 68: Storage modulus for conditioned composites with CaRaw fillers at increasing dosage. Similar trend was observed for NaRaw fillers.

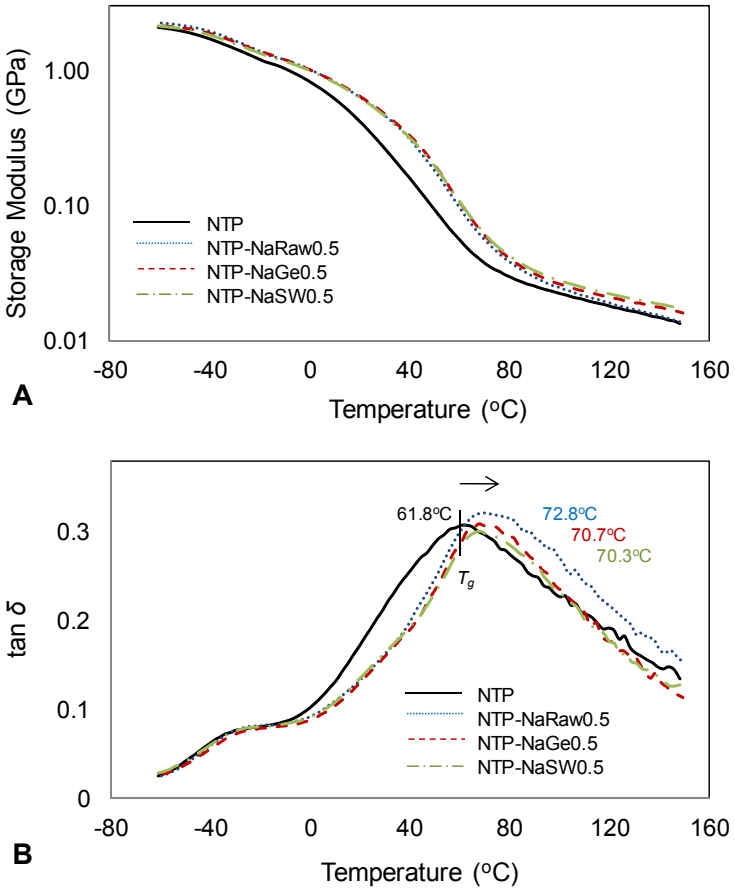

Figure 69: A) Storage modulus and B) tan δ curves for conditioned composites with NaBt fillers at 0.5 pphBM dosage.

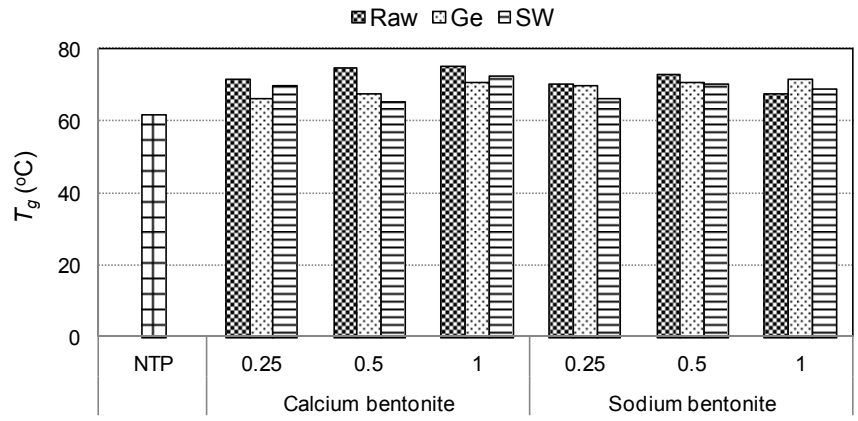

Figure 70: Summary of glass transition temperature of composites.

8.6 Crystallinity and Basal Spacing

Diffractograms of composites show scattered crystalline regions with characteristic peaks between 2θ of 5^{o} to 35^{o} (Figure 71). However, the peaks are broad and not clearly defined. The percentage crystallinity for composites was determined using the method reported elsewhere [201]. An amorphous region was graphed using a Gaussian distribution connecting five points of specified regions (Figure 71). This curve is known as halo curve and the area under the curve corresponds to amorphous region which was substracted by 100 % to yield the crystallinity of the composites as summarized in Table 59 (Appendix-17).

From Figure 72, the crystallinity of composites is generally at the maximum at 0.5 pph_{BM} filler dosage except for unmodified CaBt. Stickwater-modified bentonite gave overall higher percentage of crystallinity followed by gelatin-modified and unmodified bentonite. Addition of fillers increased the crystallinity of composites between 6 to 48 % with the highest was recorded for stickwater-modified NaBt at 0.5 pph_{BM}. This condition corresponds to the highest recorded σ and E from tensile testing, indicating the improved interactions with the matrix as the composites became more crystalline.

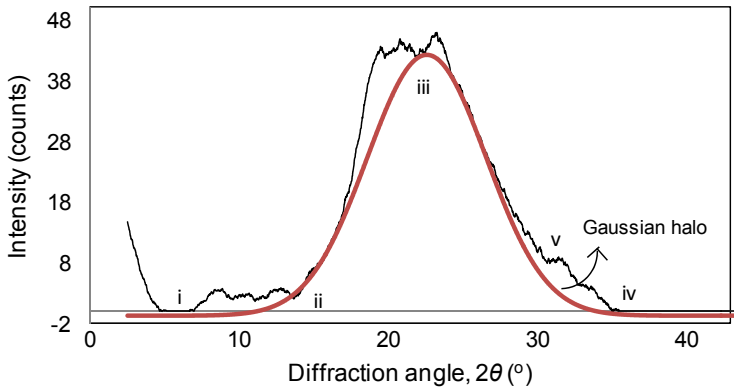

Figure 71: Gaussian halo curve for determination of crystalline region. Points i-v mark the highest intensity values of each amorphous region of pure NTP.

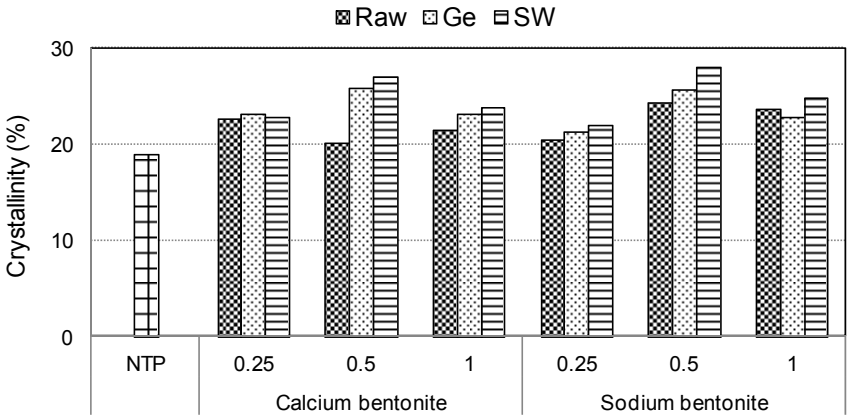

Figure 72: Crystallinity of composites.

It was expected from XRD to reveal evidence of clay intercalation or exfoliation in the matrix. Exfoliation of clays is characterized by the absence of d_{001} peak of pure clay. Selected XRD diffractograms of composites are presented in Figure 73. Previously, it has been determined that the diffraction angles at d_{001} of pure calcium and sodium bentonite correspond to basal spacing of 15.5 Å and 12.4 Å respectively. Gelatin intercalation increased the spacing up to 19.9 Å and 23.1 Å while stickwater intercalation enhanced the spacing to 14.3 Å and 15.7 Å respectively (Table 30, Section 6.7.1).

However, when fillers were incorporated into NTP, these peaks were not observed (Figure 73). The diffraction patterns of composites are mostly identical to NTP with

no noticeable bentonite peaks. Although the d_{001} deflection peak was absent, this alone can not confirm the clay exfoliation because the peaks could have been masked by the deflection of NTP due to the small amount of fillers used. Examples of clay exfoliation determined by XRD include 4 wt% octadecylammonium montmorillonite in natural rubber [152] and 5 wt% octadecylamine montmorillonite in polypropylene [177]. The filler dosages in both cases are much higher than what was used in this work.

Clay exfoliation signifies the optimum integration of fillers into composites because of very high aspect ratio, well dispersed and high degree of interactions with the matrix. Exfoliation of clay layers has been highlighted by many authors for being the reason behind properties improvement [13, 163, 202]. It was shown earlier that the bentonite reinforcement had improved the σ and E of NTP of up to 23 % and 17 % while ε at 23.5 %. At such a low filler loading (maximum of 1 pph_{BM}), these improvements could strongly suggest the exfoliation of clay layers in the matrix which could potentially yield nanocomposites. Due to the inconclusive finding from XRD, further validation using TEM was performed to verify the clay exfoliation.

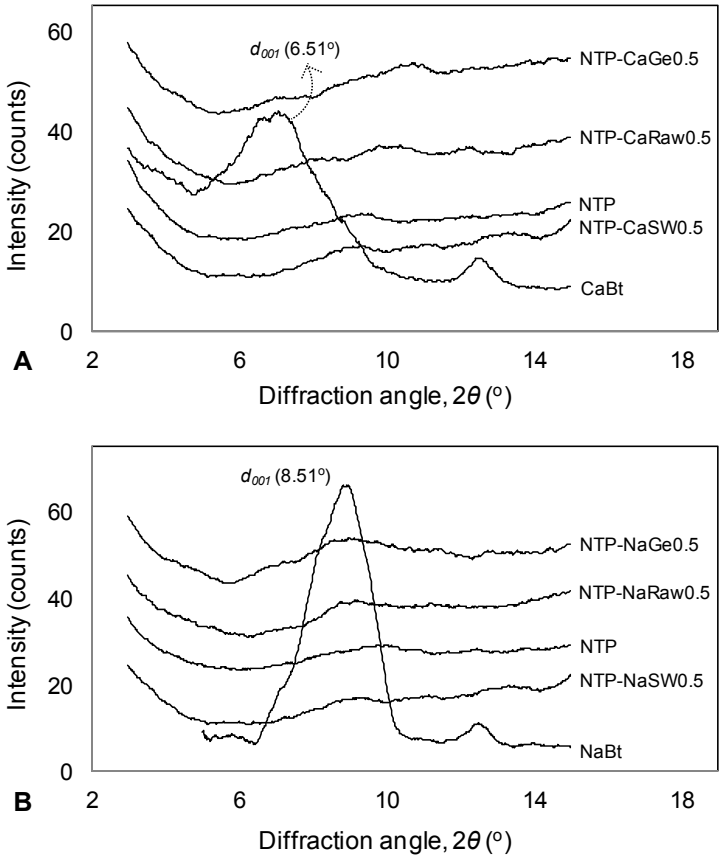

Figure 73: XRD diffractograms of NTP reinforced with A) calcium and B) sodium bentonite fillers at 0.5 pph_{BM} dosage. Basal spacings of pure bentonite at d_{001} are also presented for comparison.

8.7 Thermal Degradation Properties

Thermal decomposition curves of selected composites are presented in Figure 74 and Figure 75. The tabulated data for all samples at different temperature intervals are summarized in Table 60 (Appendix-18). Thermal degradation of raw materials in Figure 45 (Section 6.7.1) shows that calcium and sodium bentonite lost surface water at temperatures above 100 ^{o}C and remained thermally stable until 200 ^{o}C. This implies that the organic degradation did not occur during composite fabrication because the highest temperature applied was 120 ^{o}C (Table 17, Section 5.7.2). Therefore, the mass loss percentages depicted in Figure 74 and Figure 75 are attributed to constituents of the composites.

It can be seen from Figure 74 and Figure 75 that there are five stages of thermal degradation of composites; these are from 0 to 150 ^{o}C, 150 to 230 ^{o}C, 230 to 390 ^{o}C,

390 to 500 ^{o}C and 500 to 600 ^{o}C. The first stage of decomposition curve corresponds to loss of bound water on the surface. Degradation of urea, interlayer water and low molecular mass compounds occurred at the second stage up to 230 ^{o}C.

The third stage is attributed to cleavage of S–S, O–N and O–O linkages of the bloodmeal chains and surface organics of bentonite [183]. The fourth degradation region is obvious with a well defined onset at 390 ^{o}C, marked the decomposition of intercalated organics and hydroxyl water from bentonite galleries as well as hydroxyl groups on NTP which originated from polypeptide chains of bloodmeal and the plasticizer (TEG) [183, 203].

The final stage from 500 to 600 ^{o}C is attributed to degradation of low volatility organics of bentonite fillers. The difference in mass loss was diminished as the temperature reached 600 ^{o}C with an average mass loss percentage of less than 2 % (Table 60), indicating that equilibrium has been reached. This is in contrast to raw bentonite on its own where the equilibrium was not achieved at 600 ^{o}C (Figure 45). This trend could suggest that for composites, much of the low votality organics were possibly exchanged with NTP components.

From Figure 74 and Figure 75, it can be seen that composites decomposed at higher temperature (between 400 to 600 ^{o}C) compared to NTP that shows an abrupt decrease after 390 ^{o}C. The enhancement in thermal stability can be attributed to thermal resistance and nanodispersion of bentonite in the matrix which could have imparted hybrid properties deriving from interactions between components. At such low filler content, the trend observed is consistent with the improved thermal stability of nanocomposites of polyethylene and polypropylene at application of a small amount of rectorite clay [13].

Thermal degradation curves for all composites generally overlapped until about 390 ^{o}C. Above that, the behaviour changed for CaBt (Figure 74A) but less obvious for NaBt (Figure 74B). This was attributed to intercalated organics from both types of bentonite. The onset for this degradation at 390 ^{o}C is much higher compared to at 220 ^{o}C for phosphonium intercalated montmorillonite which is weakly bonded via

van der Walls forces [204]. This suggests strong electrostatic interactions between intercalated organics (from gelatin and stickwater solutions) with the bentonite layers.

Above 390 ^{o}C, gelatin-modified CaBt appeared to be more thermally stable compared to the rest of composites (Figure 74A, inset). Reinforcement with stickwater-modified CaBt indicated a larger drop in mass loss after 400 ^{o}C. This suggested that at high temperature, gelatin-modified CaBt is more thermally resistant than modification with stickwater. Long gelatin chains could be attributable for this thermal improvement, in contrast to stickwater organics that comprises of short chain molecules. The former could possibly have increased the electrostatic interaction with the charged solid-phase from abundant gelatin side groups. The same finding was obtained for thermal degradation of alkylammonium intercalated montmorillonite where it was observed that long molecular intercalants resulted in better thermal stability [204].

Composites with unmodified CaBt resulted in a marginal increase in thermal resistance compared to NTP and stickwater-modified CaBt, however is less thermally stable than gelatin-modified bentonite (Figure 74 inset). Thermally stable materials imply that they can retain structural integrity at high temperature. Therefore, if improving thermal properties of NTP is the aim, reinforcement with gelatin-modified CaBt is more beneficial followed by its unmodified form and finally modification with stickwater.

NTP composites with NaBt fillers showed a similar overlapping trend to CaBt until 390 ^{o}C (Figure 74B). However, the onset of the fourth thermal degradation stage is less visible to those of CaBt composites. The maximum difference in mass loss for NaBt composites this region is 4.6 % which occurred at 530 ^{o}C while its CaBt counterparts showed a 7.1 % difference at 500 ^{o}C (Figure 74A). This small variation shown by NaBt composites indicates the consistent performance between its raw form and organically-modified forms. A possible reason for this is because NaBt layers exfoliated in solution (as viewed under cryo-SEM) and had a higher aspect ratio in the matrix, resulting in more uniform performance of composites compared to CaBt fillers that aggregated into platelet stacks under certain conditions.

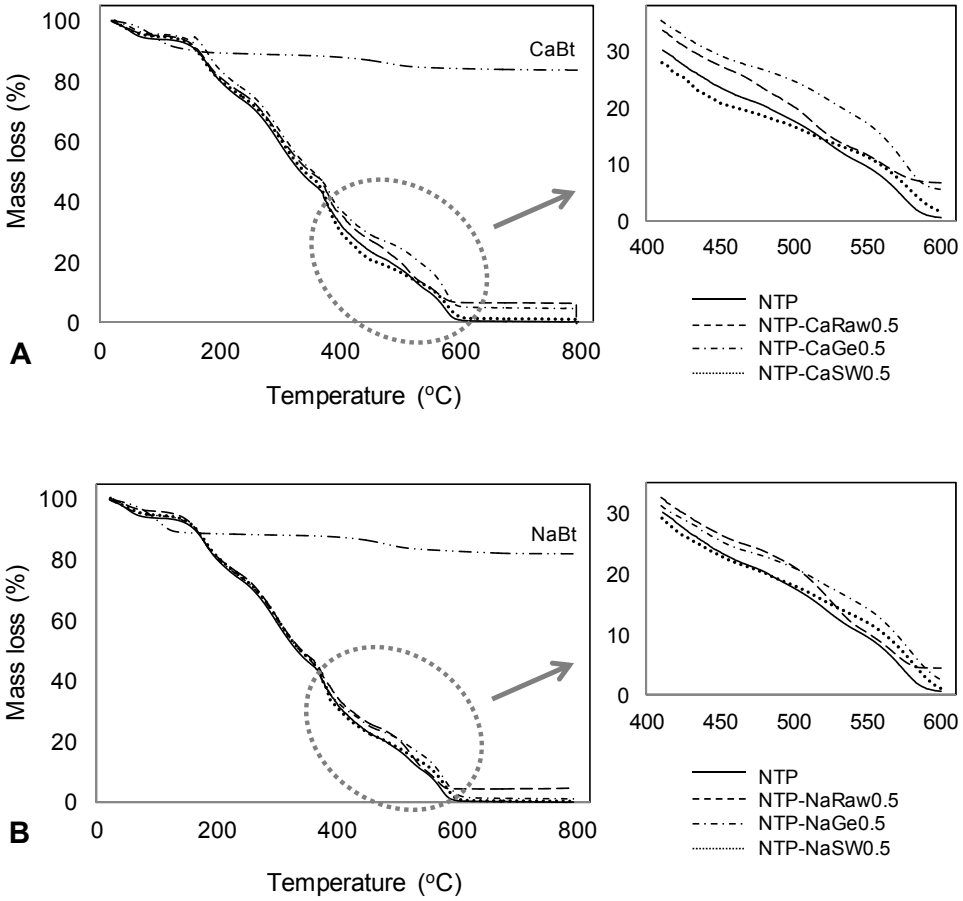

Figure 74: Thermal degradation curves of NTP composites with A) calcium and B) sodium bentonite fillers at 0.5 pph_{BM}. The area showing of the fourth degradation regions (420 to 600 ^{o}C) are expanded.

For fillers at all dosage levels (Figure 75), it is apparent that the overall features of the curves resemble the degradation pattern of pure NTP. The difference in organic content for the composites with 0.25 to 1 pph_{BM} fillers is less than 2 % (Table 60, Appendix-18). This indicates that the small amount of fillers did not cause any significant change in the mass loss and thermal stability of composites. The latter was demonstrated to improve with the addition of fillers but the filler dosage is less important. Therefore, it can be said that the proportional increment in fillers did not result in linear increment of thermal stability of the composites.

Based on the TGA curves, NaBt-based fillers could potentially be better fillers in NTP by promoting more consistent performance until 600 ^{o}C in all forms (raw and organically-modified). Furthermore, NaBt with a higher percentage of organic

content (Table 60, Appendix-18) could increase the interfacial bonding between fillers and matrix. Higher adsorption capacity of NaBt was also demonstrated earlier by high gelatin adsorbed, C_r and larger increase in *d*-value from XRD. These findings compliment the improved mechanical properties of NTP with NaBt fillers. However, it should be noted that the properties enhancements observed at using CaBt or NaBt fillers are often comparable. Therefore, both types of fillers could be ideal for NTP reinforcement but NaBt fillers might be more advantageous due to layers exfoliation.

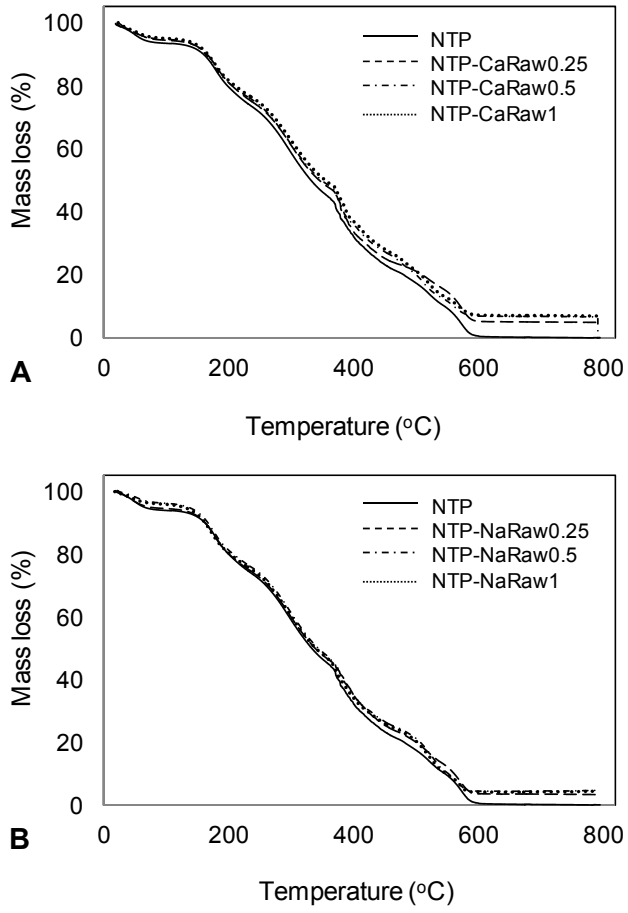

Figure 75: Thermal degradation curves of NTP composites with A) calcium and B) sodium bentonite fillers at increasing filler content.

8.8 Filler Distribution

TEM was used to evaluate qualitatively the clay exfoliation and distribution in the matrix. The images are presented in Figure 76 where light regions and dark bands indicate the NTP matrix and bentonite fillers respectively. The observation suggests the filler distribution ranging from micro-scale to nano-scale. Despite few attempts on TEM, it was unexpected for the fillers to display the majority of platelet's faces for unmodified and gelatin-modified NaBt. Logically, from the direction of sample sectioning, it should have revealed more whisker-like objects (platelet's edges) as pictured in Figure 22 (Section 4.5.3) rather than the face side.

It is apparent from the images obtained that the filler dispersion was a combination of non-exfoliated (unmodified), partially-exfoliated (gelatin-modified) and exfoliated (stickwater-modified) NaBt layers. The filler formations include aggregates (Figure 76A), combination of platelet stacks and single sheets (Figure 76B) and exfoliated layers (Figure 76C). The aggregates of unmodified bentonite were in microscopic scale while the organically-modified particles were in nanoscopic scale. Particle dispersion can be seen to improve with organic modification. This is attributed to the presence of organic on bentonite which reduces the electrostatic interaction between clay layers via cations exchange on the surface and within the interlayer gallery [177]. Reduced clay interactions resulted in greater layer separation (as evidenced from increased basal spacing) and could have facilitated the exfoliation.

In nanocomposites, higher dispersion and exfoliation signify greater SSA of fillers available for specific interactions with the matrix polymers. The observation compliments the improvement of mechanical properties determined earlier where organically-modified NaBt demonstrated higher σ and E compared to the unmodified form that had a low level of filler dispersion (Figure 76A). The latter had fewer filler / matrix interactions and was observed to have greater elongation at break.

Exfoliation of clay in nanocomposites was observed in PLA [119], soy protein isolate [16], polypropylene [14, 177], polystyrene [119], polyisoprene [205], gelatin [20, 80], polycarbonate [161] and polybutylene succinate [119]. The authors proposed the

exfoliation behaviour corresponded to improved mechanical properties of the composites.

Occasionally, tear marks can be seen at filler / matrix interface and the formation could be attributed to the stress applied during microtoming was higher than the interfacial bonding between the two components. This behaviour was also expected to occur during tensile testing. For highly crystalline composites, tear marks could initiate the crack propagation pattern at the crystallographic planes and could be visible on the fracture surface [164, 166].

Although the TEM images did not fully depicting the ideal features of clay exfoliation as illustrated in Figure 22 (Section 4.5.3), the extent of exfoliation in this work could not directly be compared to literature because only 1 pph_{BM} (<1 wt%) of filler was used instead of 13 wt% which gave a very clear TEM image of clay exfoliation in Figure 22 [175]. This is the main reason of the sparsely dispersed fillers in the matrix. It was established in this work that the mechanical, viscoelastic and thermal properties were increased for almost all conditions at such a low filler loading. These improvements in properties could strongly suggest the formation of NTP nanocomposites.

8.9 Composite Reinforcement Summary

Bentonite had been showed to have potential in organic recovery from stickwater and the spent bentonite from adsorption was applied successfully in NTP. Significant improvements in mechanical, thermal and viscoelastic properties of the composites were achieved at low level of filler dosage. Organically-modified bentonite resulted in better overall properties except at elongation at break where unmodified bentonite was superior.

The increased in mechanical properties are in harmony with the increased crystallinity from XRD, higher organic content and thermostability from TGA and better filler dispersion in the matrix as observed from TEM. These improvements are in agreement to composite enhancement at using nano-fillers suggested in literature which the authors postulated the formation of nanocomposites.

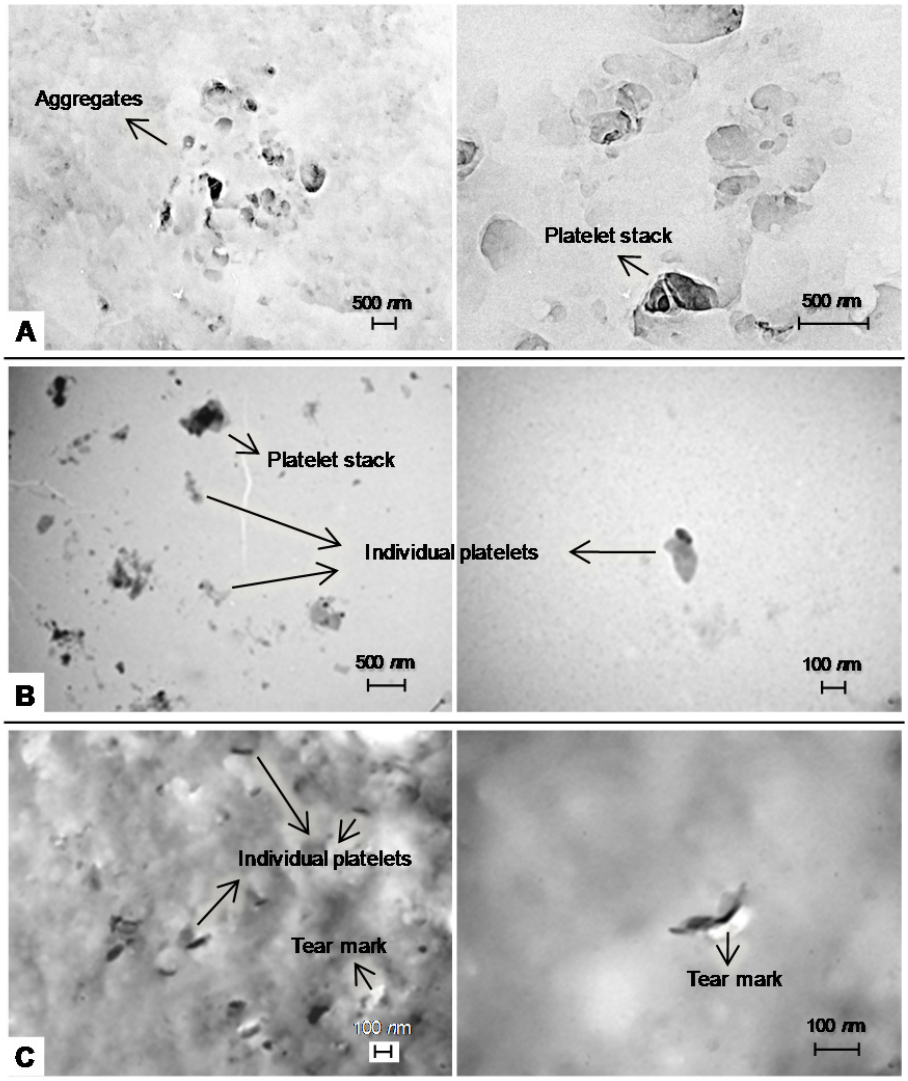

Figure 76: TEM images of NTP composites with A) unmodified, B) gelatin-modified and C) stickwater-modified NaBt at 1 pph_{BM} loading.

CHAPTER 9

CONCLUSIONS AND FUTURE WORK

9.1 Experimental Findings

Gelatin adsorption onto calcium (CaBt), sodium (NaBt) and octadecylamine-modified (amine Bt) bentonite clay was carried out in model solution (gelatin) and meat rendering plant waste water (stickwater). The gelatin solution at different pH and concentration was used to determine the best adsorption conditions and to study the adsorption kinetics. The following conclusions were made:

- CaBt and NaBt had a much higher adsorption capacity than amine Bt for gelatin, 371.98 mg/g at pH 9 for CaBt and 404.85 mg/g at pH 5.23 for NaBt compared to 239.23 mg/g at pH 9 for amine Bt. Gelatin recovery from solution was 58.9, 60.4 and 28.5 % respectively at these conditions. CaBt and NaBt were selected for recovering gelatin from stickwater.
- pH 3 gave the best adsorption conditions for gelatin recovery from stickwater with CaBt and NaBt adsorbing at 245.92 and 234.42 mg/g respectively.
- Conventional adsorption isotherm models showed excellent fits with experimental data for gelatin adsorption which amongst all, the Langmuir-Freundlich (L-F) model had resulted in the best fit (R^2 of 0.99).
- Model parameters obtained from gelatin adsorption could be applied to stickwater modelling provided that the mineral and fat content are considered. A competitive multi-components L-F model showed good success in fitting the experimental data (R^2 of 0.90). Fitting the competitive L-F model showed that fat content influenced protein adsorption on NaBt but had no affect on CaBt. Organic adsorption from stickwater was independent of mineral concentration but was dependent of mineral equilibrium term, K_M for both NaBt and CaBt.

- Increased XRD basal spacing (*d*-value) and TGA mass loss between 200 to 600 ^{o}C showed that organic adsorption onto bentonite was a combination of surface and interlayer adsorption.
- Microscopic observations revealed that NaBt layers exfoliated while CaBt layers agglomerated in solution. The former gave a higher SSA to volume ratio and resulted in higher protein adsorption compared to CaBt.

Settling experiments were conducted for bentonite in gelatin and stickwater solutions to determine the possibility of using settling for particle recovery. It was found that:

- Bentonite settling in gelatin solution can be achieved for CaBt at pH 3 and 5.23 while no settling was observed for NaBt. Both CaBt and NaBt settled in stickwater at pH 3. The highest clay recoveries in gelatin and stickwater solutions were 91 and 95 % for CaBt at pH 3.
- Bentonite settled readily in the absence of gelatin (PBS solvent) indicating the role of gelatin network trapping the particles. This observation is supported by the cryo-SEM images where gelatin chains appeared to crosslink the particles into a scaffold structure.
- Stoke's law particle settling velocity showed similarity with the experimental values where high settling velocities were predicted for the conditions where settling did occur. Since the model did not consider interactions between bentonite particles and protein molecules, adaptations would need to be made to compensate for the differences between predicted and experimental values.
- A settling model developed based on physical interactions gave acceptable R^2 when comparing it to the experimental results. However, the modelling was limited by computer resources to solve the model equations. Initial results suggest that the interactions in the bentonite / gelatin system can be well represented by physical laws alone.
- Settling observed in gelatin solution corresponded to conditions with low gelatin adsorption, further emphasizing the role of gelatin behind network formation and settling.

The unmodified and organically-modified bentonite were utilized as reinforcement materials in bloodmeal-based plastic (NTP). Bentonite was modified using gelatin and stickwater via adsorption under the optimum conditions established earlier. Some key findings determined at introduction of small amount of bentonite are:

- Organically-modified bentonite resulted in higher tensile strength and Young's modulus and unmodified bentonite was superior at elongation at break. This suggests improved interfacial bonding between the bentonite and matrix as a result of organic modification of bentonite.
- The highest improvement in σ and E was recorded at 23 % (11.45 MPa) and 17 % (727.45 MPa) for stickwater-modified NaBt at 0.5 pph_{BM} while 23.5 % increase in ε was observed for unmodified NaBt at 0.5 $pph_{BM.}$
- An increase in T_g from 61.8 to 75.2 ^{o}C and an overall improvement in thermal stability for composites indicate good filler distribution in the matrix.
- Crystallinity of composites increased when reinforced with bentonite especially after modification with stickwater. The state of filler exfoliation could not be established by XRD due to small filler content.
- TEM revealed some features of platelet stacks for unmodified NaBt, combination of stacks and exfoliated sheets for gelatin-modified NaBt and exfoliated layers of stickwater-modified NaBt.
- The TEM observations clarified the composites' improvements in mechanical, viscoelastic and thermal properties where composites with exfoliated fillers generally showing higher property improvements and at such a small filler content, this is in-line with improvements observed for nanocomposites.

9.2 Future Work and Suggestions

The potential use of calcium and sodium benonite in organic recovery and as nanocomposite fillers has been demonstrated. Stickwater adsorption using bentonite and utilizing the spent adsorbent for bio-composite reinforcement is a new field of research. Therefore, the following areas are identified and recommended as future work for improvement.

Part 1: Organic adsorption from stickwater

The model solution made from gelatin in buffer solution should be expanded by introducing stickwater's mineral term to account for binding competition on CaBt while mineral and fat terms should be introduced for NaBt.

Adsorption on model solution at stickwater's equivalent protein concentration should be performed instead of diluting it to a certain concentration to avoid gelation. This could be done by conducting the experiments at a higher temperature. The reason for this is because stickwater was not diluted proportionally to dilution made on basis of protein concentration. Without dilution, the effect of minerals, fats and dissolved organics on adsorption can be better represented.

Sodium bentonite was shown to have higher gelatin adsorption than CaBt, however settling was poor. Therefore, it could be useful to conduct adsorption using trivalent hydrophilic clays such as chromium montmorillonite which could give a good compromise between adsorption and settling.

Part 2: Settling of bentonite from solution

The aspect of flocculant addition can be investigated such as addition of multivalent ions to suppress the electrical double layer between clay particles and liquid, reducing the interparticle repulsion and increasing the tendency for particles to aggregate. In the case of NaBt, addition of divalent cations such as Ca^{2+} can replace the Na^{+} ions within the interlayer and would possibly give settling as displayed by CaBt.

The settling model should be improved by considering other assumptions such as particle stacking mechanism during sedimentation, particles smaller than the gelatin pores should permeate through to settle and using a particle size distribution rather

than an average value of particle size. Recent key findings on hindered settling models from the literatures should also be considered for model improvement [206-208]. The modelling might require a powerful computer for simulations.

A more comprehensive cost estimation study should be performed to determine the feasibility of settling over existing treatments such as centrifugation, drying and aerobic and anaerobic digestions. Apart from cost, other factors to consider are treatment rapidity, regulations imposed by government bodies, area required or foot-print and the product values.

Part 3: Organically-modified bentonite for composite fillers

Both CaBt and NaBt demonstrated a significant potential as composite fillers by improving the overall properties of NTP. However, the test conducted was limited to only three levels of dosage for raw and organic forms of CaBt and NaBt. Reinforcement at higher dosage should be considered to investigate the change in properties with increasing filler loading in order to find the optimum dosage in NTP.

It would also be interesting to see the effect of stickwater-modified bentonite on other bio-based polymers such as poly-ε-caprolactone (PCL), polyesteramide (PEA), polylactic acid (PLA) and polyhydroxybutyrate (PHB). This could make the treatment of stickwater by bentonite more appealing, serving dual functions to cleanse the waste water and to modify the adsorbents for potential use in nanocomposites.

REFERENCES

[1] Grim, R. E.; Guven, N. *Bentonites - Geology, Mineralogy, Properties and Uses*; Elsevier Scientific Publishing Company: New York, 1978.

[2] Kim, H. T. *Principles of Soil Chemistry*, 2nd ed.; Marcel Dekker Inc.: New York, 1993.

[3] Abend, S.; Lagaly, G. Sol–gel transitions of sodium montmorillonite dispersions. Applied Clay Science **2000**, *16*(3–4), 201-227.

[4] Murray, H. H. Overview — clay mineral applications. Applied Clay Science **1991**, *5*(5–6), 379-395.

[5] Doulia, D.; Leodopoulos, C.; Gimouhopoulos, K.; Rigas, F. Adsorption of humic acid on acid-activated Greek bentonite. Journal of Colloid and Interface Science **2009**, *340*(2), 131-141.

[6] Putra, E. K.; Pranowo, R.; Sunarso, J.; Indraswati, N.; Ismadji, S. Performance of activated carbon and bentonite for adsorption of amoxicillin from wastewater: Mechanisms, isotherms and kinetics. Water Research **2009**, *43*(9), 2419-2430.

[7] Zheng, H.; Liu, D.; Zheng, Y.; Liang, S.; Liu, Z. Sorption isotherm and kinetic modeling of aniline on Cr-bentonite. Journal of Hazardous Materials **2009**, *167*(1-3), 141-147.

[8] Zheng, H.; Wang, Y.; Zheng, Y.; Zhang, H.; Liang, S.; Long, M. Equilibrium, kinetic and thermodynamic studies on the sorption of 4-hydroxyphenol on Cr-bentonite. Chemical Engineering Journal **2008**, *143*(1-3), 117-123.

[9] Auerbach, S. M.; Carrado, K. A.; Dutta, P. K. *Handbook of Layered Materials*; M. Dekker, 2004.

[10] Mallick, P. K. *Fiber-reinforced composites: materials, manufacturing, and design*; CRC Press, 2008.

[11] Wallenberger, F. T.; Weston, N. E. *Natural Fibers, Plastics and Composites*; Kluwer Academic Publishers, 2004.

[12] Chen, B. Q.; Evans, J. R. G. Poly(epsilon-caprolactone)-clay nanocomposites: Structure and mechanical properties. Macromolecules **2006**, *39*(2), 747-754.

[13] Ma, X.-Y.; Liang, G.-Z.; Liu, H.-L.; Fei, J.-Y.; Huang, Y. Novel intercalated nanocomposites of polypropylene/organic-rectorite/polyethylene-octene elastomer: Rheology, crystallization kinetics, and thermal properties. Journal of Applied Polymer Science **2005**, *97*(5), 1915-1921.

[14] Manias, E.; Touny, A.; Wu, L.; Strawhecker, K.; Lu, B.; Chung, T. C. Polypropylene/Montmorillonite Nanocomposites. Review of the Synthetic Routes and Materials Properties. Chemistry of Materials **2001**, *13*(10), 3516-3523.

[15] Messersmith, P. B.; Giannelis, E. P. Synthesis and barrier properties of poly(ε-caprolactone)-layered silicate nanocomposites. Journal of Polymer Science Part A: Polymer Chemistry **1995**, *33*(7), 1047-1057.

[16] Yu, J.; Cui, G.; Wei, M.; Huang, J. Facile exfoliation of rectorite nanoplatelets in soy protein matrix and reinforced bionanocomposites thereof. Journal of Applied Polymer Science **2007**, *104*(5), 3367-3377.

[17] Zhu, J.; Morgan, A. B.; Lamelas, F. J.; Wilkie, C. A. Fire properties of polystyrene-clay nanocomposites. Chemistry of Materials **2001**, *13*(10), 3774-3780.

[18] Zhu, J. X.; Shen, W.; Ma, Y. H.; Ma, L. Y.; Zhou, Q.; Yuan, P.; Liu, D.; He, H. P. The influence of alkyl chain length on surfactant distribution within organo-montmorillonites and their thermal stability. Journal of Thermal Analysis and Calorimetry **2012**, *109*(1), 301-309.

[19] Lin, J.-J.; Cheng, I. J.; Wang, R.; Lee, R.-J. Tailoring Basal Spacings of Montmorillonite by Poly(oxyalkylene)diamine Intercalation. Macromolecules **2001**, *34*(26), 8832-8834.

[20] Zheng, J. P.; Li, P.; Ma, Y. L.; Yao, K. D. Gelatin/montmorillonite hybrid nanocomposite. I. Preparation and properties. Journal of Applied Polymer Science **2002**, *86*(5), 1189-1194.

[21] Krochta, J. M.; De Mulder-johnston, C. Edible and biodegradable polymer films: challenges and opportunities. Food Technology **1997**, *51*(2), 61-74.

[22] Martucci, J. F.; Ruseckaite, R. A. Biodegradable three-layer film derived from bovine gelatin. Journal of Food Engineering **2010**, *99*(3), 377-383.

[23] Castillo, P. F.; Rao, R. M.; Liuzzo, J. A. Potential of acid activated clays in the clarification of Menhaden stickwater. Journal of Environmental Science and Health - Part B Pesticides, Food Contaminants, and Agricultural Wastes **1987**, *B22*(4), 471-489.

[24] Higham, C.; Lay, M.; Verbeek, J. (2008), Organic Matter Adsorption to Clay Nanomaterial, Paper presented at SCENZ, Hamilton, New Zealand.

[25] Bickers, P. O.; van Oostrom, A. J. Availability for denitrification of organic carbon in meat-processing wastestreams. Bioresource Technology **2000**, *73*(1), 53-58.

[26] EPA (2000), *Abattoirs,* viewed http://www.environment.nsw.gov.au/mao/abattoirs.htm

[27] Swan, J. E. Animal By-Product Processing. In *Encyclopedia of Food Science and Technology*; Francis, F. J., Ed.; John Wiley: New York, 2000; 35-42.

[28] Bioextracts, T. (2009), *Gel Bone Plant - Summary*, Taranaki Bioextracts, New Plymouth.

[29] Council, H. C. (2010), *Wastewater and stormwater - fees and charges 2010/11*, Hamilton City Council, Hamilton, NZ.

[30] Bigi, A.; Cojazzi, G.; Panzavolta, S.; Roveri, N.; Rubini, K. Stabilization of gelatin films by crosslinking with genipin. Biomaterials **2002**, *23*(24), 4827-4832.

[31] Commerce, N. Z. M. (1996), *New Zealand Annual Mining Review 1994*, Publicity Unit, Ministry of Commerce, Wellington.

[32] Zheng, J. P.; Li, P.; Yao, K. D. Preparation and characterization of gelatin/montmorillonite nanocomposite. Journal of Materials Science Letters **2002**, *21*(10), 779-781.

[33] Foo, K. Y.; Hameed, B. H. Adsorption characteristics of industrial solid waste derived activated carbon prepared by microwave heating for methylene blue. Fuel Processing Technology **2012**, *99*, 103-109.

[34] Guerrero, P.; Stefani, P. M.; Ruseckaite, R. A.; de la Caba, K. Functional properties of films based on soy protein isolate and gelatin processed by compression molding. Journal of Food Engineering **2011**, *105*, 65-72.

[35] Edalatmanesh, M.; Sain, M.; Liss, S. N. Utilization of secondary sludge as filler in composites: surface energy and final mechanical properties. Journal of Reinforced Plastics and Composites **2011**, *30*(10), 864-874.

[36] Rountree, B. (2007), *Rendering New Zealand*, Meat and Wool NZ Economic Services, Wellington.

[37] Harrison, G. (2008), *Agriculture to New Zealand is what the Silicon Valley is to California: A Meat Industry Perspective*, Anzco Foods, Wellington.

[38] Statistics NZ (2010), *Agricultural Production Statistics: June 2009*, Ministry of Statistics, New Zealand.

[39] Verbeek, C. J. R.; Lay, M. C.; Higham, C. Protein intercalated bentonite recovered using adsorption from stickwater. Waste and Biomass Valorization **2012**, *3*(1), 109-115.

[40] Higham, C. (2010), Quantification of Collagen, Chondroitin and Elastin in TBE1 Process Streams, Thesis, Waikato University.

[41] Arvanitoyannis, I. S.; Ladas, D. Meat waste treatment methods and potential uses. International Journal of Food Science and Technology **2008**, *43*(3), 543-559.

[42] Bier, J. M.; Verbeek, C. J. R.; Lay, M. C. An eco-profile of thermoplastic protein derived from blood meal Part 1: allocation issues. International Journal of Life Cycle Assessment **2012**, *17*(2), 208-219.

[43] Verbeek, C. J. R.; van den Berg, L. E. Development of Proteinous Bioplastics Using Bloodmeal. Journal of Polymers and the Environment **2011**, *19*(1), 1-10.

[44] van den Berg, L. (2009), Development of 2nd Generation Proteinous Bioplastics, Thesis, University of Waikato.

[45] Doi, Y.; Fukuda, K. *Biodegradable plastics and polymers: proceedings of the Third International Scientific Workshop on Biodegradable Plastics and Polymers, Osaka, Japan, November 9-11, 1993*; Elsevier, 1994.

[46] Avella, M.; De Vlieger, J. J.; Errico, M. E.; Fischer, S.; Vacca, P.; Volpe, M. G. Biodegradable starch/clay nanocomposite films for food packaging applications. Food Chemistry **2005**, *93*(3), 467-474.

[47] Verstappen, E. (2008), *Protein Extraction From Stickwater Using Nanoclay*, WaikatoLink, Hamilton.

[48] Seader, J. D.; Henley, E. J. *Separation process principles*; Wiley, 2006.

[49] Schmidhalter, U.; Kahr, G.; Evequoz, M.; Studer, C.; Oertli, J. J. Adsorption of thiamin (vitamin B-1) on soils and clays. Soil Science Society of America Journal **1994**, *58*(6), 1829-1837.

[50] Bayramoglu, G.; Çelik, G.; Arica, M. Y. Biosorption of Reactive Blue 4 dye by native and treated fungus Phanerocheate chrysosporium: Batch and continuous flow system studies. Journal of Hazardous Materials **2006**, *137*(3), 1689-1697.

[51] Liu, Y.; Zheng, Y. A.; Wang, A. Q. Effect of biotite content of hydrogels on enhanced removal of methylene blue from aqueous solution. Ionics **2011**, *17*(6), 535-543.

[52] Nogueira, F. G. E.; Lopes, J. H.; Silva, A. C.; Gonçalves, M.; Anastácio, A. S.; Sapag, K.; Oliveira, L. C. A. Reactive adsorption of methylene blue on montmorillonite via an ESI-MS study. Applied Clay Science **2009**, *43*(2), 190-195.

[53] Anwar, J.; Shafique, U.; Waheed uz, Z.; Salman, M.; Dar, A.; Anwar, S. Removal of Pb(II) and Cd(II) from water by adsorption on peels of banana. Bioresource Technology, *101*(6), 1752-1755.

[54] Hu, X.-j.; Wang, J.-s.; Liu, Y.-g.; Li, X.; Zeng, G.-m.; Bao, Z.-l.; Zeng, X.-x.; Chen, A.-w.; Long, F. Adsorption of chromium (VI) by ethylenediamine-modified cross-linked magnetic chitosan resin: Isotherms, kinetics and thermodynamics. Journal of Hazardous Materials, *185*(1), 306-314.

[55] Oliveira, L. C. A.; Rios, R. V. R. A.; Fabris, J. D.; Sapag, K.; Garg, V. K.; Lago, R. M. Clay-iron oxide magnetic composites for the adsorption of contaminants in water. Applied Clay Science **2003**, *22*(4), 169-177.

[56] Mittal, G. S. Treatment of wastewater from abattoirs before land application - a review. Bioresource Technology **2006**, *97*(9), 1119-1135.

[57] Boon, A., Personal communication, 2012.

[58] Veis, A. *The macromolecular chemistry of gelatin*; Academic Press, 1964.

[59] Woodhead-Galloway, J. *Collagen: The Anatomy of a Protein*; E. Arnold, 1980.

[60] Garrett, R. H.; Grisham, C. M. (eds) (2005), *Biochemistry*, Thomson Learning Inc.,

[61] Zamora, A. (2005), *Amino acid profiles of food proteins,* viewed January 2009 http://www.scientificpsychic.com/fitness/aminoacids1.html

[62] Zhang, Z. K.; Li, G. Y.; Shi, B. Physicochemical properties of collagen, gelatin and collagen hydrolysate derived from bovine limed split wastes. Journal of the Society of Leather Technologists and Chemists **2006**, *90*(1), 23-28.

[63] Ramachandran, G. N.; Reddi, A. H. *Biochemistry of collagen*; Plenum Press, 1976.

[64] Schilling, M. W.; Mink, L. E.; Gochenour, P. S.; Marriott, N. G.; Alvarado, C. Z. Utilization of pork collagen for functionality improvement of boneless cured ham manufactured from pale, soft, and exudative pork. Meat Science **2003**, *65*(1), 547-553.

[65] Patil, R. D.; Mark, J. E.; Apostolov, A.; Vassileva, E.; Fakirov, S. Crystallization of water in some crosslinked gelatins. European Polymer Journal **2000**, *36*(5), 1055-1061.

[66] Phillips, G. O.; Williams, P. A. *Handbook of Hydrocolloids*; CRC Press, 2000.

[67] GMIA (2012), *Gelatin handbook*, Gelatin Manufacturers Institute of America, Massachusetts.

[68] De Cristofaro, A.; Violante, A. Effect of hydroxy-aluminium species on the sorption and interlayering of albumin onto montmorillonite. Applied Clay Science **2001**, *19*(1-6), 59-67.

[69] Causserand, C.; Kara, Y.; Aimar, P. Protein fractionation using selective adsorption on clay surface before filtration. Journal of Membrane Science **2001**, *186*(2), 165-181.

[70] Sun, X.; Li, C.; Wu, Z.; Xu, X.; Ren, L.; Zhao, H. Adsorption of Protein from Model Wine Solution by Different Bentonites. Chinese Journal of Chemical Engineering **2007**, *15*(5), 632-638.

[71] Itoh, T.; Mikami, B.; Maru, I.; Ohta, Y.; Hashimoto, W.; Murata, K. Crystal structure of N-acyl-D-glucosamine 2-epimerase from porcine kidney at 2.0 angstrom resolution. Journal of Molecular Biology **2000**, *303*(5), 733-744.

[72] Ward, A. G.; Courts, A. *The Science and technology of gelatin*; Academic Press, 1977.

[73] Tosh, S. M.; Marangoni, A. G. Determination of the maximum gelation temperature in gelatin gels. Applied Physics Letters **2004**, *84*(21), 4242-4244.

[74] Papon, P.; Leblond, J.; Meijer, P. H. E. *The Physics of Phase Transitions*; Springer-Verlag, 2006.

[75] Arvanitoyannis, I. S.; Nakayama, A.; Aiba, S.-i. Chitosan and gelatin based edible films: state diagrams, mechanical and permeation properties. Carbohydrate Polymers **1998**, *37*(4), 371-382.

[76] Gomez-Estaca, J.; Gimenez, B.; Montero, P.; Gomez-Guillen, M. C. Incorporation of antioxidant borage extract into edible films based on sole skin gelatin or a commercial fish gelatin. Journal of Food Engineering **2009**, *92*(1), 78-85.

[77] GMIA (2001), *Edible gelatine,* viewed http://www.gelatin-gmia.com/html/rawmaterials_app.html

[78] Choi, Y. S.; Lee, S. B.; Hong, S. R.; Lee, Y. M.; Song, K. W.; Park, M. H. Studies on gelatin-based sponges. Part III: A comparative study of cross-linked gelatin/alginate, gelatin/hyaluronate and chitosan/hyaluronate sponges and their application as a wound dressing in full-thickness skin defect of rat. Journal of Materials Science-Materials in Medicine **2001**, *12*(1), 67-73.

[79] Van Vlierberghe, S.; Cnudde, V.; Dubruel, P.; Masschaele, B.; Cosijns, A.; De Paepe, I.; Jacobs, P. J. S.; Van Hoorebeke, L.; Remon, J. P.; Schacht, E. Porous gelatin hydrogels: 1. Cryogenic formation and structure analysis. Biomacromolecules **2007**, *8*(2), 331-337.

[80] Martucci, J.; Vázquez, A.; Ruseckaite, R. Nanocomposites based on gelatin and montmorillonite. Journal of Thermal Analysis and Calorimetry **2007**, *89*(1), 117-122.

[81] de Carvalho, R. A.; Grosso, C. R. F. Characterization of gelatin based films modified with transglutaminase, glyoxal and formaldehyde. Food Hydrocolloids **2004**, *18*(5), 717-726.

[82] Apostolov, A. A.; Fakirov, S.; Evstatiev, M.; Hoffmann, J.; Friedrich, K. Biodegradable Laminates Based on Gelatin, 1. Macromolecular Materials and Engineering **2002**, *287*(10), 693-697.

[83] Apostolov, A. A.; Fakirov, S.; Hoffmann, J.; Friedrich, K. Biodegradable Laminates Based on Gelatin, 2. Macromolecular Materials and Engineering **2003**, *288*(3), 228-234.

[84] Natarajan, N.; Shashirekha, V.; Noorjahan, S. E.; Rameshkumar, M.; Rose, C.; Sastry, T. P. Fibrin-Chitosan-Gelatin Composite Film: Preparation and Characterization. Journal of Macromolecular Science, Part A: Pure and Applied Chemistry **2005**, *42*(7), 945 - 953.

[85] Bigi, A.; Cojazzi, G.; Panzavolta, S.; Rubini, K.; Roveri, N. Mechanical and thermal properties of gelatin films at different degrees of glutaraldehyde crosslinking. Biomaterials **2001**, *22*(8), 763-768.

[86] Ruiz-Hitzky, E.; Ariga, K.; Lvov, Y. M. *Bio-inorganic Hybrid Nanomaterials*; Wiley, 2008.

[87] Garreth, S. (2011), *Assessment of Stickwater as an Anaerobic Digestion feedstock*, Waikato University, Hamilton.

[88] Aguilar, M. I.; Saez, J.; Llorens, M.; Soler, A.; Ortuno, J. F. Microscopic observation of particle reduction in slaughterhouse wastewater by coagulation-flocculation using ferric sulphate as coagulant and different coagulant aids. Water Research **2003**, *37*(9), 2233-2241.

[89] Goodwin, J. W. *Colloids and interfaces with surfactants and polymers: an introduction*; J. Wiley, 2004.

[90] Tien, C. *Adsorption Calculations and Modelling*; Butterworth-Heinemann: New York, 1994.

[91] King, C. J. *Separation processes*; McGraw-Hill, 1980.

[92] McNaught, A. D.; Wilkinson, A.; Pure, I. U. o.; Chemistry, A. *Compendium of Chemical Terminology: Iupac Recommendations*; Blackwell Science, 1997.

[93] Knaebel, K. S. *Adsorbent Selection*, Adsorption Research Inc., Ohio.

[94] Masuda, H.; Higashitani, K.; Yoshida, H. *Powder Technology: Fundamentals of Particles, Powder Beds, And Particle Generation*; Taylor & Francis Group, 2006.

[95] Donohue, M. A new classification of adsorption isotherms. Johns Hopkins University.

[96] Donohue, M. D.; Aranovich, G. L. Classification of Gibbs adsorption isotherms. Advances in Colloid and Interface Science **1998**, *76*, 137-152.

[97] Murray, A. P. Protein adsorption by suspended sediments: Effects of pH, temperature, and concentration. Environmental Pollution (1970) **1973**, *4*(4), 301-312.

[98] Parfitt, G. D.; Rochester, C. H. *Adsorption from Solution at the Solid/Liquid Interface*; Academic Press Inc. LTD.: London, UK, 1983.

[99] Bulut, E.; Özacar, M.; Sengil, I. A. Equilibrium and kinetic data and process design for adsorption of Congo Red onto bentonite. Journal of Hazardous Materials **2008**, *154*(1-3), 613-622.

[100] Hameed, B. H.; Mahmoud, D. K.; Ahmad, A. L. Equilibrium modeling and kinetic studies on the adsorption of basic dye by a low-cost adsorbent: Coconut (Cocos nucifera) bunch waste. Journal of Hazardous Materials **2008**, *158*(1), 65-72.

[101] Hidayat, C.; Nakajima, M.; Takagi, M.; Yoshida, T. Multivalent binding interaction of alcohol dehydrogenase on dye-metal affinity matrix. Journal of Bioscience and Bioengineering **2003**, *96*(2), 168-173.

[102] Kurth, T. L.; Byars, J. A.; Cermak, S. C.; Sharma, B. K.; Biresaw, G. Non-linear adsorption modeling of fatty esters and oleic estolide esters via boundary lubrication coefficient of friction measurements. Wear **2007**, *262*(5-6), 536-544.

[103] Li, W.; Li, S. A study on the adsorption of bovine serum albumin onto electrostatic microspheres: Role of surface groups. Colloids and Surfaces A: Physicochemical and Engineering Aspects **2007**, *295*(1-3), 159-164.

[104] Vijayaraghavan, K.; Yun, Y.-S. Bacterial biosorbents and biosorption. Biotechnology Advances **2008**, *26*(3), 266-291.

[105] Sharma, S.; Agarwal, G. P. Interactions of Proteins with Immobilized Metal Ions: A Comparative Analysis Using Various Isotherm Models. Analytical Biochemistry **2001**, *288*(2), 126-140.

[106] Cano, T.; Offringa, N. D.; Willson, R. C. Competitive ion-exchange adsorption of proteins: Competitive isotherms with controlled competitor concentration. Journal of Chromatography A **2005**, *1079*(1-2), 116-126.

[107] Lin, P.-C.; Lin, S.-C.; Hsu, W.-H. Adsorption behaviors of recombinant proteins on hydroxyapatite-based immobilized metal affinity chromatographic adsorbents. Journal of the Chinese Institute of Chemical Engineers **2008**, *39*(5), 389-398.

[108] Tsai, S.-Y.; Lin, S.-C.; Suen, S.-Y.; Hsu, W.-H. Effect of number of poly(His) tags on the adsorption of engineered proteins on immobilized metal affinity chromatography adsorbents. Process Biochemistry **2006**, *41*(9), 2058-2067.

[109] Yang, Y.-H.; Wu, T.-T.; Suen, S.-Y.; Lin, S.-C. Equilibrium adsorption of poly(His)-tagged proteins on immobilized metal affinity chromatographic adsorbents. Biochemical Engineering Journal **2011**, *54*(1), 1-9.

[110] Yi, X. S.; Shi, W. X.; Yu, S. L.; Wang, Y.; Sun, N.; Jin, L. M.; Wang, S. Isotherm and kinetic behavior of adsorption of anion polyacrylamide (APAM) from aqueous solution using two kinds of PVDF UF membranes. Journal of Hazardous Materials **2011**, *189*(1-2), 495-501.

[111] Johnson, R. D.; Arnold, F. H. The temkin isotherm describes heterogeneous protein adsorption. Biochimica et Biophysica Acta (BBA) - Protein Structure and Molecular Enzymology **1995**, *1247*(2), 293-297.

[112] Theng, B. K. G. *Soils with variable charge*; New Zealand Society of Soil Science, 1980.

[113] Achaerandio, I.; Pachova, V.; Guell, C.; Lopez, F. Protein adsorption by bentonite in a white wine model solution: Effect of protein molecular weight and ethanol concentration. American Journal of Enology and Viticulture **2001**, *52*(2), 122-126.

[114] Lambri, M.; Dordoni, R.; Giribaldi, M.; Violetta, M. R.; Giuffrida, M. G. Heat-unstable protein removal by different bentonite labels in white wines. LWT - Food Science and Technology (0).

[115] Sarmento, M. R.; Oliveira, J. C.; Slatner, M.; Boulton, R. B. Kinetics of the adsorption of bovine serum albumin contained in a model wine solution by non-swelling ion-exchange resins. Journal of Food Engineering **1999**, *39*(1), 65-71.

[116] Bergaya, F.; Lagaly, G. Surface modification of clay minerals. Applied Clay Science **2001**, *19*(1-6), 1-3.

[117] Fusi, P.; Ristori, G. G.; Calamai, L.; Stotzky, G. Adsorption and binding of protein on "clean" (homoionic) and "dirty" (coated with Fe oxyhydroxides) montmorillonite, illite and kaolinite. Soil Biology and Biochemistry **1989**, *21*(7), 911-920.

[118] Lin, J.-J.; Wei, J.-C.; Juang, T.-Y.; Tsai, W.-C. Preparation of Protein-Silicate Hybrids from Polyamine Intercalation of Layered Montmorillonite. Langmuir **2006**, *23*(4), 1995-1999.

[119] Koyama, T.; Tanoue, S.; Iemoto, Y.; Maekawa, T.; Unryu, T. Melt Compounding of Various Polymers With Organoclay by Shear Flow. Polymer Composites **2009**, *30*(8), 1065-1073.

[120] Pluta, M.; Paul, M. A.; Alexandre, M.; Dubois, P. Plasticized polylactide/clay nanocomposites. I. The role of filler content and its surface organo-modification on the physico-chemical properties. Journal of Polymer Science Part B-Polymer Physics **2006**, *44*(2), 299-311.

[121] Rhim, J. W.; Lee, S. B.; Hong, S. I. Preparation and Characterization of Agar/Clay Nanocomposite Films: The Effect of Clay Type. Journal of Food Science **2011**, *76*(3), N40-N48.

[122] Lin, J.-J.; Chen, Y.-M. Amphiphilic Properties of Poly(oxyalkylene)amine-Intercalated Smectite Aluminosilicates. Langmuir **2004**, *20*(10), 4261-4264.

[123] Muhlack, R.; Nordestgaard, S.; Waters, E. J.; O'Neill, B. K.; Lim, A.; Colby, C. B. In-line dosing for bentonite fining of wine or juice: Contact time, clarification, product recovery and sensory effects. Australian Journal of Grape and Wine Research **2006**, *12*(3), 221-234.

[124] Chou, C.-C.; Shieu, F.-S.; Lin, J.-J. Preparation, Organophilicity, and Self-Assembly of Poly(oxypropylene)amineâˆ'Clay Hybrids. Macromolecules **2003**, *36*(7), 2187-2189.

[125] Akelah, A.; Rehab, A.; Kenawy, E. R.; Abou Zeid, M. S. Catalytic activity of polymer-montmorillonite composites in chemical reactions. Journal of Applied Polymer Science **2006**, *101*(2), 1121-1129.

[126] Güngör, N.; Karaoglan, S. Interactions of polyacrylamide polymer with bentonite in aqueous systems. Materials Letters **2001**, *48*(3-4), 168-175.

[127] Coruh, S.; Geyikci, F. Adsorption of copper (II) ions on montmorillonite and sepiolite clays: equilibrium and kinetic studies. Desalination and Water Treatment **2012**, *45*(1-3), 351-360.

[128] Pusino, A.; Braschi, I.; Gessa, C. Adsorption and degradation of triasulfuron on homoionic montmorillonites. Clays and Clay Minerals **2000**, *48*(1), 19-25.

[129] Pusino, A.; Gelsomino, A.; Fiori, M. G.; Gessa, C. Adsorption of two quinolinecarboxylic acid herbicides on homoionic montmorillonites. Clays and Clay Minerals **2003**, *51*(2), 143-149.

[130] Everett, D. H. *Basic principles of colloid science*; Royal Society of Chemistry, 1988.

[131] Park, Y.; Shin, W. S.; Choi, S. J. Sorptive removal of cobalt, strontium and cesium onto manganese and iron oxide-coated montmorillonite from groundwater. Journal of Radioanalytical and Nuclear Chemistry **2012**, *292*(2), 837-852.

[132] Konya, J.; Nagy, N. M. Sorption of dissolved mercury (II) species on calcium-montmorillonite: an unusual pH dependence of sorption process. Journal of Radioanalytical and Nuclear Chemistry **2011**, *288*(2), 447-454.

[133] Mpofu, P.; Addai-Mensah, J.; Ralston, J. Interfacial chemistry, particle interactions and improved dewatering behaviour of-smectite clay dispersions. International Journal of Mineral Processing **2005**, *75*(3-4), 155-171.

[134] Batchelor, G. K. *An Introduction to Fluid Dynamics*; Cambridge University Press, 2000.

[135] Lamb, H. *Hydrodynamics*; Cambridge University Press, 1993.

[136] Dusenbery, D. B. *Living at Micro Scale: The Unexpected Physics of Being Small*; Harvard University Press, 2009.

[137] Rhodes, M. *Introduction to Particle Technology*; Wiley, 2013.

[138] Newman, A. C. D. *Chemistry of clays and clay minerals*; Longman Scientific & Technical: London, 1987.

[139] Worden, R. H.; Morad, S. *Clay Mineral Cements in Sandstones*; Blackwell Pub.: Malden, MA, 2003.

[140] Rankin, P. C.; Churchman, G. J. (1981), *Soils with variable charge*, in (Eds) *Soils with variable charge*, Massey University, Palmerston North, 11-18 February 1981, pp. 111.

[141] Tombácz, E.; Szekeres, M.; Baranyi, L.; Michéli, E. Surface modification of clay minerals by organic polyions. Colloids and Surfaces A: Physicochemical and Engineering Aspects **1998**, *141*(3), 379-384.

[142] USGS (2012), *The Mineral Industry in New Zealand*, 2011 Minerals Yearbook, US Department of the Interior,

[143] Minerals, T. (2006), *Bentonite*, Material Safety Data Sheet, Transform Minerals Limited, Canterbury.

[144] Mathias, L. J. (2005), *Montmorillonite Clay,* viewed http://www.pslc.ws/macrog/mpm/composit/nano

[145] Sheng, N.; Boyce, M. C.; Parks, D. M.; Rutledge, G. C.; Abes, J. I.; Cohen, R. E. Multiscale micromechanical modeling of polymer/clay nanocomposites and the effective clay particle. Polymer **2004**, *45*(2), 487-506.

[146] Chang, H. C.; Yeo, L. Y. *Electrokinetically-Driven Microfluidics and Nanofluidics*; Cambridge University Press, 2009.

[147] Murray, H. H. Traditional and new applications for kaolin, smectite, and palygorskite: a general overview. Applied Clay Science **2000**, *17*(5-6), 207-221.

[148] Lantenois, S.; Champallier, R.; Beny, J. M.; Muller, F. Hydrothermal synthesis and characterization of dioctahedral smectites: A montmorillonites series. Applied Clay Science **2008**, *38*(3-4), 165-178.

[149] Issman, L.; Talmon, Y. Cryo-SEM specimen preparation under controlled temperature and concentration conditions. Journal of Microscopy **2012**, *246*(1), 60-69.

[150] Mouzon, J.; Bhuiyan, I. U.; Forsmo, S. P. E.; Hedlund, J. Cryo-SEM method for the observation of entrapped bubbles and degree of water filling in large wet powder compacts. Journal of Microscopy **2011**, *242*(2), 189-196.

[151] Sharma, S. K.; Mudhoo, A.; Clark, J. H.; Kraus, G. A. *A Handbook of Applied Biopolymer Technology: Synthesis, Degradation and Applications*; Royal Society of Chemistry, 2011.

[152] Gu, Z.; Gao, L.; Song, G. J.; Liu, W. S.; Li, P. Y.; Shan, C. P. Octadecylammonium montmorillonite/natural rubber/cis-1,4-polybutadiene nanocomposites. Applied Clay Science **2010**, *50*(1), 143-147.

[153] Kharroubi, M.; Balme, S.; Henn, F.; Giuntini, J. C.; Belarbi, H.; Haouzi, A. Dehydration enthalpy of alkali-cations-exchanged montmorillonite from thermogravimetric analysis. Journal of Colloid and Interface Science **2009**, *329*(2), 339-345.

[154] Helios Rybicka, E.; Calmano, W. Changes in physico-chemical properties of some clay minerals by reducing extraction reagents. Applied Clay Science **1988**, *3*(1), 75-84.

[155] Ding, X.; Henrichs, S. M. Adsorption and desorption of proteins and polyamino acids by clay minerals and marine sediments. Marine Chemistry **2002**, *77*(4), 225-237.

[156] Hedges, J. I.; Hare, P. E. Amino acid adsorption by clay minerals in distilled water. Geochimica et Cosmochimica Acta **1987**, *51*(2), 255-259.

[157] Boylu, F. Optimization of foundry sand characteristics of soda-activated calcium bentonite. Applied Clay Science **2011**, *52*(1-2), 104-108.

[158] Marroquín-Cardona, A.; Deng, Y.; Garcia-Mazcorro, J. F.; Johnson, N. M.; Mitchell, N. J.; Tang, L.; Robinson, A.; Taylor, J. F.; Wang, J. S.; Phillips, T. D. Characterization and safety of uniform particle size NovaSil clay as a potential aflatoxin enterosorbent. Applied Clay Science **2011**, *54*(3–4), 248-257.

[159] Czímerová, A.; Bujdák, J.; Dohrmann, R. Traditional and novel methods for estimating the layer charge of smectites. Applied Clay Science **2006**, *34*(1-4), 2-13.

[160] Benna, M.; Kbir-Ariguib, N.; Magnin, A.; Bergaya, F. Effect of pH on rheological properties of purified sodium bentonite suspensions. Journal of Colloid and Interface Science **1999**, *218*(2), 442-455.

[161] Yoon, P. J.; Hunter, D. L.; Paul, D. R. Polycarbonate nanocomposites. Part 1. Effect of organoclay structure on morphology and properties. Polymer **2003**, *44*(18), 5323-5339.

[162] Perry, A. (2006), *AboutClay,* viewed http://www.aboutclay.com/index.htm

[163] Kojima, Y.; Usuki, A.; Kawasumi, M.; Okada, A.; Kurauchi, T.; Kamigaito, O. Synthesis of nylon 6–clay hybrid by montmorillonite intercalated with ϵ-caprolactam. Journal of Polymer Science Part A: Polymer Chemistry **1993**, *31*(4), 983-986.

[164] Taib, R. M.; Ghaleb, Z. A.; Ishak, Z. A. M. Thermal, mechanical, and morphological properties of polylactic acid toughened with an impact modifier. Journal of Applied Polymer Science **2012**, *123*(5), 2715-2725.

[165] Usuki, A.; Hasegawa, N.; Kato, M. Polymer-clay nanocomposites. In *Inorganic Polymeric Nanocomposites and Membranes*; Springer-Verlag Berlin: Berlin, 2005; 135-195.

[166] Callister, W. D. *Material Science and Engineering: An Introduction*; John Wiley & Sons Incorporated, 1999.

[167] Hull, D.; Clyne, T. W. *An Introduction to Composite Materials*; Cambridge University Press, 1996.

[168] Fowler, P. A.; Hughes, J. M.; Elias, R. M. Biocomposites: technology, environmental credentials and market forces. Journal of the Science of Food and Agriculture **2006**, *86*(12), 1781-1789.

[169] Doi, Y. *Microbial polyesters*; VCH, 1990.

[170] Li, S. H.; Wang, C. P.; Zhuang, X. W.; Hu, Y.; Chu, F. X. Renewable Resource-Based Composites of Acorn Powder and Polylactide Bio-Plastic: Preparation and Properties Evaluation. Journal of Polymers and the Environment **2011**, *19*(1), 301-311.

[171] Thielen, M. (2012), *US Demand for Bioplastics*, Bioplastics Magazine, ISSN: 1862-5258, Polymedia Publisher GmbH, Krefeld, Germany.

[172] Vasilakos, S. P.; Tarantili, P. A. Mechanical properties and nanostructure correlation of condensation-type poly(dimethyl siloxane)/layered silicate hybrids. Journal of Applied Polymer Science **2012**, *125*, E548-E560.

[173] Sinha Ray, S.; Okamoto, K.; Okamoto, M. Structure-Property Relationship in Biodegradable Poly(butylene succinate)/Layered Silicate Nanocomposites. Macromolecules **2003**, *36*(7), 2355-2367.

[174] Kojima, Y.; Usuki, A.; Kawasumi, M.; Okada, A.; Kurauchi, T.; Kamigaito, O.; Kaji, K. Fine-structure of nylon-6-clay hybrid. Journal of Polymer Science Part B-Polymer Physics **1994**, *32*(4), 625-630.

[175] Soulestin, J.; Rashmi, B. J.; Bourbigot, S.; Lacrampe, M. F.; Krawczak, P. Mechanical and Optical Properties of Polyamide 6/Clay Nanocomposite Cast Films: Influence of the Degree of Exfoliation. Macromolecular Materials and Engineering **2012**, *297*(5), 444-454.

[176] Van de Velde, K.; Kiekens, P. Biopolymers: overview of several properties and consequences on their applications. Polymer Testing **2002**, *21*(4), 433-442.

[177] Sharma, S. K.; Nema, A. K.; Nayak, S. K. Effect of modified clay on mechanical and morphological properties of ethylene octane copolymer-polypropylene nanocomposites. Journal of Composite Materials **2012**, *46*(10), 1139-1150.

[178] Alexandre, M.; Dubois, P. Polymer-layered silicate nanocomposites: preparation, properties and uses of a new class of materials. Materials Science & Engineering R-Reports **2000**, *28*(1-2), 1-63.

[179] Sigma-Aldrich (2011), *Nanoclay, surface modified*, Material Safety Data Sheet, Sigma-Aldrich NZ Ltd., Auckland.

[180] Bier, J. M., Personal communication, 2011.

[181] Babu, S. (2003), viewed 2012, http://www.plastemart.com/upload/literature/Extruder-Processing-Zone-EPZ-Co-rotating-Twin-Screw-Extruder-quality-compounded-material-output.asp

[182] Sawpan, M. A. (2009), Mechanical Performance of Industrial Hemp Fibre Reinforced Polylactide and Unsaturated Polyester Composites., Thesis, Waikato University.

[183] Verbeek, C. J. R.; van den Berg, L. E. Structural changes as a result of processing in thermoplastic bloodmeal. Journal of Applied Polymer Science **2012**, *125*, E347-E355.

[184] Johlin, J. M. The Isoelectric Point of Gelatin and its Relation to the Minimum Physical Properties of Gelatin. The Journal of Biological Chemistry **1930**.

[185] Sigma-Aldrich *Gelatin Product Information*, Sigma-Aldrich, St. Louis, MO 63103, USA.

[186] Hitchcock, D. I. The isoelectric point of a standard gelatin preparation. The Journal of General Physiology **1931**(July 20).

[187] Arai, T.; Norde, W. The behavior of some model proteins at solid-liquid interfaces 1. Adsorption from single protein solutions. Colloids and Surfaces **1990**, *51*, 1-15.

[188] Tchobanoglous, G.; Burton, F. L.; Metcalf; Eddy; Stensel, H. D. *Wastewater Engineering: Treatment and Reuse*; McGraw-Hill, 2004.

[189] BIOTOL; Universiteit, O.; Polytechnic, T. *Bioprocess technology: modelling and transport phenomena*; Butterworth-Heinemann, 1992.

[190] Janek, M.; Lagaly, G. Interaction of a cationic surfactant with bentonite: a colloid chemistry study. Colloid and Polymer Science **2003**, *281*(4), 293-301.

[191] Zoecklein, B. (1988), *Bentonite fining of juice and wine*, Virginia Polytechnic Institute and State University, Petersburg.

[192] Mehta, D.; Hawley, M. C. Wall Effect in Packed Columns. Industrial & Engineering Chemistry Process Design and Development **1969**, *8*(2), 280-282.

[193] Ogunnaike, B. A.; Ray, W. H. *Process Dynamics, Modeling, and Control*; Oxford University Press, 1994.

[194] Ugural, A. C.; Fenster, S. K. *Advanced strength and applied elasticity*; Prentice Hall PTR, 2003.

[195] Zhang, X. M.; Qiang, B.; Greenleaf, J. Comparison of the surface wave method and the indentation method for measuring the elasticity of gelatin phantoms of different concentrations. Ultrasonics **2011**, *51*(2), 157-164.

[196] Bouman, R.; Jesen, S.; Wake, M. Process Capital Cost Estimation for New Zealand 2004. W.B., E., Ed.; Society of Chemical Engineers New Zealand: Christchurch, 2004.

[197] Garcia-Martinez, J. M.; Laguna, O.; Areso, S.; Collar, E. P. Polypropylene/mica composites modified by succinic anhydride-crafted atactic polypropylene: A thermal and mechanical study under dynamic conditions. Journal of Applied Polymer Science **2001**, *81*(3), 625-636.

[198] Stamhuis, J. E. Mechanical properties and morphology of polypropylene composites. III. Short glass fiber reinforced elastomer modified polypropylene. Polymer Composites **1988**, *9*(4), 280-284.

[199] Benali, S.; Peeterbroeck, S.; Brocorens, P.; Monteverde, F.; Bonnaud, L.; Alexandre, M.; Lazzaroni, R.; Dubois, P. Chlorinated polyethylene nanocomposites using PCL/clay nanohybrid masterbatches. European Polymer Journal **2008**, *44*(6), 1673-1685.

[200] Kontou, E.; Georgiopoulos, P.; Niaounakis, M. The role of nanofillers on the degradation behavior of polylactic acid. Polymer Composites **2012**, *33*(2), 282-294.

[201] Hu, X.; Lu, Q.; Kaplan, D. L.; Cebe, P. Microphase Separation Controlled beta-Sheet Crystallization Kinetics in Fibrous Proteins. Macromolecules **2009**, *42*(6), 2079-2087.

[202] Jiménez, A.; Zaikov, G. E. *Recent Advances in Research on Biodegradable Polymers and Sustainable Composites*; Nova Science Pub Incorporated, 2009.

[203] Berg, J. M.; Tymoczko, J. L.; Stryer, L. *Lecture Notebook for Biochemistry*; W. H. Freeman, 2006.

[204] Mittal, V. Modification of montmorillonites with thermally stable phosphonium cations and comparison with alkylammonium montmorillonites. Applied Clay Science **2012**, *56*, 103-109.

[205] Jeon, H. S.; Rameshwaram, J. K.; Kim, G.; Weinkauf, D. H. Characterization of polyisoprene–clay nanocomposites prepared by solution blending. Polymer **2003**, *44*(19), 5749-5758.

[206] Coutinho, C. A.; Harrinauth, R. K.; Gupta, V. K. Settling characteristics of composites of PNIPAM microgels and TiO2 nanoparticles. Colloids and Surfaces a-Physicochemical and Engineering Aspects **2008**, *318*(1-3), 111-121.

[207] Kim, B. H.; Klima, M. S. Simulation of hindered-settling column separations for soil remediation. Journal of Environmental Science and Health Part a-Toxic/Hazardous Substances & Environmental Engineering **2004**, *39*(1), 19-33.

[208] Richardson, J. F.; Zaki, W. N. Sedimentation and fluidisation: Part I. Chemical Engineering Research and Design **1997**, *75, Supplement*(0), S82-S100.

APPENDICES

Appendix-1A

Table 41: Full sequence of collagen amino acid [40, 59].

N terminal non-helical region

pGlu- Met- Ser- Tyr- Gly- Tyr- Asp- Glu- Lys- Ser- Ala- Gly- Val- Ser- Val- Pro

Helical region

1 **Gly**- Pro- Met- **Gly**- Pro- Ser- **Gly**- Pro- Arg- **Gly**- Leu- Hyp- **Gly**- Pro- Hyp- **Gly**- Ala- Hyp- **Gly**- Pro- Gln- **Gly**- Phe- Gln- **Gly**- Pro- Hyp
28 **Gly**- Glu- Hyp- **Gly**- Glu- Hyp- **Gly**- Ala- Ser- **Gly**- Pro- Met- **Gly**- Pro- Arg- **Gly**- Pro- Hyp- **Gly**- Pro- Hyp- **Gly**- Lys- Asn- **Gly**- Asp- Asp
55 **Gly**- Glu- Ala- **Gly**- Lys- Pro- **Gly**- Arg- Hyp- **Gly**- Gln- Arg- **Gly**- Pro- Hyp- **Gly**- Pro- Gln- **Gly**- Ala- Arg- **Gly**- Leu- Hyp- **Gly**- Thr- Ala
82 **Gly**- Leu- Hyp- **Gly**- Met- Hyl- **Gly**- His- Arg- **Gly**- Phe- Ser- **Gly**- Leu- Asp- **Gly**- Ala- Lys- **Gly**- Asn- Thr- **Gly**- Pro- Ala- **Gly**- Pro- Lys
109 **Gly**- Glu- Hyp- **Gly**- Ser- Hyp- **Gly**- Glx- Asx- **Gly**- Ala- Hyp- **Gly**- Gln- Met- **Gly**- Pro- Arg- **Gly**- Leu- Hyp- **Gly**- Glu- Arg- **Gly**- Arg- Hyp
136 **Gly**- Pro- Hyp- **Gly**- Ser- Ala- **Gly**- Ala- Arg- **Gly**- Asp- Asp- **Gly**- Ala- Val- **Gly**- Ala- Ala- **Gly**- Pro- Hyp- **Gly**- Pro- Thr- **Gly**- Pro- Thr
163 **Gly**- Pro- Hyp- **Gly**- Phe- Hyp- **Gly**- Ala- Ala- **Gly**- Ala- Lys- **Gly**- Glu- Ala- **Gly**- Pro- Gln- **Gly**- Ala- Arg- **Gly**- Ser- Glu- **Gly**- Pro- Gln
190 **Gly**- Val- Arg- **Gly**- Glu- Hyp- **Gly**- Pro- Hyp- **Gly**- Pro- Ala- **Gly**- Ala- Ala- **Gly**- Pro- Ala- **Gly**- Asn- Hyp- **Gly**- Ala- Asp- **Gly**- Gln- Hyp
217 **Gly**- Ala- Lys- **Gly**- Ala- Asn- **Gly**- Ala- Hyp- **Gly**- Ile- Ala- **Gly**- Ala- Hyp- **Gly**- Phe- Hyp- **Gly**- Ala- Arg- **Gly**- Pro- Ser- **Gly**- Pro- Gln
244 **Gly**- Pro- Ser- **Gly**- Ala- Hyp- **Gly**- Pro- Lys- **Gly**- Asn- Ser- **Gly**- Glu- Hyp- **Gly**- Ala- Hyp- **Gly**- Asn- Lys- **Gly**- Asp- Thr- **Gly**- Ala- Lys
271 **Gly**- Glu- Hyp- **Gly**- Pro- Ala- **Gly**- Val- Gln- **Gly**- Pro- Hyp- **Gly**- Pro- Ala- **Gly**- Glu- Glu- **Gly**- Lys- Arg- **Gly**- Ala- Arg- **Gly**- Glu- Hyp
298 **Gly**- Pro- Ser- **Gly**- Leu- Hyp- **Gly**- Pro- Hyp- **Gly**- Glu- Arg- **Gly**- Gly- Hyp- **Gly**- Ser- Arg- **Gly**- Phe- Hyp- **Gly**- Ala- Asp- **Giy**- Val- Ala
325 **Gly**- Pro- Lys- **Gly**- Pro- Ala- **Gly**- Glu- Arg- **Gly**- Ser- Hyp- **Gly**- Pro- Ala- **Gly**- Pro- Lys- **Gly**- Ser- Hyp- **Gly**- Glu- Ala- **Gly**- Arg- Hyp
352 **Gly**- Glu- Ala- **Gly**- Leu- Hyp- **Gly**- Ala- Lys- **Gly**- Leu- Thr- **Gly**- Ser- Hyp- **Gly**- Ser- Hyp- **Gly**- Pro- Asp- **Gly**- Lys- Thr- **Gly**- Pro- Hyp
379 **Gly**- Pro- Ala- **Gly**- Gln- Asp- **Gly**- Arg- Hyp- **Gly**- Pro- Ala- **Gly**- Pro- Hyp- **Gly**- Ala- Arg- **Gly**- Gln- Ala- **Gly**- Val- Met- **Gly**- Phe- Hyp
406 **Gly**- Pro- Lys- **Gly**- Ala- Ala- **Gly**- Glu- Hyp- **Gly**- Lys- Ala- **Gly**- Glu- Arg- **Gly**- Val- Hyp- **Gly**- Pro- Hyp- **Gly**- Ala- Val- **Gly**- Pro- Ala
433 **Gly**- Lys- Asp- **Gly**- Glu- Ala- **Gly**- Ala- Gln- **Gly**- Pro- Hyp- **Gly**- Pro- Ala- **Gly**- Pro- Ala- **Gly**- Glu- Arg- **Gly**- Glu- Gln- **Gly**- Pro- Ala
460 **Gly**- Ser- Hyp- **Gly**- Phe- Gln- **Gly**- Leu- Hyp- **Gly**- Pro- Ala- **Gly**- Pro- Hyp- **Gly**- Glu- Ala- **Gly**- Lys- Hyp- **Gly**- Glu- Gln- **Gly**- Val- Hyp
487 **Gly**- Asp- Leu- **Gly**- Ala- Hyp- **Gly**- Pro- Ser- **Gly**- Ala- Arg- **Gly**- Glu- Arg- **Gly**- Phe- Hyp- **Gly**- Glu- Arg- **Gly**- Val- Glu- **Gly**- Pro- Hyp
514 **Gly**- Pro- Ala- **Gly**- Pro- Arg- **Gly**- Ala- Asn- **Gly**- Ala- Hyp- **Gly**- Asn- Asp- **Gly**- Ala- Lys- **Gly**- Asp- Ala- **Gly**- Ala- Hyp- **Gly**- Ala- Hyp
541 **Gly**- Ser- Gln- **Gly**- Ala- Hyp- **Gly**- Leu- Gln- **Gly**- Met- Hyp- **Gly**- Glu- Arg- **Gly**- Ala- Ala- **Gly**- Leu- Hyp- **Gly**- Pro- Lys- **Gly**- Asp- Arg
568 **Gly**- Asp- Ala- **Gly**- Pro- Lys- **Gly**- Ala- Asp- **Gly**- Ala- Pro- **Gly**- Lys- Asp- **Gly**- Val- Arg- **Gly**- Leu- Thr- **Gly**- Pro- Ile- **Gly**- Pro- Hyp
595 **Gly**- Pro- Ala- **Gly**- Ala- Hyp- **Gly**- Asp- Lys- **Gly**- Glu- Ala- **Gly**- Pro- Ser- **Gly**- Pro- Ala- **Gly**- Thr- Arg- **Gly**- Ala- Hyp- **Gly**- Asp- Arg
622 **Gly**- Glu- Hyp- **Gly**- Pro- Hyp- **Gly**- Pro- Ala- **Gly**- Phe- Ala- **Gly**- Pro- Hyp- **Gly**- Ala- Asp- **Cly**- Gln- Hyp- **Gly**- Ala- Lys- **Gly**- Glu- Hyp
649 **Gly**- Asp- Ala- **Gly**- Ala- Lys- **Gly**- Asp- Ala- **Gly**- Pro- Hyp- **Gly**- Pro- Ala- **Gly**- Pro- Ala- **Gly**- Pro- Hyp- **Gly**- Pro- Ile- **Gly**- Asn- Val
676 **Gly**- Ala- Hyp- **Gly**- Pro- Hyl- **Gly**- Ala- Arg- **Gly**- Ser- Ala- **Gly**- Pro- Hyp- **Gly**- Ala- Thr- **Gly**- Phe- Hyp- **Gly**- Ala- Ala- **Gly**- Arg- Val
703 **Gly**- Pro- Hyp- **Gly**- Pro- Ser- **Gly**- Asn- Ala- **Gly**- Pro- Hyp- **Gly**- Pro- Hyp- **Gly**- Pro- Ala- **Gly**- Lys- Glu- **Gly**- Ser- Lys- **Gly**- Pro- Arg
730 **Gly**- Glu- Thr- **Gly**- Pro- Ala- **Gly**- Arg- Hyp- **Gly**- Glu- Val- **Gly**- Pro- Hyp- **Gly**- Pro- Hyp- **Gly**- Pro- Ala- **Gly**- Glu- Lys- **Gly**- Ala- Hyp
757 **Gly**- Ala- Asp- **Gly**- Pro- Ala- **Gly**- Ala- Hyp- **Gly**- Thr- Pro- **Gly**- Pro- Gln- **Gly**- Ile- Ala- **Gly**- Gln- Arg- **Gly**- Val- Val- **Gly**- Leu- Iiyp
784 **Gly**- Gln- Arg- **Gly**- Glu- Arg- **Gly**- Phe- Hyp- **Gly**- Leu- Hyp- **Gly**- Pro- Ser- **Gly**- Glu- Hyp- **Gly**- Lys- Gln- **Gly**- Pro- Ser- **Gly**- Ala- Ser
811 **Gly**- Glu- Arg- **Gly**- Pro- Hyp- **Gly**- Pro- Met- **Gly**- Pro- Hyp- **Gly**- Leu- Ala- **Gly**- Pro- Hyp- **Gly**- Glu- Ser- **Gly**- Arg- Glu- **Gly**- Ala- Hyp
838 **Gly**- Ala- Glu- **Gly**- Ser- Hyp- **Gly**- Arg- Asp- **Gly**- Ser- Hyp- **Gly**- Ala- Lys- **Gly**- Asp- Arg- **Gly**- Glu- Thr- **Gly**- Pro- Ala- **Gly**- Ala- Hvp
865 **Gly**- Pro- Hyp- **Gly**- Ala- Hyp- **Gly**- Ala- Hyp- **Gly**- Pro- Val- **Gly**- Pro- Ala- **Gly**- Lys- Ser- **Gly**- Asp- Arg- **Gly**- Glu- Thr- **Gly**- Pro- Ala
892 **Gly**- Pro- Ile- **Gly**- Pro- Val- **Gly**- Pro- Ala- **Gly**- Ala- Arg- **Gly**- Pro- Ala- **Gly**- Pro- Gln- **Gly**- Pro- Arg- **Gly**- Asx- Hyl- **Gly**- Glx- Thr
919 **Gly**- Glx- Glx- **Gly**- Asx- Arg- **Gly**- Ile- Hyl- **Gly**- His- Arg- **Gly**- Phe- Ser- **Gly**- Leu- Gln- **Gly**- Pro- Hyp- **Gly**- Pro- Hyp- **Gly**- Ser- Hyp
946 **Gly**- Glu- Gln- **Gly**- Pro- Ser- **Gly**- Ala- Ser- **Gly**- Pro- Ala- **Gly**- Pro- Arg- **Gly**- Pro- Hyp- **Gly**- Ser- Ala- **Gly**- Ser- Hyp- **Gly**- Lys- Asp
973 **Gly**- Leu- Asn- **Gly**- Leu- Hyp- **Gly**- Pro- Ile- **Gly**- Hyp- Hyp- **Gly**- Pro- Arg- **Gly**- Arg- Thr- **Gly**- Asp- Ala- **Gly**- Pro- Ala- **Gly**- Pro- Hyp
1000 **Gly**- Pro- Hyp- **Gly**- Pro- Hyp- **Gly**- Pro- Hyp- **Gly**- Pro- Pro

C terminal non-helical region

Ser- Gly- Gly- Tyr- Asp- Leu- Ser- Phe- Leu- Pro- Gln- Pro- Pro- Gln- Gln- Glx- Lys- Ala- His- Asp- Gly- Gly- Arg- Tyr- Tyr

Appendix-1B

Table 42: Collagen's amino acid distribution, number of residues and pKa [40, 63].

Amino acid	Total	Polar	Charge	pKa (pH)
Alanine	121	N	N	-
Arginine	51	Y	Y	12
Aspartic acid	31	Y	Y	4.4
Glutamic acid	47	Y	Y	4.4
Glutamine	27	Y	N	-
Glycine	338	N	N	-
Histidine	2	Y	Y	6.5
Hydroxylysine	4	Y	Y	10.5
Isoleucine	7	N	N	-
Leucine	19	N	N	-
Lysine	32	Y	Y	10.5
Methionine	7	N	N	-
Phenylalanine	12	N	N	-
Proline	119	N	N	-
Serine	35	Y	N	-
Threonine	16	Y	N	-
Valine	17	N	N	-
4-Hydroxyproline	114	N	N	-
C-terminal	1	Y	Y	3.1
N-terminal	1	Y	Y	8
Total	1011			

**Y and N indicates yes or no.*

Appendix-2A

Table 43: UV_{280} of gelatin solution pH 3.

Gelatin concentration		UV absorbance at 280 nm			
(mg/ml)	(%)	1	2	3	Average
0	0	0	0	0	0
0.1	0.01	0.011	0.011	0.011	0.0110
0.5	0.05	0.053	0.053	0.052	0.0527
1	0.1	0.111	0.111	0.106	0.1093
3	0.3	0.317	0.308	0.315	0.3133
5	0.5	0.520	0.522	0.521	0.5210
10	1	1.035	1.031	1.006	1.0240
15	1.5	1.527	1.532	1.528	1.5290
20	2	2.052	2.048	2.056	2.0520
25	2.5	2.480	2.480	2.481	2.4803

Table 44: UV_{280} of gelatin solution pH 5.23.

Gelatin concentration		UV absorbance at 280 nm			
(mg/ml)	(%)	1	2	3	Average
0	0	0	0	0	0
0.1	0.01	0.007	0.008	0.008	0.0077
0.5	0.05	0.048	0.052	0.052	0.0507
1	0.1	0.107	0.101	0.109	0.1057
3	0.3	0.317	0.318	0.312	0.3157
5	0.5	0.513	0.524	0.533	0.5233
10	1	1.038	1.030	1.020	1.0293
15	1.5	1.531	1.534	1.530	1.5317
20	2	2.013	2.015	2.019	2.0157
25	2.5	2.493	2.493	2.496	2.4940

Table 45: UV_{280} of gelatin solution pH 7.

Gelatin concentration		UV absorbance at 280 nm			
(mg/ml)	(%)	1	2	3	Average
0	0	0	0	0	0
0.1	0.01	0.007	0.006	0.006	0.0063
0.5	0.05	0.046	0.046	0.045	0.0457
1	0.1	0.101	0.100	0.104	0.1017
3	0.3	0.313	0.315	0.308	0.3120
5	0.5	0.517	0.524	0.529	0.5233
10	1	1.016	1.045	1.046	1.0357
15	1.5	1.562	1.556	1.547	1.5550
20	2	2.049	2.058	2.045	2.0507
25	2.5	2.526	2.528	2.525	2.5263

Table 46: UV_{280} of gelatin solution pH 9.

Gelatin concentration		UV absorbance at 280 nm			
(mg/ml)	(%)	1	2	3	Average
0	0	0	0	0	0
0.1	0.01	0.012	0.011	0.011	0.0113
0.5	0.05	0.051	0.052	0.053	0.0520
1	0.1	0.106	0.105	0.111	0.1073
3	0.3	0.326	0.335	0.333	0.3313
5	0.5	0.549	0.559	0.565	0.5577
10	1	1.156	1.154	1.151	1.1537
15	1.5	1.730	1.714	1.729	1.7243
20	2	2.260	2.268	2.250	2.2593
25	2.5	2.788	2.795	2.798	2.7937

Appendix-2B

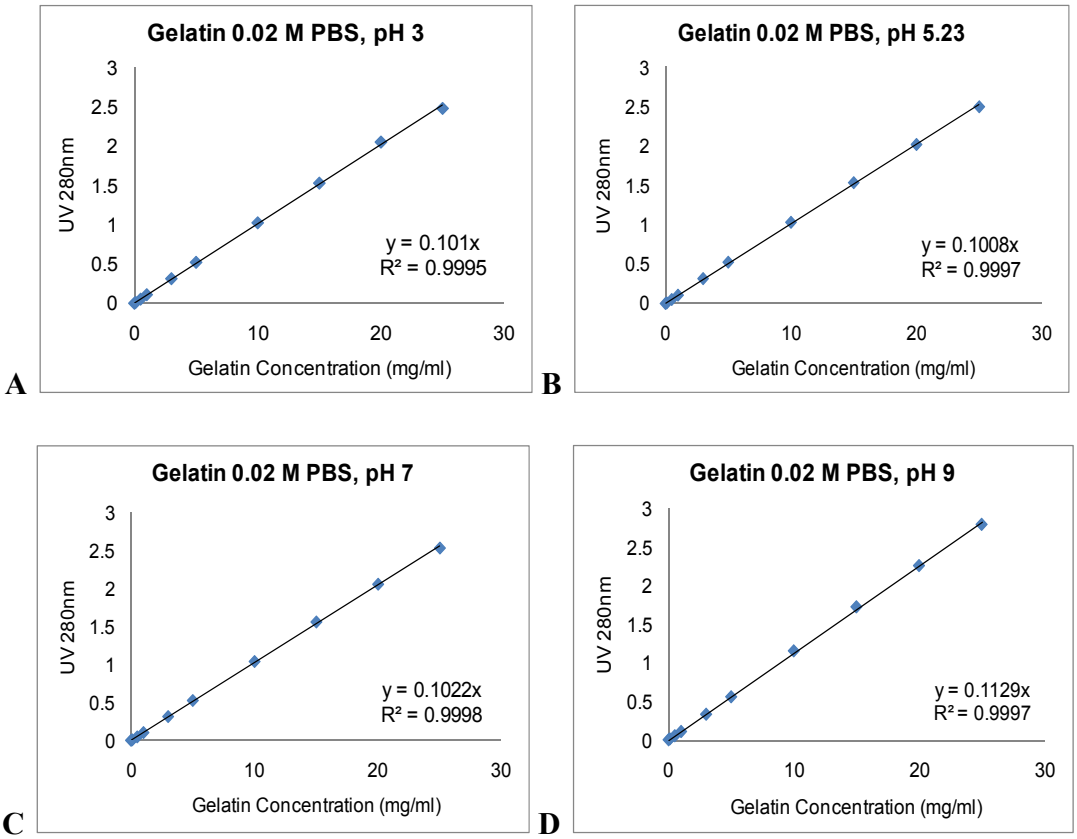

Figure 77: Gelatin standard curves in 0.02 M PBS solution at A) pH 3, B) pH 5.23, C) pH 7 and D) pH 9. Raw data are presented in Table 43-46.

Appendix-3A

Table 47: Turbidity reading for calcium and sodium bentonite in 0.02 M PBS at pH 3.

Calcium bentonite			Sodium bentonite		
Clay mass (mg / 15 ml)	Clay concentration (mg/ml)	Turbidity (NTU)	Clay mass (mg / 15 ml)	Clay concentration (mg/ml)	Turbidity (NTU)
0	0	0	0	0	0
0.36	0.0240	13	0.43	0.0287	21
1.16	0.0773	42	3.09	0.2060	137
3.42	0.2280	122	6.19	0.4127	304
5.66	0.3773	212	8.82	0.5880	447
8.05	0.5367	306	11.05	0.7367	598
12.99	0.8660	539	13.26	0.8840	696
15.25	1.0167	632	16.06	1.0707	846
18.04	1.2027	771	17.74	1.1827	977
20.73	1.3820	901			
21.60	1.4400	948			

Table 48: Turbidity reading for calcium and sodium bentonite in 0.02 M PBS at pH 5.23.

Calcium bentonite			Sodium bentonite		
Clay mass (mg / 15 ml)	Clay concentration (mg/ml)	Turbidity (NTU)	Clay mass (mg / 15 ml)	Clay concentration (mg/ml)	Turbidity (NTU)
0	0	0	0	0	0
0.30	0.0200	12	0.50	0.0333	17
1.21	0.0807	47	1.12	0.0747	42
2.87	0.1913	106	5.11	0.3407	245
4.39	0.2927	162	7.31	0.4873	374
6.49	0.4327	252	10.64	0.7093	556
11.53	0.7687	473	13.69	0.9127	773
14.10	0.9400	585	16.11	1.0740	896
16.92	1.1280	726	17.27	1.1513	973
21.62	1.4413	962			

Table 49: Turbidity reading for calcium and sodium bentonite in 0.02 M PBS at pH 7.

Calcium bentonite			Sodium bentonite		
Clay mass (mg / 15 ml)	Clay concentration (mg/ml)	Turbidity (NTU)	Clay mass (mg / 15 ml)	Clay concentration (mg/ml)	Turbidity (NTU)
0	0	0	0	0	0
0.37	0.0247	13	0.50	0.0333	22
1.18	0.0787	42	1.31	0.0873	54
2.57	0.1713	96	3.18	0.2120	149
3.55	0.2367	134	8.19	0.5460	430
5.78	0.3853	225	11.05	0.7367	604
7.56	0.5040	289	13.88	0.9253	788
11.18	0.7453	467	16.12	1.0747	932
16.08	1.0720	685	16.94	1.1293	982
20.55	1.3700	899			
22.03	1.4687	982			

Table 50: Turbidity reading for calcium and sodium bentonite in 0.02 M PBS at pH 9.

Calcium bentonite			Sodium bentonite		
Clay mass (mg / 15 ml)	Clay concentration (mg/ml)	Turbidity (NTU)	Clay mass (mg / 15 ml)	Clay concentration (mg/ml)	Turbidity (NTU)
0	0	0	0	0	0
1.19	0.0793	59	0.22	0.0147	8
1.50	0.1000	65	0.72	0.0480	31
2.05	0.1367	80	1.12	0.0747	51
3.20	0.2133	122	3.82	0.2547	188
4.22	0.2813	169	5.89	0.3927	309
6.19	0.4127	255	8.05	0.5367	435
8.42	0.5613	333	10.91	0.7273	626
10.41	0.6940	430	13.34	0.8893	776
12.73	0.8487	534	15.06	1.0040	894
14.46	0.9640	602	16.43	1.0953	983
17.16	1.1440	742			
18.69	1.2460	819			
20.64	1.3760	938			

Appendix-3B

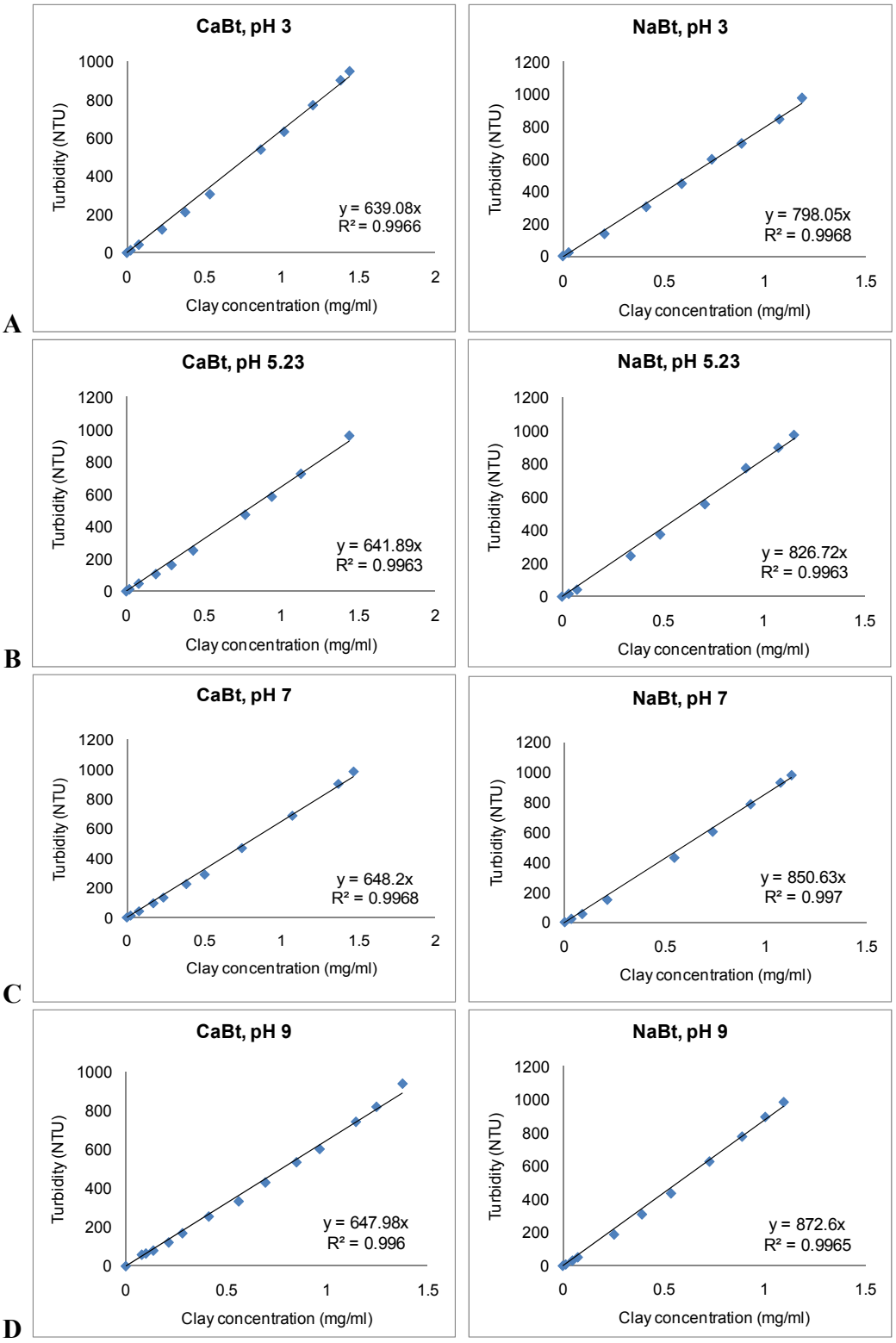

Figure 78: Turbidity standard curves for CaBt and NaBt in 0.02 M PBS at A) pH 3, B) pH 5.23, C) pH 7 and D) pH 9. Raw data are presented in Table 47-50.

Appendix-4A

Table 51: Turbidity reading for calcium and sodium bentonite in 0.02 % stickwater at pH 3.

Calcium bentonite			Sodium bentonite		
Clay mass (mg / 15 ml)	Clay concentration (mg/ml)	Turbidity (NTU)	Clay mass (mg / 15 ml)	Clay concentration (mg/ml)	Turbidity (NTU)
0	0	297	0	0	297
1.07	0.0713	323	0.48	0.032	322
5.35	0.3567	581	1.40	0.0933	406
8.07	0.5380	738	3.15	0.2100	511
10.49	0.6993	873	5.26	0.3507	597
12.13	0.8087	931	8.11	0.5407	740
			10.22	0.6813	859
			11.75	0.7833	921
			12.17	0.8113	957

Appendix-4B

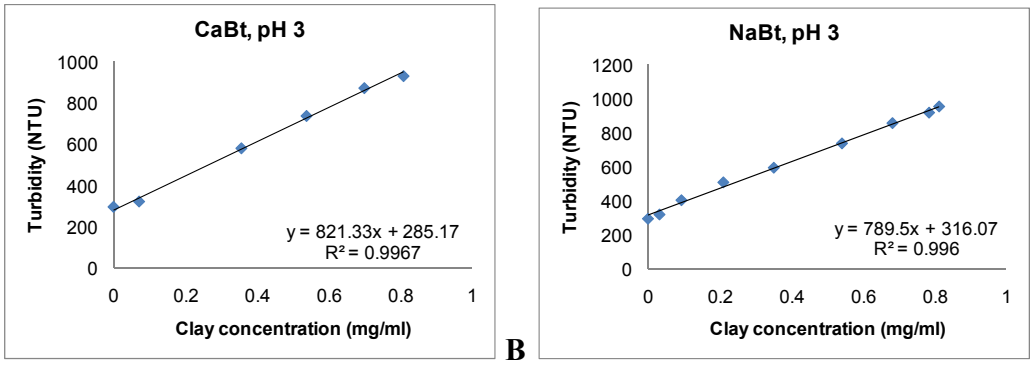

Figure 79: Turbidity standard curves of A) CaBt and B) NaBt in 0.02 % stickwater at pH 3. Raw data are presented in Table 51.

Appendix-5

A

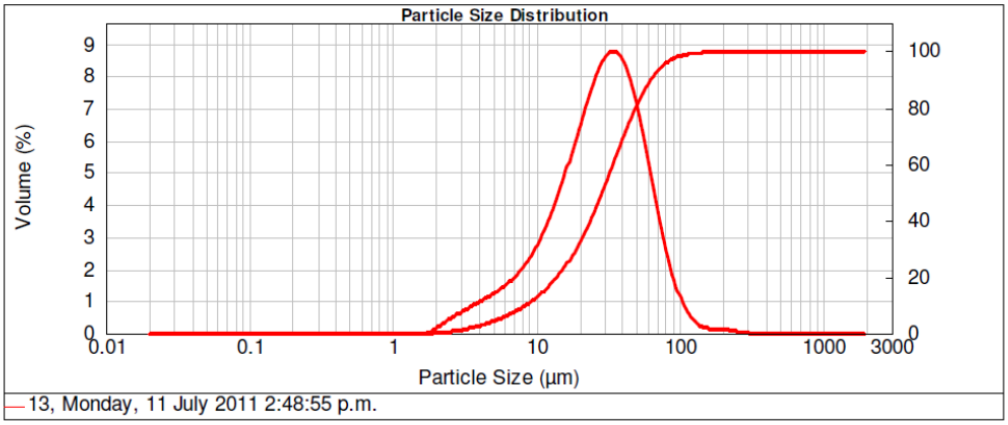

Size (µm)	Vol Under %	Size (µm)	Vol Under %	Size (µm)	Vol Under %	Size (µm)	Vol Under %	Size (µm)	Vol Under %	Size (µm)	Vol Under %
0.050	0.00	0.980	0.00	37.000	64.31	105.000	98.62	300.000	100.00	840.000	100.00
0.060	0.00	2.000	0.05	44.000	73.91	125.000	99.31	350.000	100.00	1000.000	100.00
0.120	0.00	3.900	2.51	53.000	82.97	149.000	99.60	420.000	100.00	2000.000	100.00
0.240	0.00	7.800	8.75	63.000	89.62	177.000	99.76	500.000	100.00		
0.490	0.00	15.600	22.99	74.000	94.03	210.000	99.88	590.000	100.00		
0.700	0.00	31.000	54.18	88.000	97.02	250.000	99.98	710.000	100.00		

B

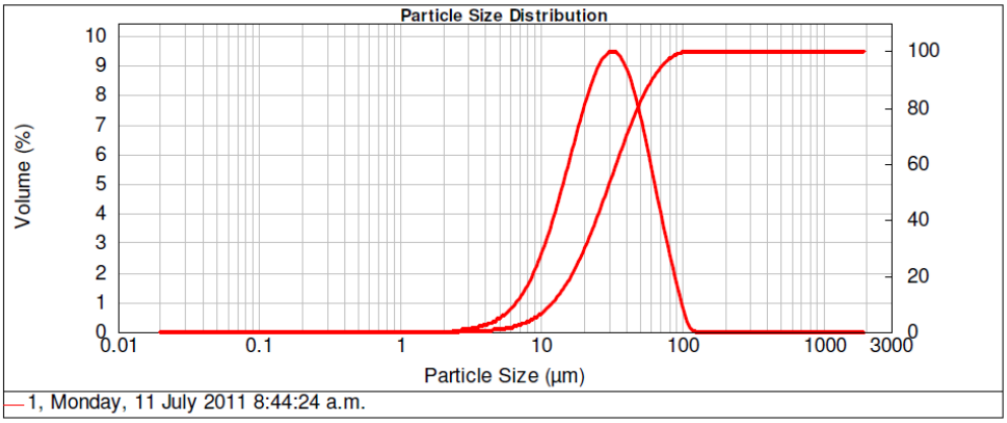

Size (µm)	Vol Under %	Size (µm)	Vol Under %	Size (µm)	Vol Under %	Size (µm)	Vol Under %	Size (µm)	Vol Under %	Size (µm)	Vol Under %
0.050	0.00	0.980	0.00	37.000	65.15	105.000	99.89	300.000	100.00	840.000	100.00
0.060	0.00	2.000	0.00	44.000	75.15	125.000	100.00	350.000	100.00	1000.000	100.00
0.120	0.00	3.900	0.29	53.000	84.41	149.000	100.00	420.000	100.00	2000.000	100.00
0.240	0.00	7.800	3.29	63.000	91.12	177.000	100.00	500.000	100.00		
0.490	0.00	15.600	18.35	74.000	95.57	210.000	100.00	590.000	100.00		
0.700	0.00	31.000	54.26	88.000	98.57	250.000	100.00	710.000	100.00		

Figure 80: Example of size distribution for treated A) CaBt and B) NaBt with gelatin 2% at pH 3.

Appendix-6A

Hill Laboratories
BETTER TESTING BETTER RESULTS

R J Hill Laboratories Limited
1 Clyde Street
Private Bag 3205
Hamilton 3240, New Zealand

Tel +64 7 858 2000
Fax +64 7 858 2001
Email mail@hill-labs.co.nz
Web www.hill-labs.co.nz

ANALYSIS REPORT

Client:	Waikato University School of Science & Engineering	Lab No:	986375	SPv1
Contact:	Mark Lay	Date Registered:	12-Mar-2012	
	C/- Waikato University School of Science & Engineeri	Date Reported:	19-Mar-2012	
	C/- University of Waikato	Quote No:	48297	
	Private Bag 3105	Order No:	1125119	
	HAMILTON 3240	Client Reference:	Bovine Stickwater	
		Submitted By:	Rashid Shamsuddin	

Sample Type: Aqueous

Sample Name:	Gelatin 20 12-Mar-2012 11:00 am	Ge20 - Treated with NaBt 12-Mar-2012 11:00 am	Ge20 - Treated with CaBt 12-Mar-2012 11:00 am		
Lab Number:	986375.1	986375.2	986375.3		
Carbonaceous Biochemical Oxygen Demand ($cBOD_5$) g O_2/m^3	14,100	5,100	7,100	-	-

SUMMARY OF METHODS

The following table(s) gives a brief description of the methods used to conduct the analyses for this job. The detection limits given below are those attainable in a relatively clean matrix. Detection limits may be higher for individual samples should insufficient sample be available, or if the matrix requires that dilutions be performed during analysis.

Sample Type: Aqueous

Test	Method Description	Default Detection Limit	Samples
Carbonaceous Biochemical Oxygen Demand ($cBOD_5$)	Incubation 5 days, DO meter, nitrification inhibitor added, dilutions, seeded. Analysed at; 25 Te Aroha Street, Hamilton. APHA 5210 B 21st ed. 2005.	2 g O_2/m^3	1-3

These samples were collected by yourselves (or your agent) and analysed as received at the laboratory.

Samples are held at the laboratory after reporting for a length of time depending on the preservation used and the stability of the analytes being tested. Once the storage period is completed the samples are discarded unless otherwise advised by the client.

Peter Robinson MSc (Hons), PhD, FNZIC
Client Services Manager - Environmental Division

Figure 81: Analysis report on $cBOD_5$ of gelatin 2 % solution before and after treatment with calcium and sodium bentonite.

Appendix-6B

Analysis Report

16 April 2012

Engineering Department, Waikato University
c/- Science Store
Gate 8, Hilcrest Road
Hamilton

Attention: *Rashid Shamsuddin*

Approved by: Wheyen Toung NZCS
On behalf of SGS New Zealand Ltd

Date Received: 3/04/12

Lab Number: 64943
Temperature: N/A
Order Number/Ref: 03/04/12
Date Completed: 16/04/12

The Results of analysis on the sample/s as received from Engineering Department, Waikato University and described below, are as follows.
The Sample/s were received in good condition. Analysis of the sample/s commenced on 3/04/2012

Test	Method	Result Unit	1 Bovine Stickwater
Protein*	AOAC 990.03 , AOAC 992.15 18th ed.2005	%	3.5
Fat*	AOAC 991.36 18th Edition, 2005	%	1.6
Nitrogen*	AOAC 4.2.08 17th Edition	%	0.57

Legend: < = less than limit of detection, > = greater than, [ND] = not detected, s = sub contracted

END OF REPORT

Figure 82: Analysis report on stickwater content.

Appendix-6C

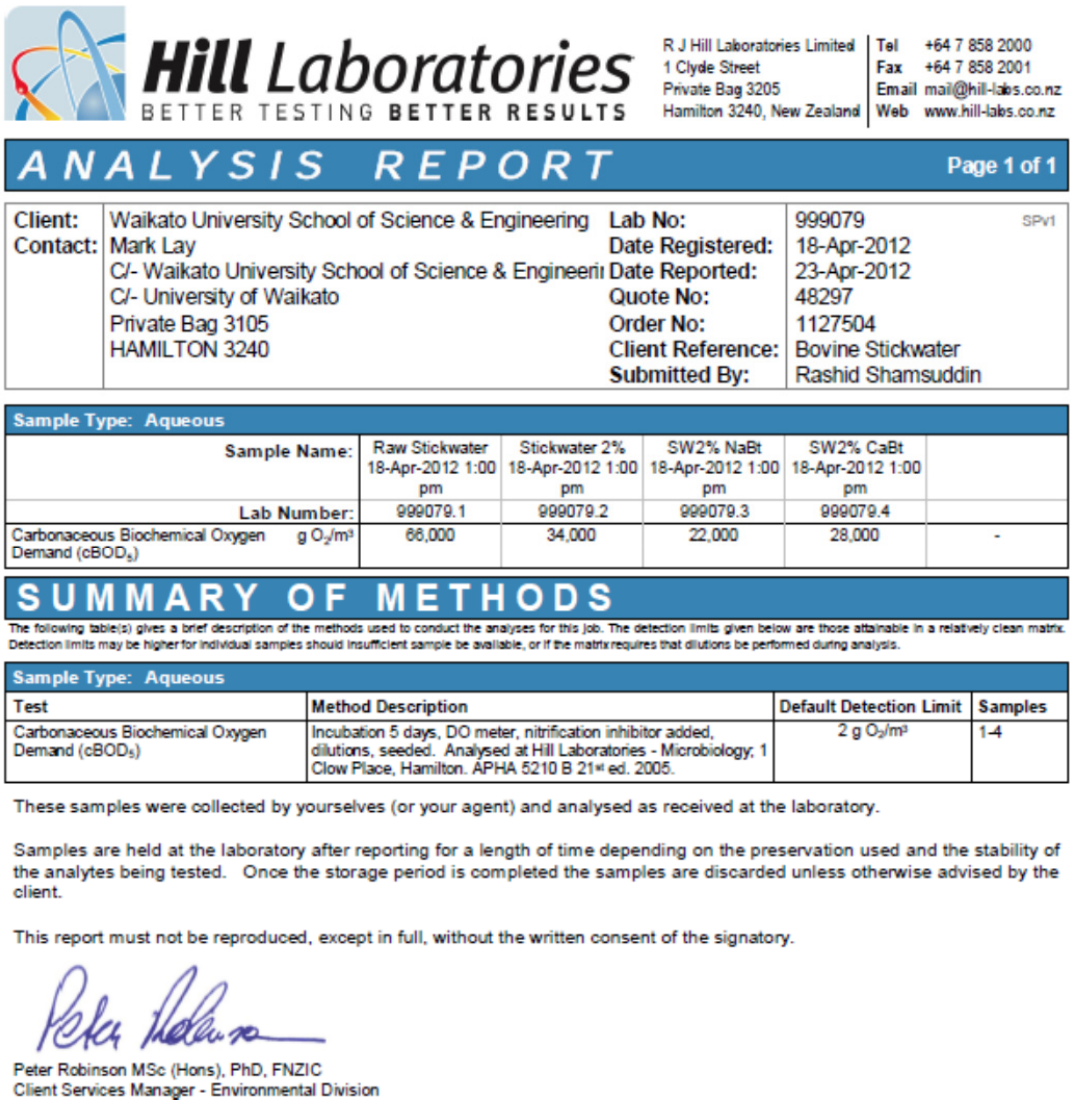

Hill Laboratories
BETTER TESTING BETTER RESULTS

R J Hill Laboratories Limited
1 Clyde Street
Private Bag 3205
Hamilton 3240, New Zealand

Tel +64 7 858 2000
Fax +64 7 858 2001
Email mail@hill-labs.co.nz
Web www.hill-labs.co.nz

ANALYSIS REPORT Page 1 of 1

Client:	Waikato University School of Science & Engineering	Lab No:	999079	SPv1
Contact:	Mark Lay	Date Registered:	18-Apr-2012	
	C/- Waikato University School of Science & Engineeri	Date Reported:	23-Apr-2012	
	C/- University of Waikato	Quote No:	48297	
	Private Bag 3105	Order No:	1127504	
	HAMILTON 3240	Client Reference:	Bovine Stickwater	
		Submitted By:	Rashid Shamsuddin	

Sample Type: Aqueous

Sample Name:	Raw Stickwater 18-Apr-2012 1:00 pm	Stickwater 2% 18-Apr-2012 1:00 pm	SW2% NaBt 18-Apr-2012 1:00 pm	SW2% CaBt 18-Apr-2012 1:00 pm	
Lab Number:	999079.1	999079.2	999079.3	999079.4	
Carbonaceous Biochemical Oxygen Demand ($cBOD_5$) g O_2/m^3	66,000	34,000	22,000	28,000	-

SUMMARY OF METHODS

The following table(s) gives a brief description of the methods used to conduct the analyses for this job. The detection limits given below are those attainable in a relatively clean matrix. Detection limits may be higher for individual samples should insufficient sample be available, or if the matrix requires that dilutions be performed during analysis.

Sample Type: Aqueous

Test	Method Description	Default Detection Limit	Samples
Carbonaceous Biochemical Oxygen Demand ($cBOD_5$)	Incubation 5 days, DO meter, nitrification inhibitor added, dilutions, seeded. Analysed at Hill Laboratories - Microbiology; 1 Clow Place, Hamilton. APHA 5210 B 21st ed. 2005.	2 g O_2/m^3	1-4

These samples were collected by yourselves (or your agent) and analysed as received at the laboratory.

Samples are held at the laboratory after reporting for a length of time depending on the preservation used and the stability of the analytes being tested. Once the storage period is completed the samples are discarded unless otherwise advised by the client.

This report must not be reproduced, except in full, without the written consent of the signatory.

Peter Robinson MSc (Hons), PhD, FNZIC
Client Services Manager - Environmental Division

Figure 83: Analysis report on $cBOD_5$ of raw and diluted stickwater solution at 2% protein concentration before and after treatment with calcium and sodium bentonite.

Appendix-7

Table 52: Gelling temperature of gelatin and stickwater solutions.

T (°C)	Solution / Solidified? (Yes/No)							
	Ge1%	Ge2%	Ge3%	Ge4%	Ge5%	Ge6%	SW	SW2%
18	Yes	Yes	Yes	Yes	Yes	Yes	No	No
20	Yes/No	Yes	Yes	Yes	Yes	Yes	No	No
25	No	Yes/No	Yes/No	Yes/No	Yes	Yes	No	No
30	No	No	No	No	Yes/No	Yes/No	No	No
35	No	No	No	No	No	No	No	No
40	No	No	No	No	No	No	No	No

Appendix-8

Table 53: Isotherm model equations for gelatin adsorption at different pH conditions.

Sample / model	Fitted isotherm model equations at different pH			
CaBt	pH 3	pH 5.23	pH 7	pH 9
Langmuir	y = 0.0079x + 0.0028 R^2 = 0.9893	y = 0.0056x + 0.0035 R^2 = 0.9767	y = 0.0083x + 0.0012 R^2 = 0.9617	y = 0.0091x + 0.0009 R^2 = 0.9654
Freundlich	y = 0.4763x + 2.0029 R^2 = 0.9899	y = 0.309x + 2.077 R^2 = 0.9036	y = 0.5882x + 2.0737 R^2 = 0.866	y = 0.6838x + 2.0354 R^2 = 0.936
Langmuir-Freundlich	y = 0.0084x + 0.002 R^2 = 0.9918	y = 0.0053x + 0.0042 R^2 = 0.999	y = 0.0076x + 0.0024 R^2 = 0.9945	y = 0.0079x + 0.0026 R^2 = 0.9975
Temkin	y = 86.774x + 88.67 R^2 = 0.9944	y = 52.074x + 118.56 R^2 = 0.9458	y = 122.77x + 114.75 R^2 = 0.9076	y = 142.64x + 101.89 R^2 = 0.9804
NaBt	pH 3	pH 5.23	pH 7	pH 9
Langmuir	y = 0.0055x + 0.0018 R^2 = 0.9902	y = 0.0061x + 0.0016 R^2 = 0.9985	y = 0.0069x + 0.0022 R^2 = 0.9599	y = 0.0122x + 0.0017 R^2 = 0.9676
Freundlich	y = 0.5115x + 2.1516 R^2 = 0.9247	y = 0.5868x + 2.1266 R^2 = 0.9747	y = 0.4366x + 2.0917 R^2 = 0.805	y = 0.6572x + 1.9021 R^2 = 0.9584
Langmuir-Freundlich	y = 0.005x + 0.0023 R^2 = 0.9966	y = 0.0058x + 0.0018 R^2 = 0.999	y = 0.0063x + 0.0032 R^2 = 0.9886	y = 0.0129x + 0.0037 R^2 = 0.9976
Temkin	y = 112.76x + 145.38 R^2 = 0.9555	y = 136.01x + 131.09 R^2 = 0.9939	y = 83.092x + 124.62 R^2 = 0.7961	y = 103.6x + 64.549 R^2 = 0.9959
Amine Bt	pH 3	pH 5.23	pH 7	pH 9
Langmuir	y = 0.0105x + 0.0044 R^2 = 0.8556	y = 0.0203x + 0.0043 R^2 = 0.9632	y = 0.0308x + 0.0052 R^2 = 0.9282	y = 0.0254x + 0.0028 R^2 = 0.9636
Freundlich	y = 0.433x + 1.867 R^2 = 0.9436	y = 0.5225x + 1.6876 R^2 = 0.9794	y = 0.5266x + 1.5568 R^2 = 0.965	y = 0.6869x + 1.6084 R^2 = 0.982
Langmuir-Freundlich	y = 0.015x - 0.0019 R^2 = 0.9177	y = 0.0233x - 0.0043 R^2 = 0.9899	y = 0.0278x + 2E-05 R^2 = 0.9382	y = 0.024x + 0.0003 R^2 = 0.9739
Temkin	y = 62.333x + 56.819 R^2 = 0.9373	y = 63.785x + 19.025 R^2 = 0.9304	y = 50.53x + 8.5432 R^2 = 0.9588	y = 91.371x - 10.126 R^2 = 0.9445

Appendix-9

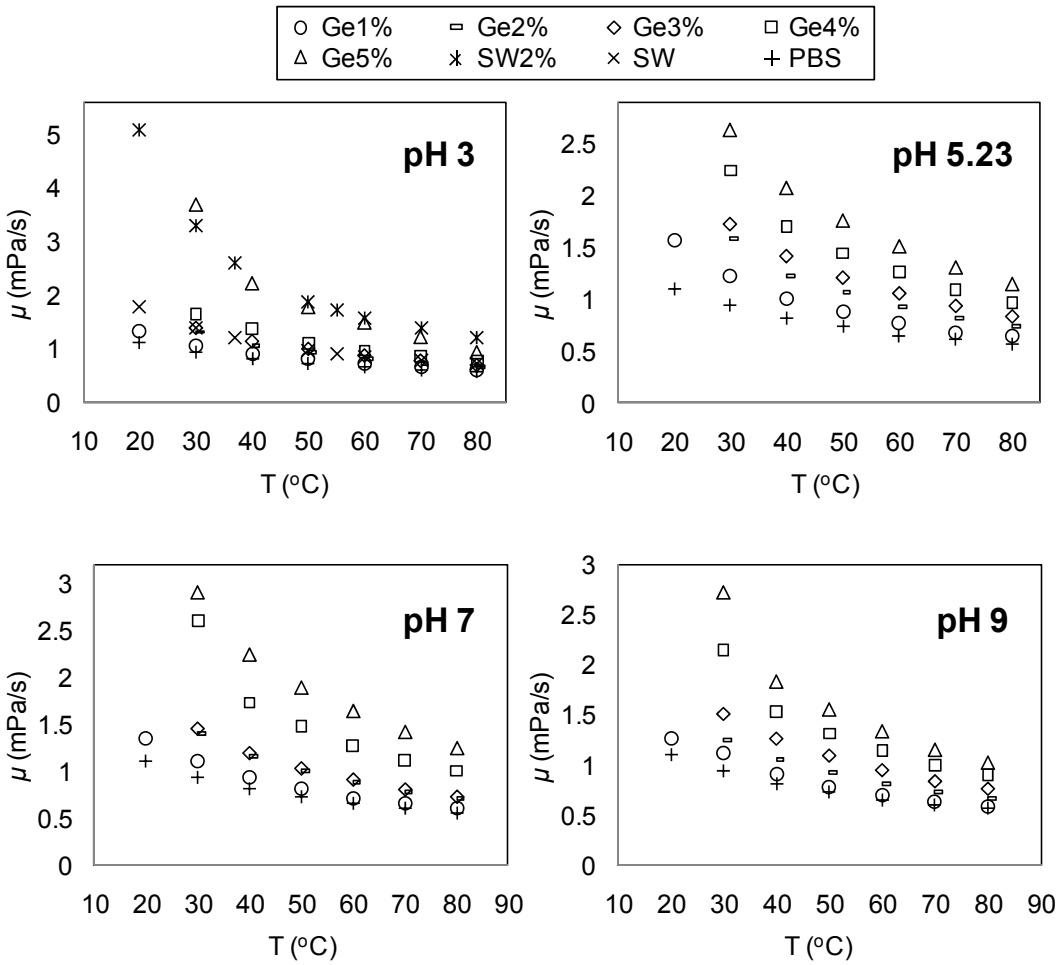

Figure 84: Viscosity profiles of gelatin and stickwater solutions at various concentrations and temperatures under for pHs (1 mPa.s = $1x10^{-3}$ kg/ms). Some data points are not available at 20 °C due to gelation.

Appendix-10

Table 54: *d*-value of sediments from settling experiment in gelatin solution and stickwater (values in brackets).

pH	2θ		*d*-value (Å)	
	CaBt	NaBt	CaBt	NaBt
3	4.71 (6.11)	4.25 (2.63)	18.8 (14.5)	20.8 (16.8)
5.23	4.43	4.19	19.9	21.1
7	4.13	4.27	21.4	23.4
9	4.01	4.15	22.0	21.3

Appendix-11A

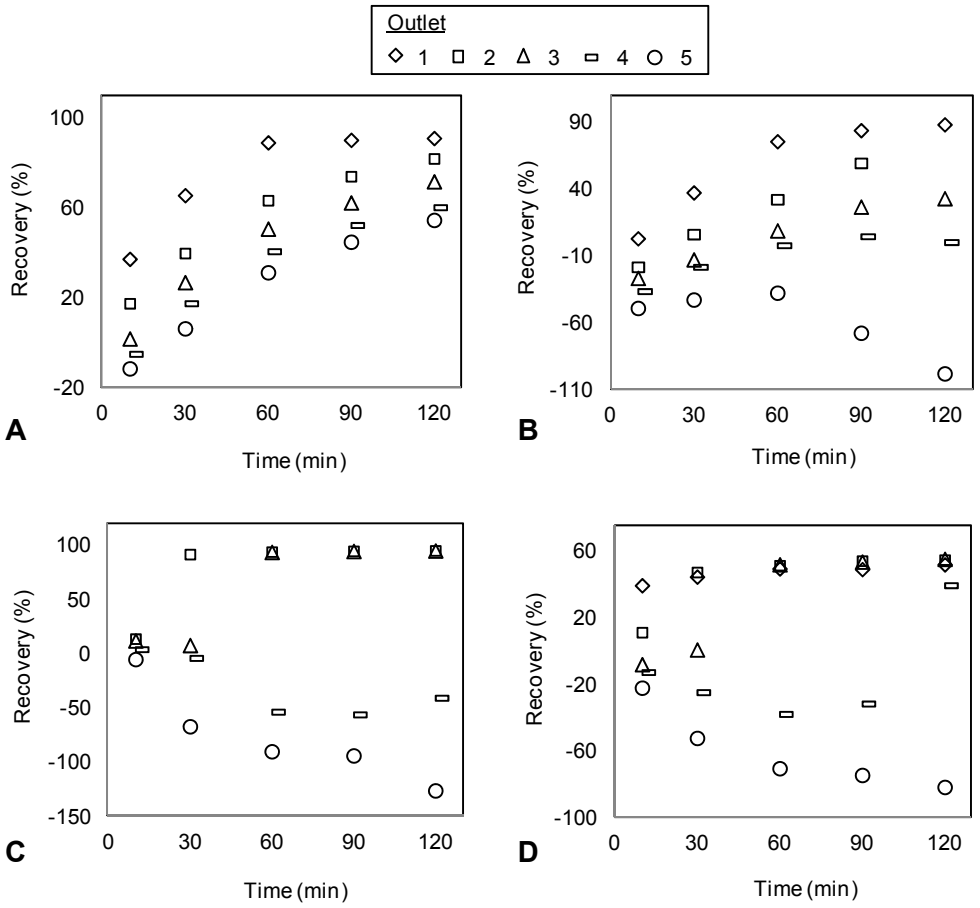

Figure 85: Percentage recovery of CaBt in gelatin solutions at A) pH 3 and B) pH 5.23 and in stickwater solutions at pH 3 for C) CaBt and D) NaBt.

Appendix-11B

Table 55: Percentage of clay recovery after overnight at outlet 4.

Treated sample	Clay recovery (%)	
	Gelatin 2 %	Stickwater 2 %
CaBt- pH 3	93.9	95.8
- pH 5.23	93.3	-
NaBt- pH 3	-	63.1

Appendix-12

Table 56: Percentage removal and settling velocity of bentonite in solutions at settling conditions.

Time (min)	Distance corresponding to outlet (mm), measured from top (outlet 1) to bottom				
	Change in settling height over time (x10^{-5} m/s)				
	70	140	210	280	350
10	11.70	23.30	35.00	46.70	58.30
30	3.89	7.78	11.70	15.60	19.40
60	1.94	3.89	5.83	7.78	9.72
90	1.30	2.59	3.89	5.19	6.48
120	0.97	1.94	2.92	3.89	4.86
Calcium bentonite, gelatin 2 %, pH 3					
Time (min)	Percentage of organic removal (%)				
10	37.26	17.54	1.85	-4.94	-11.41
30	65.56	39.85	26.92	17.54	6.38
60	89.01	63.30	50.68	40.66	31.28
90	90.14	73.97	62.33	52.30	44.86
120	90.95	81.89	71.70	60.22	54.57
Calcium bentonite, gelatin 2%, pH 5.23					
Time (min)	Percentage of organic removal (%)				
10	2.91	-18.40	-26.69	-36.56	-49.18
30	37.25	6.07	-12.88	-18.40	-42.87
60	75.53	32.12	8.83	-2.22	-37.74
90	83.82	59.35	26.59	4.49	-67.73
120	88.16	85.40	32.91	0.15	-98.12
Calcium bentonite, stickwater 2 %, pH 3					
Time (min)	Percentage of organic removal (%)				
10	* *not recorded*	13.59	11.90	3.93	-5.24
30		91.48	7.67	-4.15	-67.10
60		93.76	93.46	-53.68	-90.16
90		94.40	94.33	-56.14	-94.00
120		94.87	94.73	-40.81	-126.18
Sodium bentonite, stickwater 2%, pH 3					
Time (min)	Percentage of organic removal (%)				
10	39.38	11.22	-8.05	-12.76	-22.15
30	44.58	47.37	0.77	-24.83	-52.34
60	49.49	51.43	52.00	-37.90	-70.55
90	49.09	54.17	53.60	-31.68	-74.61
120	51.94	54.80	55.25	39.44	-81.79

Appendix-13

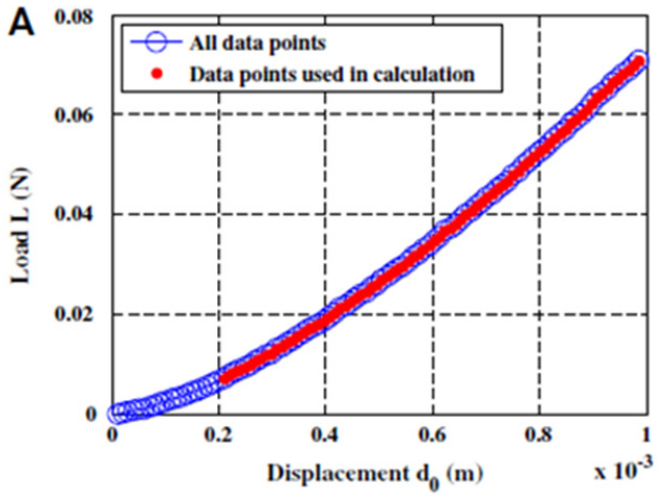

Figure 86: A load-displacement measurement of 15 % gelatin phantom [195].

Appendix-14

Matlab settling model:

```
ht=0.4;                 %tube height (m)
Dt=0.06;                %tube width (m)
Ns=400;                 %number of tube sections
hts=ht./Ns;             %tube section height (m)
ats=(pi().*Dt.*Dt./4);  %tube cross sectional area (m2)
Vts=ats.*hts;           %tube section volume(m3)

mco=0.036;              %mass bentonite clay added to tube (kg)
mcs=mc./Ns;             %mass clay per section (kg)
Dcp=0.00003572;         %average clay particle diameter (m)
Pcp=1353.9;             %clay density (kg/m3)
Pf=998.654;             %gelatin 2% density (kg/m3)
g=9.8067;               %gravitational acceleration (m/s2)
uf=0.0012171;           %viscosity solution (kg/ms)
Vcp=(4./3).*pi().*((Dcp./2).^3);        %clay particle volume (m3)
mcp=Vcp.*Pcp;                           %mass clay particle (kg)
ncps=mcs./mcp;                          %number of clay particles in one section

Fg=mcs.*g;              %force due to gravity (kg.m/s2)
Fb=Vcp.*ncps.*g.*Pf;    %force due to buoyancy (kg.m/s2)

ks=0.22;                %spring constant for gelatin (kg/s2)
kf=0.000002;            %flux coefficient
```

```
Rt=2.*60.*60;                   %run time (seconds)
delt=0.05;                      % change in time (seconds)
T=ceil(Rt./delt);               %number of time steps
eo=1-((Vcp.*ncps)./Vts);        %start void fraction
ef=0.75252;                     %final void fraction

Fr=zeros(T,Ns);                 %resultant force
%Fd=zeros(T,Ns);                %Fd equation moved into Ft equation to reduce memory use
V(1:T,1:Ns)=Vts;
e(1:T,1:Ns)=eo;
%Fs=zeros(T,Ns);                %Fs equation moved into P equation to reduce memory use
x(1:Ns)=hts;
Q=zeros(T,Ns);                  %flowrate (m3/s)
P=zeros(T,Ns);                  %pressure (kg/ms2)
xh=zeros(T,1);                  %vertical distance (m)
time=zeros(T,1);                %time (s)

for t=2:T;
   for n=1;
      %Fd(t,n)=6.*pi().*uf*(Dcp./2).*Q(t,n);
      %Fs(t,n)=0;
      Fr(t,n)=Fg-(6.*pi().*uf.*(Dcp./2).*Q(t,n))-Fb;
      P(t,n)=(sum(Fr(t,1:n-1))-Fs(t,n))./ats;
      e(t,n)=1-((Vcp.*ncps)./V(t-1,n));
      V(t,n)=V(t-1,n)+(kf./x(t-1,n)).*ats.*e(t-1,n).*(P(t-1,n+1)-P(t-1,n)).*delt;
      Q(t,n)=(((kf./x(t-1,n)).*ats.*e(t-1,n).*(P(t-1,n+1)-P(t-1,n)).*delt)./ats)./delt;
      x(t,n)=V(t,n)./ats;
   end
   for n=2:Ns-1;
      %Fd(t,n)=6.*pi().*uf.*(Dcp./2).*Q(t,n);
      %Fs(t,n)=ks.*(hts-x(t-1,n));
      Fr(t,n)=Fg-(6.*pi().*uf.*(Dcp./2).*Q(t-1,n))-Fb;
      P(t,n)=(((sum(Fr(t,1:n-1))-((((ks.*(hts-x(t-1,n)))+abs(ks.*(hts-x(t-
1,n)))))/2))./ats)+abs((sum(Fr(t,1:n-1))-((((ks.*(hts-x(t-1,n)))+abs(ks.*(hts-x(t-1,n)))))/2))./ats))/2;
      e(t,n)=1-((Vcp.*ncps)./V(t-1,n));
      V(t,n)=V(t-1,n)-((kf./x(t-1,n-1)).*ats.*e(t-1,n).*(P(t-1,n)-P(t-1,n-1)).*delt)+((kf./x(t-
1,n)).*ats.*e(t-1,n+1).*(P(t-1,n+1)-P(t-1,n)).*delt);
      Q(t,n)=(((kf./x(t-1,n-1)).*ats.*e(t-1,n).*(P(t-1,n+1)-P(t-1,n)).*delt)./ats)./delt;
      x(t,n)=V(t,n)./ats;
   end
   for n=Ns;
      %Fd(t,n)=6.*pi().*uf.*(Dcp./2).*Q(t,n);
      %Fs(t,n)=ks.*(hts-x(t-1,n));
      Fr(t,n)=Fg-(6.*pi().*uf.*(Dcp./2).*Q(t-1,n))-Fb;
      P(t,n)=(((sum(Fr(t,1:n-1))-((((ks.*(hts-x(t-1,n)))+abs(ks.*(hts-x(t-
1,n)))))/2))./ats)+abs((sum(Fr(t,1:n-1))-((((k.*(hts-x(t-1,n)))+abs(ks.*(hts-x(t-1,n)))))/2))./ats))/2;
      e(t,n)=1-((Vcp.*Ncps)./V(t-1,n));
      V(t,n)=V(t-1,n)-((kf./x(t-1,n)).*ats.*e(t-1,n).*(P(t-1,n)-P(t-1,n-1)).*delt);
      Q(t,n)=(((kf./x(t-1,n-1)).*ats.*e(t-1,n).*(P(t-1,n)-P(t-1,n-1)).*delt)./ats)./delt;
      x(t,n)=V(t,n)./ats;
   end
   xh(t)=sum(x(t,4:Ns));
   time(t)=((t-1).*delt)/60;
end
for t=1:T,
```

```
   xh(t)=sum(x(t,57:Ns));
   time(t)=((t-1).*delt)/60;
end

A=time(1:T,1);
B=xh(1:T,1);
figure
plot(A,B);

%finding concentration at specific heights for 100 time spots.
%height = 70 140 210 280 350mm @ outlet 1 2 3 4 5
Y=100;
for y=1:Y+1;
   ty(y)=ceil((T./Y).*(y-1));
   if ty(y)==0;
      ty(y)=1;
   end
   time2(y)=time(ty(y));
   for n=1:Ns;
      xht(y,n)=ht-(sum(x(ty(y),n:Ns)));
      cht(y,n)=mcs./V(ty(y),n);

   end
   for j=1:5;
      h=j.*0.07;
      index(y,j)=min(find(xht(y,2:Ns)>=h));
      c(y,j)=cht(y,index(y,j));
   end
end
A=time2(1:Y+1);
B=c(1:Y+1,1);
C=c(1:Y+1,2);
D=c(1:Y+1,3);
E=c(1:Y+1,4);
F=c(1:Y+1,5);
figure;
plot(A,B,A,C,A,D,A,E,A,F);
```

Appendix-15

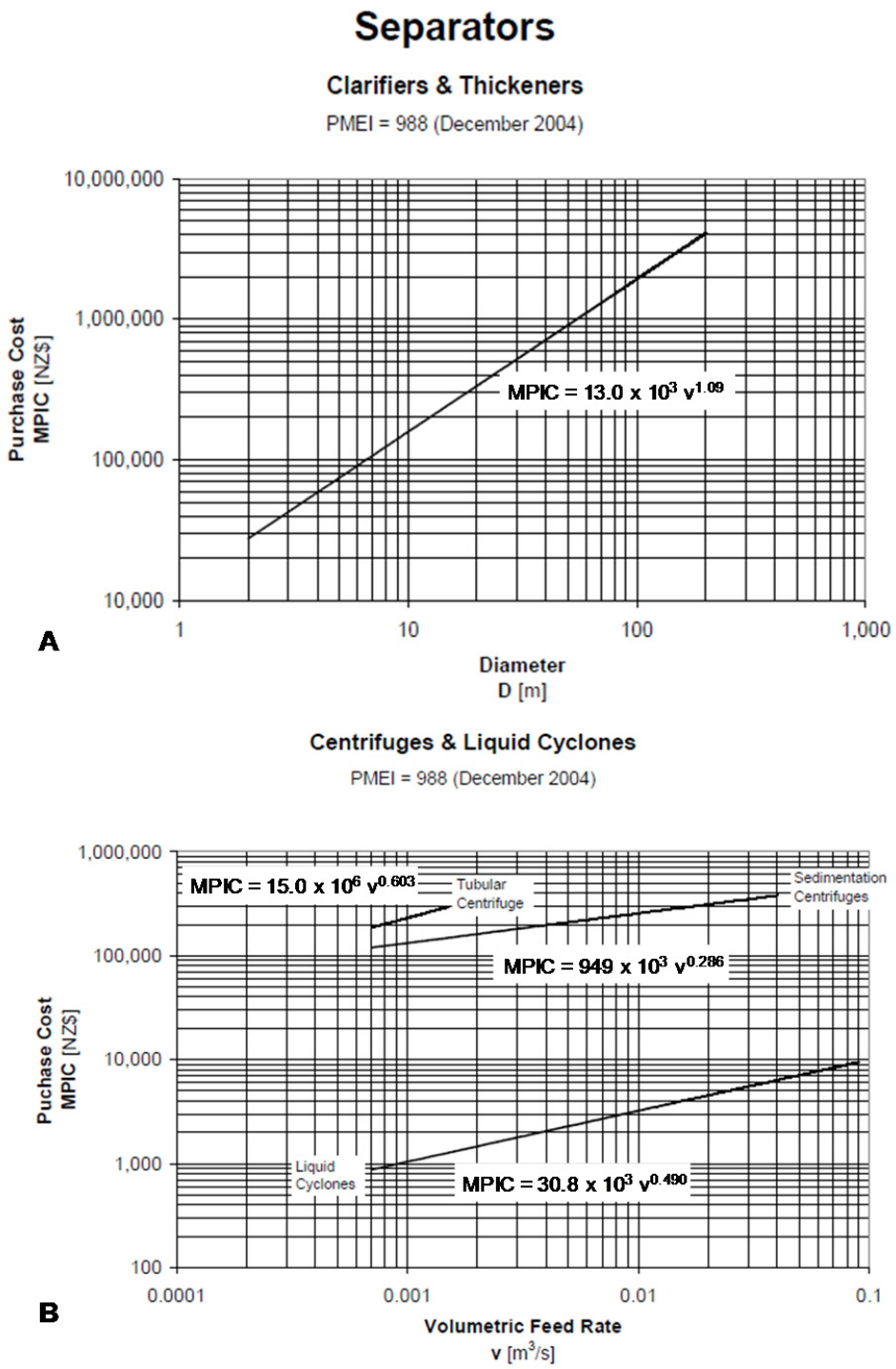

Figure 87: Purchased equipment costs for A) clarifiers and thickeners and B) centrifuges and liquid cyclones. MPIC is the main plant item cost [196].

Appendix-16A

Table 57: Tensile properties of conditioned NTP composites (mean ± standard error of the mean).

Sample	Tensile strength, σ (MPa)	Young's modulus, E (MPa)	Elongation at break, ε (%)	Toughness (MPa)
NTP	9.34 ± 0.10	622.33 ± 24.66	71.96 ± 3.56	3.14 ± 0.21
NTP-CaRaw0.25	8.78 ± 0.15	430.25 ± 9.11	87.93 ± 2.61	3.90 ± 0.17
NTP-CaRaw0.5	9.15 ± 0.16	517.46 ± 9.36	74.95 ± 1.68	3.43 ± 0.17
NTP-CaRaw1	9.81 ± 0.20	550.07 ± 20.75	69.86 ± 1.98	3.01 ± 0.47
NTP-CaGe0.25	8.97 ± 0.21	571.79 ± 18.35	86.43 ± 2.32	3.97 ± 0.21
NTP-CaGe0.5	8.55 ± 0.06	442.07 ± 16.09	81.21 ± 2.79	3.42 ± 0.09
NTP-CaGe1	10.23 ± 0.10	601.31 ± 17.51	69.31 ± 1.74	3.41 ± 0.32
NTP-CaSW0.25	10.57 ± 0.18	649.64 ± 21.31	70.09 ± 3.77	3.91 ± 0.20
NTP-CaSW0.5	10.51 ± 0.12	655.24 ± 42.02	73.13 ± 1.23	4.05 ± 0.09
NTP-CaSW1	10.30 ± 0.13	654.87 ± 26.49	67.52 ± 3.82	3.72 ± 0.21
NTP-NaRaw0.25	8.43 ± 0.07	446.98 ± 19.62	78.68 ± 1.57	3.28 ± 0.09
NTP-NaRaw0.5	8.52 ± 0.07	417.73 ± 7.06	88.84 ± 3.72	3.70 ± 0.11
NTP-NaRaw1	9.96 ± 0.13	526.28 ± 6.61	77.86 ± 3.41	4.30 ± 0.23
NTP-NaGe0.25	9.06 ± 0.14	447.26 ± 18.07	76.63 ± 2.86	3.51 ± 0.20
NTP-NaGe0.5	11.46 ± 0.16	711.00 ± 31.44	46.25 ± 5.62	2.74 ± 0.30
NTP-NaGe1	10.70 ± 0.11	639.87 ± 16.63	56.64 ± 5.59	3.72 ± 0.24
NTP-NaSW0.25	11.08 ± 0.06	705.75 ± 19.39	58.74 ± 3.24	3.27 ± 0.20
NTP-NaSW0.5	11.45 ± 0.07	727.45 ± 35.38	63.10 ± 3.69	3.85 ± 0.21
NTP-NaSW1	9.85 ± 0.16	577.46 ± 35.21	64.21 ± 5.68	3.31 ± 0.23

Appendix-16B

Table 58: Tensile properties of unconditioned NTP composites (mean ± standard error of the mean).

Sample	Tensile strength, σ (MPa)	Young's modulus, E (MPa)	Elongation at break, ε (%)	Toughness (MPa)
NTP	1.94 ± 0.061	31.08 ± 2.00	73.63 ± 1.09	0.50 ± 0.012
NTP-CaRaw0.25	2.18 ± 0.029	42.38 ± 1.64	61.49 ± 1.24	0.43 ± 0.021
NTP-CaRaw0.5	2.28 ± 0.034	43.77 ± 1.96	60.06 ± 2.86	0.46 ± 0.045
NTP-CaRaw1	2.11 ± 0.012	43.09 ± 1.53	60.37 ± 9.30	0.44 ± 0.082
NTP-CaGe0.25	1.88 ± 0.032	34.22 ± 0.92	62.04 ± 3.71	0.38 ± 0.025
NTP-CaGe0.5	1.89 ± 0.027	34.59 ± 1.72	60.86 ± 3.75	0.37 ± 0.024
NTP-CaGe1	1.79 ± 0.034	28.22 ± 1.31	64.33 ± 2.91	0.38 ± 0.023
NTP-CaSW0.25	1.95 ± 0.020	40.04 ± 0.94	61.32 ± 1.54	0.40 ± 0.019
NTP-CaSW0.5	2.13 ± 0.017	42.84 ± 1.01	52.94 ± 1.36	0.37 ± 0.013
NTP-CaSW1	2.01 ± 0.018	37.51 ± 0.88	54.98 ± 1.34	0.35 ± 0.011
NTP-NaRaw0.25	2.10 ± 0.031	35.56 ± 2.55	54.04 ± 0.86	0.36 ± 0.001
NTP-NaRaw0.5	1.87 ± 0.010	36.13 ± 1.52	62.96 ± 0.49	0.40 ± 0.012
NTP-NaRaw1	2.03 ± 0.017	44.14 ± 2.24	64.59 ± 0.91	0.45 ± 0.020
NTP-NaGe0.25	1.99 ± 0.020	33.07 ± 1.46	58.20 ± 0.74	0.36 ± 0.015
NTP-NaGe0.5	2.12 ± 0.045	42.02 ± 1.56	58.07 ± 0.43	0.38 ± 0.012
NTP-NaGe1	1.75 ± 0.021	27.37 ± 0.95	63.31 ± 1.46	0.32 ± 0.023
NTP-NaSW0.25	2.03 ± 0.036	47.73 ± 1.38	62.35 ± 0.50	0.48 ± 0.021
NTP-NaSW0.5	2.34 ± 0.027	54.71 ± 2.48	54.14 ± 0.61	0.42 ± 0.019
NTP-NaSW1	2.07 ± 0.012	39.50 ± 1.01	55.29 ± 0.73	0.39 ± 0.020

Appendix-17

Table 59: Summary of T_g and crystallinity of conditioned NTP composites.

Samples	DMA mass loss (%)	T_g at 1Hz (°C)	Increase in T_g (%)	Crystallinity (%)
NTP	4.04	61.8	-	18.89
NTP-CaRaw0.25	3.82	71.8	16.18	22.59
NTP-CaRaw0.5	3.27	74.6	20.71	20.14
NTP-CaRaw1	3.57	75.2	21.68	21.50
NTP-CaGe0.25	3.44	66.2	7.12	23.20
NTP-CaGe0.5	3.63	67.6	9.39	25.89
NTP-CaGe1	3.31	70.7	14.40	23.07
NTP-CaSW0.25	3.55	70.0	13.27	22.71
NTP-CaSW0.5	3.23	65.2	5.50	26.91
NTP-CaSW1	3.46	72.4	17.15	23.73
NTP-NaRaw0.25	3.75	70.1	13.43	20.43
NTP-NaRaw0.5	3.61	72.8	17.80	24.25
NTP-NaRaw1	3.34	67.4	9.06	23.57
NTP-NaGe0.25	3.82	69.8	12.94	21.32
NTP-NaGe0.5	3.40	70.7	14.40	25.72
NTP-NaGe1	3.62	71.6	15.86	22.85
NTP-NaSW0.25	3.40	66.3	7.28	22.01
NTP-NaSW0.5	3.40	70.3	13.75	28.02
NTP-NaSW1	3.59	68.9	11.49	24.74

Appendix-18

Table 60: Summary of thermal degradation of NTP composites.

Sample	TGA composition (wt%) *						Organic (wt%)	Ash (wt%)
	A	B	C	D	E	F		
	0-150°C	150-230°C	230-390°C	390-500°C	500-600°C	600-800°C		
NTP	8.14	16.95	39.33	17.74	16.91	0.56	91.49	0.38
NTP-CaRaw0.25	7.32	16.49	38.75	15.99	15.98	0.36	87.56	5.12
NTP-CaRaw0.5	7.47	15.74	38.59	17.76	13.31	0.38	85.79	6.74
NTP-CaRaw1	7.02	15.71	37.95	18.16	14.01	0.41	86.24	6.75
NTP-CaGe0.25	7.73	16.40	39.86	17.03	16.12	0.82	90.22	2.05
NTP-CaGe0.5	6.73	14.71	38.79	14.83	19.19	0.66	88.18	5.09
NTP-CaGe1	9.84	15.57	38.16	11.20	20.41	0.86	86.21	3.95
NTP-CaSW0.25	8.82	15.80	43.78	19.35	10.00	0.97	89.89	1.29
NTP-CaSW0.5	7.54	16.31	41.94	17.36	14.87	0.86	91.35	1.11
NTP-CaSW1	7.39	15.64	50.14	11.19	14.74	0.24	91.95	0.66
NTP-NaRaw0.25	7.85	16.71	36.79	18.27	16.59	0.28	88.62	3.53
NTP-NaRaw0.5	6.61	16.74	38.52	16.67	16.84	~0	88.47	4.92
NTP-NaRaw1	7.06	16.63	38.91	16.50	16.19	~0	87.92	5.02
NTP-NaGe0.25	7.23	16.44	46.80	15.91	12.43	0.88	92.46	0.31
NTP-NaGe0.5	7.54	16.68	40.33	14.17	18.52	1.48	91.18	1.28
NTP-NaGe1	7.05	15.97	38.42	9.94	21.29	1.84	87.46	5.50
NTP-NaSW0.25	8.03	16.31	49.43	13.06	13.37	0.09	92.26	~0
NTP-NaSW0.5	7.49	16.72	42.28	15.35	16.98	0.95	92.28	0.23
NTP-NaSW1	6.73	15.57	51.88	13.16	9.95	0.58	91.14	2.13

***** A: Surface/pore water and low molecular mass compounds; B: Surface organics and degradation of urea; C: Cleavage of S–S, O–N and O–O linkages; D: Hydroxyl water, intercalated organics and reduction in peptide bonds; E: Low volatility organics/compounds and F: Traces of organics [80, 183, 203].